Unravelling the binding mechanism of selected bioactive compounds with human plasma proteins

Thesis submitted for the Degree of

Doctor of Philosophy

Y Daniel Pushparaju

Department of Plant Sciences
School of Life Science
University of Hyderabad
Hyderabad-500 046

INDIA

December 2016

University of Hyderabad School of Life Sciences
Department of Plant Sciences
Hyderabad-500 046

DECLARATION

I, Y Daniel Pushparaju, hereby declare that this thesis entitled **"Unravelling the binding mechanism of selected bioactive compounds with human plasma proteins"** submitted by me under the guidance and supervision of Prof. S.Rajagopal is an original and independent research work. I also declare that it has not been submitted previously in part or in full to this University or any other University or Institution for the award of any degree or diploma.

Date:

Name: Y Daniel Pushparaju

Signature:

Regd. No.: 12LPPH09

CERTIFICATE

This is to certify that this thesis entitled "**Unravelling the binding mechanism of selected bioactive compounds with human plasma proteins**" submitted Y. Daniel Pushparaju, bearing registration number 12LPPH09 in partial fulfillment of the requirements for award of Doctor of Philosophy in the School of Life Sciences is a bonafide work carried out by him under my supervision and guidance.

This thesis is free from plagiarism and has not been submitted previously in part or in full to this or any other University or Institution for award of any degree or diploma.

Parts of this thesis have been:

A. Published in the following publication

1. Molecular Pharmaceutics , ISSN 1543-8384 ,Chapter 3,4 and 5
2. Molecular Biosystems, ISSN:1742-206X , Chapter 1,3 and 4
3. Journal of Biomolecular Structure and Dynamics, ISSN: 0739-1102, Chapter 3, 4 and 5
4. RSC Advances, ISSN 2046-2069, Chapter 3, 4 and 5
5. Journal of Photochemistry and Photobiology B, ISSN: 1011-1344 ,Chapter 3,4 and 5
6. Journal of Biomolecular Structure and Dynamics,ISSN: 0739-1102, Chapter ,1,4 and 5
7. RSC Advances, ISSN 2046-2069, Chapter 3, 4 and 5

B. Presented in the followinng conferences

1. Indo-German symposium on the system biology (International)
2. Recent Advance in computational Drug Design (International)
3. Nanoscitech (International)

Further, the student has passed the following courses towards fulfillment of coursework reqirements for Ph.D

	CourseCode	Name	Credits	Pass/Fail
1.	PL 801	Seminar	1	Pass
2.	PL 802	Research Ethic & Mangment	2	Pass
3.	PL 803	Biostatics	2	Pass
4.	PL 804	Analytical Techiques	3	Pass
5.	PL 805	Lab Work	4	Pass

Supervisor **Head of the Department** **Dean of the School**

DEDICATION

I gratefully dedicate this thesis to my parents and my aunt

Bishop Pushpa

-Daniel Yeggoni-

ACKNOWLEDGEMENTS

I express my whole hearted thanks to my research supervisor, ***Prof. S. Rajagopal****, for believing in me and offering me the chance to work in his research group on this interesting topic and for scientific and encouragement he extended during times of thick and thin.*

I sincerely thank the present and former Deans, ***Prof. A.S.Raghavendra, Prof. Aparna Dutta Gupta, Prof. P. Reddanna****, School of Life Sciences, for allowing me to use school facilities.*

I would like to express my thankfulness to present and former Heads, ***Prof. Attipalli R.Reddy*** *and* ***Prof. Ch. Venkata Ramana****, Department of Plant Sciences for their support and encouragement during my research tenure and allowing me to use department facilities.*

I would like to thank ***Prof. Rainer Haag****, Department of Chemistry, Biochemistry and Pharmacy, FU Berlin, Germany for giving me the opportunity to work in his group.*

I am extremely indebted to my doctoral committee members ***Prof.T. Sarada Devi*** *and* ***Dr. Irfan Ahmad Ghazi*** *for their constant support and valuable suggestions during my research period.*

I also thank ***Prof. S. Naresh babu*** *for scientific discussion and valuable suggestions.*

My sincere thanks, ***Dr. A.G. Damu*** *and* ***Dr. Mark Manidhar*** *Department of Chemistry, Yogi Vemana University and Sri Venkateswara University for providing coumarin derivatives*

I would like to thank ***Dr. Aparna Rachamallu****, NIAB for helping with cell culture facilities.*

It would like to express my sincere thanks to all the faculty members of School of Life Sciences for their support and encouragement.

I thank the nonteaching and technical staff of School of Life Sciences for their kind help and support.

I would also like to thank central instrumentation laboratory, UOH, for allowing me to use CD spectroscopy. I thank proteomic facility, School of Life Sciences, for MALDI analysis. I thank CMSD and bioinformatics facility (SLS facility) for providing servers for molecular simulation studies.

I am very much grateful to my senior colleagues ***Dr.Mahesh and Late Chandra Mouli*** *for their guidance and help in acquiring the technical skills and scientific insight.*

My heartfelt thanks to my colleagues ***Dr.N.Veerababu, Dr.Monika, Dr.Dinesh, Saikiran, Elsinraju, Srilatha, Aparna, Shreya, Srilatha, Aparna, Ranay, Nisha, Argha, Varma, Arijit and lab assistant Ganesh*** *for their cooperation and providing me a peaceful atmosphere during my bench work.*

I'm grateful to all my friends, ***Girija Brahma, RohitRaj, Yogendrakumar, Himadri Medhi and Obaidullah*** *for their ever responsiveness and being the very special part of my life.*

I expand my thanks to all my friends at School of Life Sciences for maintaining a lively and amicable atmosphere.

I take this opportunity to sincerely acknowledge the funding agencies ***DST-FIST, DBT-CREBB*** *and* ***UGC-SAP*** *for infrastructure and also thank* ***DST, DBT, CSIR*** *and* ***UPE-II*** *for financial support to the lab.*

I'm thankful for Erasmus+ program, funding for my stay in Germany.

I would like to take the privilege to thank my family members without whose support and encouragement I would not have been able to successfully complete my doctoral research, who have been eagerly looking forward to this personal milestone with much patience. My parents have been a true inspiration all along, they stood by me in every step I took and every decision I made. Their simplicity, revered advice, love, and affection have helped me be what I am.

Daniel Yeggoni..

CONTENTS

LIST OF FIGURES

LIST OF TABLES

ABBREVIATIONS

[Q]	Quencher concentration
6-SGL	6-Shagoal
7HC-1	(E)-2-cyano-N-(3,5-dimethoxybenzyl)-3-(7-hydroxy-2-oxo-2H-chromen-8-yl) acrylamide
7HC-2	(E)-N-benzhydryl-2-cyano-3-(7-hydroxy-2-oxo-2H-chromen-8-yl)acrylamide
7HC-3	(E)-2-cyano-3-(7-hydroxy-2-oxo-2H-chromen-8-yl)-N-(1-phenylethyl) acrylamide
ADG	Andrographolide
A_{emi}	Absorption at emission
A_{exc}	Absorption at excitation
AFM	Atomic force microscopy
AGP	α-1-glycoprotein
APO	Apocynin
ART	Artemisinin
AT	Ar-tumarone
BAC	Bacosine
CHG	Chebulagic acid
CHN	Chebulinic acid
COR	Corilagin
DEA	De Andrographolide
DEF	De Forskolin
EMB	Embelin
F	Fluorescence intensity in presence quencher
Fcor	Corrected fluorescence intensity
FDA	Federal Drug Administration.
Fo	Fluorescence intensity in absence of quencher.
Fobs	Observed fluorescence
HSA	Human serum albumin
IC_{50}	Half maximal inhibitory concentration
K	Binding constant

KD	Stern-Volmer quenching constant.
Kq	Bimolecular quenching rate constant.
LDA	L-dopa
MEL	Menthol
MOL. CD	Molar circular dichroism
MTT	3-(4,5-Dimethylthiazol-2-Yl)-2,5-Diphenyltetrazolium Bromide.
PBS	Phosphate Buffered Saline
PIP	Piperine
PLN	Psoralen
PTE	Pterostiblene
R	Gas constant
Rg	Radius of gyration
RMA	Rosmaric acid
RMSD	Root mean square deviation
RMSF	Root mean square fluctuation
SDS-PAGE	Sodium dodecyl sulfate polyacrylamide gel electrophoresis
STL	Stigmasterol
t_0	Lifetime of the fluorophore in the absence of quencher
TdCD	Temperature-dependent circular dichroism
TEM	Transmission electron microscopy
UMB-1	2-Cyano-N-(2,5-dihydro-thiazol-2-yl)-3-(7-hydroxy-2-oxo-2H-chromen-8-yl)-acrylamide
UMB-2	2-Cyano-3-(7-hydroxy-2-oxo-2H-chromen-8-yl)-N-[2-(2-methoxy-phenoxy)-ethyl]-acrylamide
ΔG	Free energy
λ_{em}	Emission wavelength
λ_{ex}	Excitation wavelength

CHAPTER 1

INTRODUCTION

1. Introduction

Plasma proteins and their binding mechanism to various drugs have a vital implication for drug action and disposition. Plasma protein binding property strongly affects the drug distribution pharmacokinetic properties, which leads to all pharmacological action. The effect of a drug depends on the available of plasma that is in a free state in plasma for binding to receptor sites and employ pharmacological action. Most of the drugs bind reversibly to the plasma proteins. As a result, drugs are transported, in plasma in an aqueous state, either in free, dissolved state or in complex form proteins (Otagiri et al., 2009). Hence the binding capacity of drugs to proteins is an important factor, which determines and helps us to understand the pharmacodynamics and pharmacokinetics effects of drugs. Among the plasma proteins, considerable efforts are focused towards understanding the drug binding mechanisms to human serum albumin (HSA) as most of the drugs bind to it and to an extent with the second crucial protein α-1-acid glycoprotein (AGP) which is an acute phase protein, which plays an important role in clinical therapy (Israili & Dayton 2001; Bailey & Briggs 2004).

1.1. Albumins

Blood, the major constituent of the human circulatory system, is a specialized body fluid that delivers necessary substances like nutrients, oxygen to cells and transports away waste products. Blood accounts for 5% of the total body weight and its components are plasma, cells like red blood cells, white blood cells, and platelets. Plasma accounts for 55% of human blood composition in which it contains 92% water, 7% plasma proteins, 1% other solutes such as inorganic ions and trace amounts of other materials. Plasma devoid of clotting factors is called serum (Anderson & Anderson 1977). Total serum protein in blood is 7g/dl which accounts for 7% of total blood volume. Albumin comprises of 60% of the total plasma protein. Numerous types of albumins are present and most familiar examples are ovalbumin found in egg white, and HSA. The protein comprises is globular and water soluble.

1.1. A. Protein under study: human serum albumin

In human blood plasma, HSA is the most abundant protein, present at a concentration of ~7×10^{-4} M. It is synthesized in the liver. The chromosome 4 is where the gene for albumin is located with 16,961 nucleotides long. This protein contains one polypeptide chain of 609 amino acids in the case of immature protein, i.e. synthesized in the liver as pre pro-albumin. This nascent protein is then transported to endoplasmic reticulum where approximately 24 amino acids long signal peptide chain at the N-terminal end is spliced off to give rise to pro-albumin, which is further transported to Golgi vesicles and secreted as albumin of 585 amino acids, having half-life of approximately 20 days (Anderson & Anderson 1977; He & Carter 1992; Sugio et al., 1999). Since, HSA, abundant blood plasma protein; the binding efficacy of this protein towards various drug entities plays a critical role in studying pharmacokinetic and pharmacodynamics of drugs. Besides, transporting various hormones, exogenous drug molecules HSA also possess antioxidant activity, further, it also maintains osmotic pressure, pH of blood vessels, sequestering metal ions, and scavenge free radicles from the plasma (Kragh-Hansen et al., 1981). HSA has a molecular weight of 67 KDa with a serum half-life of 20 days. It is a well-known point that HSA has a robust affinity to a wide range of materials, including metals such as $Cu^{2+}$and Zn^{2+}, fatty acids, amino acids, metabolites (e.g. bilirubin) and for many drug compounds (Sugio et al., 1999).

1.1.B. Structural insights of HSA

HSA, non-glycosylated single chained polypeptide with a molecular mass of 66-kD mass, which organizes to form a heart-shaped protein with approximately 67% α-helical (He & Carter 1992; Curry et al., 1998; Curry et al., 1999; Sugio et al., 1999; Bhattacharya et al., 2000; Petitpas et al., 2001; Ghuman et al., 2005). HSA is a widely studied protein because its primary structure is well known and its tertiary structure has been determined by X-ray crystallography (Carter et al., 1989; He & Carter 1992). HSA is helical protein assemble asymmetrically, with approximate dimensions of 80-80-30 Å. It possesses three domains, I (residues1-195), II (196-383) and III (384-585), seven water molecules and the whole structure is stabilized by a conserved set 17 disulfide bridges, one free thiol group (Cys34) and a Tryptophan residue (Trp214). Due to the presence of 17 disulfide bridges, the tertiary structure of HSA engraves nine loops that were centered by eight sequential Cys-Cys pairs. This structural feature of S-S bonds

was also observed in sheep, frog, salmon, mouse, pig, bovine and human, suggesting that the protein was evolved from a common ancestor of approximately 190 amino acid sequences (Fig.1.1). Further this protein also acquires thermal stability due to the presence of 17 disulfide bridges (Sudlow et al., 1975; Sudlow et al., 1976) studied the structure of HSA by probing fluorescence methods and found two major binding sites having high affinity with most drugs, which they named as site I and site II. An electron density corresponding to residues 1-4 and residues 583-585 of the HSA molecule is not clearly observed, probably due to the conformational flexibility at both termini (Fig.1.2) (Sugio et al.,1999). X-ray crystallographic studies reveal that its alpha-helical region is divided into three domains I (residue 1-195), II (residue 196-383), III (residue 384-585); each domain is further divided into two sub-domains A and B (Lichenstein et al., 1994; Sugio et al., 1999). Aromatic and heterocyclic ligands have been found to bind within two hydrophobic pockets in sub-domains IIA and IIIA, a namely site I and site II (Peters Jr et al., 1996). Subdomain I and II are almost perpendicular to each other, between subdomain IA and IB by hydrophobic and hydrogen bond interaction IIA being connected at the interface region. Domain III interacts only with subdomain IIB, forming a Y-shaped assembly with domains II and III. A big channel created by subdomains IB, IIIA and IIIB separates domains I and III which are connected only by few contacts. Fatty acids have seven binding sites and are localized in sub-domains IB, IIIA and IIIB, and on the subdomain interfaces. At the N-terminus end, HSA has a high affinity for metal binding. Digitoxin site has been recognized more recently and is consider as a third specific drug-binding site (Curry et al., 2009; Zsila et al., 2013). This binding pocket, located in subdomain IB, has been described as the primary binding site of various compounds such as lidocaine, hemin and fusidic acid (Zunszain et al., 2008).

\

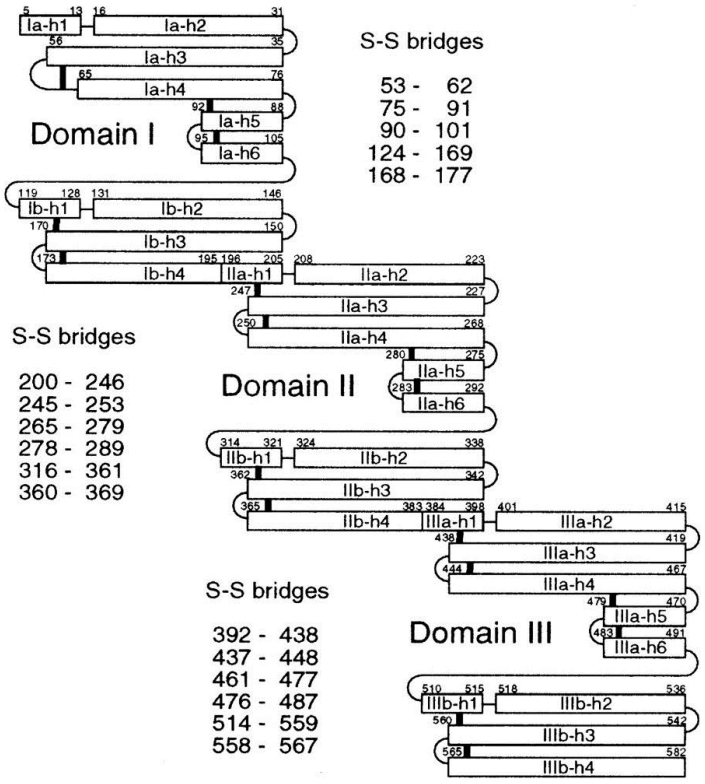

Fig.1.1. Schematic drawing of secondary structural elements and disulfide bridges of HSA. Helices are represented by rectangles, and loops and turns by thin lines. Disulfide bridges are drawn with thick lines (Adapted from Sugio et al.,1999).

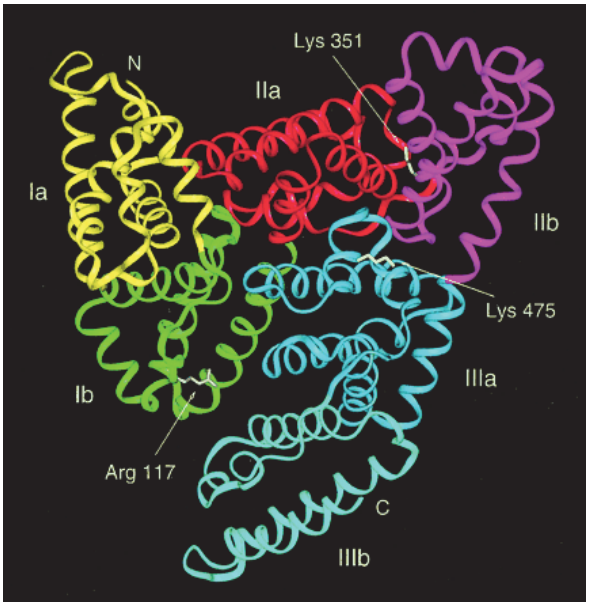

Fig.1.2. HSA with its sub-domains IA, IIA, IB, IIB, IIIA, IIIB. Each sub-domain is marked with a different color (yellow for sub-domain IA; green, IB; red, IIA; magenta, IIB; blue, IIIA; and cyan, IIIB). N-and C-termini is marked as N and C, respectively. Arg117, Lys351, and Lys475, which may be binding sites for long-chain fatty acids, are colored white.Adapted from (Sugio et al.,1999).

1.1.C. Modes of Ligand Binding

Several studies suggest that the extraordinary ligand binding with HSA reflect its multidomain organization. Indeed, although monomeric, HSA functional properties are similar of those of multimeric proteins. Binding of nonsteroidal anti-inflammatory drugs (NSAIDs) and serum albumin are stereoselective with different degrees depending on the properties of the drug (ibuprofen, indoprofen, carprofen, etodolac, ketoprofen, and flurbiprofen). For other drugs, they are bound to a similar extent (pirprofen and fenoprofen). This stereoselective nature of HSA could vary with the various experimental conditions, such as protein or drug concentration (ketoprofen, etodolac) (Chuang & Otagiri 2006). Binding of several exogenous (e.g., therapeutic and diagnostic agents) and endogenous (e.g. heme and FAs) ligands to HSA. Usually, drug binds to one or very few high-affinity sites with typical association constant in the range of 10^3-$10^6 M^{-1}$. The binding can affect the metabolic fate and clearance and ultimately decides its bioavailability. Binding with HSA helps insolubilizing compounds, otherwise gets aggregated and resulting in poor distribution (Chuang & Otagiri 2006). Two mechanisms have been proposed for the covalent interactions between drug and HSA (Fasano et al., 2005).

1.1.D. Extra Corporeal Clearance

Albumin can be used to clear the endogenous toxin from the body. Liver failure and renal failure associated with jaundice and excretory insufficiency usually result in accumulation of various endogenous toxins which, in turn, have been shown to induce hepatocellular apoptosis and necrosis and thereby create a vicious cycle of the disease. The toxin that contributes substantially to the development of multiorgan dysfunction such as cardiovascular, kidney, and cerebral impairment, are albumin-binding compounds such as bilirubin, bile acids, and uremic toxins. During clinical situation, hemodialysis is done to remove the toxin from patients. By passing blood through columns with immobilized albumin endotoxins such as lipopolysaccharides and cytokines, and possibly other toxins can be removed (Kragh-Hansen et al., 2002).

1.1. E. Enzymatic Properties of HSA

In some cases, enzymatic activity results due to the interaction between a small molecule and albumin. Thus albumin has an enolase activity towards

dihydrotestosterone, and the active-site for this property has been assigned to the amino-terminal end of the molecule Drmanovic et al., 1998). HSA is also able to act as a thioesterase because it has a free sulfhydryl group at 34 Cys. The protein can degrade disulfiram (antabuse), a clinically important process (Agarwal et al., 1986). HSA can catalyze dehydration of prostaglandin D2 (Fitzpatrick & Wynalda 1983), dehydration and subsequent isomerization of 15-ketoprostaglandin E2 (Yang et al., 2002). Amino acid residues of the site I can also degrade at sulbenicillin, with the R-isomer being degraded much faster than the S-isomer (Kragh-Hansen et al., 2002).Thus the enzymatic properties of HSA can, best stereospecific, like the ligand binding properties. Among other possible catalytic properties of sub-domain IIA is an esterase reaction, which results in the transfer of the acetyl group from acetylsalicylic acid to Lys199 (Walker et al., 1976).

Sub-domain IIIA of HSA possesses a well-known esterase-like activity towards substrates such as p-nitrophenyl acetate (Means & Bender 1975) and several N-carbobenzoxy-D(L)-alanine-nitrophenyl esters (Kurono et al., 1992). Residues in sub-domain IIIA of HSA are also able to detoxify cyanide by reaction with elemental sulfur to form thiocyanate (Jarabak & Westley 1989). The esterase-like activity of HSA in sub-domain IIIA is due to the close proximity of Arg410 and Tyr411. From the pharmaceutical and clinical points of view, it is interesting that the esterase-like activity of HSA can be used to activate prodrugs. Human plasma converts inactive olmesartan medoxomil to active olmesartan by hydrolysis, with a half-life of a few seconds (Ma et al., 2005). In addition, both serum and cytosolic HSA possesses an intrinsic enolase activity, converting the 3-keto form of dihydrotestosterone to the 3-enol form, which is much lower in cytosol from malignant tumors. Lower albumin concentration and partly polymerization or binding of the protein to other intracellular proteins may reduce the activity.

1.1.F. Binding sites on HSA for endogenous and exogenous compounds

HSA has few sites for high-affinity the interaction with drug molecule often influences the simultaneous binding of other drugs. Alterations in binding may lead to a difference in the pharmacokinetic properties. HSA globular domain structural organization provides multiple binding sites for various ligands and thus makes it an important determinant of pharmacokinetic behavior of several ligands (Fig.1.3).

Usually, drugs bind to one or very few high-affinity sites with typical association constants in the range of 10^{3} - 10^{6} M^{-1} (Varshney et al., 2010). HSA interacts reversibly with a broad spectrum of therapeutic agents. The binding can ultimately decide its bioavailability and it affects the metabolic fate and clearance. Albumin binding helps insolubilizing compounds, otherwise get aggregated and results in a poor distribution. Drugs with an excessively high affinity for HSA are distributed slowly to sites of action and may not be efficiently eliminated (Ghuman et al., 2005).

The crystallographic analysis gives a good information of various complexes of HSA with a range of drugs reveals the accurate architecture of two drug binding sites1,2 situated in subdomain IIA and IIIA on the HSA, along with numerous secondary sites. Residues which are the key determinants of binding specificity, flexible accommodation were identified. Overall, HSA plays vital role in various physiological functions in the transport and distribution of many endogenous molecules i:e fatty acids, bilirubin and thyroxine (Curry et al., 1999; Bhattacharya et al., 2000; Zunszain et al., 2008) and various exogenous drug molecules like warfarin, ibuprofen, digitoxin and quinidine with binding constants of 3.3×10^{-5}, 2.6×10^{-6}, 0.4×10^{-5}, and 1.6×10^{-3} M, respectively (Table.1).

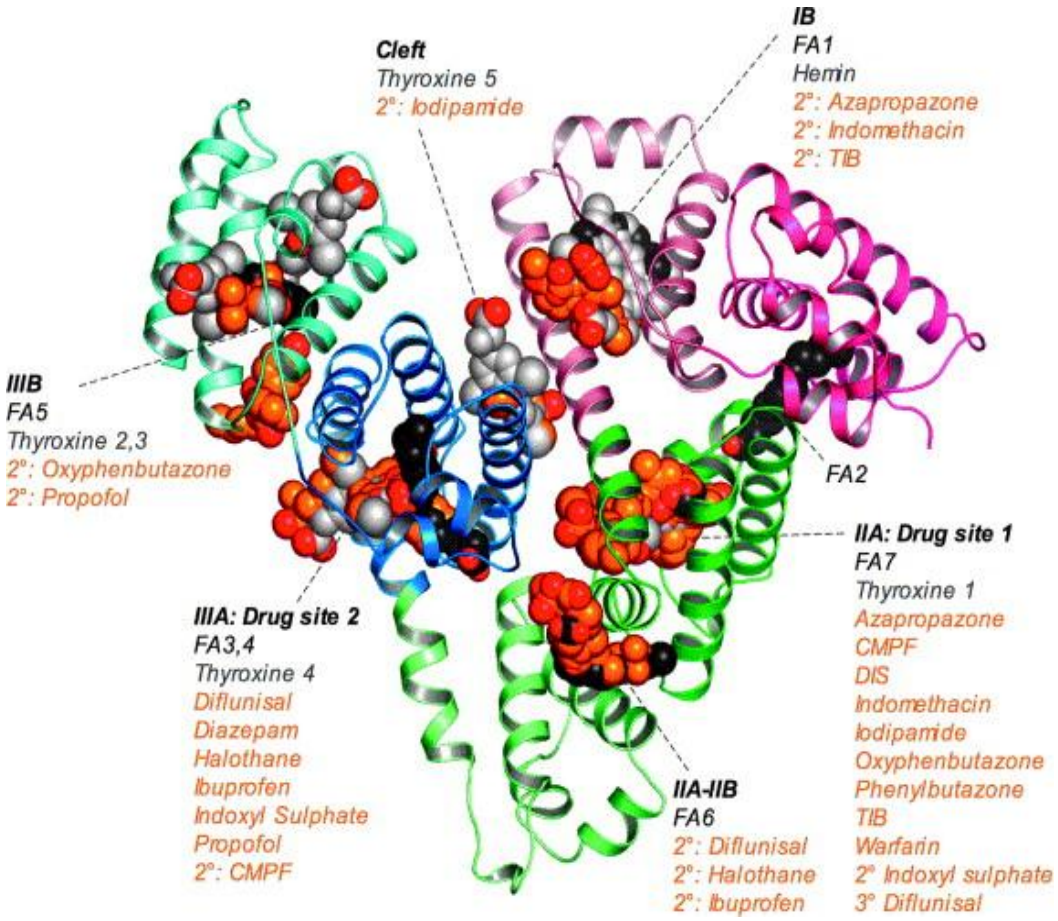

Fig.1.3. Summary of the ligand binding capacity of HSA as defined by crystallographic studies to date. Ligands are depicted in space-filling representation; oxygen atoms are colored red; all other atoms in fatty acids (Myristic acid), other endogenous ligands (Adapted from Ghuman et al., 2005).

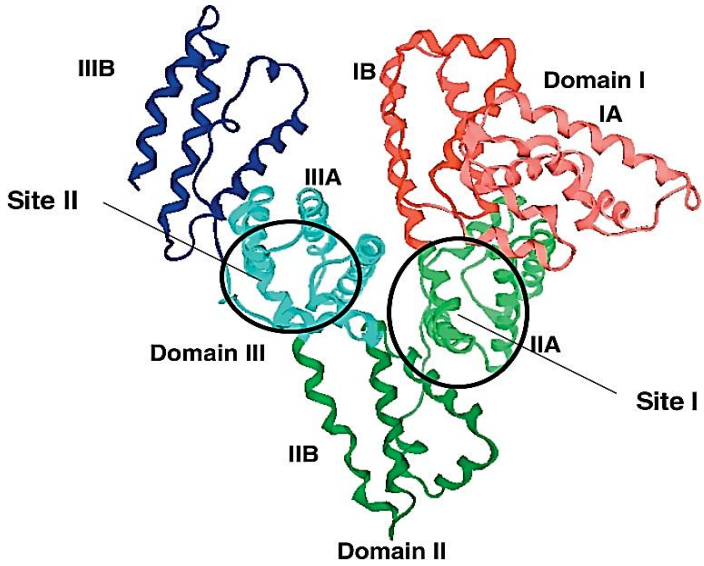

Fig.1.4. Crystal structure of HSA. The subdivision of HSA into the domain (I – III) and subdomains are indicated, and approximate locations of Sudlow's site I and site II are shown (Chuang & Otagiri 2006).

1.1.G. Binding of drugs to HSA

Binding to HSA controls the free, active concentration of a drug, provides a reservoir for a long duration of action, and ultimately affects drug absorption, metabolism, distribution, and excretion. The free concentration of a drug can also be affected by interaction with co-administered drugs or by pathological conditions that can modify to a significant extent to the binding properties of the carrier, resulting in important clinical impacts for drugs that have a relatively narrow therapeutic index.

The clinical consequences of drug-albumin interactions are now well understood. Dosage schedules that have been empirically devised for highly albumin-bound drugs are based on normal concentrations and drug-binding behavior of albumin. HSA has a limited number of binding sites for endogenous and exogenous ligands, so that drug binding to the protein may be affected by a variety of factors. The effects on the pharmacokinetics of drug-drug competition for the same sites on HSA are generally held to be of little clinical importance. Physiological or disease states that cause variations in the plasma levels of albumin or its primary endogenous ligands can influence drug binding and may require dosages to be closely monitored. Added to this, genetic polymorphisms in HSA can also alter drug binding and may further complicate the clinical picture. To understand the molecular basis of these effects, structural information is required to fully delineate the binding sites for drugs and endogenous ligands. Such information will also be invaluable to efforts to exploit the carrier properties of HSA in the development of novel therapeutic reagents for drug targeting or oxygen transport. Structural studies have mapped the locations of the fatty acid binding sites and the primary drug binding sites on the protein.

The fatty acid binding sites are distributed throughout the protein and involve all six sub-domains; by contrast, many drugs bind to one of the two primary binding sites on the protein, known as Sudlow's sites I and II (Fig.1.4). Although examples of drugs binding elsewhere on the protein have been documented, most work has focused on the primary drug sites. These investigations have largely employed competitive binding methods to investigate the selectivity of the primary drug binding sites.

1.1H. Details of the three sites on HSA for drug binding

1.1.H.i. *Drug site1 (Sub-domain IIA)*

It was determined from the crystal structure of HSA that site I is formed as a hydrophobic pocket at subdomain IIA. In which the lone Tryptophan residue (Trp214) of the protein play a major role drug binding. The inside wall of this large pocket is made up of hydrophobic side chains, whereas the entrance to the pocket is surrounded by positively charged residues. In this sub-domain, Lys 199, His 242, and Arg 257 binds sterically and electrostatically with ligands. The hydrophobic end of the IIA cavity is truncated relative to IIIA by the presence of bulkier hydrophobic side chains. Moreover, helix h1 in IIA is displaced outward and presents a very hydrophilic surface toward the cavity (Curry et al., 1998). This site must be large because large ligands like bilirubin can bound easily within it. It is also very flexible because ligands with very varied chemical structures bind with higher affinity. Thus, a site I appear to be capacious and flexible. Mutual interactions between bound ligands have been observed, that is due to the conformational changes in the protein molecule called allosteric effects or anti-cooperativity. But several studies suggest that site I may not be the proper site for stereoselective binding with HSA and warfarin. Also binding of fatty acids with HSA induce a conformational change in the domain I and III relative to domain II (Chuang & Otagiri 2006).

1.1.H.ii. *Drug site2 (Sub-domain IIIA)*

Site II i.e. subdomain IIIA contains a hydrophobic, branched, T-shaped cavity. This cavity has two hydrophilic entrances which are separated by approximately 10Å and the residues each interacts with the carboxylic group of the drug molecules. This binding pocket shares two hydrogen bonds. The first one is formed by Ser 342, located in the II and III domain interface and Arg 348 from IIB and by Arg 485 from IIIA sun-domain. The another one is formed by Arg 410, Tyr 411, and Ser 489 in subdomain IIIA. In this subdomain, Arg 410 and Tyr 411 help in the binding with various drug molecules. In the case of ligands binding to this site (also named as Sudlow site II), aromatic carboxylic acids binds to it where the acidic group located away from a hydrophobic center (e.g., NSAIDs). As no large ligands apparently bind to site II, it appears to be smaller, more narrow, than site I. It also appears to be less flexible, as the binding with ligand is strongly affected by stereoselectivity approved by some research experiments (Kragh-Hansen et al., 2002).

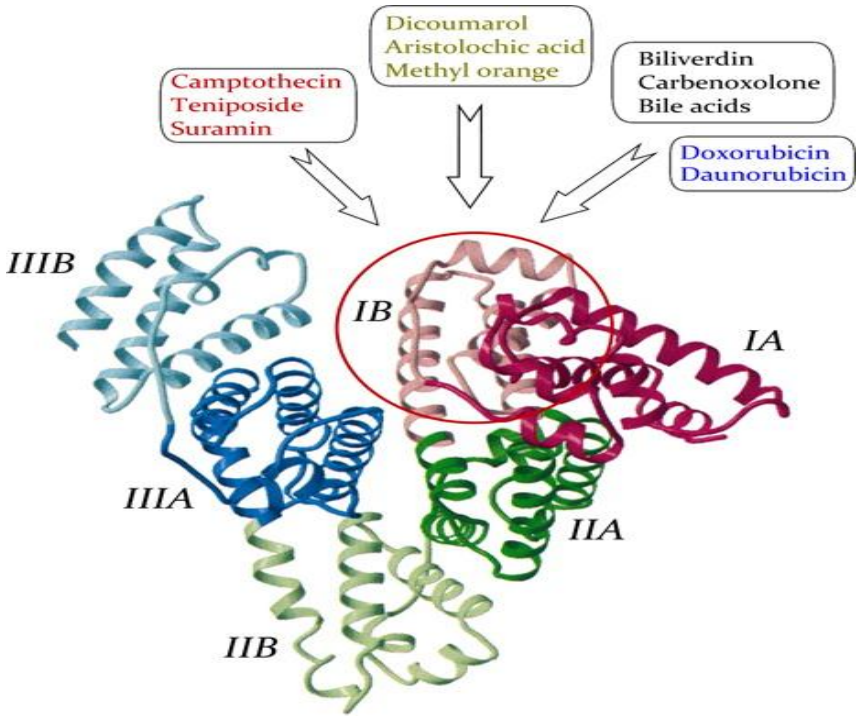

Fig.1.5. Subdomain IB Is the Third Major Drug Binding Region of Human Serum Albumin (Zsila et al., 2013)

1.1.H.iii. *Drug site 3 (Sub-domain IB)*

A third binding pocket within subdomain IB has recently been identified as the primary binding site of a bilirubin photoisomer, hemin, and the steroid antibiotic fusidic acid. Crystallographic studies have also shown that the large crevice of subdomain IB harbors secondary binding sites for some additional compounds (Fig.1.5) (Zunszain et al., 2008; Zsila et al., 2013).

Table 1. High-Affinity Binding of Ligands to site I, site II and site IB of HSA (Kragh-Hansen et al., 2002; Zunszain et al., 2008).

Site 1 (Sub-domain IIA)		**Site 2 (Sub-domain IIIA)**	
Drug	Binding const (M^{-1})	Drug	Binding const (M^{-1})
Warfarin	3.3×10^{5}	Diazepam	3.83×10^{5}
Azapropazone	2.83×10^{5}	Ketoprofen	2.53×10^{6}
Phenylbutazone	1.53×10^{6}	Chlofibrate	7.63×10^{5}
Salicylate	1.93×10^{5}	Ibuprofen	2.6×10^{6}
Acenocoumarol	2.23×10^{5}	Carprofen	$>10^{6}$

(Sub-domain IB)		**Endogenous compounds**	
Drug	Binding const (M^{-1})	Drug	Binding const (M^{-1})
Lidocaine	10^5	Bilirubin (IIA)	9.53×10^7
Fusidic acid	10^5	Octanoate (IIIA)	1.63×10^6
Hemin	10^8	L-Tryptophan (IIIA)	4.43×10^4
15*E*-bilirubin-IXα photo isomer	10^5	L-Thyroxine (IIIA)	3.03×10^5
Estradiol	10^5	Cl^{-1} (IIIA)	7.23×10^2

1.2. α-1-Acid-Glycoprotein

Next to HSA, the most second critical plasma protein is α-1-acid glycoprotein (AGP), also called *orosomucoid*, present at a much low concentration (~1-3× 10^{-5}M). AGP is an acute phase protein in blood comprises of 183 amino acid residues and five N-linked oligosaccharides. After synthesized in the liver cells, AGP secreted into the blood stream (2.5 mg/ml). Human AGP presents in the plasma of healthy individuals at concentrations between 0.6 and 1.2 mg/ml with a molecular weight of approximately 3 8 - 44 kDa protein (Fournier et al., 2000). The five carbohydrate chains account for about 40% of the total mass and render AGP very soluble and confer acidic (pI) between 2.8-3.8 due to the presence of sialic acid and with a net negative charge at physiological pH (Fournier et al., 2000; Hochepied et al., 2003). While AGP is mainly biosynthesized in the liver and secreted into the circulation (Sarcione et al., 1963; Athineos et al., 1964), other organs including the heart, stomach and lungs have also been reported to synthesize and secrete AGP (Fournier et al., 2000). The basal level of AGP is maintained at approximately 20μmol/L in healthy individuals. The biological role of AGP is not completely understood, albeit numerous *in vitro* and *in vivo* activities such as inhibition of platelet aggregation, modulation of lymphocyte proliferation and drug transport have been reported (Bories et al., 1990; Pos et al., 1990; Gambacorti-Passerini et al.,2003; Hochepiedet al.,2003;).

Similar to HSA, the binding and transportation of a range of endogenous and exogenous compounds is one of the major physiological functions of AGP (Otagiri et

al., 2009). One of the main roles of AGP is the transportation of endogenous ligands like lysophospholipids and biliverdin, while it may also function as a transporter for anticancer and antibiotic drug candidates (Azad et al., 2012). Therefore, drug binding to AGP is an important in terms of the accurate understanding of the pharmacokinetics of drugs, especially during acute phase conditions. Drug-binding specificity and pharmacokinetic properties of AGP were under investigation using various biophysical and biochemical analytical methods such as spectrophotometry and protein engineering for the past twenty years. There are few studies showed the structure of the AGP (variant A) and its complex with drugs (Nishi et al., 2011).

1.2.A. The structure of AGP

It consists of the single polypeptide chain (183 amino acids) in which 21 positions of the sequence contains two alternative amino acids. The polypeptide chain of AGP attached to five asparaginyl linked glycans (Yoshima et al., 1981; Fournier et al., 2000; Katori et al., 2011). AGP is composed of (i) different linkages of sugars (in particular sialic acid to galactose) and (ii) a very few number of amino acid substitutions were found in the sequence. Several analysis suggesting that polymorphism is the one of the main reason for heterogeneity in its amino acid sequences (Schmid et al., 1977; Dente et al., 1987; Imamura et al., 2002).

1.2.B. Function of AGP

Unlike HSA, glycoprotein AGP has no definitive function but some documents have been reported saying that it has immunosuppressive properties along with that activation of dampening neutrophil and stimulation of lymphocyte, these functions may be correlating with its glycosylation properties (Fig.1.6). Also, it has been described that AGP has angiogenic properties (Chiu et al., 1977; Costello et al., 1984; Heegaard et al., 2013). It has invariably been described as a positive acute phase protein in all species studied, including human, cow, mouse, dog, cat, rabbit, rat, and chicken (Hochepied et al., 2003; Heegaard et al., 2013). This phenomenon, involving several other proteins, is referred as the acute phase reaction and the affected proteins are called acute phase reactants. This phenomenon is common to all mammals so far investigated, even though the set of acute phase reactants are not identical in the various species. The molecular mechanism of this phenomenon is unknown. However, growing evidence that the hepatocyte responds to acute phase signals produced by

macrophages by increasing the rate of transcription of the acute phase genes and the stability of the corresponding mRNAs (Ritchie & Fuller 1983; Dente et al., 1987).

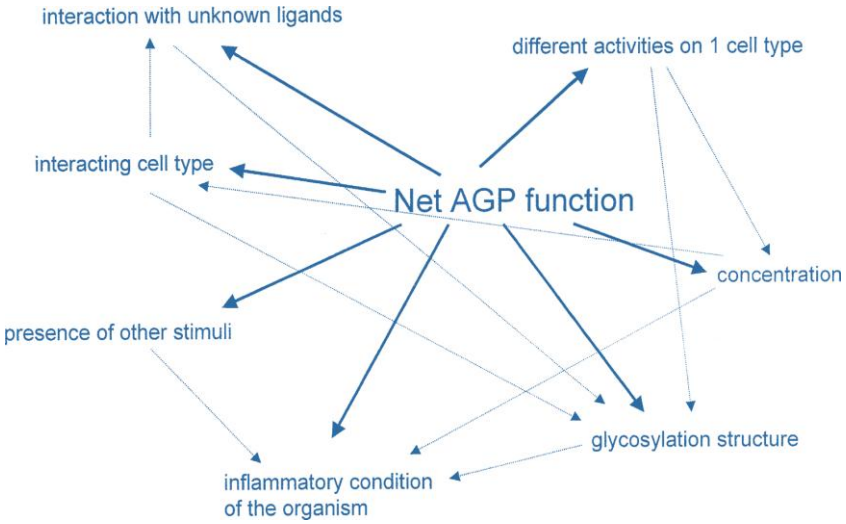

Fig.1.6. Chart representing various functions of AGP (Hochepied T et al., 2003)

1.2.C. Drug Binding to AGP

AGP has the ability to bind and transport several basic and neutral drugs of endogenous and exogenous origin. AGP belongs to the lipocalin family, bind to the small lipophilic/cationic molecules (Kremer et al., 1988; Heegaard et al., 2013). AGP has only one drug-binding site, thus it is different from other albumin proteins. In the case of AGP, the drug-binding properties are saturable and displaceable (Huang & Ung 2013). Although the binding activities of many racemic drugs to AGP are known to be stereoselective, the effect of the AGP subfractions has not been fully elucidated (Shen et al., 2013).

Since HSA and AGP are negative and positive acute-phase proteins respectively, binding studies with both HSA and AGP play a crucial role in deciding the pharmacokinetic behavior of the bioactive compounds in various pathological and inflammatory states. Therefore, binding studies of bioactive compounds with AGP along with HSA is pivotal in terms of the accurate understanding of pharmacokinetics properties, especially during normal conditions and in acute phase conditions.

1.3. Dendritic core-multishell Nanocarriers

Core-multishell (CMS) nanocarriers with hyperbranched polyglycerol-amine (hPG) and hyperbranched polyester-ester (hPE) as a core in the structure of the nanocarriers raised the question of the biocompatibility of the polymers. PEIs have been widely used in the environment for more than 40 years and no sign of acute or chronic toxicity has been reported. Nevertheless, the cytotoxicity data showed PEI toxicity on the cellular level. This toxicity might be a consequence of the endo/lysosomal enzyme release into the cytoplasm, consecutive to feeding a cell with membrane-disrupting particles (Boussif et al., 1995; Ihm et al., 2003) This should be considered as an important drawback for the use of PEI for *in vivo* applications. The PEI toxicity can be reduced up to 100 times by functionalization with poly(ethylene glycol) chains(Petersen et al., 2002; Merdan et al., 2005; Shuai et al., 2005). Nevertheless, hPG-amine and hPES-ester core nanocarriers demonstrate that changes of the amino groups on the periphery of nanocarrier with PEG changes chains reduces the toxicity and increases the biocompatibility of resulting the polymer as PEG is water soluble, nonimmunogenic and nontoxic with other substrates produces conjugates that combine the properties of both the polymer nad substrate.However, conjugates formation can alter the binding affinity of hPG-amine and hPES-ester core nanocarriers to drugs protein in general. Thus, the universal abilities of the new type of CMS nanocarrier systems were assumed to remain unchanged, although it was still questionable if the CMS nanocarriers and its interaction with HSA. Therefore, it was present interest to me for carrying study the binding mechanism of CMS nanocarriers with HSA in aqueous solutions in order to examine the properties of nanocarrier on conformation, and secondary structure. I have studied out the interaction of the different nanocarriers with HSA (Chapter 6).1.4. Bioactive compounds under study: properties and functions

In this study I have chosen selected bioactive compounds; Apocynin (APO), Andrographolide (ANDR), Bacosine (BAC), Chebulinic acid (CHN), Chebulagic acid(CHG), 7-Hydroxy coumarin derivatives (7-HC-1, 7HC-2 and 7HC-3), Corilagin (COR), Embelin (EMB), L-dopa (LDA), Piperine (PIP) and Novel 8-substituted Coumarin derivatives (UMB-1 and UMB-2). All are phytochemicals except 7-Hydroxy coumarin derivatives and novel 8-substituted coumarin derivatives.

There are several major groups of phytochemicals like phytoestrogens,

terpenoids, carotenoids, limonoids, phytosterols, terpenoids, phytosterols glucosinolates, polyphenols, flavonoids, isoflavonoids anthocyanidins, phytoestrogens, and anthocyanidins. These phytochemicals, in combination or alone, have the remarkable therapeutic potential for curing several chronic diseases. They play specific pharmacological effects in human health. In our study I selected bioactive compounds which are having potent biological functions; details of structures and specific biological functions of bioactive compounds under study are mentioned below.

1.4. BOACTIVE COMPOUNDS: PROPERTIES AND FUNCTIONS

1. Artemisinin (ART)

Structure

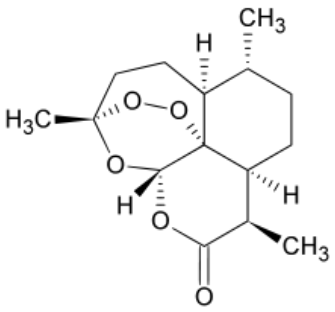

Empirical formula: $C_{15}H_{22}O_5$ **Molecular weight: 282.33**

Function

Artemisinin, a sesquiterpenoid endoperoxide, was derived from *Artemisia annua* L, It has various pharmacological effects such as anti-malaria, anti-tumor, antibacterial, anti-fetation, anti-fibrosis, heat-clearing, detoxicating and immune function regulation. However, studies had shown that artemisinin is toxic to neuronal and glial cells in culture (et al., 1994; Jeffrey et al., 1995).

2.Ar-tumarone (AT)

Structure

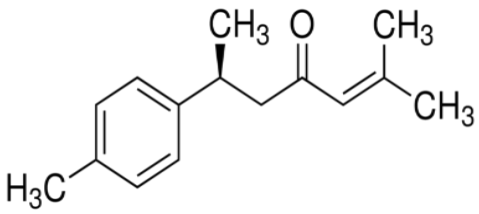

Empirical formula: $C_{15}H_{20}O$ **Molecular weight: 216.3**

Function

AT is isolated from *Curcuma longa* here are several data in the literature indicating a great variety of pharmacological activities of *Curcuma longa L. (Zingiberaceae)*, which exhibits anti-inflammatory, anti-human immunodeficiency virus, anti-bacteria, antioxidant effects and nematocidal activities. Other extracts of this plant have been showing potency too. In *in vitro*, AT exhibit antiparasitic, antispasmodic, anti-inflammatory and gastrointestinal effects and also inhibits carcinogenesis and cancer growth (Araujo & Leon 2001).

3.Apocynin (APO)

Structure

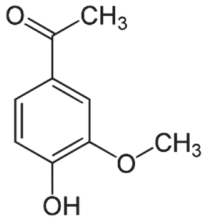

Empirical formula: $C_9H_{10}O_3$ **Molecular weight: 166.1**

Function

Apocynin, also known as acetovanillone, is a natural organic compound which structurally related to vanillin, having several pharmacological properties. Apocynin possesses anti-arthritic, anti-asthmatic properties and it is also used in the treatment of atherosclerosis (Peters et al., 2001; Van den Worm et al., 2001).

4. Andrographolide (ANDR)

Structure

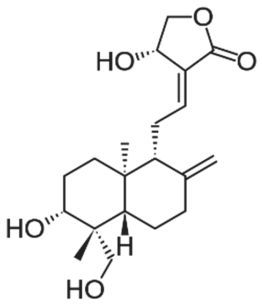

Empirical formula: $C_{20}H_{30}O_5$ **Molecular weight: 350.45**

Function

Andrographolide is a diterpenoid an important phytocompound from the *Andrographis paniculate* which is a medical plant (Chakravarti & Chakravarti et al.,1951). Andrographolide has been reported to have a wide range of biological activities, such as those that are anti-inflammatory (Shen et al., 2002), antiallergic (Xia et al., 2004), antiplatelet aggregation (Amroyan et al.,1999), hepatoprotective (Trivedi et al., 2007), and anti-HIV. In biological systems, ANDR has an ability to interact with many inter- and intracellular constituents as a bipolar compound, thus trigger in various biological responses.

5.Bacosine (BAC)

Structure

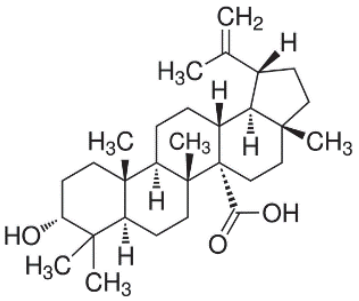

Empirical formula: $C_{30}H_{48}O_6$ **Molecular weight: 456.70**

Function

Bacosine, a triterpene isolated from the ethyl acetate fraction of the ethanolic extract of Bacopamonnieri. It has a significant effect on the decrease in the blood glucose level (Ghosh et al., 2011; Gonzalez-Burgos & Gomez-Serranillos 2012).

6. Corilagin (COR)

Structure

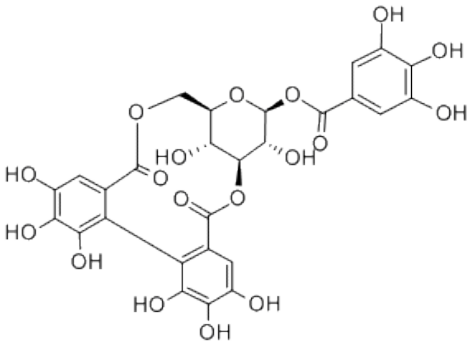

Empirical formula: $C_{27}H_{24}O_{18}$ **Molecular weight: 636.46**

Function

It has been shown to exhibit versatile medicinal activities. There has been little research on the effect of Corilagin on cancer and mostly focused on its use as an antiviral, hypolipemic, hypotensive and anticoagulation agent (Liu et al.,1999). Some pharmacological activities of corilagin have already been described, such as antiatherogenic (Duan et al., 2005), antioxidant (Chen & Chen 2011), hepatoprotective (Kinoshita et al., 2007) anti-tumor (Hau et al., 2010).

7. Chebulinic acid (CHN)

Structure

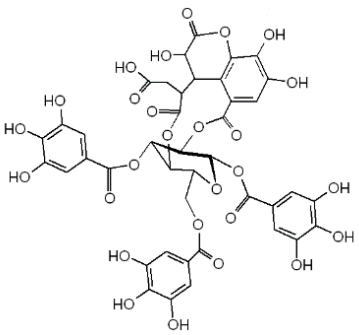

Empirical formula: $C_{41}H_{32}O_{27}$ **Molecular weight: 956.67**

8. Chebulagic acid (CHG)

Structure

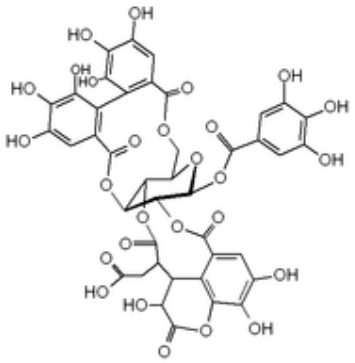

Empirical formula: $C_{41}H_{30}O_{27}$ **Molecular weight: 954.66**

Function of CHN and CHG

Chebulinic acid (CHN) is an ellagitannin found in the seeds of Euphoria longana, in the leaves of *Terminalia macroptera* (Klika et al., 2004). This indicates that the above compounds will be used for controlling many diseases like cancer, diabetes, HIV etc. Chebulagic acid (CHG), is a benzopyran tannin. It is found in the plant's species of *Terminnalia chebula* and *Teriminalia citrine*. These compounds are natural anti-oxidant, showed potent anti-inflammatory effects in LPS-stimulated RAW 264.7, a mouse macrophage cell line (Reddy & Reddanna 2009) and found to be immunosuppressive, alpha-glucosidase inhibitor and hepatoprotective (Kinoshita et al., 2007; Sasidharan et al., 2012). Reactive oxygen species are produced in the cells by cellular metabolism and it is known that chebulinic acid and chebulagic acid protect the formation of ROS.

9. 14-Deoxy-11, 12-didehydroandrographolide

Structure

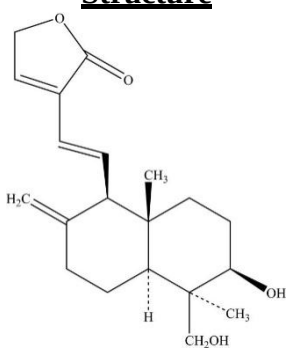

Empirical formula: $C_{20}H_{28}O_4$ **Molecular weight: 332.439**

Function

Deoxydidehydroandrographolide is derivative of andrographolide is a labdane diterpenoid that is the main bioactive component of the medicinal plant *Andrographis paniculate* (Chakravarti & Chakravarti 1951). A recent study demonstrated that *A.paniculate* polysaccharides combined with andrographolide and andrographolide can ease their cover of diabetic nephropathy (Xu et al., 2012).

10. 1,9-Dideoxyforskolin

Structure

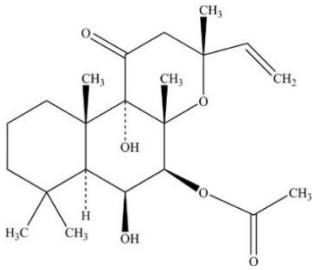

Empirical formula: $C_{22}H_{34}O_6$ **Molecular weight: 394.51**

Function

Dideoxyforskolin also called Coleonol is a labdane diterpene that is produced by the Indian Coleus plant (*Coleusforskohlii*). Forskolin provides a route to inhibition of colon cancer cell growth and survival (McEwan et al., 2007). It helps in controlling the underlying cause of glaucoma. Reduce urinary tract infections and enhance the ability of antibiotics to kill bacteria that normally survives (Abraham et al., 2008). In addition to these functions, various experimental studies are underway in using dideoxy forskolin as an adjuvant treatment for diseases such as Parkinson's and/or nerve damage caused by trauma/accident.

11. Embelin (EMB)

Structures

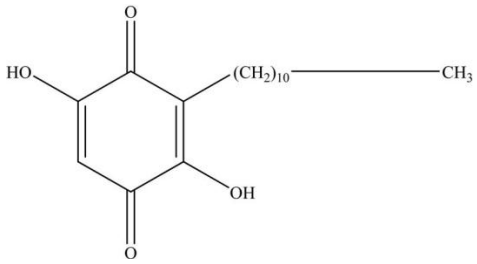

Empirical formula: $C_{17}H_{26}O_4$ **Molecular weight: 294.390**

Function

Embelin is a novel cell-permeable inhibitor of XIAP (X-linked inhibitor of apoptosis) which was discovered by screening a library of natural products derived from traditional Chinese medicine (Nikolovska-Coleska et al., 2004).

12. L-dopa (LDA)

Structure

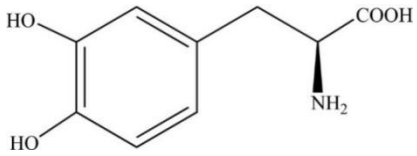

Empirical formula: $C_9H_{11}NO_4$ **Molecular weight: 197.190**

Function

L-Dopa is found in *Mucuna pruriens*, *Tamarindus indica*, *Sesbania bispinosa*, *Acacia leucophloea*, *Canavalia gladiate* (Gautam et al., 2012). L-dopa is a precursor to the neurotransmitters of dopamine, norepinephrine (noradrenaline), and epinephrine (adrenaline) collectively known as catecholamines. Apparently, it crosses the protective blood–brain barrier, whereas dopamine could not do this function. In the treatment of Parkinson's disease, the L-dopa is used to increase the dopamine concentration (Hauser & Zesiewicz 1999) and dopamine-responsive dystonia.

13. Menthol (MEL)

Structure

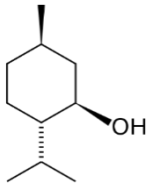

Empirical formula: $C_{10}H_{20}O$ **Molecular weight: 156.2**

Function

Menthol, a natural product of the peppermint plant such as corn mint, peppermint or other mint oils (Lamiaceae), is a monoterpene which is widely used as a natural product in cosmetics, a flavoring agent, and as an intermediate in the production of other compounds. The cooling characteristic of Menthol is because of the activation of

sensory neurons i.e. transient receptor potential (TRP) channels, in particular, transient receptor potential melastatin family member 8 (TRPM8) and transient receptor potential subfamily A, member 1 (TRPA1). Menthol binds to TRPM8 receptors in the skin and activates sodium and calcium transporter channels, therefore, depolarization resulting in the generation of action potential. and followed by inducing cold response signals at the application site. Besides this, menthol exhibits anti-cancer as well as anti-inflammatory capabilities and it has synergistic effects by acting on GABA receptors and also activating sodium ion channels which induce analgesia (Farco & Grundmann 2013).

14. Piperine (PIP)

Structure

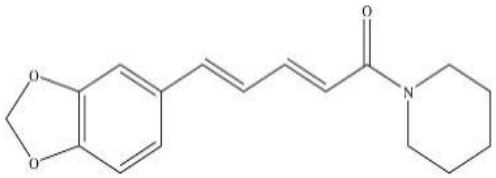

Empirical formula: $C_{17}H_{19}NO_3$ **Molecular weight: 285.34**

Function

Piperine is a main alkaloid phytochemical found in plants from the family of Piperaceae. This compound can be obtained from the fruits of *Piper nigrum*, also both in black and long pepper grains which are *Piper nigrum* and *Piper longum L*. Further piperine is one of the major constituents of *Sitopaladi churna*. The biological properties of piperine have been extensively studied (Atal et al., 1981; Atal et al., 1985). It was liable and found to possess central nervous system, depressant properties (Pei et al., 1983; Lee et al., 1984). In general, piperine is found to act on anti-mutagenic and anti-tumour properties (Srinivasan et al., 2007). Also, it has been demonstrated in *in vitro* studies to protect against oxidative damage by inhibiting or quenching free radicals and reactive oxygen species. Further, piperine is used successfully thwart morphine-induced respiratory depression in experimental animal models (Singh et al., 1973). Altogether, piperine is helpful in reducing inflammation, improving digestion and revealing pain and asthma. Also, it has been found to have immune-modulatory, anti-oxidant, anti-asthmatic, anti-carcinogenic, anti-inflammatory and antiulcer (Bang et al., 2009).

15. Psoralen (PSO)

Structure

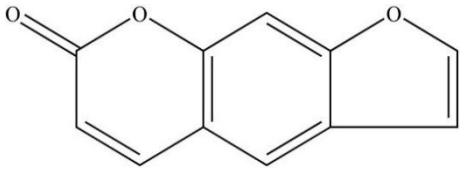

Empirical formula: $C_{11}H_6O_3$ **Molecular weight: 186.17**

Function

Psoralen (PSO) is a main active ingredient extracted from the fruits of *Psoralea corylifolia* L (Tang et al., 2011). and has been used as a drug for the treatment of alopecia areata, vitiligo, and tinea (Spiegel & Magistrato 2006), etc. It was also reported that PSO exerts other biological activities, such as preventing the proliferation of mucoepidermoid carcinoma, mammary cancer cells and bladder carcinoma *in vitro* (Leite et al., 2004). In recent years, many new psoralen derivatives were isolated and identified from different plants, and some of them were found to possess interesting biological activities (Zhou et al., 2014).

16. Pterostilbene

Structure

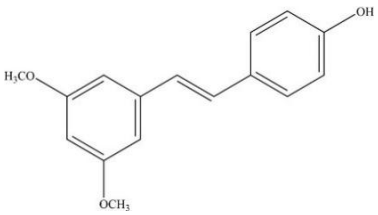

Empirical formula: $C_{16}H_{16}O_3$ **Molecular weight: 256.301**

Function

Pterostilbene is a natural analog of resveratrol. It possesses a variety of biological activities and has been used as anticancer, antioxidant, anti-inflammatory agents (Remsberg et al., 2008). Numerous publications reported the therapeutic potential of resveratrol in various ailments, including cancer, heart, diabetes, stroke and Alzheimer disease (Baur & Sinclair 2006). Pterostilbene may be effective in correcting dyslipidemia that leads to atherosclerosis and coronary disease, as it can increase the HDL/LDL cholesterol ratio (Schmidlin et al., 2008).

17. Rosmarinic acid

Structure

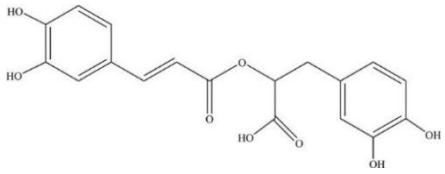

Empirical formula: $C_{18}H_{16}O_8$ **Molecular weight: 360.32**

Function

Rosmarinic acid occurs throughout the Boraginaceae family, whereas within the Lamiaceae it is restricted to the subfamily Nepetoideae (Litvinenko et al., 1975). Main activities are astringent, antioxidative, anti-inflammatory, antimutagen, antibacterial and antiviral (Parnham & Kesselring 1985) Phenolic compounds like rosmarinic acid can provide protection against cancer and rosmarinic acid contributes to the antioxidant activity of plants used in the cosmetic industry, such as *Rosmarinus officinalis* and *Sanicula europaea (Botanicals 1999).*

18. Stigmasterol

Structure

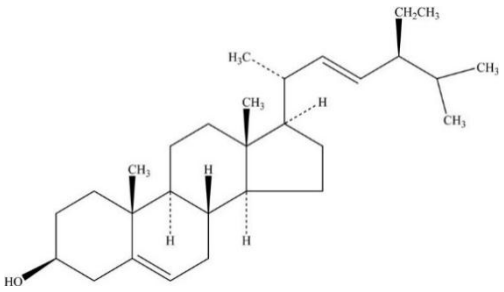

Empirical formula: $C_{29}H_{48}O$ **Molecular weight: 412.698**

Function

Stigmasterol an unsaturated plant sterol occurring in the plant fats of soybeans rape seeds and Calabar and a number of medicinal herbs, in *Mirabilis jalapa* (Siddiqui et al., 1990). Stigmasterol is also found in various vegetables, legumes, nuts seeds and unpasteurized milk. Edible oils contain higher amount than vegetables (Jun-Hua et al., 2008). Stigmasterol is used as a precursor in the manufacture of semisynthetic progesterone which is used to rebuild the mechanism related to estrogen effects; as well

it acts as an intermediate in the synthesis of androgens and corticoids. It is also used as a precursor of vitamin D_3 (Sundararaman & Djerassi 1977; Kametani & Furuyama 1987). Stigmasterol may be useful in the prevention of certain types of cancers like ovarian, prostate, breast and colon cancers, It also possesses potent antioxidant, hypoglycemic and thyroid inhibiting properties (Panda et al., 2009).Stigmasterol has a potential anti-osteoarthritic and anti-inflammatory properties (Gabay et al., 2010). It is a component of soy-derived lipids, has antagonist activity against a central NR involved in the adaptive response to Bile acid-mediated hepatotoxicity, FXR (Carter et al., 2007).

19. 6-Shagoal

Structure

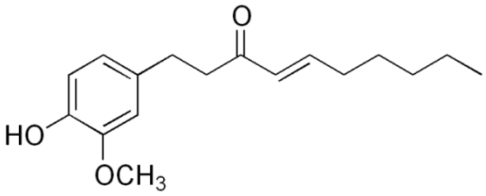

Empirical formula: $C_{17}H_{24}O_3$ **Molecular weight: 276.3**

Function

Several studies suggest that 6-Shogaol, considerable pharmacologic effects which include anti-cancer, anti-inflammatory, antioxidant as well as antiemetic properties. Also, it was reported that it could induce cell death or apoptosis in a variety of cancer cells such as human lung cancer, colorectal carcinoma, hepatocarcinoma, ovarian cancer and breast cancer cells (Pan et al., 2008).

20. Novel 8-substituted coumarin derivatives (Umb-1 and Umb-2)

Structure

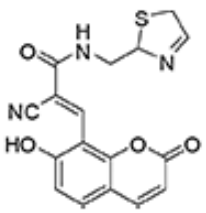	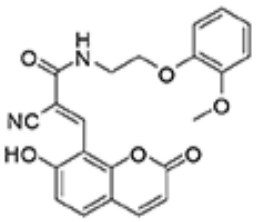
Umb-1 Molecular weight: 355.3	Umb-2 Molecular weight: 406.9

Function

Coumarins with phenolic hydroxyl groups have the capability to scavenge reactive oxygen species and thus prevent the formation of 5-hydroxyicosatetraenoic acid (5-HETE) and hydroxy heptadecatrienoic acid (HHT) in the arachidonic pathway of inflammation suppression (Dighe et al., 2010).Coumarin and its derivatives like 7-hydroxy coumarin and 7-hydroxy-4-methyl coumarin occur in nature especially in plant species in high concentrations, they exhibit numerous biological activities such as lipid lowering , anti-hepatitis C, antiparkinson and anti-cancer activities like novel coumarin substances that has been reported (Madhavan et al., 2003; Santana et al., 2006; Donnelly et al., 2008; Mazzei et al., 2008; Sashidhara et al., 2010).

21. 7-Hydroxy Coumarin Derivatives (7HC-1, 7HC-2, and 7HC-3)

Structure

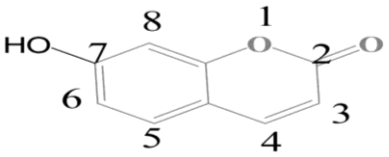

7-hydroxy Coumarin
(umbelliferone)

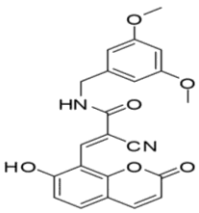

7HC-1

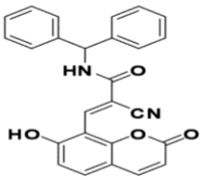

7HC-2

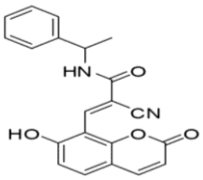

7HC-3

Function

Coumarin is categorized as a member of benzopyrone family compounds, which consists of a benzene ring joined to pyrone ring (Ojala et al., 2001). Coumarins comprise a very large class of compounds found throughout the plant kingdom (Egan et al., 1990; Finn et al., 2002). Most coumarins occur in higher plants with the richest source being the Rutaceae and Umbelliferae. Many coumarins and their derivatives exert, anti-tumor, (Lacy & O'Kennedy 2004; Riveiro et al., 2010) anti-viral, anti-coagulate, anti-inflammatory, anti-oxidant and vasorelaxant,(Campos-Toimil et al.,2002; Kontogiorgis & Hadjipavlou-Litina 2003) effects as well as anti-microbial,(Gormley et al.,1996; Ostrov et al., 2007) and enzyme inhibition properties (Kabeya et al., 2007).

Mentioning the importance of plasma proteins, understanding of the specific binding site of proteins is of potential importance in the field of drug delivery research, an example in the investigation of drug–drug interactions. Co-administered drugs may exert a competition for the binding to the same albumin binding site, the free fraction of the low-affinity drug is enhanced. Similarly, competition for a certain binding site may occur between drugs and endogenous substances (Tesseromatis & Alevizou 2008). I have selected these bioactive compounds because they all have a potent role in protecting many diseases; here the chosen bioactive compounds are mostly phytochemicals. As we all know that phytochemicals are having fewer side effects, and known as traditional medicine in India. Since HSA is an important protein as a transporter and maintains the efficacy of the drug but binding of all these compounds has not been understood well. In present study, I analyzed the cytotoxic activity of these selected bioactive compounds on different cell lines like hepatocellular carcinoma (HepG2), Michigan Cancer Foundation (MCF-7),cervical cancer (HeLa), mouse leukaemic monocyte macrophage cell line (Raw 264.7) and adenocarcinoma human alveolar basal epithelial cells (A549) and its binding, conformational, docking, molecular simulation studies with HSA. Also, comparative binding studies were carried out with another important plasma protein, AGP. Taking these into consideration, I have framed four major objectives for my work.

OBJECTIVES

1. **Cytotoxic and binding studies of bioactive compounds with human serum albumin.**

   1. A. Cytotoxic studies with different cell lines.

   1. B. Unraveling the binding mechanism using fluorescence spectroscopy and surface plasmon resonance.

   1. C. Study of protein conformational changes of plasma protein with bioactive compounds.

2. ***In silico* binding studies of human serum albumin with bioactive compounds.**

   2. A. Binding studies using in silico docking.

   2. B. Stability of HSA-Drug conformer by using molecular dynamics simulation.

3. **Comparative binding studies of bioactive compounds with plasma proteins.**

4. **Interaction studies of core-multi shell nanocarriers with human serum albumin.**

CHAPTER 2

MATERIALS AND METHODOLOGY

2. MATERIALS AND METHODS

2.1. Cell Response Assay

For different cell line like (HepG2, MCF-7, HeLa, Raw 264.7 mouse macrophages and A549) was purchased from National Center for Cell Science (NCCS), Pune, India. Different cells were grown at 37 ^{o}C in a humidified incubator under 5% CO_2/95% air in Dulbecco's Modified Eagle's Medium (DMEM) supplemented with 10% fetal bovine serum (FBS), 200 IU/ml penicillin, 200µg/ml of streptomycin, and 1mM sodium pyruvate. Culture medium was replaced every next day. After the cells were confluency, the cells were subcultured followed by trypsinization and cell response assay was assessed by the MTT [3-(4,5-Dimethylthiazol-2-yl)-2,5-Diphenyltetrazolium Bromide staining method (Mosmann et al., 1983). Cells were harvested from four to five-day-old cultures and were seeded in 96-well plates at the density of $5x10^3$ cells. Cell lines were treated with selected bioactive compounds in increasing concentrations of 20, 40, 60, 80, and 100 µM for 48 h in a final volume of 100 µL. At an optical density of 570nm cell response was calculated on a microplate reader (µ Quant Bio-tek Instruments, Inc.). Three independent experiments were carried in triplicates and mean ± SE (*n*=4) was calculated and reported as the cell response (%) *vs* concentration (µM).

2.2. Cell Viability Assays

Cytotoxicity of the nanocarriers was evaluated through impedance measurement with an xCELLigence real-time cell analyzer (RTCA) from Roche Applied Science (Mannheim, Germany). In short, A549 cells (adenocarcinoma human alveolar basal epithelial cells) were cultured in Dulbecco's Modified Eagle Medium supplemented with 10% fetal bovine serum (Bio Chrom KG, Berlin, Germany), 100 U mL^{-1} penicillin, and 100 µg mL^{-1} streptomycin at 37 °C, 5% CO_2, and 99% humidity and seeded in a 96-well E-plate (10000 cells per well). The plate was placed in the RTCA and impedance was measured at least every 15 minutes. The plate was removed from the RTCA after approximately 24 h and the nanocarriers were added in various concentrations. Here, doxorubicin, piperine, and untreated cells served as a control. The plate was placed back in the RTCA and the real-time impedance measurement was

continued for another 48 h.

2.3. The Evaluation of Anticancer Activity by Apoptosis

The programmed cell death i.e apoptosis was measured by using Annexin V-FITC detection Kit (Sigma cat no: APOAF). HeLa cells were treated with 29.1µM of embelin for 24h, after that cells were washed twice with PBS and resuspended in binding buffer (100mM HEPES, pH 7.5) provided by Kit and stained with 5 µl of Annexin V-FITC, staining precedes the loss of membrane integrity which accompanies the latest stages of cell death resulting from either apoptotic or necrotic processes. It conjugates with a fluorescent isothiocyanate (FITC) to label phospholipid phosphatidylserine (PS) sites on the membrane surface and 10 µl of Propidium Iodide (PI) for 10 min to label the cellular DNA (Zhang et al., 1997). Flow cytometry (BD LSR Fortessa) was done to determine the percent apoptosis induced by embelin.

2.4. Cellular Uptake of CMS-ICC Dye Conjugates

The cellular uptake of ICC-labeled nanocarriers (cms-mPEG350) was monitored by confocal laser scanning microscopy (cLSM) and flow cytometry. For cLSM 50000 A549 cells were seeded on 9 mm glass coverslips in each well of a 24-well plate and cultured for 24 h before adding the nanocarriers for 5 and 24 hours, respectively. Cells were grown at 37 °C, 5% CO2, and 99% humidity and maintained in Dulbecco's Modified Eagle Medium (D-MEM) supplemented with 10% fetal bovine serum (BioChrom KG, Berlin, Germany), 100 U mL^{-1} penicillin, and 100 µg mL^{-1} streptomycin. For a qualitative analysis by cLSM, the cells were washed 3 times with PBS and fixed with 4% paraformaldehyde (PFA) for 20 min. Afterward, cell nuclei were stained with 4′,6-diamidino-2-phenylindole (DAPI), cell light lyso and cell light endo. Cells were observed and imaged using a confocal laser scanning microscope (Leica DMI6000CSB stand) and Leica LAS AF software. For flow cytometry, 150000 A549 cells were seeded in each well of a 24-well plate and cultured for 24 h before adding the nanocarriers at 5, and 24 hours, respectively. Cells were grown as described above. For a qualitative analysis by flow cytometry, the cells were washed 3 times with PBS and detached by trypsin. The detached cells were then transferred to a flow cytometry tube and centrifuged at 138 g for 5 min. Supernatants were discarded and cells were fixed with 4% PFA for 10 min at 4 °C. The cells were centrifuged at 138g

for 5 min to remove the PFA. The supernatants were discarded and the cells were re-suspended in 100 µl PBS supplemented with 1% FCS and 0.1% sodium azide. The fluorescence of the cells was measured in an FACScantor (Becton Dickinson, Heidelberg, Germany) and the analysis was done with Flowing Software 2.0.

2.5. Preparation of stock solutions

Fat-free human serum albumin and α-1-glycoprotein were dissolved in PBS (1.5mM) of 0.1mM phosphate buffer pH 7.4. The purity of plasma proteins (HSA and AGP) was then confirmed by SDS-PAGE using12% gel (Laemmli et al., 1970). The SDS-PAGE results showed no contaminations thus the HSA/AGP are in pure (Fig 2.1). Non-fluorescent selected bioactive compounds were prepared by dissolving (2 mM) in 20:80 (ethanol: water mixture). It is noted that absorption spectra of HSA/AGP, its structure does not affect due to the presence of 20% ethanol. In order to find out the optimum physiological conditions, I have suspended the HSA/AGP in different pH and measure the maximum absorption. At pH 7.4 the maximum absorption was observed, thus, for entire parameters I have used pH 7.4 of 0.1 mM phosphate buffer. Also optimized the time of bioactive compounds binding to HSA/AGP by absorption, fluorescence emission, and circular dichroism (CD) spectra and we found that 5 min is the maximum binding time. Thus, we have fixed the incubation of bioactive compounds with HSA/AGP for 5min in all parameters. All other chemicals including proteins were bought from Sigma-Aldrich.

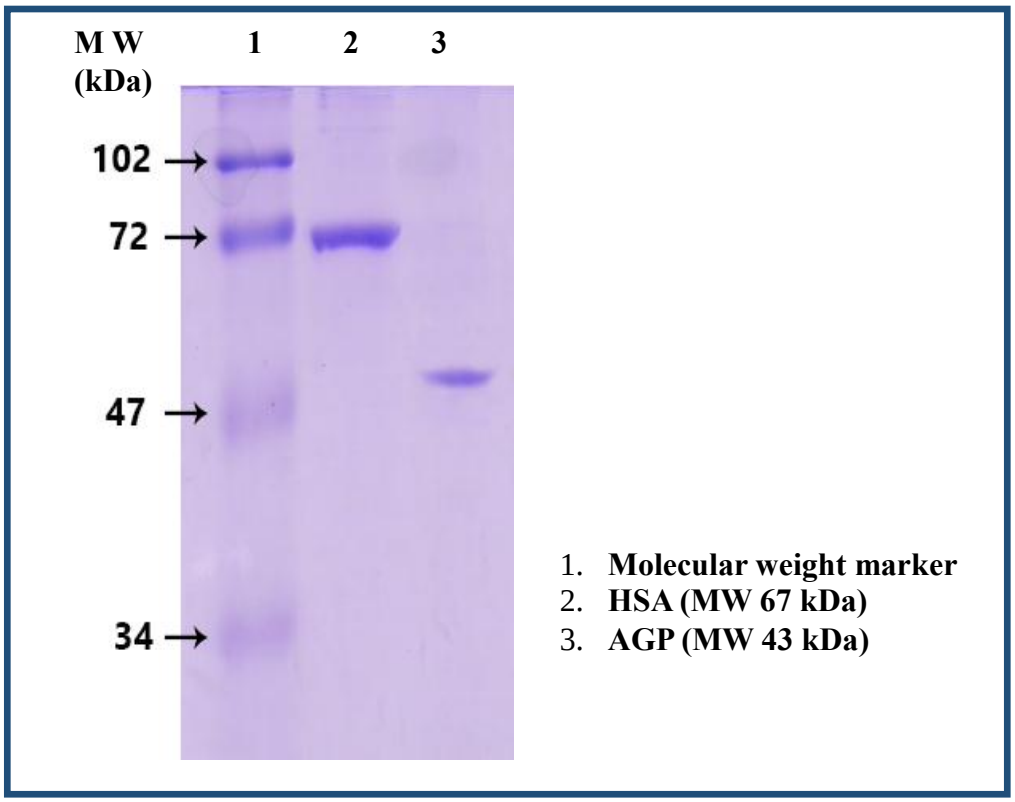

Fig. 2.1. HSA and AGP proteins were separated using 12% SDS-PAGE. Equal protein concentration (30µg) was loaded in each lane. Lane 1) Molecular weight marker; lane 2) HSA sample (molecular weight 67 kDa); lane 3) AGP sample (molecular weight 43 kDa).

2.6. Fluorescence Spectroscopy

The fluorescence emission spectra were recorded on Perkin Elmer LS55 fluorescence spectrometer from 300 to 500 nm, with excitation at 285nm, and slit width of 5.0 nm for both emission and excitation (Subramanyam et al., 2009a & b). The final concentrations of the bioactive compounds was diluted to 0.001, 0.002, 0.003, 0.004, 0.005, 0.006, 0.007, 0.008 and 0.009 mM with 0.1 mM phosphate buffer pH (7.4) and the protein concentration was fixed 0.001 mM. The binding constant was calculated using the maximum fluorescence value at 360 and 340 nm. All experiments were measured in triplicate and spectra which are identical were presented.

2.6a. Displacement Experiment

The concentration of HSA and the site-specific marker were maintained at a constant concentration of 1 µM, bioactive compounds were titrated with increased in concentration from 0 to 9µM. The excitation wavelength for site-specific makers

lidocaine (IB specific marker) in which lidocaine has a unique binding site on the subdomain IB of HSA (Hein et al., 2010), phenylbutazone (a site I specific marker) and ibuprofen (site II specific marker) with HSA was 285 nm.

2.7. Surface Plasmon Resonance (SPR) Measurements

Experiments performed by using Biacore X100 device (GE Healthcare, Uppsala, Sweden). A carboxymethylated dextran chip (CM5-Chip, GE Healthcare, Uppsala, Sweden) was fully coupled on Fc2 with HSA or AGP (GE Healthcare) using amine coupling strategy. Response level reached ~14650 RU for HSA and ~7803 RU for AGP on Fc2. Non-binding Fc1 was mock treated. Therefore, ANDR was diluted in running buffer (PBS + 5% DMSO) at concentrations of 5 µM, 25 µM, 50 µM, 200 µM and 1000 µM. After solvent correction, sensorgrams were analyzed by plotting the binding signal at the end of injecting against analyte concentration. Isotherm result was fitted to obtain K_A values using the steady state model.

2.7a. Solvent refractive index correction

Since DMSO has a high refractive index, a solvent correction procedure was performed to account for the small variations of DMSO percentage between samples and running buffer (Frostell-Karlsson et al., 2000). PBS/DMSO mixtures ranging from 4.5% to 5.8% (v/v) (pH 7.4), were injected over the active and reference flow cells and a calibration curve was obtained. This procedure is very important while working with small molecules–macromolecules interactions, especially when the ligand is immobilized at high density (5000 RU or more). In this experimental setup, the expected response has the same magnitude as, or lower magnitude than, the signal arising from refractive index mismatches, therefore including a correction protocol during the evaluation of the data becomes of great significance.

2.8. Electrospray Ionisation (ESI) Mass spectrometry (Q-TOF)

The ESI-Q-TOF-MS (Bruker Daltonics, Bremen, Germany) were used to record the positive ion mode mass spectra. In order to measure, the HSA concentration was reduced to 0.15nM and the embelin concentration to 5nM, free fatty HSA, and HSA-Embelin were prepared in 0.1% formic acid in water/acetonitrile (1:1(v/v)), with help of syringe pump (KD Scientifics Inc., Hilliston, MA) at 3µL/min the sample is

introduced into the mass spectrometer, the spray voltage maintained at around 4.5 kV. The time of flight (TOF) pressure was maintained at less than 3×10^{-7} Torr. Scanning was performed over an *m/z* range of 50-3000, with a collision energy of 10 eV. The data were averaged for about 2min and then smoothed using the Gaussian algorithm in Brucker Data Analysis 3.4 software program. The instrument was calibrated using ES tuning Mix (Agilent Technologies, Part No.G2421-60001), before injecting I have diluted it 1:60 (v/v) times with water and introduced through a divert valve jute before application of the sample.

2.9. Transmission Electron Microscopy

The size and external morphology of HSA and HSA-EMB complexes in aqueous solution at a pH 7.4 are determined by transmission electron microscopy (TEM) using FE1 Tecnai G^2S-Twin-200kv. The samples [HSA (0.001mM), HSA solution (0.001M) + EMB solution (0.002 mM)] were prepared freshly by placing one preparation drop (5–10 µL) on a carbon coated copper grids and the sample was dried completely, if there is any excess liquid present on the grid, a piece of filter paper is used to absorbed. Finally at room temperature a drop of 2% uranyl acetate negative stain was added before drying and further observed the structure of HSA and HSA plus EMB under TEM.

2.10. Atomic Force Microscopy (AFM)

To observe the morphological changes of free HSA and HSA-bioactive compounds corilagin and menthol, AFM experiment is carried out by NT-MDT solver scanning probe microscopy (Germany) equipment. The cantilever (0.3mm) have an Au high reflectivity coating, tip height 14-16 µm, force constant (5, 5 N/m) and the typical imaging resonance frequency was 140 kHz. The samples are imaged by AFM in noncontact mode. All of the samples were prepared as follows: (1) before washing with water, free HSA with 30 μL of 1.5μmol·L^{-1} HSA was added to a glass slide and incubated for 15 min at 288K; (2) HSA-bioactive compounds complexes with free HSA samples were prepared as defined in step (1) earlier to adding 20 μL of a 15 μmol·L^{-1} bioactive compounds solution, incubating for 15min, washing with water, drying under N_2 for 5 min, later samples are dried overnight for taking AFM image in air.

2.11. Circular Dichroism (CD) Spectroscopy

The Circular dichroism spectra of HSA and HSA- bioactive compounds were recorded with Jasco J-815 spectropolarimeter, using a quartz cell with a path length of 0.02 cm. Three scans were accumulated at a scan speed of 50 nm/min with data being collected every 1 nm from 190 to 300 nm. For CD studies, the final concentration of HSA was 0.001 mM and the concentration of bioactive compounds was taken as 0.001, 0.005 and 0.009 mM. The verification of the secondary structure determination was done using CDNN 2.1 version software (Subramanyam et al., 2009 a & b).

2.12. Molecular Modeling and Docking

Molecular docking is an important computational procedure performed to find out the exact binding site on the protein which fit geometrically and energetically by using Auto Dock 4.2.3 software, which has been used widely because it shows acceptable fee energy values relative to experimentally observed docking data (Gorelik & Goldblum 2008). The HSA (PDB Id: 1A06) and AGP (PDB Id: 3KQ0) crystal structure were obtained from the Brookhaven Protein Data Bank. Three-dimensional structure of selected bioactive compounds was built from the 2D structure and geometry was optimized by using Discovery studio 3.5 software. Molecular docking was performed using AutoDock (4.2.3) program. The PDB structures were optimized and used as input for AutoDock Tools. To find the binding site and types of interactions involved in the formation of HSA-corilagin complexes, docking was performed using the Lamarckian genetic algorithm implemented in AutoDock 4.2.3. We found this is to be the best performing docking method in terms of its ability to find the lowest energy and its structure prediction accuracy; it also incorporates ligand flexibility. AutoDock 4.2.3 takes water as a solvent by default, and polar hydrogens were added using the MGL tools interface (Morris et al., 1998; Morris et al., 2009). For each docking simulation of bioactive compounds, 30 different conformers were obtained from AutoDock, the conformer with the least binding free energy must match with experimental data for further analysis as reported earlier (Malleda et al., 2012).

2.13. Molecular Dynamics Simulation

Molecular dynamics simulation (MDS) is an important parameter to find out the stability of protein-drug complex. Here a 10000ps MD simulation of the complex was

carried out with the Gromacs v4.6.3 package with force field GROMOS96 43a1, was used for unliganded HSA, HSA-bioactive complexes (Berendsen et al., 1995; Wang et al., 2002). The initial conformation was chosen as the least binding energy docking conformation. The topology parameters of HSA were created by using the Gromacs program. The topology parameters of HSA-bioactive were built by the Dundee PRODRG2.5 server (Lindahl et al., 2001). Then the complex was immersed in a cubic box (7.335× 6.135 × 8.119 nm) of an extended simple point charge (SPC) water molecules, $15Na^+$ counter ions, and 43623 solvent atoms were added to each simulation box to maintain electroneutrality and to release conflicting contacts. Simulations were performed in the NPT (i.e., constant number of molecules, constant pressure and constant temperature) ensemble, at a temperature of 300 K and 1 bar respectively maintained using a Berendsen thermostat (Schuttelkopf & van Aalten 2004) with a coupling constant of 1.0 ps. Protein and water/ions were coupled independently. Pressure coupling used the Berendsen barostat with a coupling constant of 1.0 ps. Long-range electrostatic interactions were calculated using the particle mesh Ewald method (Berendsen et al., 1984) with a 10 Å cut-off. LINCS algorithm (Darden et al.,1993), was used to restrain bond lengths. Each system was energy minimized followed by a short 200 ps simulation during which the protein, and if present ligand, non-hydrogen atoms were harmonically restrained with a force constant of 1000 kJ/mol/Å2 (Hess et al., 1997; Kiselev et al., 2001; Sudhamalla et al., 2010; Yeggoni et al., 2014a).

2.14. Dynamics Light Scattering (DLS)

DLS experiments were performed by using Malvern Zetasizer Nano instrument Core-multi shell nanocarriers were dissolved in physiological pH 7.4, mixed by a Vortex shaker for 2 min, and then filtration was done by using a 0.45 µm RC syringe filter. 100 µL of the filtered solution was added to a disposable Plastibrand®micro cuvette (Brand GmbH + Co KG, Wertheim, Germany).Measurements were carried out at 25°C, four different runs were done at this temperature by equilibrating the system for120s. s

2.15. Encapsulation of Piperine in CMS Nanocarrier

Film uptake method was used to encapsulate the piperine (Fleige et al., 2012), solute ethanol was used to solubilize later at reduced pressure 40 °C is maintained to dry the

sample. A thin dry film was observed at the bottom of the vial. CMS nanocarrier was dissolved in distilled water at concentration 10 $mg.mL^{-1}$. The mixture was subject to a constant stirring at around RT for 24 h for1200 min^{-1} and afterward, excess piperine was filtrated using 0.45µmPTFEsyringefilter. The amount of piperine in the CMS nanocarriers solution was determined by UV-visible spectroscopy measurement relative to a piperine calibration curve.The obtained values from UV-visible spectroscopy measurements, piperine-loaded CMSnanocarriers. Loading capacity (LC) is calculated by using following equation.

$$\text{Loading capacity} = n(\text{encapsulated piperine}) / n(\text{nanocarrier}) \times 100$$

2.16. Stability and Release Experiments

The piperine-loaded pH-CMS nanocarriers and its stability were evaluated with UV-visible measurements. , Piperine -loaded pH-CMS nanocarrier solutions were kept at pH 7.4 and pH 5, at 37 °C for different time intervals. 1ml of medium containing 6mg of PIP @CMS 2 was placed in a dialysis bag (MWCO3.5kDa) and dialyzed it in falcon tube containing15ml of PBS.During this time, a sample of 5 mL volume was periodically removed and the same volume of PBS was replenished. The released amount of PIP was determined by UV-visible spectroscopy. The release studies were performed in triplicate and the error bar in the plot represent the standard deviation.

2.17. Peak Force Quantitative Nanomechanics (QNM)

Muscovite mica was used as a substrate, at a constant temperature, all the measurements were performed in a liquid state using fluid cell. Before sample deposition, the outer layers of the mica were cleaved with regular adhesive tape and 10-15µl solution of 15µl of Poly-L-lysine (Conc: 0.1mg/ml) was deposited and let it dry. Then 10µl of the sample was deposited and incubated for at least 20 minutes. Samples were kept to dry for a while. Afterward, the samples were mounted onto the AFM head and a fluid cell was assembled.For calibration, a well established thermal noise procedure is used for cantilever spring constant on a clean hard surface. Nanoscope analysis software is used for analyzing the particle size.

2.18. Isothermal calorimetry (ITC)

ITC experiments were carried out using MicroCalITC200, Northampton, MA, USA) at 298.15 K. Binding conditions were optimized for CMS-mPEG 2000. All the experiments were conducted at physiological pH 7.4. The thermodynamic and binding constants of binding(K_b) the number of binding sites per one molecule(n) and enthalpy of binding (ΔH_b) were computed from actual calorimetric data by a non-linear fitting using origin ITC software origin, using output of ΔH_b and K_b, the free energy of binding ΔG_b and its entropic component $-T\Delta S_b$ were simply determined using standard thermodynamics relationships(i:e ΔG_b= -RT ln K_b and $-T\Delta S_b$= ΔG_b-ΔH_b). The K_b was calculated from three independent experiments with multiple runs.

CHAPTER 3

CYTOTOXIC AND BINDING MECHANISM OF BIOACTIVE COMPOUNDS WITH HUMAN SERUM ALBUMIN

3. 1. Introduction

Protein-drug interactions play an important role in a variety of biological processes. The studies on this aspect may provide information of the structural features that determine the therapeutic effectiveness of drugs, and become an important research field in life sciences, chemistry, and clinical medicine. Depending on a specific drug's affinity for plasma protein, a proportion of the drug may become bound to plasma proteins, with the remainder being unbound. If the protein binding is reversible, then a chemical equilibrium will exist between the bound and unbound states, such that:

$$\text{Protein} + \text{Drug} \rightleftharpoons \text{Protein-Drug Complex}$$

Protein binding can influence the drug's biological half-life in the body. There are several mechanisms by which drugs may interact, but most of them can be categorized as pharmacokinetic (absorption, distribution, metabolism, excretion), pharmacodynamics, or combined interactions. Knowledge of the mechanism by which a given drug interaction occurs is often clinically useful, since the mechanism may influence both the time course and the methods of circumventing the interaction. Some important drug interactions occur as a result of two or more mechanisms.

Reversible binding to serum proteins modulates the distribution of drugs and then affects the pharmacokinetics and pharmacodynamic properties. Once administered, the free concentration of a drug can change due to its interaction with other drugs and endogenous factors, to its binding to plasma proteins, or to significant changes of the serum carrier concentration. Therefore, investigation studies on the plasma protein drug binding site aimed at the determination of the binding parameters are relevant when studying a drug profile.

In our study, we used fluorescence spectroscopy, surface plasmon resonance (SPR), and mass spectrometry to obtain the binding constants, a number of binding sites, free energy and binding site of bioactive compounds with HSA.

3.2.A Results and Discussion

3.2.A.1. Cytotoxic Studies with different Cell lines

I have used MTT assay method to examined the effect of Andrographolide, 7-Hydroxy coumarin derivatives, Corilagin, Embelin, Piperine, Stigmasterol, Rosmarinic acid and Menthol on the viability of HepG2, MCF-7, HeLa, Raw mouse macrophages, and A549cells. HepG2, MCF-7, HeLa, Raw mouse macrophages and A549 cells are appropriate *in vitro* model system for the study of polarized human hepatocytes including liver diseases. Further, Apocynin, Andrographolide, Bacosine, 7-Hydroxy coumarin derivatives, Corilagin, Embelin, Piperine, Stigmasterol, Rosmarinic acid, Menthol, and 6-Shagoal decreased the cell viability for different cell lines in a dose-dependent manner with an IC_{50} values (Table.3.1). These result clearly indicated the cytotoxic activity of these selected phytocompounds/bioactive compounds, wherein viability is decreased for particular cell lines (Fig. 3.1), however, no effect on other cell lines. Hence, this reports exhibits different levels cytotoxicity on different cell lines indicates that these selected bioactive compounds are very specific to certain diseases.

Table.3.1. Cytotoxic (IC_{50} values) of selected bioactive compounds against different cell lines.

Compound Name	**IC_{50}(µM) HepG2**	**IC_{50} (µM) Hela**	**IC_{50} (µM) Raw 264.7**	**IC_{50} (µM) Mcf-7**
Stigmasterol	40	_	_	_
Andrographalide	57	30	80	55
Piperine	21	_	63.5	_
Rosmarinic acid	18	_	_	11
Bacosine	34	_	_	_
Apocynin	40	_	_	_
Corilagin	-	_	69.5	_
Embelin	_	29	_	_
7HC-1	_	_	78	_
7HC-2	_	_	63	_
7HC-3	_	_	50	_
Menthol	_	43	24	_
6-Shagoal	_	36	13	_

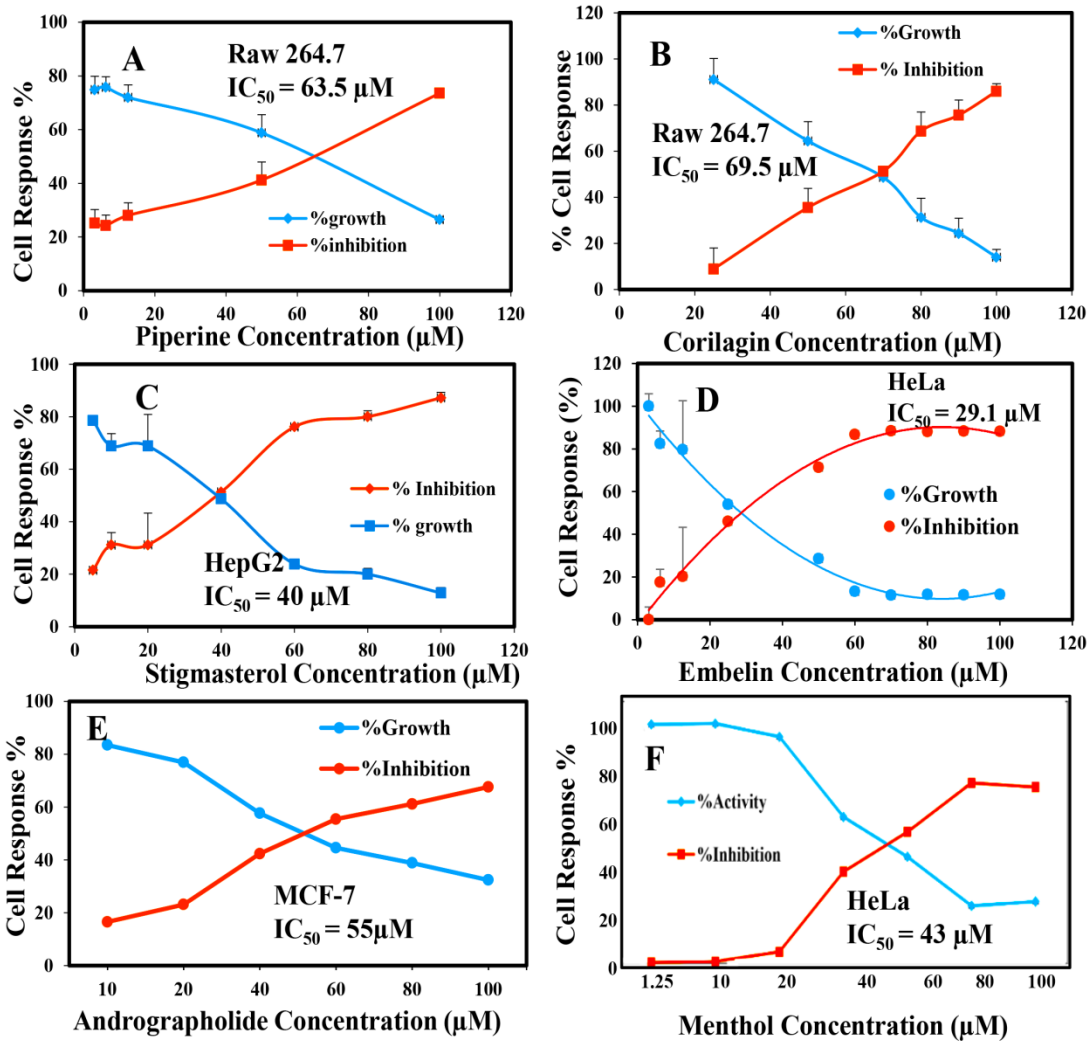

Fig. 3.1. Cytotoxic studies on different cell lines. (A) piperine (B) corilagin, (C) stigmasterol (D) embelin (E) andrographolide (F) menthol reduces the viability of specific cell lines. Cells treated for 48 h with or without each concentration of corilagin, piperine, stigmasterol, embelin, and menthol was analyzed for viability by using MTT assay.

3.2.A.2. The Evaluation of Anti-cancer Activity by Apoptosis

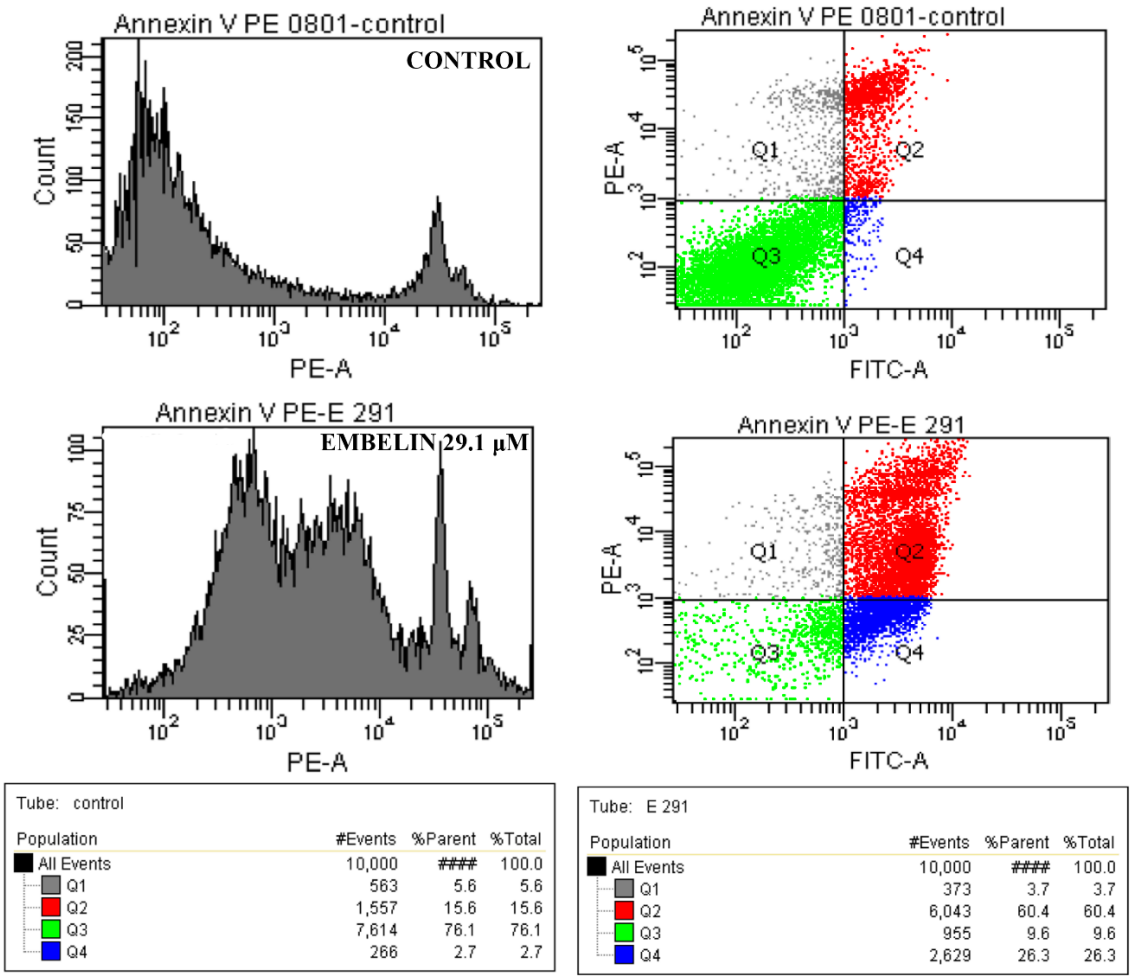

Fig. 3.2. Apoptosis activity at an induction of 29.1 µM EMB on the 24h culture of HeLa cell line. Flow cytometry was used to govern the fluorescence. Quadrants were assessed as a percentage of the cell, i.e. Q1 as late apoptotic or necrotic cells, Q2 dead cells, Q3 as live cells and Q4 as apoptotic cells.

In this study, HeLa cells were treated with embelin (IC_{50} value 29.1±1.52 µM) for cell viability assay for 24h to measure the cell death by using apoptotic detection kit as described in material and methods (2.2). The results are shown as dot-plot representation (FITC-A on x-axis and PE-A on the y-axis) in quadrants and histogram (Fig.3.2). The results showed that embelin was inducing apoptotic cell death about 26.3% at its IC_{50} value. The percentages of different cells in quadrants are shown in Fig.3.2. Other natural compounds berberine and alternate showed similar results as that of embelin and thus it might strengthen our results (Mantena et al., 2006; Tang et al., 2014). Hence, the compound embelin leads to a promising and optimization of developing a new class of anticancer potent drugs and promoting apoptosis in cancer

cell lines of HeLa cell lines. Further, an investigation into the molecular mechanisms that mediate the antitumor activities were needed to develop chemo preventive agents and cancer therapeutics in the current encounter against cancer.

3.3.B Unravelling the Binding Mechanism using Fluorescence Spectroscopy and Surface Plasmon Resonance.

Binding Studies using Fluorescence Spectroscopy

Fluorescence quenching is a useful method to study the reactivity of chemical and biological systems since it allows non-intrusive measurements of substances in low concentration under physiological conditions. It can reveal accessibility of quenchers to HSA fluorophores. Fluorescence measurements can help to understand HSA binding phenomenon such as the binding mechanism, binding constants, number of binding sites, intermolecular distances, etc., (Lakowicz et al., 2009).

For HSA, there are only three intrinsic fluorophores i.e., tryptophan, tyrosine, and phenylalanine. HSA has a single tryptophan residue (Trp-214) located in the hydrophobic cavity of the subdomain IIA corresponding to the so-called sudlow's drug binding site I region (Brown et al., 1977).

Tryptophan (shown as free amino acid) has much stronger fluorescence and higher quantum yield than the other two aromatic amino acids. The intensity, quantum yield, and wavelength of maximum fluorescence emission of tryptophan is very solvent dependent. The fluorescence spectrum shifts to shorter wavelength and the intensity of the fluorescence increase as the polarity of the solvent surrounding the tryptophan residue decrease. Tryptophan residues which are buried in the hydrophobic core of proteins can have spectra which are shifted by 10 to 20 nm compared to tryptophans on the surface of the protein. Tryptophan fluorescence can be quenched by neighboring protonated acidic groups such as Asp or Glu.

Tyrosine, like tryptophan it has strong absorption bands at 280 nm, and when excited by light at this wavelength it has characteristic emission profile. Tyrosine is a weaker emitter than tryptophan, but it may still contribute significantly to protein fluorescence because it usually presents in larger numbers. The fluorescence from tyrosine can be easily quenched by nearby tryptophan residues because of energy

transfer effects. Also, tyrosine can undergo an excited state ionization which may result in loss of the proton on the aromatic hydroxyl group that leads to quenching of tyrosine fluorescence.

Phenylalanine with only a benzene ring and a methylene group is weakly fluorescent. The experimental sensitivity (the product of quantum yield and molar absorptivity maximum) is especially low for this residue. Phenylalanine fluorescence is observed only in the absence of both tyrosine and tryptophan. The simple structure of phenylalanine may predominantly demonstrate the effect of structure on fluorescence. Adding a hydroxyl group, as in tyrosine, causes a 20 fold increase in fluorescence. If an indole ring is added as in tryptophan, the relative fluorescence increases to 200 times that of phenylalanine.

Thus, the intrinsic fluorescence of HSA is almost contributed by tryptophan alone, because phenylalanine has a very low quantum yield and the fluorescence of tyrosine is almost totally quenched if it is ionized, or near an amino group, a carboxyl group, or a tryptophan (Lakowicz et al., 2009). The intrinsic fluorescence of the unique tryptophan is very sensitive to the environment around the amino acid residues. Binding of small molecules with HSA sometimes induces changes in protein conformation and consequently, it gives fluorescence. Therefore, the fluorescence of Trp-214 has been employed frequently in the study of the interaction of the protein with drugs (Ma et al., 2009a). The interaction of bioactive compounds to HSA resulted in a substantial change in the fluorescence. Fig. 3.3–3.23 shows the fluorescence emission of HSA/AGP is obtained at 360 and 340nm when excited at 285 nm. Our results showed that with increasing concentrations of bioactive compounds (0.001 to 0.009 mM for all other bioactive compounds) and a fixed concentration of HSA/AGP (0.001 mM), the maximum fluorescence (360 nm) of HSA/AGP was quenched upon binding of bioactive compounds (Fig. 3.3-3.23). This indicates that bioactive compounds bind to HSA causes microenvironment changes in HSA/AGP and leads to HSA/AGP-bioactive complexes formation. With increasing concentrations of bioactive compounds with HSA absorption at excitation (285 nm) and emission (360 nm) wavelength introduces inner filter effect, which may decrease the fluorescence intensity and results in a non-linear relationship between the observed fluorescence intensity and the concentration [Q] of the bioactive compounds. Such effect was corrected using the following equation

$$F_{cor} = F_{obs}10\,(A_{exc} + A_{emi})/2 \text{ - [1]}$$

Where, F_{cor} is the corrected fluorescence intensity, A_{exc} and A_{emi} represent the absorbance at the fluorescence excitation (285 nm) and emission wavelengths (360 nm) of HSA and (340 nm) of AGP, Fobs is the observed fluorescence (Lakowicz et al., 2009).

Different mechanisms of quenching are classified as either dynamic quenching or static quenching. Dynamic and static quenching can be distinguished by temperature and viscosity, or by the difference of their fluorescence lifetime (Lakowicz et al., 2009). Dynamic quenching is a process in which the fluorophore and the quencher come into contact during the transient existence of the excited state. Static quenching refers to fluorophore (HSA)-quencher (bioactive compounds) complex formation. To verify whether the quenching is by static or dynamic in HSA-bioactive complexes, I have plotted *Fo/F* against Q to determine the static and dynamic quenching. The *Kq* was estimated according to the Stern-Volmer equation:

$$F_0 / F = 1 + K_q t_0 [Q] = 1 + K_D [Q] \text{ - [2]}$$

Where, F_0 and F are the fluorescence intensities in the absence and presence of quencher, [Q] is the quencher concentration and K_D is the Stern-Volmer quenching constant (Kq), which can be written as $K_D = kqt0$; where kq is the bimolecular quenching rate constant and $t0$ is the lifetime of the fluorophore in the absence of quencher, lifetime of fluorophore for HSA is 5.6 ns (Tayeh, Rungassamy & Albani 2009). From the biomolecular quenching constants (Table 3.4) all the HSA-bioactive complexes followed the static quenching mechanism which is evident from the quenching constants which are much greater than the maximum collisional quenching constant of HSA (2.0×10^{10} M^{-1} s^{-1}) (Zhang et al., 2008; Agudelo et al., 2012).

Binding constant and Number of binding sites

When small molecules bind independently to a set of equivalent sites on a macromolecule, the equilibrium between free and bound molecules could be represented by the modified stern-Volmer equation (Kragh-Hansen et al., 1981).

$$\text{Log } (F_0 - F)/ F = \log K + n \log[Q] \text{ - [3]}$$

Where, K and n are the binding constant and number of binding sites, respectively. The values of K and n for HSA/AGP -bioactive compounds system were calculated from the intercept and slope of the plot of $\log(F_0-F)/F$ versus log[Q] and the same plot for a representative system, HSA-bioactive compounds are given in (Fig.3.3-3.23). The values of K and n are summarized in Table. 3.4. It was noticed that the binding constant values are in the range and in agreement with known binding constants of (10^3-10^6 M^{-1}); Federal Drug Administration (FDA) approved drugs (see Table. 1). The K values indicates strong binding with HSA and n values for HSA-bioactive complexes **(**Table 3.4) were noticed to be almost unity indicating that there was one independent class of binding sites on HSA for all the bioactive compounds (Fig.3.3-3.23), suggesting that HSA interacts with bioactive compounds in a one-to-one ratio. The differential binding constants obtained for different molecules because of their structural difference (Gokara et al., 2010; Garg et al., 2013; Yeggoni et al., 2014 a & b; Yeggoni et al., 2015a & b; Yeggoni et al., 2016 a & b).

Thermodynamic parameters and the nature of binding forces

Generally, the interaction forces between small organic molecules and biological macromolecules can include the hydrophobic force, hydrogen bonds, the van der Waals force, electrostatic interactions etc (Leckband et al., 2000). Thermodynamic parameters for a binding interaction can provide major evidence about the nature of the intermolecular forces. The binding constant K of bioactive compounds with HSA/AGP at 298K is used to calculate the standard free energy according to a well-known equation (see eq 4).

$$\Delta G^\circ = -RT\ln K \qquad -[4]$$

Where, ΔG is free energy, K is the binding constant at the corresponding temperature, which can be obtained from fluorescence data, and R is the gas constant. The calculated free energy change of HSA/AGP-bioactive compounds is summarized in Table. 3.4. The negative sign for free energies of the compounds is given in Table.3.4. I have also carried out the using different temperatures to find out the free energies, for most of the molecules, the free energy changes were minimal. Hence, I am providing the free energies only the room temperature data.

These data indicates that the interaction process is spontaneous. The negative free energy and the docking data which is explained in the docking studies of individual studies suggest the type of interactions of HSA/AGP -bioactive complexes include both hydrogen bond and hydrophobic interactions. Earlier, our group have reported similar kind free energies for other natural bioactive compounds (trans-feruloyl maslinic acid, betulinic acid, β-sitiosterol, lupeol, L-dopa, 7-hydroxycoumarin, trimethoxy flavone, embelin, corilagin *etc.* (Subramanyam et al., 2009 a & b; Gokara et al., 2010; Yeggoni et al., 2014 a & b; Yeggoni et al., 2016 a & b). The detail binding mechanism of different bioactive compounds with HSA has been discussed below.

3.2.B.1 Andrographolide

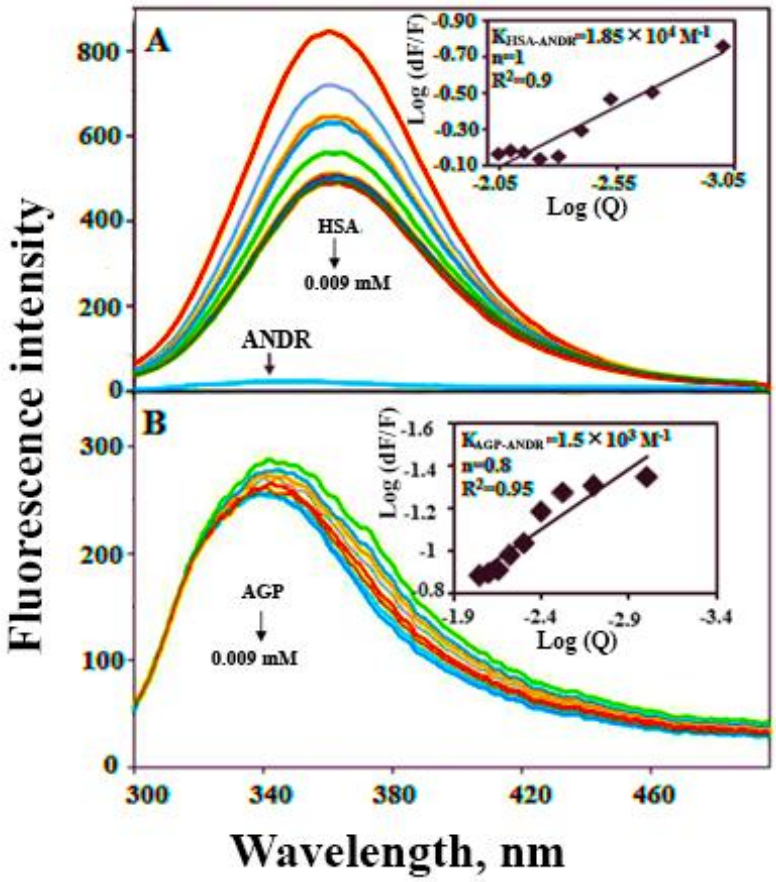

Fig. 3.3. Fluorescence emission spectroscopy of (A) Free HSA (0.001mM) and free HSA with different concentration of ANDR (0.001, 0.002, 0.003, 0.004, 0.005, 0.006, 0.007, 0.008, 0.009mM) in 0.1 M phosphate buffer pH 7.4, λex = 285 nm, temperature = 25^{o}C**,** inset, Modified Stern-Volmer plot ; Plot of log (dF/F) against log [Q] λex = 285nm. , λex = 360 nm. (B) Free AGP (0.001 mM) and free AGP with different concentrations ANDR of 0.001, 0.002, 0.003, 0.004, 0.005, 0.006, 0.007, 0.008, and 0.009 mM. Inset Plot of log (dF/F) against log [Q]. λex = 285 nm and λem = 340 nm.

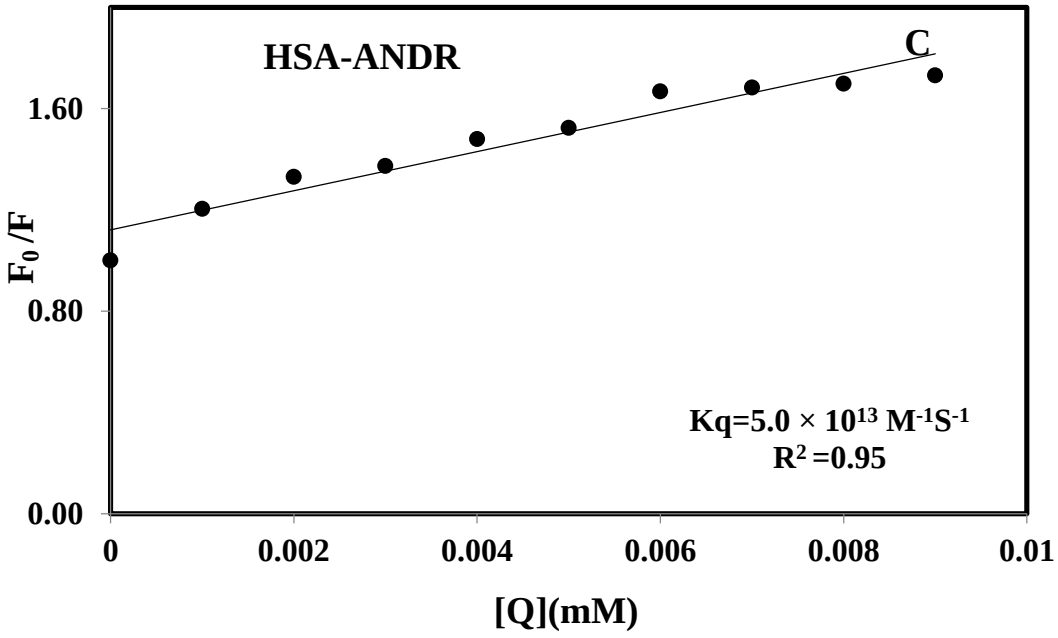

Fig.3.4. (C) Stern-Volmer plots of HSA-ANDR complexes showing fluorescence quenching constant (K_q). Here the plot is showing F_0/F against [Q] for ANDR.

T (K)	**K_b** ($\times 10^4$ M^{-1})	**ΔG** (kcal M^{-1})
298	1.85± .01	-5.1
310	1.22 ± .03	-5.5

Table.3.2. Binding parameters of ANDR interaction to HSA in 0.1 M phosphate buffer pH 7.4 at a different temperature obtained and calculated from fluorescence quenching results.

I have used fluorescence spectroscopy to unravel the binding mechanism or binding mode of andrographolide (ANDR) to HSA or AGP. The fluorescence quenching of AGP and HSA is due to intrinsic tryptophan residue used to understand the interaction of ANDR with these proteins (Fig. 3.3). While titrating ANDR to the HSA the fluorescence maximum intensity at 360 nm was decreased with the addition of ANDR. Due to the presence of Trp-214 HSA major fluorescence of HSA is obtained when its excited at 285 nm. It even indicates that ANDR binding site exists near to the tryptophan residue which is located to the IIA subdomain of HSA.

The static quenching constants, $K_q(s)_{(ANDR)}$ =5.0 ± 0.03 × 10^{13} $M^{-1}s^{-1}$ (Fig.3.4.C). According to the standard procedures, if K_q is more than the maximum

collisional quenching constant then the static quenching is dominant. I found that the dynamic quenching constant is $2.06 \pm 0.03 \times 10^{10}$ $M^{-1}s^{-1}$ (Tayeh et al., 2009; Agudelo et al., 2012). Hence the binding of ANDR to HSA is 'static' as $K_q(s)$ is very much greater than colloidal constant. This indicates the formation of the fluorophore-quencher complex formation. The results demonstrated that HSA fluorescence quenching by ANDR may follow a static mechanism and was initiated by HSA-ANDR complex formation rather than dynamic collision.

Also the binding constant (Fig. 3.3) to be K_{ANDR} =1.85 ± 0.02×10^4 M^{-1}, indicates the strong binding of ANDR with HSA. This data are very much correlated with the data found *in silico i.e.* 1.2 ± 0.03×10^4 M^{-1}. The same experimental procedures were followed at 37 ^oC where I found that on increasing temperature the fluorescence emission decreases, or in other words, the extent of lowering in fluorescence emission was higher at a lower temperature. For ANDR, the value of K_b and n were calculated at 37 ^oC temperature and the observed values are K_b= 1.2 ± .03 × 10^4 M^{-1}, ΔG=-5.5 kcal M^{-1} at 37 °C (Table.3.2). Thus the data shows a slight decrease in K_b on increasing the temperature is a clear indication of static quenching (Feroz et al., 2012). As we know that a very few drug molecules binds efficiently with AGP, therefore, I have also calculated the binding constant and found to be K_{ANDR} = 1.5±0.03×10^3 M^{-1}, *in silico* binding affinity of AGP is 7.7 ± 0.05×10^4 M^{-1} which is in the range of known FDA approved drug values (10^3 – 10^6 M^{-1}) (Varshney et al., 2010). Recently, we have reported that few phytochemicals binds to AGP and HSA (Yeggoni et al., 2015 a & b; Yeggoni et al., 2016a) from this point of view, I can state that due to an acute phase protein AGP binds with ANDR and hence in chronic inflammation/cancer conditions the ANDR can bind to overexpressed AGP. Thus, these results indicate that the ANDR binds to both HSA and AGP and this has been discussed in chapter 5. It even reveals that there is only one binding site for ANDR for serum proteins also suggests that both the proteins may be used as a carrier for ANDR in different diseased conditions. The free energy change for ANDR has been calculated and found to be -5.79 ± 0.031 kcal/mol at 25 °C, when binding with HSA. Interestingly, this data also supports the *in silico* analysis (discussed in chapter 4) of HSA-ANDR complex, where $\Delta G°_{ANDR}$ = -5.6 ± 0.031 kcal/mol. Therefore, this data suggests that the binding between protein and ligand can be stabilized by hydrophobic interaction and hydrogen bond formation.

From the fluorescence quenching mechanism, it is found to be a static mechanism which is evident from the bimolecular quenching constants ANDR are 5.27± 0.02 × 10^{13} M^{-1} s^{-1}. It is observed that quenching of emission maximum at 340 nm of AGP was observed with ANDR. Interestingly blue shift and red shifts were observed in the peaks of AGP- ANDR (Fig. 3.3B) whereas with HSA there is no shift in the peaks of these ANDR. This phenomenon might be due to the unfolding and refolding of the protein after the binding. The possible explanation for the shift might be due to the differential exposure of tryptophan residues at various positions in the protein, which may be exposed differentially to the polar environment leading to the shift in the emission maximum at 340nm. The binding constants with ANDR are 10 times lesser than HSA. ANDR binds with AGP in 1:1 ratio indicating that only one molecule is bound with AGP, similarly with HSA. The negative free energy of all these ANDR is less than the values obtained with HSA. These findings suggest that HSA plays a major role in binding, however, it should be verified *in vivo* in various pathological conditions where AGP expression is upregulated.

Displacement studies of ANDR binding to HSA

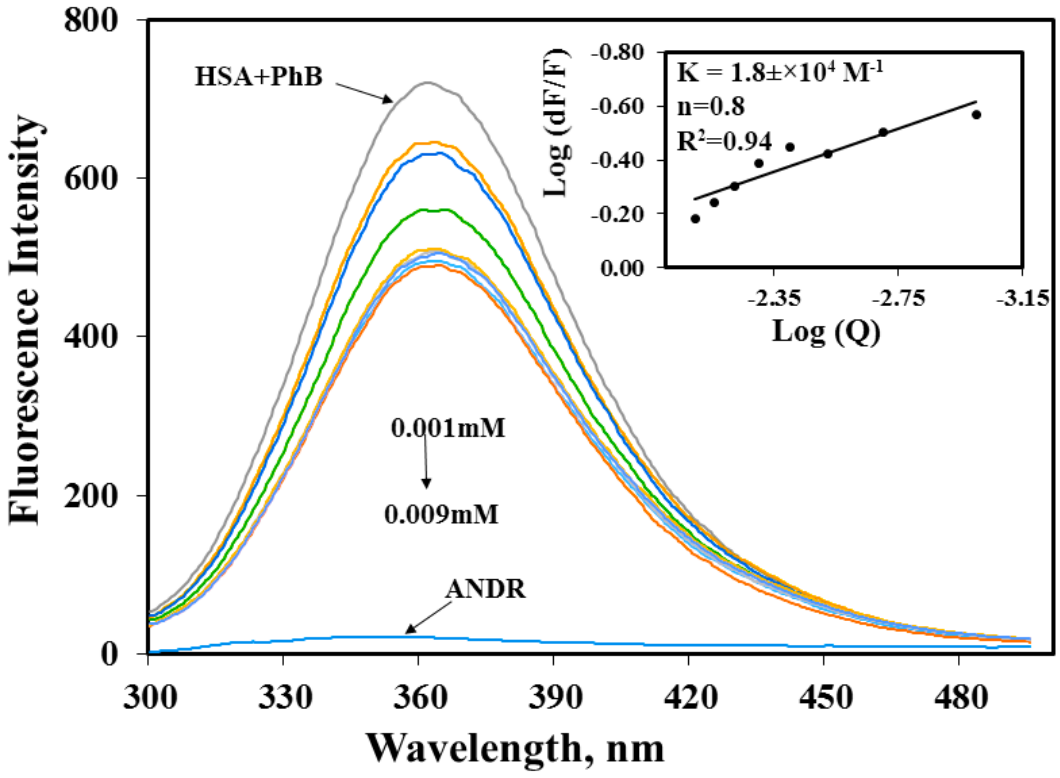

Fig.3.5. Competitive binding of a ligand with HSA. Displacement of phenylbutazone from the HSA-phenylbutazone complex by ANDR. In the graph log dF/F vs log Q (Inset) was plotted to calculate binding constant and a number of binding sites.

To determine the exact binding pocket of HSA upon interaction of ANDR, molecular displacement studies were carried out using site-specific marker fluorescence probes for monitoring site I and site II of HSA. Here, I took two site-specific markers for HSA; phenylbutazone that binds at IIA and ibuprofen for IIIA, to know the specific binding of ANDR with HSA through site competitive displacement experiments. The concentration of HSA and that of site-specific markers are kept constant (0.001mM) and titrated with ANDR at increasing concentrations, it showed a decrease in fluorescence emission intensity when titration of different concentrations of ANDR into HSA-phenylbutazone. The binding constant obtained were close to HSA-ANDR alone. From the displacement experiment, the binding constant value decreased slightly in presence of phenylbutazone found to be K_{ANDR} = 1.8 ± 0.03×10^4 M^{-1} (Fig.3.5), which was very much close to the intrinsic fluorescence data, where it shows K_{ANDR}=1.85 ± 0.02 × 10^4 M^{-1}.

Therefore, indicating a competition between phenylbutazone and ANDR for the binding site of IIA of HSA, data was harmonized with the docking results which showed that ANDR binding to the IIA subdomain of HSA (discussed in chapter 4). However, there are no observed changes in the binding constants of another site-specific marker for IIIA subdomain of HSA (2.1 ± 0.05×10^4 M^{-1}) compared with the absence of the site-specific probe, thus ANDR displaces only phenylbutazone from subdomain IIA. Therefore, from this study, ANDR displaces the phenylbutazone molecule and forms a stable complex due to hydrophobic interactions at the IIA domain.

Surface Plasmon Resonance (SPR)

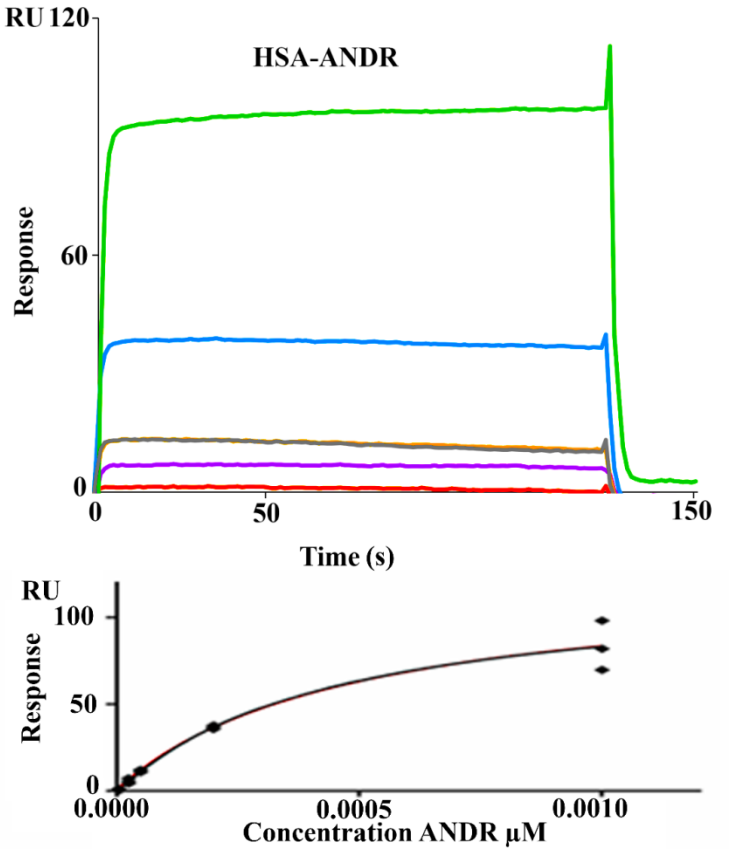

Fig.3.6. Sensorgrams of binding of ANDR to HSA immobilized on CM 5 sensor chip (top) and respective R_{eq} values fitted to the steady state model giving the final binding isotherm (bottom). Increasing concentrations of analyte are denoted by different colors: 5 µM (orange), 25 µM (purple), 50 µM (light black and yellow), 200 µM (blue) and 1000 µM (green) for ANDR–HSA.

There are various techniques to understand molecular interactions, among them fluorescence and SPR spectroscopy are widely used. Interactions between macromolecules and small molecules by fluorescence spectroscopy are based on the interaction of quencher and a fluorophore. Measuring fluorescence quenching, binding constants, and mechanisms of molecular interaction can be analyzed. SPR is an optical technique which is based on the refractive index change near to a metal (Au) surface. The refractive index changes reflect the absorbance of analyte in solution onto the ligand HSA is immobilized on the surface Fig.3.6. The advantage of SPR is that it can monitor the surface-constrained interaction in real time without the requirement for labeling.

As the interaction of ANDR to HSA by SPR is formed under flow conditions that usually exhibit shear stress and takes place between an immobilized ligand and a

mobile analyte, it might be a bit weaker than binding affinities derived from assays with both binding partners in solution without any shear stress forces like fluorescence spectroscopy. The association constants obtained from the fluorescence and SPR experiments were very close i:e $1.85 \pm 0.02\times10^{4}$ M^{-1} (fluorescence) and $3.1 \pm 0.04\times10^{3}$ M^{-1} (SPR), respectively. Additionally, covalent coupling of HSA to the chip surface takes place randomly via primary amines in the protein. If these amines are situated next to the binding pocket for ANDR, interactions may be sterically hindered reducing binding affinity in contrast to fluorescence spectroscopy where no attachment is needed.

3.2.B.2 Corilagin (COR)

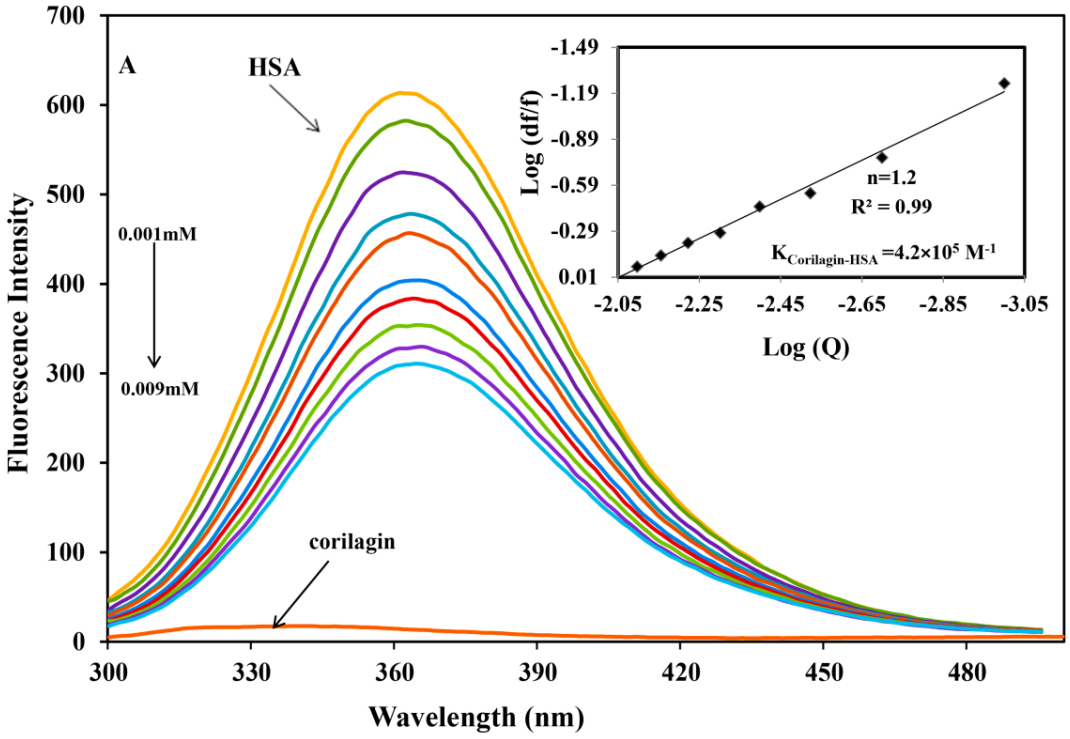

Fig. 3.7. Fluorescence emission spectra of HSA– Corilagin in 0.1 M phosphate buffer with pH 7.4, λex = 285 nm, and temperature = 25 °C. (A) Free HSA (0.001 mM) and free HSA with different concentrations Corilagin of 0.001- 0.009 mM. (B) Plot of log (dF/F) against log [Q]. λex = 285 nm and λem = 360 nm.

From the slope of the plot, binding constants of corilagin were calculated from the intercept as $4.2 \pm .02 \times 10^{5}$ M^{-1} which indicates strong binding of corilagin to HSA (Fig. 3.7). There is a good correlation with the computational calculated binding constant as 1.5×10^{4} M^{-1} obtained as lowest free energy. The binding constants and free

energy of the best docking conformer are close and consistent with the binding constants and free energy determined by fluorescence studies. Thus these results corroborate with the experimental data. Interestingly, I have reported that natural compounds binding to HSA showed similar results on betulinic acid, feruloyl masalinic acid, trimethoxy flavone, and coumaroyltyramine, and their binding constants were K_{BA} = 1.685 ±0.01 × 10^6 M^{-1}, K_{FMA} = 1.42 ± 0.01 × 10^8 M^{-1}, K_{TMF} = 1.0 ± 0.01 × 10^3 M^{-1}, and K_{CT} = 4.5 ± 0.01 × 10^5 M^{-1} (Subramanyam et al., 2009 a & b; Gokara et al., 2010; Neelam et al., 2010). The calculated free energy change of COR-HSA is -7.6 kcal M^{-1} at 25 °C. The calculated computational free energy value is -5.71 kcal M^{-1} and the results are in agreement with the experimental data. Here the lower free energy value is mainly due to the hydrophobic interaction of corilagin binding to HSA.

Energy transfer from HSA to Corilagin (Fluorescence Resonance Energy Transfer)

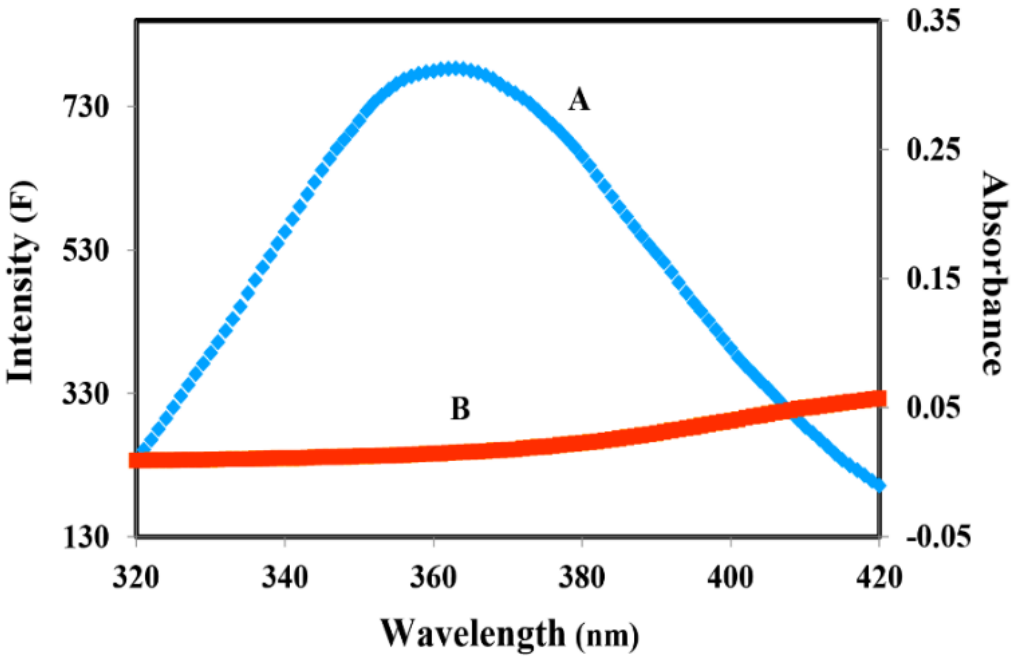

Fig.3.8. The overlap of fluorescence spectrum of HSA (A) and absorbance spectrum of corilagin (B) [λ_{ex}=285 nm , λ_{em}=360 nm c(HSA)/c(corilagin)=1:1].

HSA has a single tryptophan residue (Trp-214). The distance *r* between the Trp-214 in HSA and the bound corilagin could be determined using fluorescence resonance energy transfer (FRET). FRET has been widely used to determine the molecular distance between the acceptor and donor molecules. Generally, FRET occurs whenever the emission spectrum of a fluorophore (donor) overlaps with the absorption spectrum of

another molecule (acceptor). The overlap of the UV absorption spectrum of corilagin with the fluorescence emission spectra of HSA is shown (Fig.3.8). The distance between the donor and acceptor and extent of spectral overlaps determines the extent of energy transfer. The distance between the donor and acceptor can be calculated according to Fösters theory (Förster et al., 1996). The efficiency of energy transfer, *E*, can be calculated as

$$E=1-F/F_{0=} R^6_0/ R^6_0+r^6 \qquad -[5]$$

Where, F and F_o are the fluorescence intensities of HSA in the presence and absence of corilagin, *r* the distance between acceptor and donor and R_o is the critical distance when the transfer efficiency is 50%. R_o can be determined as

$$R_o^6 = 8.8\times10^{-25} \times K^2 \times N^{-4} \times \phi \times J \quad -[6]$$

Where, K^2 is the spatial orientation factor of the dipole N the refractive index of the medium, ϕ the fluorescence quantum yield of the donor and *J* is the overlap integral of the fluorescence emission spectrum of the donor and the absorption spectrum of the acceptor. *J* can be calculated as

$$J = \sum F(\lambda)\varepsilon(\lambda)\, \lambda^4 \Delta\lambda / \sum F(\lambda)\Delta\lambda \qquad -[7]$$

Where, $F(\lambda)$ is the fluorescence intensity of the fluorescent donor of wavelength, λ, and $\varepsilon(\lambda)$ is the molar absorption coefficient of the acceptor at a wavelength, λ. In the present case, $K^2=2/3$, N=1.336 and ϕ=0.118 for has (Epps et al., 1998). From the above-mentioned equations 5, 6 and 7 were able to calculate that $J= 9.41\times10^{-15}$ Cm^3 L mol^{-1}, R_0=2.57nm, E=0.49 and r=1.32 nm for HSA. The donor-acceptor distance, r < 8nm (Hu et al., 2004; Valeur & Brochon 2012) indicates that energy transfer from HSA to corilagin occurs with high possibility, thus the existence of static quenching due to complex formation between HSA (Trp-214) and corilagin.

Displacement Studies of Corilagin binding to HSA

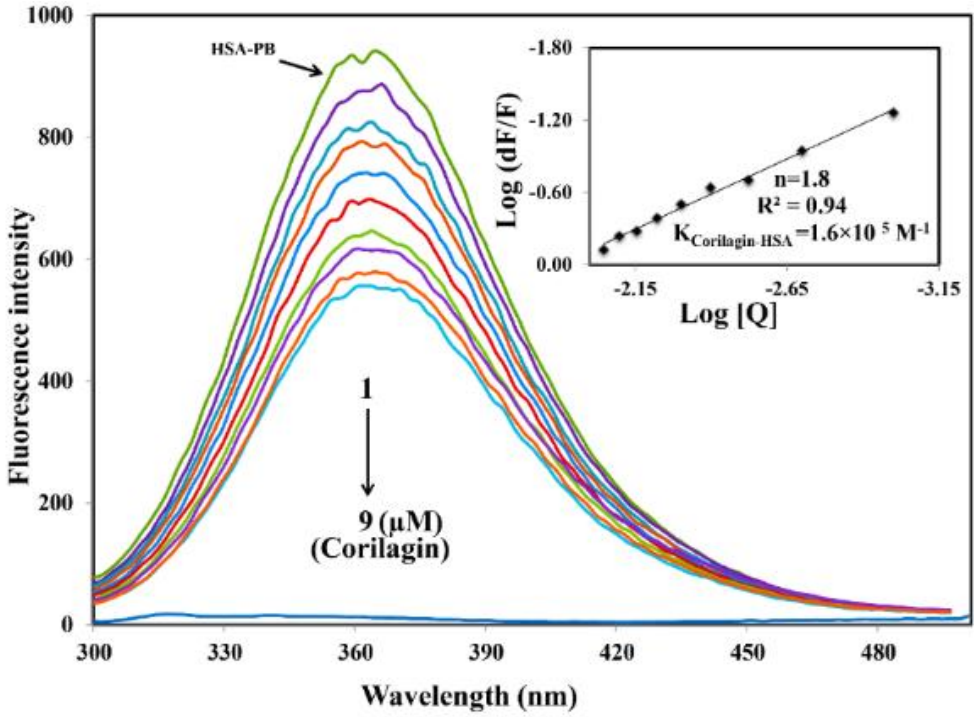

Fig. 3.9. Displacement of phenylbutazone from HSA-phenylbutazone complex by corilagin**.** Fluorescence emission spectra were recorded on Perkin Elmer LS55 fluorescence spectrometer for corilagin with HSA in presence of site probe markers. Phenylbutazone is referred as a site-I probe. The concentrations of HSA and phenylbutazone were maintained constant at a concentration of 1µM whereas, the corilagin was varied from 0 to 9 µM. Inset: Modified Stern-Volmer plot. Plot of log (dF/F) against log [Q] λex = 285 nm, λem = 360 nm.

Corilagin has to compete with lidocaine (subdomain IB marker), phenylbutazone (a site I marker) and ibuprofen (site II marker**)** to get the chance to bind to HSA if they bind to HSA in the same site. This is proved by the gradual decrease in fluorescence intensity, but the intensity is much lower in the absence of site-specific markers. The binding constant of corilagin- HSA system is ~3.9 ± 0.02 × 10^4 (lidocaine), 1.6 ± 0.01× 10^5 (phenylbutazone) and 3.7 ± 0.02× 10^4 M^{-1} (ibuprofen), respectively. The original binding constants of HSA-corilagin is 4.2 ± 0.02 × 10^5 M^{-1}. The binding constants in the presence of phenylbutazone and in its absence are close to each other, whereas binding constants in presence of other site-specific markers like lidocaine and ibuprofen are less which indicates that corilagin compete and displaced phenylbutazone from the binding site. Thus the displacement measurement confirms that the corilagin is bound to Sudlow's site I of HSA (Fig. 3.9). Similar kind of competitive displacement studies was reported in my previous papers (Yeggoni et al., 2014a; Yeggoni et al., 2015b).

Atomic Force Microscopy (AFM)

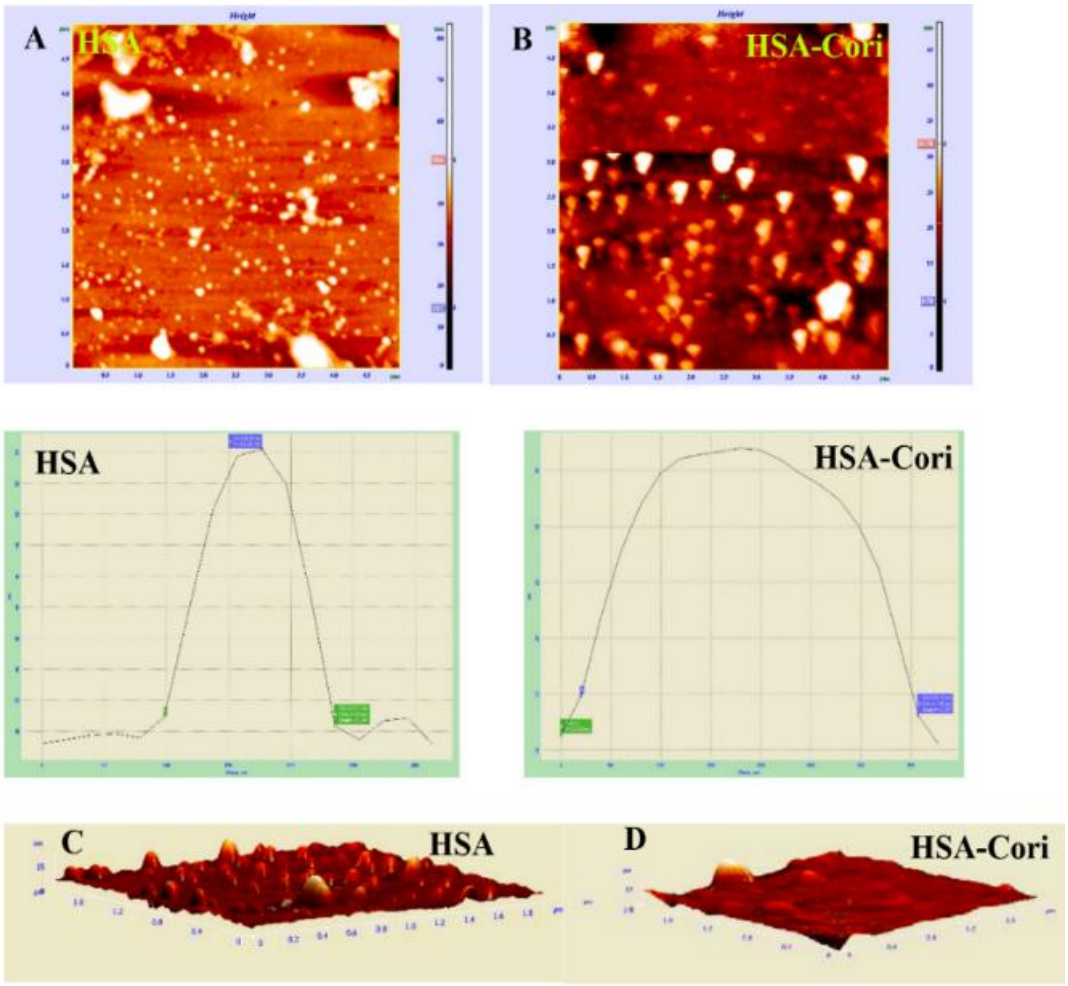

Fig. 3.10. 2D AFM images of (A) Free HSA (B) HSA–Corilagin complex. The corresponding 3D images are given by (C) and (D) respectively, the scan area is given in brackets.

To investigate topography changes in HSA upon addition of corilagin, the free HSA and HSA-corilagin complexes were clearly visualized by using AFM in triplicate. Fig. 3.10 shows the results obtained from AFM for the unliganded HSA and HSA-corilagin complexes. The data shows that HSA was absorbed evenly on the mica glass surface. The mean height of the different HSA molecules was 137.3 ± 2.47 nm. These dimensions are nearer to the previous report of HSA (Kowalczyk et al.,1996).Later after addition of the corilagin, the HSA molecule became swollen, and the mean height of HSA reached 337.5 ± 3.05 nm, which indicates the aggregation or HSA- corilagin complexation. Thus the microenvironment surrounding the HSA became more hydrophobic after interacting with corilagin. Therefore minimizing some factors

unfavorably affecting the formation of a stable complex structure, the HSA molecule reduced its surface area of contact with water by molecular aggregation.

Mostly proteins are aggregated under certain conditions like special composition ion, appropriate pH value, and concentration of the protein solution. Moreover, protein–protein hydrophobic interaction is an important factor in causing proteins aggregation (Privalov et al., 1979). The different shapes and size distributions point towards distinctly different forms of the morphology of free HSA and HSA–Corilagin complex. These results again support the formation of protein-ligand complex, as a result, the morphology is different from the free protein (Fig. 3.10). Hence, the results expose that a hydrophobic interaction between HSA and corilagin may exist.

3.2.B.3 Embelin (EMB)

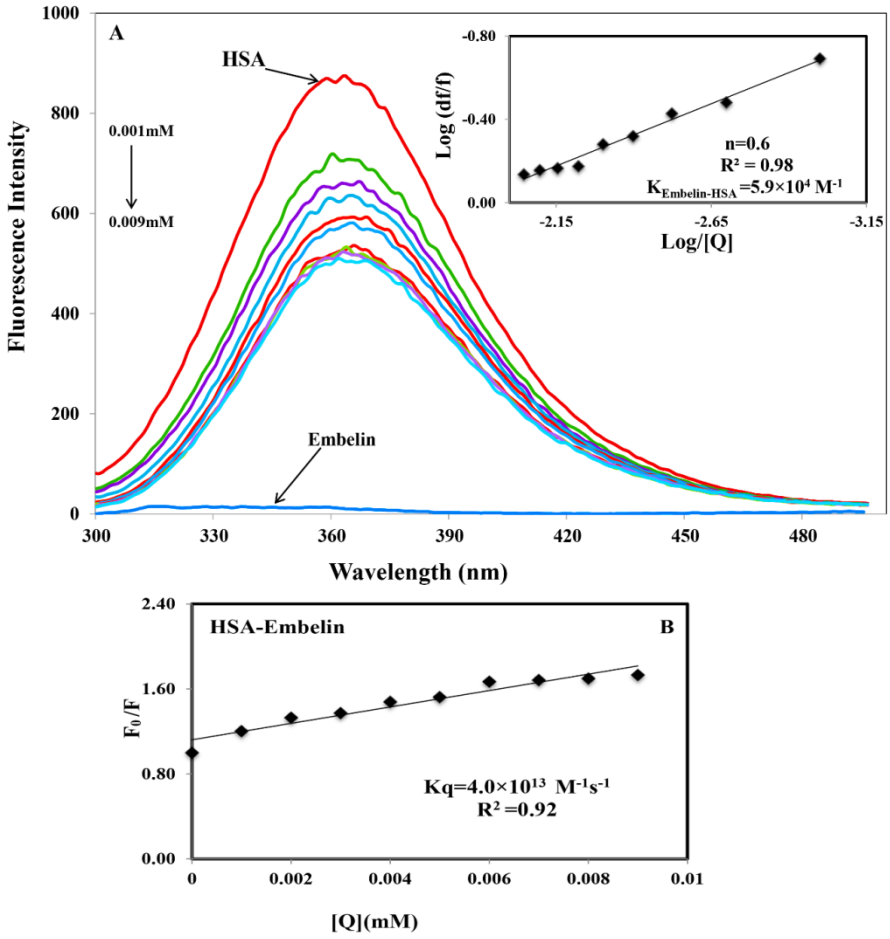

Fig. 3.11. Room temperature fluorescence emission spectra were measured at physiological pH 7.4 (A) Free HSA (0.001 mM) and free HSA with different concentrations EMB of 0.001- 0.009 mM. Inset Plot of log (dF/F) against log [Q]. (B) Stern-Volmer plots of HSA- EMB complexes showing fluorescence quenching constant (k_q) and plot of Fo/F against [Q] for EMB λex = 285 nm and λem = 360 nm.

T (K)	**K_b** ($\times 10^4$ M^{-1})	**ΔG** (kcal M^{-1})
298	5.9± .01	-5.1
310	1.5 ± .01	-5.0

Table. 3.3. Binding parameters of EMB interaction to HSA in 0.1 M phosphate buffer pH 7.4 at a different temperature obtained and calculated from fluorescence quenching results.

From above-mentioned equation, the plotted results indicated a good linear relationship with the value of n=0.6 approximately equal to 1. This indicates the presence of a single class of binding site for EMB in HSA. Further, linearity in the plot of log (d*F*/*F*) against log[*Q*] confirms that HSA interacts with EMB in a one-to-one ratio (Fig. 3.11). The binding constants of EMB were calculated from the intercept as 5.9 ± 0.01 × 10^4 M^{-1} which indicates strong binding of EMB to HSA. The fluorescence intensity decreases continuously but a higher concentration of EMB the decreasing pattern of emission gets saturated which is clear indication of binding of EMB to a specific binding site on HSA. The same experimental procedures were followed at 37 ^oC where I found that on increasing the temperature, the quenching also decreases, or in other words, the extent of lowering in fluorescence emission was higher at a lower temperature. For EMB, the value of K_b and n were calculated at 37 ^oC temperature and the observed values are K_b= 1.5 ± 0.01×10^4 M^{-1} ΔG= -5.0 kcal M^{-1} at 37 °C (Table .3.3). Thus the data shows a slight decrease in K_b on increasing the temperature is a clear indication of static quenching (Feroz et al., 2012). There is a good correlation with the computational calculated binding constant as 4.0 × 10^3 M^{-1} obtained as lowest free energy. Thus, the calculated free energy change is -5.1 kcal M^{-1} at 25 °C. I have also used a computational method to calculate the free energy and found to be -4.92 kcal M^{-1} for the lowest confirmation. Thus, the experimental results are in agreement with the theoretical or computational data.

Displacement Studies of EMB binding to HSA

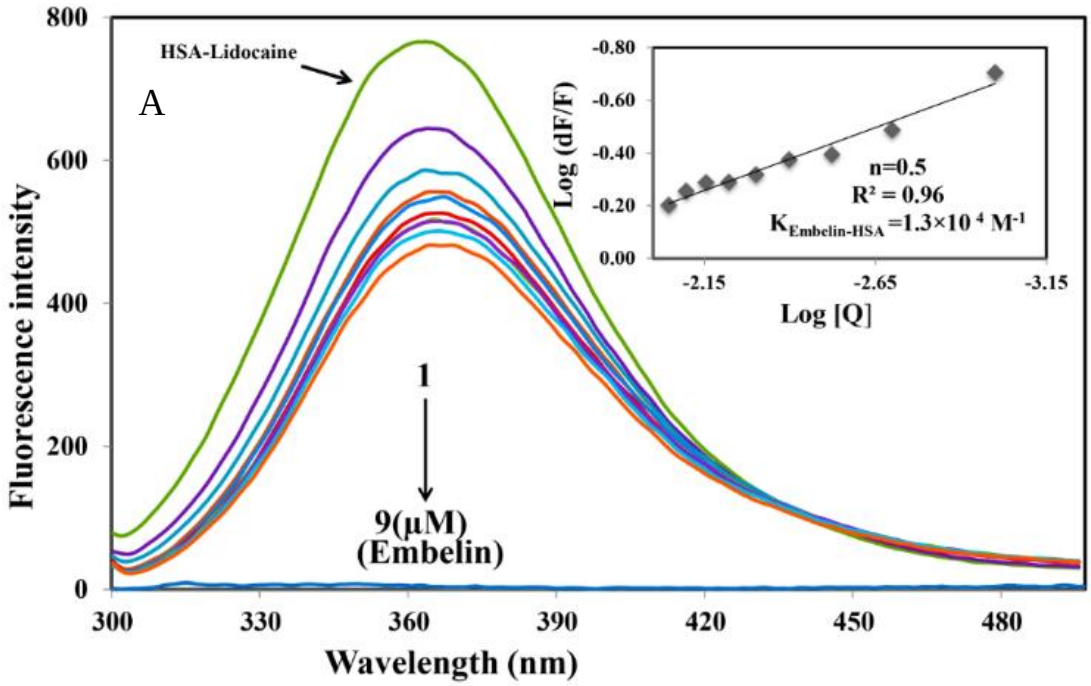

Fig. 3.12. Displacement of Lidocaine from HSA-Lidocaine complex by EMB**.** (A)The concentrations of HSA and lidocaine were maintained constant at a concentration of 1µM whereas, the EMB was varied from 0 to 9 µM. Inset Modified Stern-Volmer plot. Plot of log (dF/F) against log [Q] λex = 285 nm, λem = 360 nm.

To compare the effects of lidocaine (subdomain IB marker), phenylbutazone (Site I marker) and ibuprofen (Site II marker) on the binding of EMB to HSA, I have calculated the binding constant and other parameters. The binding constant of EMB-HSA with different site markers are $1.3 \pm 0.02 \times 10^4$ (lidocaine), $1.3 \pm .01 \times 10^3$ (phenylbutazone) and $5.2 \pm 0.02 \times 10^3$ (ibuprofen), respectively. The binding constants in the presence of lidocaine are higher than that of its absence, whereas binding constants in the presence of other site-specific probes like phenylbutazone and ibuprofen are lesser which indicates that EMB has displaced lidocaine from the binding site. Hence, the displacement measurement confirms that the EMB is bound to IB subdomain of HSA (Fig. 3.12). There are reports stating that IB is the third major drug binding region (Zsila et al., 2013).

Analysis of Electrospray Ionisation Mass spectrometry (Q-TOF)

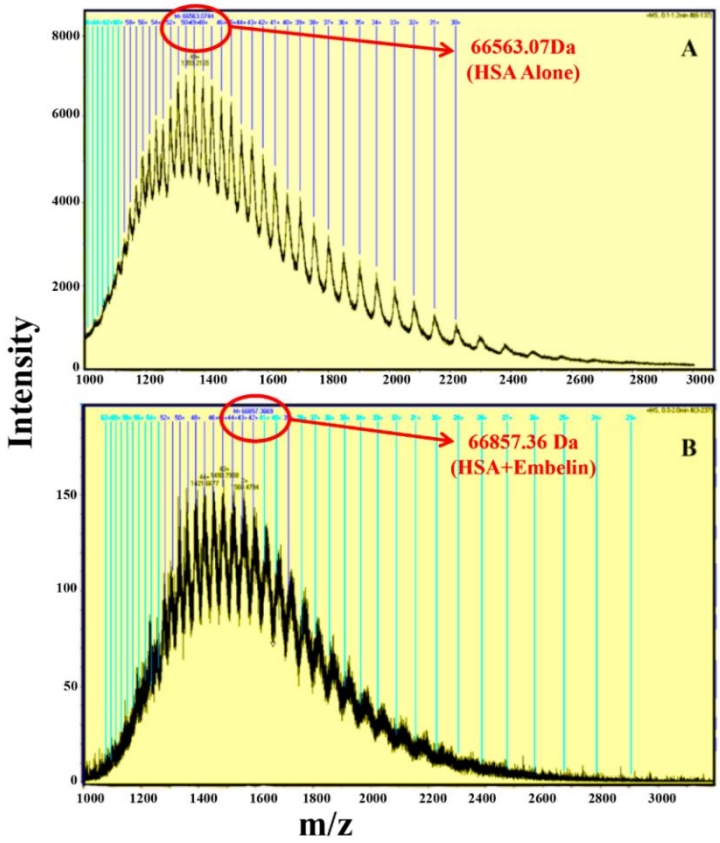

Fig. 3.13. Q-TOF mass spectra of free HSA, and HSA along with EMB. The concentration of free HSA(A) and HSA-EMB(B) were 0.15 nM and 5 nM, respectively (m=mass; z=change).

ESI-MS is an important tool to identify the small molecules, their masses and also the binding characterization of ligands to the macromolecules can be studied since it is a very sensitive technique. Here I have used Q-TOF MS to demonstrate protein-ligand complexation at nanomolar levels. The mass spectra of free HSA and HSA-EMB complexes can be seen in (Fig. 3.13). The numbers above the vertical lines indicate the matched charge states of HSA and HSA-EMB complexes. Thus, deconvolution of the multiply charged states resulted in the identification HSA and HSA-EMB complex masses. I observed an increase in the molecular mass from 66563 Da to 66857 Da when EMB binds to HSA. As the molecular weight of EMB is 294.39 Da, the additional mass of 294Da indicates that EMB binds to HSA in 1:1 ratio. Hence, the mass spectra data is very well in agreement with fluorescence data showing that HSA-EMB complexes were formed. Our group has shown similar binding of betulinic acid, feruloyl maslinic acid, and tri methoxy flavone bound to HSA in 1:1, 1:2, 2:1and 1:1 from Q-TOF MS which was similar agreement with the fluorescence data (Subramanyam et al., 2009 a & b; Gokara et al., 2010).

3.2.B.4 Piperine (PIP)

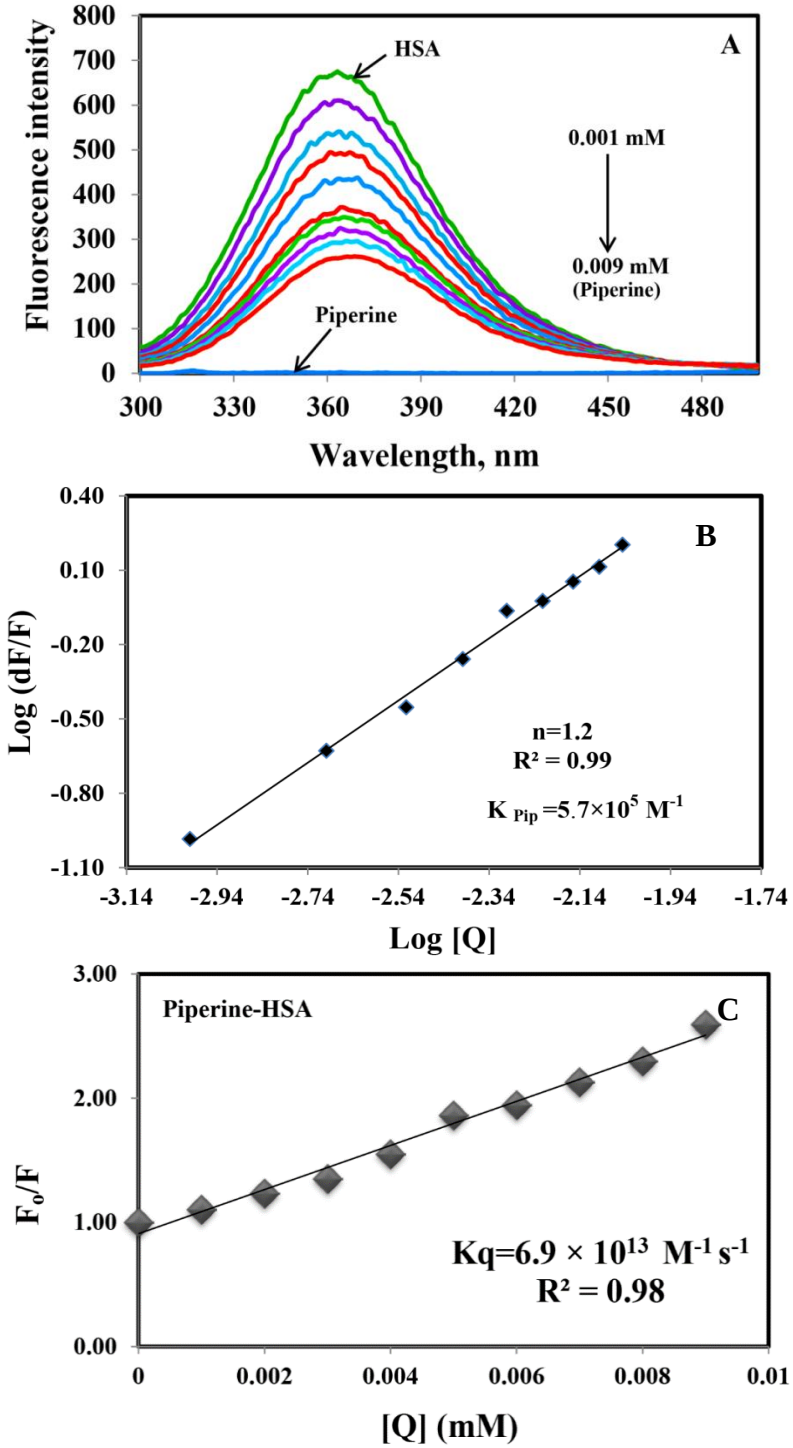

Fig. 3.14. Fluorescence emission spectra of HSA–piperine in 0.1 M phosphate buffer with pH 7.4, λex = 285 nm, and temperature = 25 ± 1°C. (A) Free HSA (0.001 mM) and free HSA with different concentrations piperine of 0.001, 0.002, 0.003, 0.004, 0.005, 0.006, 0.007, 0.008, and 0.009 mM. (B) Plot of log (dF/F) against log [Q]. λex = 285 nm and λem = 360 nm.(C) Stern-Volmer plots of HSA-piperine complexes showing fluorescence quenching constant (Kq) and plot of Fo/F against [Q] for piperine.

The quenching constant (Kq) for piperine is calculated (Fig. 3.14) to be 6.9×10^{13} $M^{-1}s^{-1}$. As this value is much greater than the maximum collisional quenching

constant $2.0 \times 10^{10}\ M^{-1}\ s^{-1}$ (Agudelo et al., 2012; Zhang et al., 2012) hence the static quenching mechanism is predominant in these HSA-Piperine complex. From this equation, the plotted results indicated a good linear relationship. The number of piperine molecule binding to HSA was calculated to be 1.2 suggesting that HSA interacts with piperine in a close relationship of one- to-one ratio (Fig. 3.14). The binding constants of piperine were calculated from the intercept as $5.7 \times 10^{5}\ M^{-1}$ which indicates strong binding of piperine to HSA. There is a good correlation with the computational calculated binding constant as $3.3 \times 10^{5}\ M^{-1}$ obtained as lowest free energy. Thus, the calculated free energy change is -7.8 kcal M^{-1} at 25 °C. I have also calculated the free energy (-6.8 kcal M^{-1}) from computational modeling and results are in agreement with the experimental data. Here, the lower free energy value is mainly due to the hydrophobic interaction of piperine binding to HSA.

Displacement Studies of PIP binding to HSA

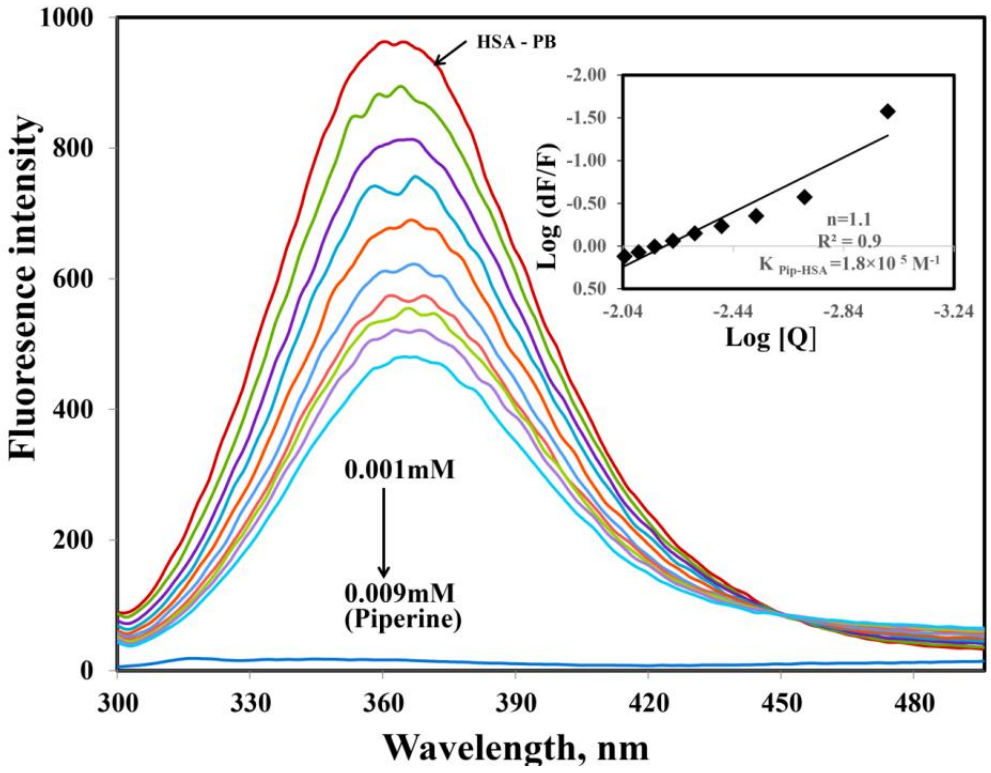

Fig. 3.15. Displacement of phenylbutazone from HSA-phenylbutazone complex by piperine. Phenylbutazone is referred as a site-I probe. The concentrations of HSA and phenylbutazone were maintained constant at a concentration of 1µM whereas, the piperine was varied from 0 to 9 µM. Inset Modified Stern-Volmer plot. Plot of log (dF/F) against log [Q] λex = 285 nm, λem = 360 nm.

The titration of the different concentration of piperine to HSA- phenylbutazone showed the decrease in the fluorescence emission as the piperine replaces the phenylbutazone. Further, the binding constant values obtained for this displaced fluorescence quenching of piperine + HSA-phenylbutazone found to be 1.8×10^5 M^{-1} which is closely correlated with the HSA-piperine complexes 5.7×10^5 M^{-1} (Fig. 3.14). Thus the observed emission of HSA- phenylbutazone was decreased upon increasing the concentration of piperine which reveals that there is competition between the piperine and phenylbutazone for the site I subdomain of HSA. I have also performed the experiments with another site-specific markers like lidocaine, ibuprofen for subdomain IB and site II probe. However, the binding constants are not close to the value which was obtained from HSA-piperine complex, indicate that there is no competition between the piperine with lidocaine and ibuprofen (Fig. 3.15)**.** Thus, the experimental evidence indicates that the piperine is specifically bound to the site I domain.

3.2.B.5 7-Hydroxy Coumarin Derivatives (7HC-1, 7HC-2, and 7HC-3)

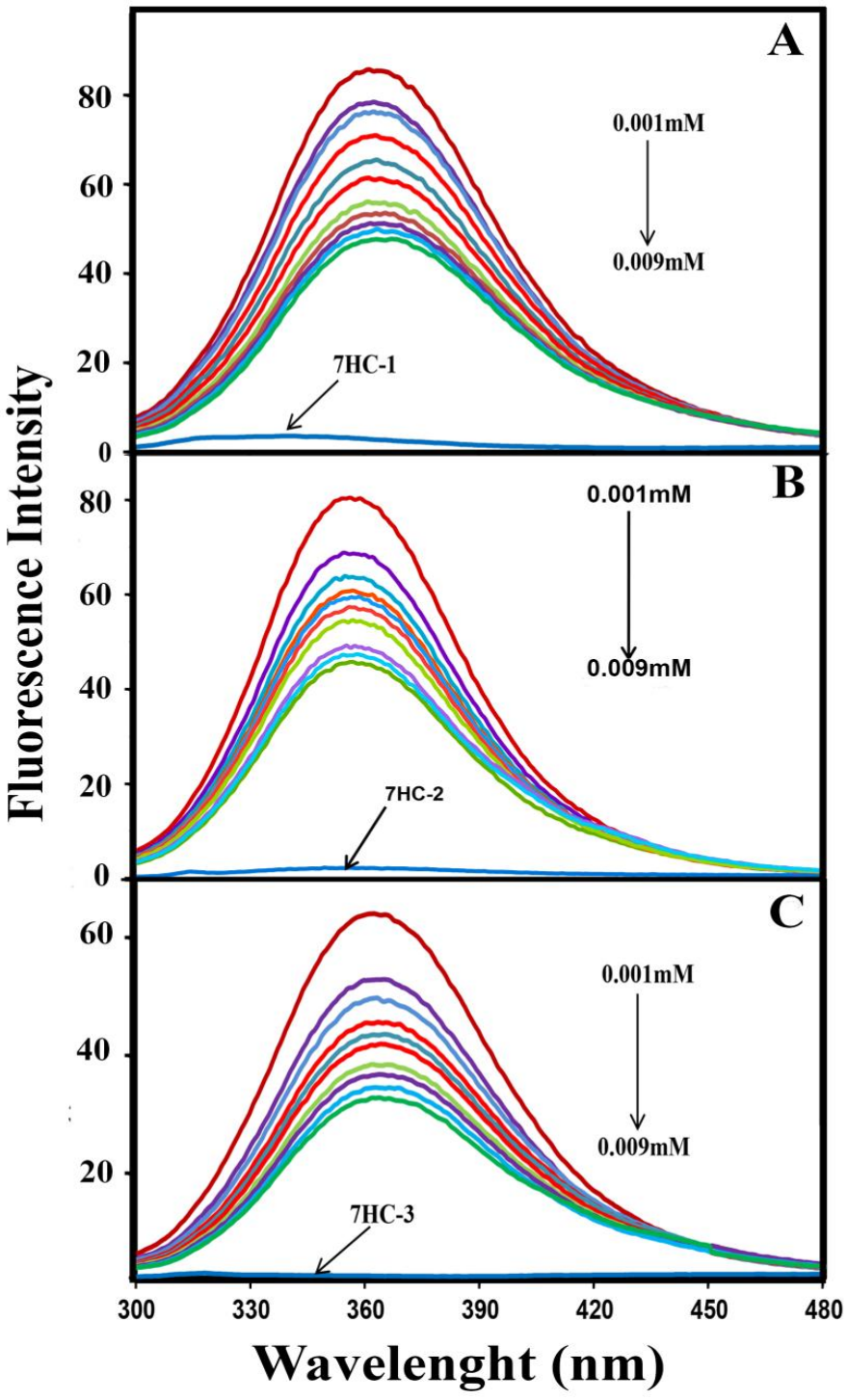

Fig.3.16. Room temperature fluorescence emission spectra were recorded on Perkin Elmer LS55 fluorescence spectrometer for coumarin derivatives (7HC-1(A), 2(B) and 3(C)). The slit width for both excitation and emission were 5 nm. Three independent experiments were carried out and each time identical spectra were obtained.

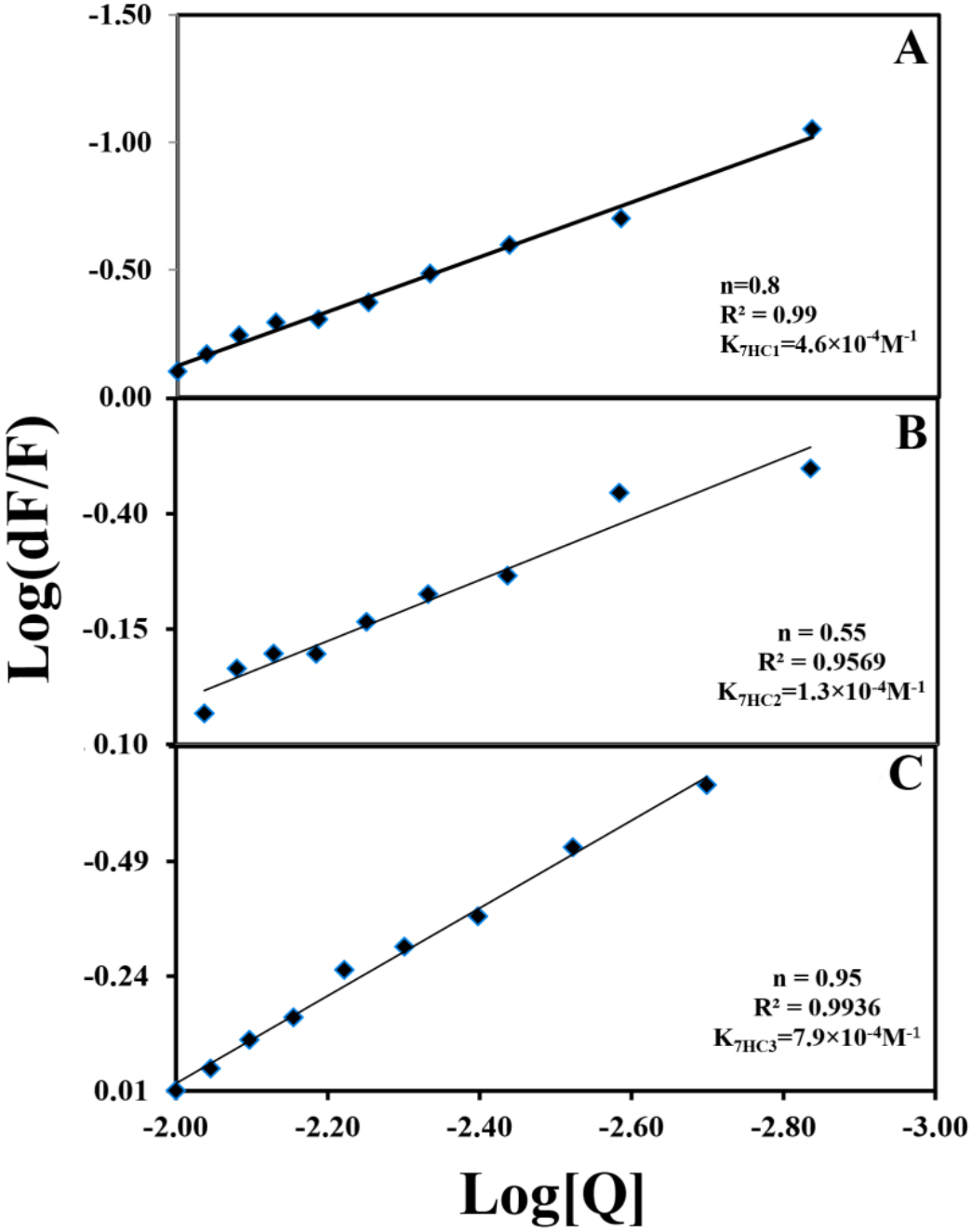

Fig. 3.17. Modified Stern-Volmerplot. Fluorescence emission spectra of HSA–Coumarin derivatives (7HC-1(A), 7HC-2(B) & 7HC-3(C)) in 0.1mM phosphate buffer pH 7.4, λex = 285 nm, temperature = 25^{o}C. Plot of log(dF/F) against log [Q]λex = 285 nm, λem = 360 nm.

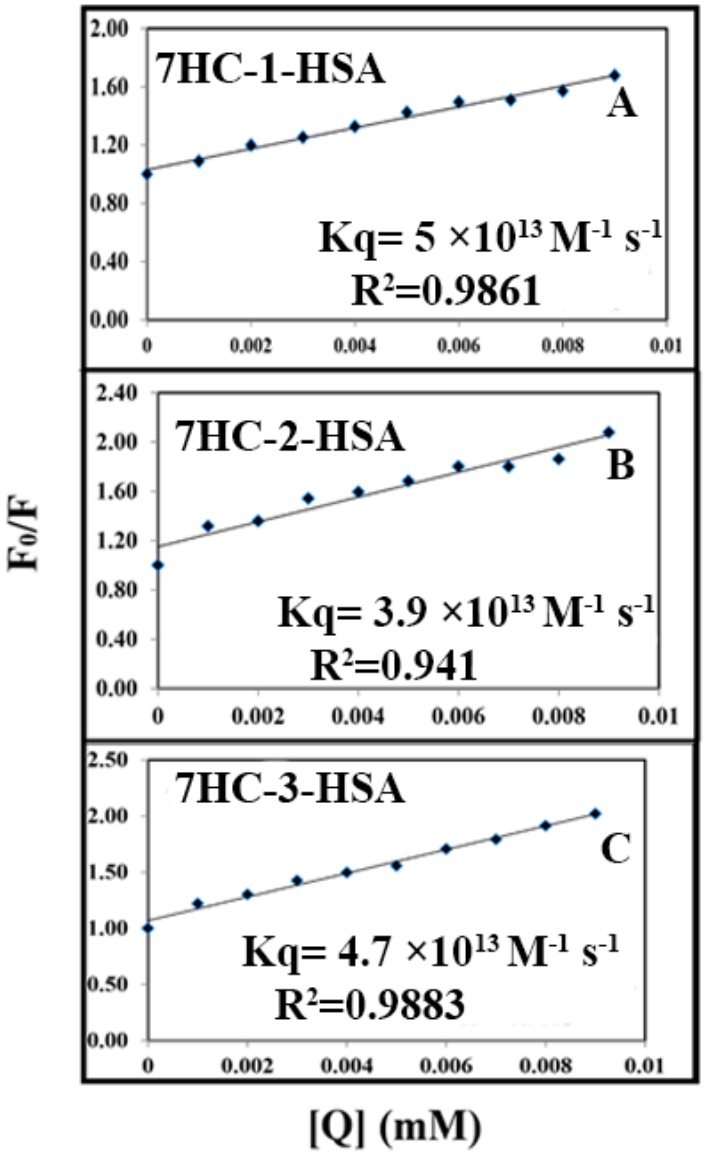

Fig. 3.18. Stern-Volmer plots of fluorescence quenching constant (Kq) for the Coumarin derivatives-HSA complexes at different drug concentrations (A) 7HC-1-HSA and (B) 7HC-2-SA and (C) 7HC-3-HSA.

The number of binding ligands was calculated to be 0.89, 0.53 and 0.9 for 7-hydroxy coumarin derivatives (7HC-1, 7HC-2 and 7HC-3) suggesting that HSA interacts with different coumarin derivatives in a one-to-one ratio (Fig. 3.16 and 3.17). The binding constants of coumarin derivatives (7HC-1, 7HC-2 and 7HC-3) were calculated from the intercept as 4.6×10^4 M^{-1},1.3×10^4 M^{-1} and 7.9×10^4 M^{-1} respectively, which indicates strong binding of these derivatives to HSA. It also has good correlations with the computationally calculated binding constants as $5.9\pm0.01\times10^4$, $9\pm0.01\times10^4$, and

$5.2\pm0.01\times10^4$ M^{-1}, respectively for 7HC-1, 7HC-2 and 7HC-3, obtained as lowest free energy. The quenching constants (Kq) were calculated to be 5×10^{13} M^{-1} s^{-1} for 7HC-1-HSA and 3.9×10^{13} M^{-1} s^{-1} for 7HC-2-HSA and 4.7×10^{13} M^{-1} s^{-1} for 7HC-3-HSA, respectively (Fig. 3.18). Since these values obtained were far greater than the maximum collisional quenching constant ($2.0\times10^{10}M^{-1}s^{-1}$), (Agudelo et al., 2012; Zhang et al., 2012) thus the static quenching is prevailing in these coumarin derivative-protein complexes. It is known that binding constant obtained from fluorescence emission can be used to calculate the free energy and also different binding interactions like hydrogen bonds, hydrophobic, van der Waals forces, and electrostatic interactions. Thus, the free energy change calculated upon binding of coumarin derivatives (7HC-1, 7HC-2 and 7HC-3) to HSA were -6.34,-5.58, -6.65 Kcal M^{-1} respectively, at 25 ºC. This indicates that the free energy of HSA-7HC derivative complexes is derived mainly from hydrophobic and possibly hydrogen bond interactions. Interestingly, the computationally calculated free energy is also closely matching to the experimental values which are -6.15, -5.65 and -6.31 Kcal $M^{-1}$of 7HC-1, 7HC-2 and 7HC-3 upon binding to HSA at 25 ºC.

Displacement Studies of 7HC-1, 7HC-2 and 7HC-3 binding to HSA

The intensity of HSA-site probe was recorded with the increasing concentrations of coumarin derivatives and the comparable results were shown in (Fig. 3.19). Interesting, titration of different concentration of 7HC-1, 7HC-2 and 7HC-3 to ibuprofen-HSA showed quenching the fluorescence emission. The binding constant values obtained for coumarin derivatives (7HC-1,7HC-2 and 7HC-3)-HSA were noticed to be 3.8×10^4 M^{-1}, 1.7×10^4 M^{-1} and 1.3×10^4 M^{-1} in the presence of ibuprofen which is closely matching to the HSA-7HC-1,7HC-2 and 7HC-3 experimental values found to be, $K_{7HC-1} = 4.6x10^4$ M^{-1} , $K_{7HC-2} = 1.3x10^4$ M^{-1} and $K_{7HC-3} = 7.9x10^4$ M^{-1}, respectively. Hence the observed fluorescence emission of coumarin derivatives (7HC-1,7HC-2 and 7HC-3)- HSA reduced considerably in the presence of ibuprofen which indicates that there is competition between coumarin derivatives and ibuprofen for site II subdomain of HSA. In the presence of phenyl butazone which is a site I probe have no compelling effects were observed (Kalanur et al., 2010).

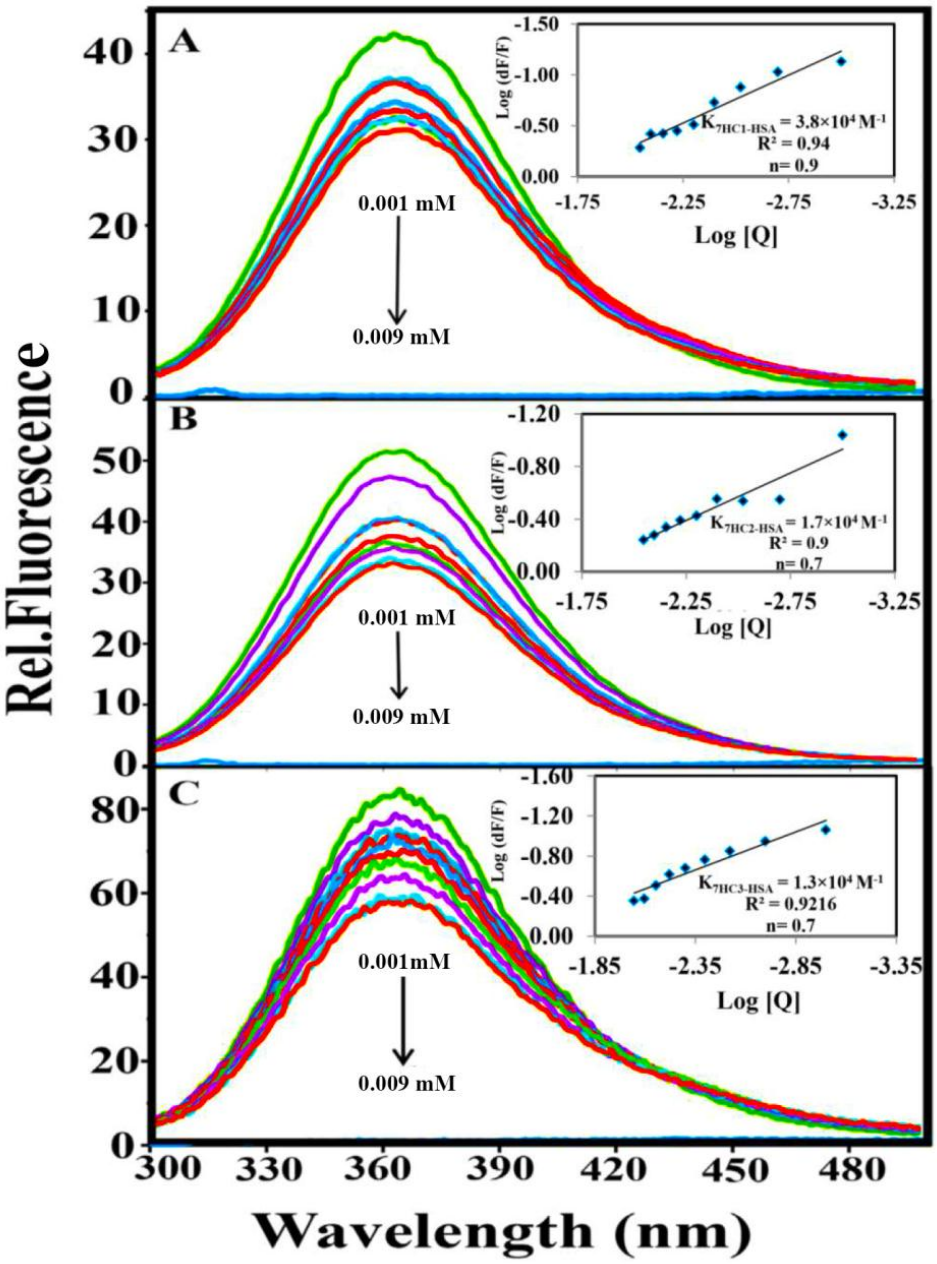

Fig. 3.19. Displacement of ibuprofen from HSA-ibuprofen complex by coumarin derivatives (7HC-1(A), 7HC-2(B) & 7HC-3(C)). Fluorescence emission spectra were recorded on Perkin Elmer LS55 fluorescence spectrometer for coumarin derivatives (7HC-1, 2 and 3)-HSA in the presence of site probe. In this, ibuprofen is referred to site probe. The concentrations of HSA and site probe were maintained constant at a concentration of 1µM whereas, the coumarin derivatives (7HC-1, 2 and 3) was varied 0.001mM-0.009mM. Inset Modified Stern-Volmer plot. Fluorescence emission spectra of coumarin derivatives (7HC-1(A), 7HC-2(B) & 7HC-3(C))-HSA in the presence of site probe. Plot of log (dF/F) against log [Q]λex = 285 nm, λem = 360 nm.

3.2.B.6 Novel 8-substituted Coumarin Derivatives

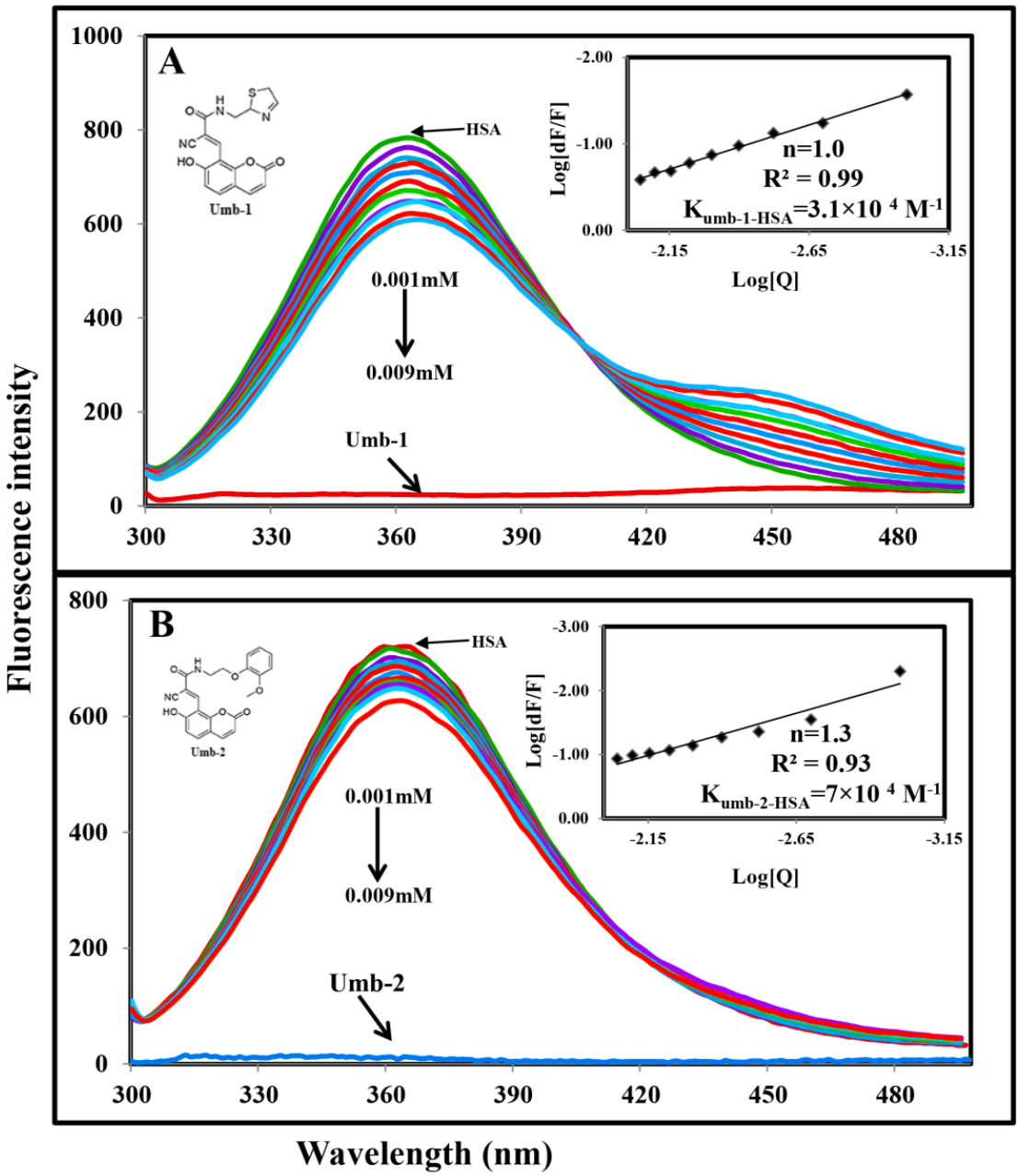

Fig. 3.20. Fluorescence emission spectra of HSA-Umb-1(A) and Umb-2(B) in 0.1 M phosphate buffer pH 7.4, λex = 285 nm, temperature 25 °C. (A) Free AGP (0.001 mM) and free HSA with different concentrations of Umb-1(0.001 to 0.009mM mM). Inset: Modified Stern-Volmer plot. Fluorescence emission spectra of HSA–Umb-1 and Umb-2, 10 mM phosphate buffer pH 7.4, λex = 285 nm, temperature = 25 °C. Plot of log (dF/F) against log [Q]λex = 285 nm, λem = 340 nm.

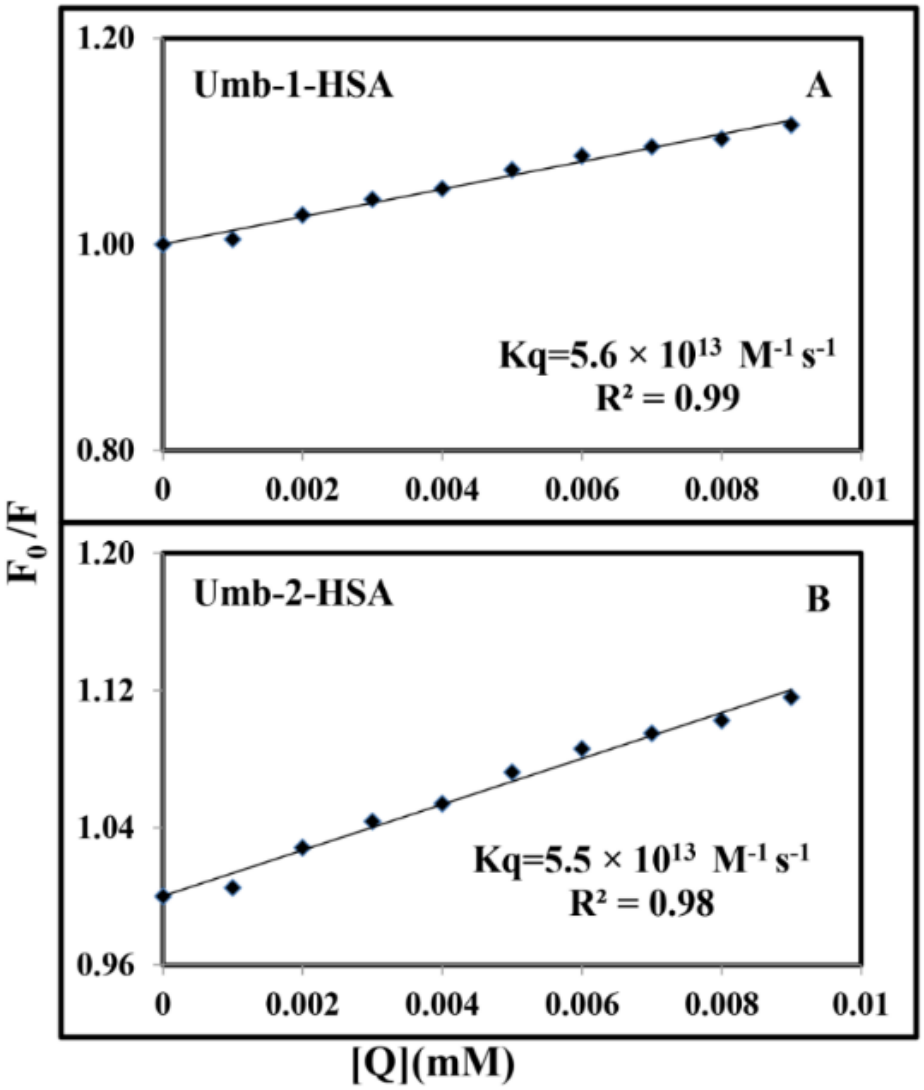

Fig. 3.21. Stern-Volmer plots of fluorescence quenching constants (Kq) for the Umb-coumarin derivative-HSA complexes at different ligand concentrations to determine static and dynamic quenching. (A) Umb-1-HSA and (B) Umb-2-HSA.

Binding constant obtained from fluorescence emission data was found to be $K_{umb\text{-}1}$ = 3.1± 0.01×10^4 M^{-1}, $K_{umb\text{-}2}$ = 7 ± 0.01×10^4 M^{-1}, which corresponds to -6.1 kcal/mol and -6.5 kcal/mol of free energy for Umb-1 and Umb-2, respectively, suggesting that these derivatives bind strongly to HSA. From the stern-volmer equation, the quenching constants (k_q) were calculated to be 5.6 ×10^{13} M^{-1} s^{-1} for Umb-1-HSA and 5.5 ×10^{13} M^{-1} s^{-1} for Umb-2-HSA, respectively (Fig. 3.20 and Fig. 3.21). Since these values obtained were greater than the maximum collisional quenching constant (2.0×10^{10} M^{-1} s^{-1}) (Agudelo et al., 2012; Zhang et al., 2012) and thus the static quenching is prevailing in these Umb-coumarin derivative-HSA complexes.

Energy transfer from HSA to 8-substituted Coumarin Derivatives

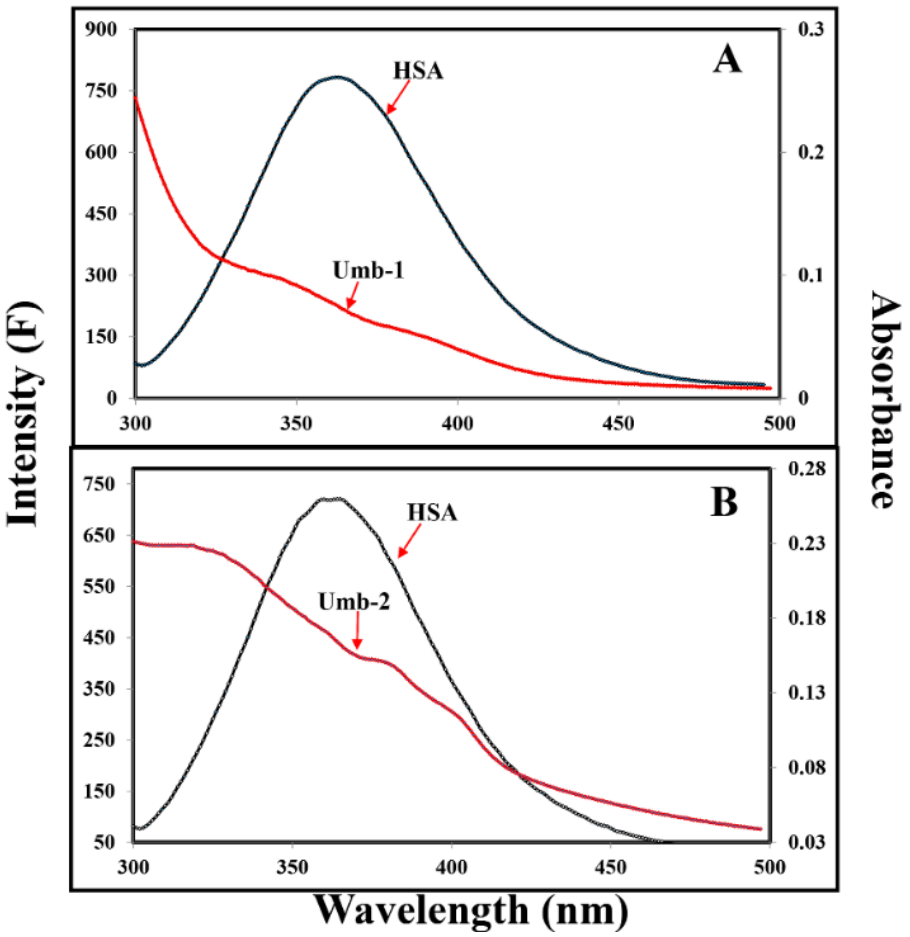

Fig. 3.22. Overlap of fluorescence emission HSA (A) and (B) with absorption spectra of Umb-1(A) and Umb-2(B) at room temperature.

From the Fösters theory, I was able to calculate that J= 7.53×10^{-15}, $2.06\times10^{-16}$$Cm^3$ L mol^{-1}, R_0=2.48, 1.36 nm, E=0.20, 0.10 and r = 1.14, 1.29 nm for HSA. Finally, the values of r were obtained by using equation 5 and were found to be 1.14 and 1.29nm for umb-1-HSA and umb-2-HSA, respectively. The donor-acceptor distance, r < 8nm (Fig. 3.22) (Hu et al., 2004; Valeur & Brochon 2012) indicates that energy transfer from HSA to umb-coumarin derivatives occurs with high possibility.

Displacement studies of Umb-1 and Umb-2 binding to HSA

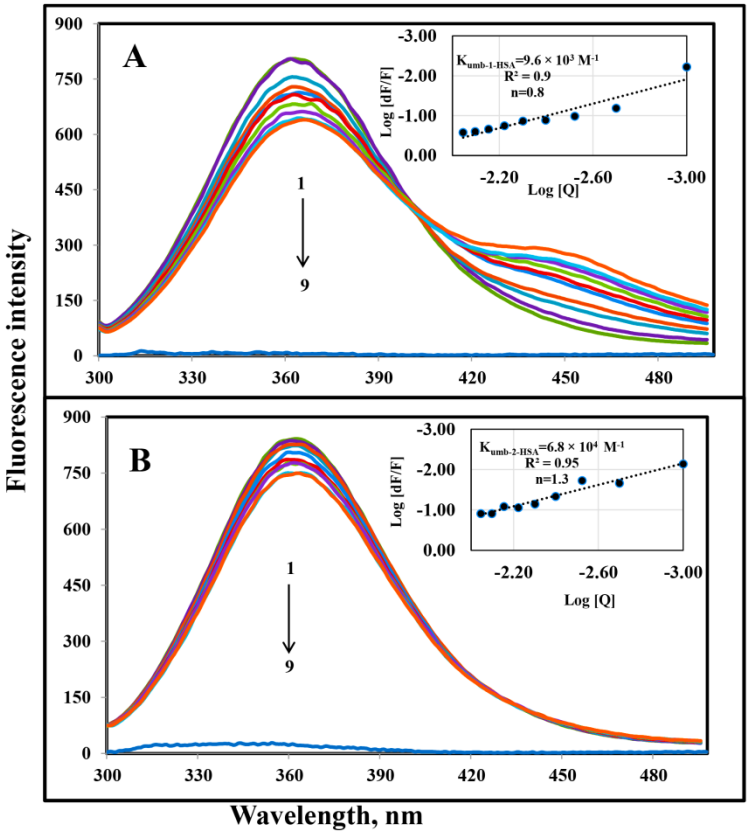

Fig. 3.23. Displacement experiment of ibuprofen from HSA- ibuprofen complex by umb coumarin derivatives (Umb-1 and 2)**.** HSA (Umb-1(A) and Umb-2(B) in the presence of site probe. Phenylbutazone is referred as site-I probe Ibuprofen is referred as a site-II probe. The concentrations of HSA and site probe were maintained constant at a concentration of 1:1 µM whereas, the Umb coumarin derivatives (Umb-1(A) and Umb-2(B)) was varied: 1-9 µM. Inset Modified Stern-Volmer plot. Fluorescence emission spectra of Umb derivatives (Umb-1 and Umb-2)-HSA in the presence of site probe. Plot of log (dF/F) against log [Q]λex = 285 nm, λem = 360 nm.

The binding constant of the Umb-1- HSA system is ~9.3± .02 × 10^3 (lidocaine), 4.8 ± 0.01× 10^5 (phenylbutazone) and 9.6 ± 0.02×10^3 (ibuprofen) respectively. The binding constants in the presence of ibuprofen is near than that of HSA+Umb-1, whereas in the presence of lidocaine and phenylbutazone the binding constants are insignificant which indicates that Umb-1 have displaced ibuprofen from the binding site, thus the displacement measurement confirms that the Umb-1 is bound to Sudlow's Site II of HSA (Fig. 3.23). Whereas in the case of other Umb-coumarin derivative (umb-2) the binding constant of different site-specific markers is ~7.9 ± 0.02 × 10^3 (lidocaine), 1.9 ± 0.02× 10^4 (phenylbutazone) and 6.8 ± 0.01× 10^4 (ibuprofen) respectively. The binding constants with the presence of ibuprofen are closer than that of HSA+Umb-2, whereas binding constants in presence of other site-specific markers

like lidocaine and phenylbutazone are insignificant which indicates that Umb-2 have displaced ibuprofen from the binding site.Thus the displacement measurement confirms that the Umb-2 is bound to Sudlow's Site II of HSA (Fig. 3.23). It is not surprising that both Umb-1 and Umb-2 bind to HSA in Sudlow's site II only and thus, binding of Umb-1 and 2 to the same site of HSA which is expected because of similar structure prevails to the Umb. Therefore, I have even observed similar results for our synthesized 7-hydroxy coumarin derivatives which emphasize that the binding of synthesized coumarin derivatives to IIIB sub-domain which may influence the displacement of site-specific marker ibuprofen from site II (Yeggoni et al., 2014a).

Table. 3.4. Showing *in vitro* binding constants free energy constants, number of binding sites and Biomolecular quenching constant

S.No	Drug	Binding Constants(M^{-1})	Free energy (ΔG^0) (Kcal/mol)	Number of Binding sites(n)	Quenching constant ($(Kq)s^{-1}\ M^{-1}$)
1	Artemisinin	5.5×10^4	-6.4	1	5.2×10^{13}
2	Ar-tumarone	5.6×10^3	-5.0	1	4.0×10^{13}
3	Apocynin	1.87×10^4	-5.8	1	5.5×10^{13}
4	Andrographalide	1.85×10^4	-5.79	1	4.12×10^{13}
5	Bacosine	2.97×10^4	-6.07	1	5.7×10^{13}
6	Corilagin	4.2×10^5	-7.6	1	4.2×10^{13}
7	Chebulinic acid	1.2×10^5	-6.9	1	3.3×10^{13}
8	Chebulagic acid	3.7×10^5	-7.4	1	3.5×10^{13}
9	DeAndrographalide	1.2×10^4	-5.5	1	7.6×10^{13}
10	deForskolin	1.7×10^4	-5.7	1	5.5×10^{13}
11	Embelin	5.9×10^4	-6.30	1	4.0×10^{13}
12	L-dopa	1.8×10^4	-5.48	1	6.5×10^{13}
13	Menthol	2.7×10^4	-6.02	1	5.4×10^{13}
14	Piperine	3×10^4	-6.09	1	6.9×10^{13}
15	psoralen	2.2×10^5	-7.2	1	5.5×10^{13}
16	Pterostiblene	3.9×10^4	-6..2	1	4.9×10^{13}
17	Rosmaric Acid	2.64×10^4	-6.0	1	6.0×10^{13}
18	Stigmasterol	1.8×10^5	-7.1	1	5.6×10^{13}
19	6-shagoal	2.24×10^4	-5.90	1	6.4×10^{13}
20	Umb-1	3.1×10^4	-6.1	1	5.6×10^{13}
	Umb-2	7.1×10^3	-6.9	1	5.5×10^{13}
21	7HC-1	4.6×10^4	-6.3	1	5.0×10^{13}
	7HC-2	3.1×10^4	-5.5	1	3.9×10^{13}
	7HC-3	7.9×10^4	-6.65	1	4.7×10^{13}

3.2.C Study of Protein Conformational Changes of Plasma Protein with Bioactive Compounds using Circular Dichroism

Circular dichroism (CD) spectroscopy is an extraordinarily sensitive technique to monitor the secondary structural conformational changes in the protein. The change in CD spectra of HSA may deduce that there must be a conformational change in HSA. CD is the differential absorption of left- and right-handed circularly polarized light by a substance. The biological molecules exhibit their dextrorotary and levorotary in nature which can be observed from CD. The most important thing is even a secondary structure will also impart a distinct CD to its respective molecules. Therefore, the α-helix of proteins and the double helix of nucleic acids have CD spectral signatures representative of their structures. Secondary structure can be determined by CD spectroscopy in the "far-uv" spectral region (190-250 nm). The protein CD spectra in the "near-uv" spectral region between 250-350 nm can be subtle to the tertiary structure. At these wavelengths, the chromophores are the aromatic amino acids and disulfide bonds, and the CD signals they produce are sensitive to the overall tertiary structure of the protein. Signals in the region from 250-270, 270-290 and 280-300 nm are attributable to phenylalanine, tyrosine and tryptophan residues. Disulfide bonds give rise to broad weak signals throughout the near UV-spectrum.

The amide chromophore of the peptide bond dominates the CD spectra of proteins below 250 nm. Amides have 2 electronic transitions of low energy that are well characterized with transitions n-π^* and π_o- π^* showing circular dichroism at 215-230 nm and 185–200 nm, respectively (Woody & Koslowski 2002; Correcirc & Ramos 2009). In my study I determined the percentage of α-helix, β-sheets, and random coils of HSA upon interaction of bioactive compounds to elucidate the effect on the secondary structure. I used CDNN v.2.1 software (Poschner et al., 2007) for the determination of secondary structural elements.

3.2.C.1 Results and Discussion

Fig. 3.24-3.32 shows the circular dichroism spectra of HSA in presence and absence of bioactive compounds. The influence of bioactive compounds (back ground noise) was eliminated by using corresponding concentration of bioactive compounds as reference solution during the measurement. As can be seen from the Fig. 3.24 -3.32, HSA has

two absorption peaks at 208 and 222 nm, these peaks are originated from α-helix in the protein (Corrêa & Ramos, 2009). The addition of bioactive compounds to HSA resulted in a decrease of absorbance intensity at 208 nm and a subtle change at 222 nm, which indicated a decrease in the α-helix with an increase in the β-sheets and random coils, induced by a specific interaction between bioactive compounds and HSA. It is clearly evident from all graphs that two transitions at far-UV (<240 nm) in the negative bands between 190 -250 nm of HSA alone with respect to each compound (see Fig.3.24-3.32). This indicates that after complexation of HSA-bioactive compounds, there is unfolding of HSA secondary structure.

That is the reason why there is a decrease in the α-helix accompanied by an increase in the β-sheets and random coils. Similar phenomenon were reported with HSA from our group (Subramanyam et al., 2009 a & b;Garg et al., 2013; Yeggoni et al., 2014a) and other groups with different pharmaceutically important drugs (Maiti, et al., 2008; Agudelo et al., 2012; Roy et al., 2012). Interestingly it is observed that few compounds showed less conformational changes with high affinity and vice versa, this might be due to the orientation, structural complexity and hindrance of the drugs which may induce more or less conformational changes with reciprocal binding affinities. The details of conformational changes of individual bioactive compounds with HSA are discussed as follows.

3.2.C.1.a Andrographolide (ANDR)

Circular Dichroism Spectra of HSA and ANDR Complexes

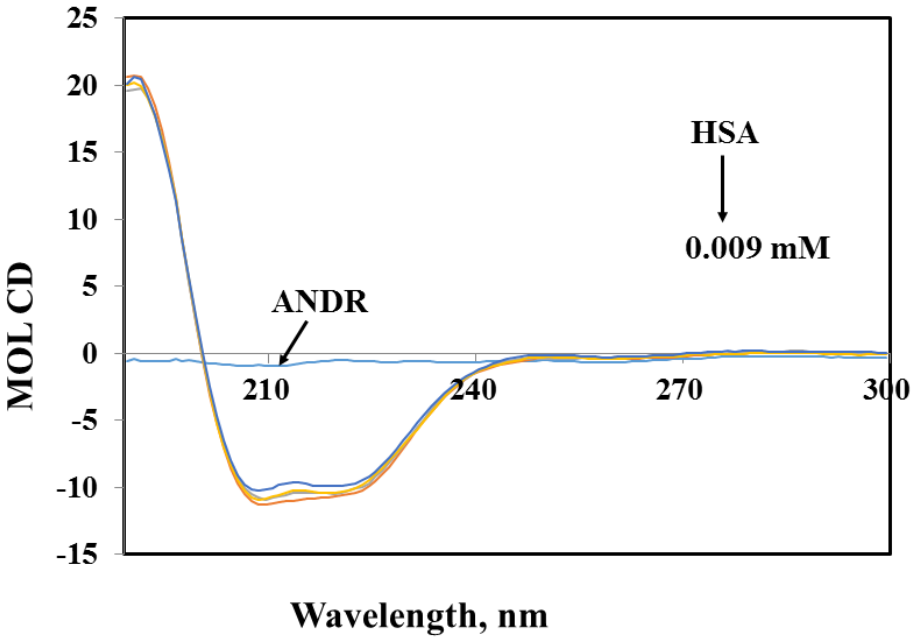

Fig. 3.24. Circular dichroism of the free HSA and HSA-ANDR complexes. The free HSA and HSA-ANDR complexes in PBSwith a protein concentration of 0.001 mM and ANDR concentrations were 0.001, 0.005 and 0.009 mM.

Table.3.5. Percentage of the secondary structure of HSA and HSA-ANDR complex. Mean SE ± (n=3)

Secondary structure (%)	HSA	HSA-0.001 (mM)	HSA- 0.005 (mM)	HSA- 0.009 (mM)
α–Helix %	56.0±2.5	56.4±2.5	54.8±2.3	50.9±2.25
β-Turn%	25.6±0.62	25±0.62	26±0.62	29.4±0.74
Random coil %	18.4±0.82	18.6±0.82	19.2±0.83	19.7±0.84

The percent of each portion of secondary structural elements of HSA-ANDR complex was evaluated. The addition of increased concentration of ANDR to HSA, the CD-spectral behavior changes marginally (Fig. 3.24). There were changes in α-helix, β-sheet, and random coil content, as ANDR concentration increases. The free HSA contains 56.0 ± 2.5% α-helix, 25.6 ± 0.62% β-sheet and 18.4 ± 0.82% random coil (see Table 3.5). After addition of ANDR gradually from 0.001 to 0.009mM, the α-helical content decreased to 50.9 ± 2.25%. While the percentage of β-sheet and random coil content increased to 29.4 ± 0.74% and 19.7±0.84%, respectively. It is clearly evident that only a marginal decrease in the negative ellipticity in the region of far- UV CD without any significant shift of peaks.

The similarity between the CD spectra of free HSA and HSA-ANDR suggested the structure of HSA was also predominantly α-helix (Table 3.5) indicating that the binding of the drug to HSA induced a slight decrease in the α-helical structure content of the protein with a minor increase in the β-sheets and random coils. The changes in α-helix of HSA indicated that the ANDR might have bound with the amino acid residues present in the HSA polypeptide chain and destroyed the hydrogen bonding networks (Cheng et al., 2009). This might, in turn, exerted a change in the secondary structure of the HSA. The CD spectroscopy revealed the conformational changes on the HSA due to the change in the physiological environment of HSA after the addition of ANDR. Thus, ANDR created a variation in the local environment of HSA and changed the nature of HSA, indicates that the binding of ANDR to HSA induced a slight decrease in the α-helical structure content of the protein with a minor increase in the β-sheets and random coils. Though the binding of ANDR is more (1.85×10^{4} M^{-1}) to HSA, however, the protein conformation is not much observed due to orientation changes upon binding of ANDR to HSA.

3.2.C.1.b Corilagin (COR)

Circular Dichroism Spectra of HSA and Corilagin Complexes

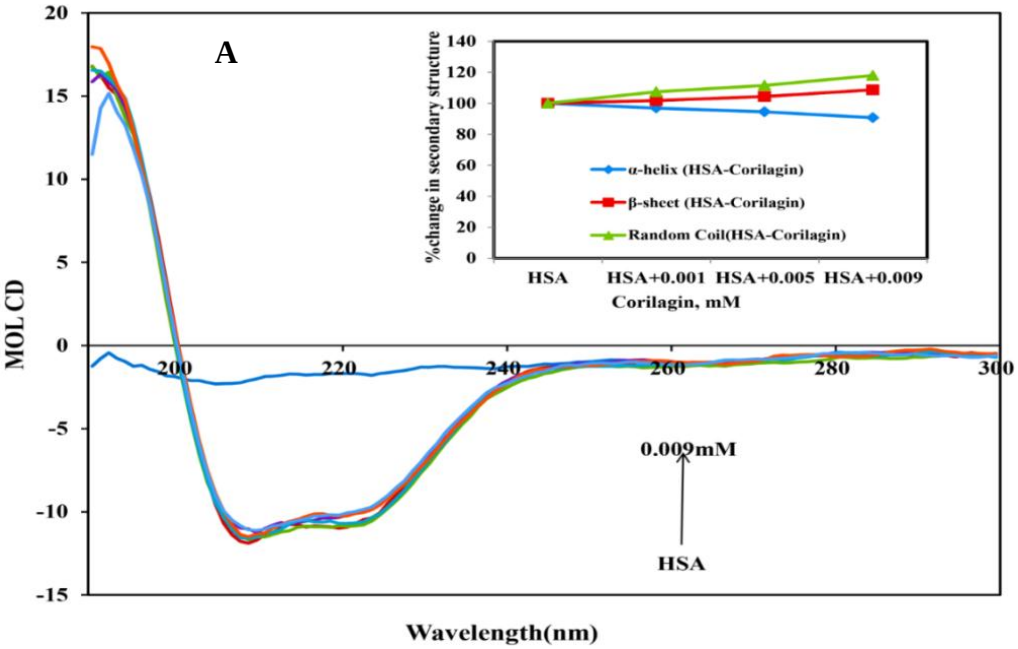

Fig. 3.25.(A)Circular dichroism spectra of free HSA and its corilagin complexes in PBS with a protein concentration of 0.001 mM and corilagin concentrations were 0.001, 0.005 and 0.009 mM. .Inset: The secondary structural changes of HSA and HSA- corilagin, the plot represent the concentration-dependent secondary structural changes of free HSA and HSA- corilagin.

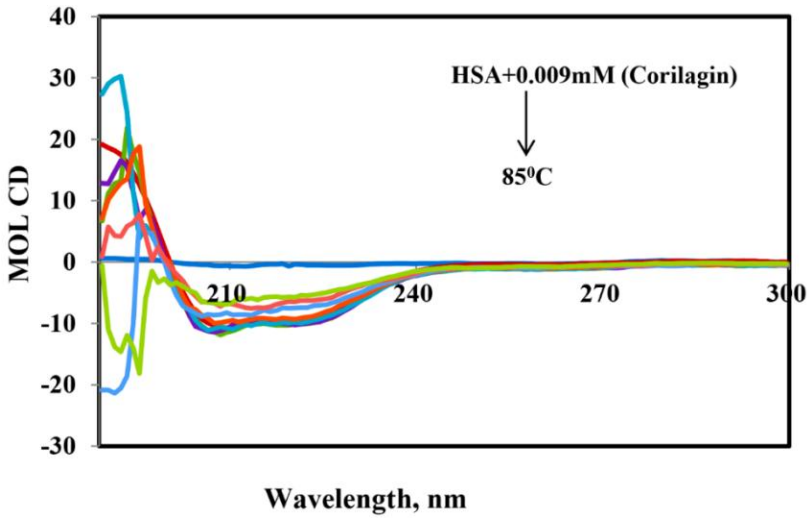

Fig. 3.26. Temperature-dependent CD-Spectra of HSA+COR complexes (25°C to 85°C).

Table.3.6. The Secondary structural study of the HSA alone and its interaction with COR.

Corilagin	**HSA**	**HSA+0.001mM**	**HSA+0.005mM**	**HSA+0.009mM**
α-Helix%	58±2.5	56.2±2.03	54.8±2.04	52.6±1.8
β-Sheet%	23±0.73	23.4±0.6	24 ±0.8	25 ±0.1
Random coils%	19 ±1.0	20.4±0.6	21.2±0.4	22.4±0.8

The data analyzed by web-based software CDNN 2.1

The conformational changes induced by corilagin on the overall structure of HSA and resultant formation of HSA–corilagin complexes. Free HSA has 58% α-helix, 23% β-sheets, and 19 % random coils, which is in agreement with the previous reports (Subramanyam et al., 2009a; Gokara et al., 2010; Yeggoni et al., 2015a). The original crystal structure, however, reported being 67% of the α-helical content (He & Carter 1992), in our study, it was 58%. The differences in α-helical contents could be originated to the different structural arrangements of the protein in the solid state (X-ray structure) and in PBS (CD measurements). However, there was no change in the tertiary structure of HSA when corilagin binds to HSA. The percentages of the secondary structural elements of HSA and corilagin–HSA complex is shown in Table.3.6. A slight decrease in the α-helical content from 58 ± 2.5 to 52.6 ± 1.8 and an increase in the β-turns from 23 ± 0.73 to 25 ±0.1 and random coils from 19 ±1.0 to 22.4±0.8 indicates that the addition of corilagin induced a partial unfolding of the secondary structure of HSA (Fig. 3.25). The partial unfolding may be due to the microenvironment changes within the proximity of tryptophan residue while binding to

corilagin, which was revealed by a decrease in fluorescence emission quenching and AFM data.

Thermal Stability of HSA and HSA-COR Complexes

In order to determine the stability of HSA-corilagin complexes, temperature-dependent CD was carried out for HSA and HSA with 0.009 mM of corilagin, from 25–85 ^{o}C. The secondary structural conformation of a protein is not significantly changed up to 60 ^{o}C in HSA-corilagin complexes (Fig. 3.26). Above 65 ^{o}C, the α-helical content decreased dramatically due to thermal denaturation, while the β-sheets and random coil content increased in both HSA-corilagin complexes. An earlier report showed that the T_m of the HSA alone was around 65 ^{o}C, which shows that the unfolding of protein occurs only after this point. (Gokara et al., 2010) The secondary structural conformation was noticed in corilagin plus HSA complexation (0.009 mM) that the α-helical contents were 52.6±1.8 % and 33.7±2.0%, β-sheets 25±0.73 % and 38.2±1.0%, and random coils 22.4±0.8 % and 28.1±2.0%, respectively, which indicate that there is no release of corilagin from its complexation. Thus this results indicated that even at 60 ^{o}C the HSA-corilagin complex is stable, thus the protein complex is thermodynamically and conformationally stable.

3.2.C.1.c Embelin (EMB) *Circular Dichroism Spectra of HSA and Embelin Complexes*

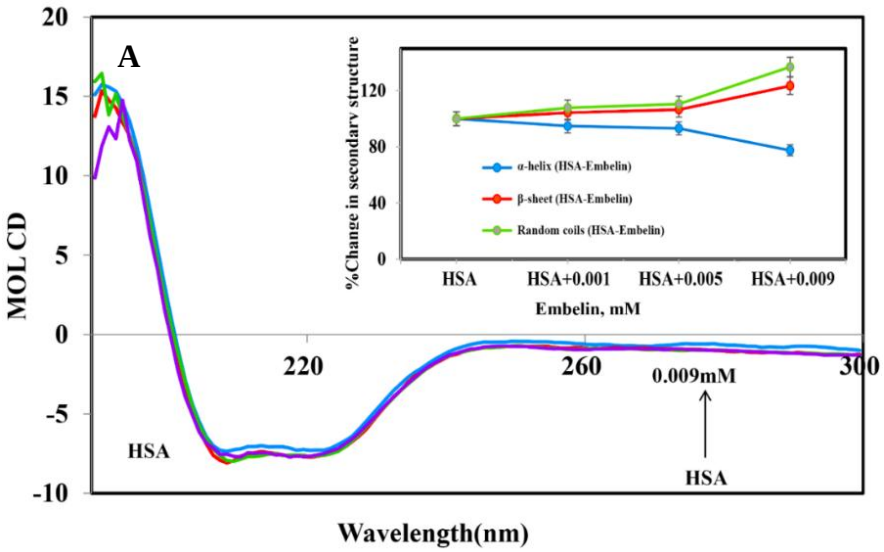

Fig. 3.27. (A) CD spectra of the EMB-HSA complex at different concentrations of drug to HSA ratios at pH 7.4, with a protein concentration of 0.001 mM and EMB concentrations were 0.001- 0.009 mM. Inset: The changes in the secondary structural of HSA and HSA-EMB, the plot represent the concentration-dependent secondary structural changes of free HSA and HSA- EMB.

Table.3.7. The Secondary structural study of the HSA alone and its interaction with EMB.

	HSA	HSA+0.001mM	HSA+0.005mM	HSA+0.009mM
α-Helix%	58±2.3	55±2.0	54±2.2	45.6±1.8
β-Sheet%	23±0.74	24±0.8	25±0.7	28.4±0.2
Random coils%	19±1.0	20.5±0.6	21±0.7	26±0.8

The data analyzed by web-based software CDNN 2.1

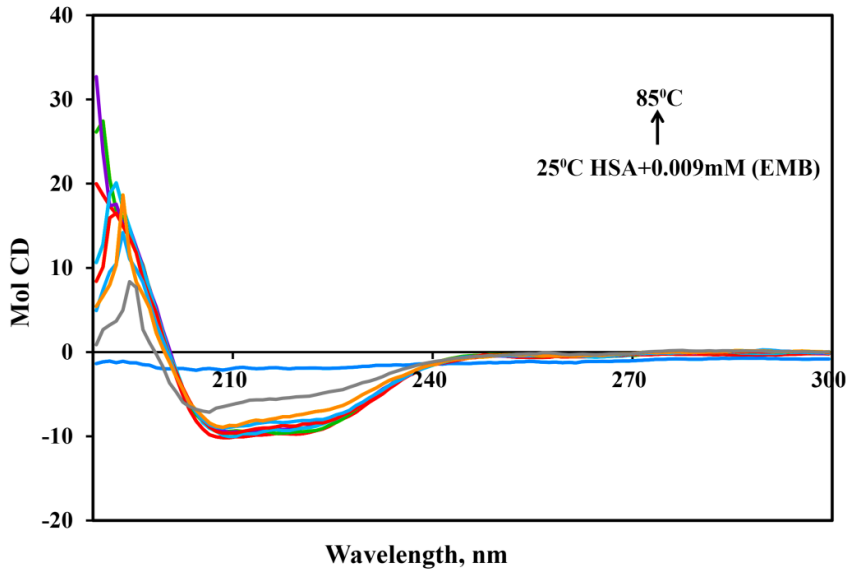

Fig. 3.28. Temperature-dependent CD-Spectra of HSA+EMB complexes (25°C to 85°C).

From the above method it was found that upon complexation of HSA with EMB (0.001, 0.005, 0.009 mM), the α-helical content of the protein decreased from 58±2.3 to 45.6±1.8% with an increase in β-sheets from 23±0.74 to 28.4±0.2%, and random coils 19±1.0 to 26±0.8%, respectively (Table 3.7). The results indicate that there is a partial change in the secondary structure of protein upon binding to EMB. The conformational changes may be due to local rearrangement of secondary structural elements, also, it may lead to the orientation and structural complexity in the protein upon binding of EMB to HSA Fig. 3.27. (Neelam et al., 2010; Sudhamalla et al., 2010). Therefore a decrease in the α-helix is due to the marginal unfolding of the protein which is further supported by the RMSD (from molecular dynamics simulation) of HSA and HSA–EMB complexes, which showed a consistent stability (chapter 4, Fig.4.9B). Furthermore, a decrease in the percentage of β-sheets and random coils an increase in α-helix were observed it is not due to the destabilization of the HSA, which suggested that the binding of EMB to HSA induced unfolding of the polypeptides of protein.

Thus, the conformational changes were synchronizing with the RMSD and Rg data (chapter 4, Fig.4.9B).

Thermal Stability of HSA and HSA-EMB Complexes

The secondary structural conformation was noticed in EMB plus HSA complexation (0.009 mM) that the α-helical contents were 45.6±1.8 and 30±0.8%, β-sheets 28.4±0.2 and 39±1.2%, and random coils 26±0.8 and 31±1.0%, respectively (Fig. 3.12c.ii). These results indicate that there is no release of EMB from its complexation below 60 ^{o}C. Hence, these results confirmed that even at 60 ^{o}C the HSA-EMB complex is stable, thus the HSA-EMB complex is thermodynamically and conformationally stable. From this result, it can be concluded that HSA-EMB complex was functionally stabilized by non-covalent interactions and hence requires high temperature to break down these complexes.

Topography changes observed from Transmission Electron Micrographs

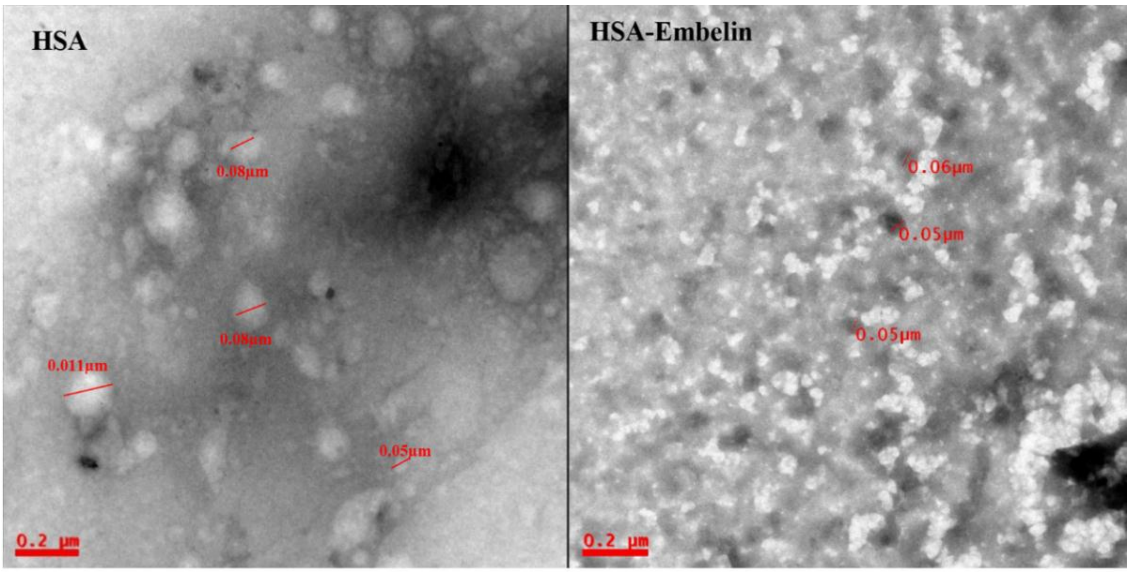

Fig. 3.29. TEM micrographs the morphological feature of HSA alone and HSA-EMB complex at pH 7.4 and 25 °C. The concentration of free HSA and EMB were 0.1 mM and 0.4 mM, respectively.

The electron microscopy is one of the best tools to see the protein topology upon binding of EMB with HSA. Here the mean particle diameter of HSA was 0.08±5µm and majority of them are spherical in shape without any indiscretions. Aqueous solutions of HSA and HSA-EMB complex at pH 7.4 were viewed under transmission electron microscopy (Fig.3.29). Thus results of the TEM images are in

good support in the formation of HSA-EMB complex that the morphology is totally different from that of the free EMB or the free HSA. We have observed that the HSA EMB complexation in terms of aggregation (0.05±5μm) it might be probably because EMB altered the molecular structure of HSA upon interaction. HSA-EMB gets compacted to form hard and thick, which makes the electron beam tough to get through it. Hence distinct configuration of the adsorbed protein was observed compared to the blurred ones of HSA alone in which conforms the binding of EMB on HSA(Zhao et al., 2011; Zhao et al., 2015). Most of the protein aggregate under some special conditions such as pH value, the concentration of the protein solution and ion composition. Moreover, protein stability and protein–protein hydrophobic interaction is an important factor in causing protein aggregation (Privalov & Gill 1988). Furthermore, upon addition, after interacting of EMB with HSA, the local environment around the HSA has become more hydrophobic. To ease the number of unfavorable factors for the formation of a stable structure, the HSA molecule reduces its surface area on contact with water by molecular aggregation. Hence, these results show that a hydrophobic interaction between HSA and EMB may occur. The morphological difference of HSA upon addition of EMB are attributed to slight structural changes of HSA upon complexation. The TEM results are very well supported by the CD data where we can see a decrease in the α-helix and increase in β-sheets and random coils, which specify that protein forms broad aggregate for HSA-EMB complex.

3.2.C.1.d Piperine (PIP)

Circular Dichroism Spectra of HSA and Piperine Complexes

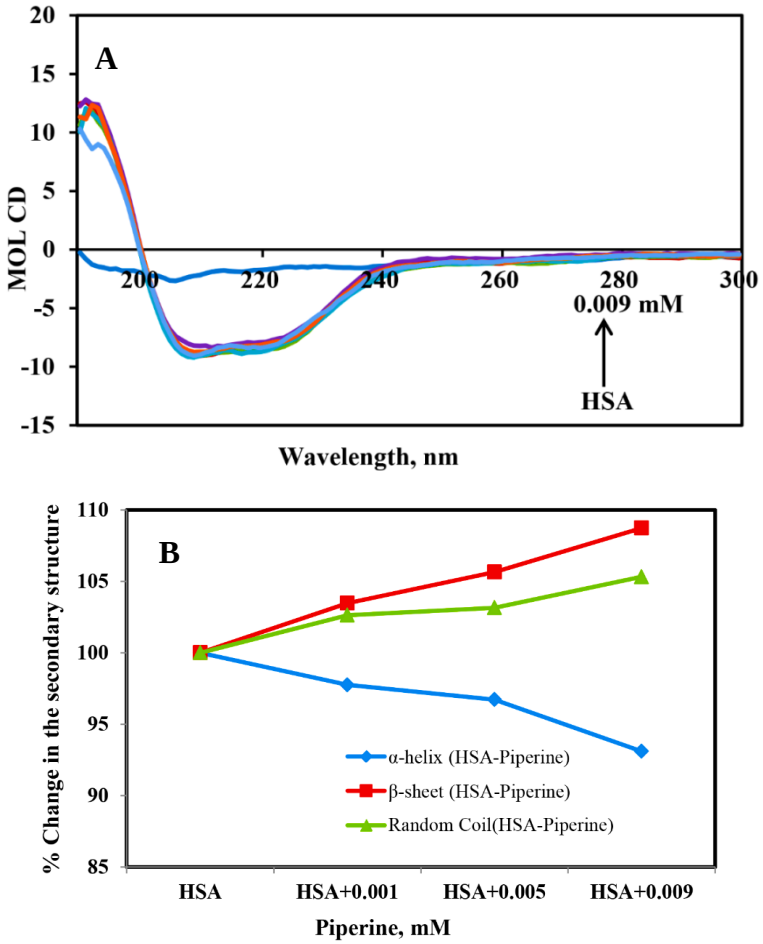

Fig. 3.30 (A) Circular dichroism spectra of free HSA and its piperine complexes in aqueous solution with a protein concentration of 0.001 mM and piperine concentrations were 0.001, 0.005 and 0.009 mM. Inset: The secondary structural changes of HSA and HSA-piperine, the plot represent the concentration-dependent secondary structural changes of free HSA and HSA-piperine.

From this method it was found that upon complexation of HSA with different concentrations of piperine (0.001, 0.005, 0.009 mM), the α-helical content of the protein decreased from 58 to 54% with an increased in β-sheets from 23 to 25 %, and random coils from 19 to 20%, respectively, Therefore, the results suggest that changes in the secondary structural elements arise from the marginal unfolding of HSA upon binding of piperine (Fig.3.30). Earlier reports also indicate that conformational changes occur in HSA upon complexion with ligand (Zsila et al., 2003; Beauchemin et al., 2007; Kanakis et al., 2007; Jiang et al., 2008; Subramanyam et al., 2009; a &b).Thus the protein conformation in our experiment arises due to change in the local structural mobility in the secondary structural elements.

3.2.C.1.e . 7-Hydroxy Coumarin Derivatives (7HC-1, 7HC-2, and 7HC-3)

At low concentrations of 7HC derivatives, there are marginal changes in the secondary structural elements (Fig.3.31), however, there was an apparent change in the secondary structure conformation of protein at high concentration. The proportion of secondary structural elements undergoes marginal variation at low concentrations of 7HC derivatives. However, with the addition of 0.009mM of 7HC derivatives, there was a significant change in the protein conformation. At 0.009 mM concentration, the α-helical stability decreased to ~36.5%, 52% and 46%, while the proportion of β-sheets increased to ~32%, 23.6% and 25.6%, and random coils were increased to 31%, 24, and 28.5%, respectively for 7HC-1, 7HC-2 and 7HC-3 (Fig.3.31). These results have indicated that the secondary structure of HSA became partially disordered due to HSA-7HC derivatives complex formation. The order of conformational changes of α-helix, in the ascending order, follows; 7HC-1>7HC-3>7HC-2 whereas for β-sheets and random coils 7HC-1>7HC-3>7HC-2. This influence the coumarin derivative binding to HSA may be attributed to the difference in the functional groups. Moreover, it is clearly observed that 7HC-2 has less influence than 7HC-3 and 7HC-1 which might be due to the additional phenyl ring. Very recently our group reported that different methyl coumarin derivatives bound to HSA showed similar conformational changes of protein (Garg et al., 2013).

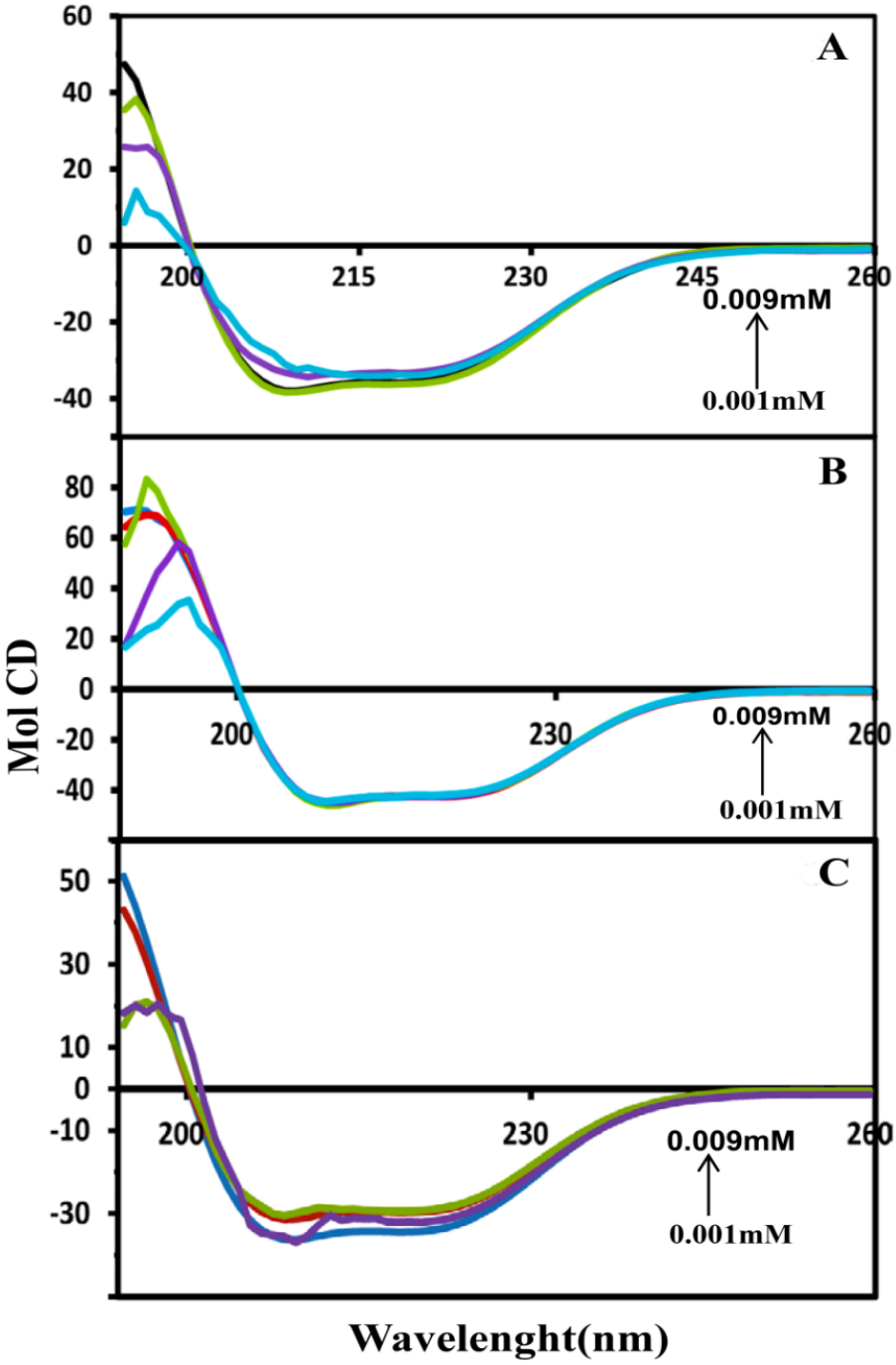

Fig. 3.31. Circular dichorism (CD) spectra of HSA and its complexes with coumarin derivatives (7HC-1(A), 7HC-2(B) & 7HC-3(C)).

3.2.C.1.f Novel 8-substituted Coumarin Derivatives

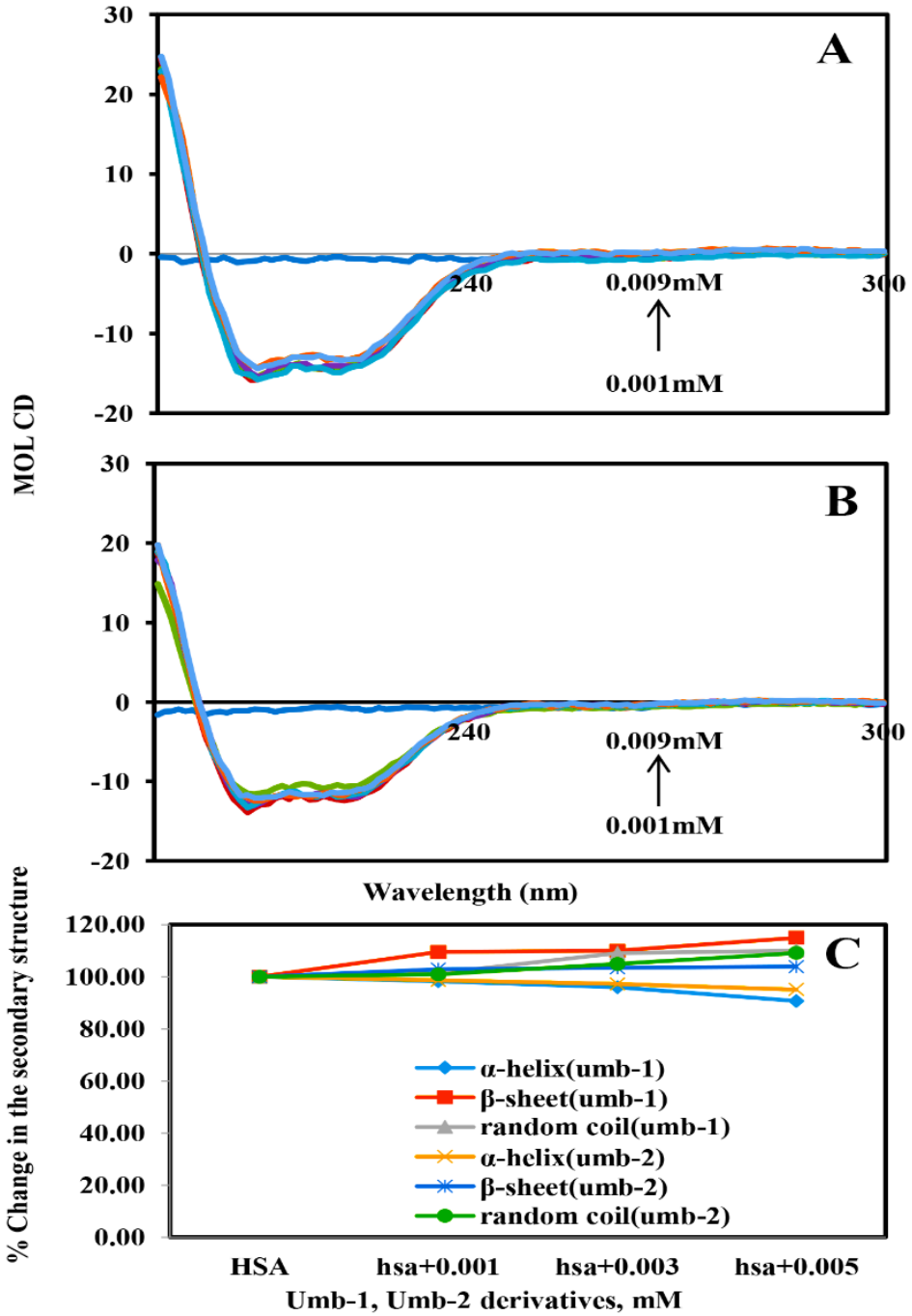

Fig.3.32. CD spectra of free HSA and its Umb-1(A) and Umb-2(B) analogue complexes in aqueous solution with a protein concentration of 0.001mM (1×10^{-6}M) and Umb-1 concentrations of 0.01, 0.005 and 0.009mM. (C)Secondary structure composition calculated. Concentration-dependent secondary structure change for free HSA, HSA-umb-1 complex and HSA-umb-2 complex and secondary structural analysis of HSA and its interaction with umb-1, 2. The data is analyzed by web-based software CDNN 2.1.

In fact, the secondary structural elements undergo marginal variation at low concentrations of Umb-1 and Umb-2 (Fig.3.32) while titrated with HSA. However, with the addition of 0.001 and 0.009 mM of Umb-1 and Umb-2, there was a significant change in protein conformation. At final concentration (0.009mM), the loss of α -helical content is ~52.7 and 54.7%, while the proportion of β -sheets increased to ~23 and ~21%, random coils increased to ~24.3 and ~24.6% respectively for Umb-1 and 2 (Fig.3.32).Thus, upon binding of umb derivatives to HSA, the conformational changes of HSA appears to be partially unfolded. Such unfolding of HSA may be due to orientation changes of the umb derivatives during binding to HSA. The results suggest that due to the binding between umb derivatives and HSA induced a partial unfolding of the protein that contains constitutive polypeptides and resulted in structural changes in HSA, hence the hydrophobic regions that were buried are exposed in increasing manner (Pasban Ziyarat et al., 2014). Also the conformational change in the secondary structure of HSA upon binding of Umb- coumarin derivatives might be due to the difference in functional groups or orientation of Umb- coumarin derivatives. Similar results were observed upon binding of other ligands like coumarin derivatives, 7-hydroxycoumarin derivatives, piperine, and L-dopa & to HSA, thus indicating a major decrease of α -helices and an increase of β -sheets and random coils as well (Garg et al., 2013; Yeggoni, et al., 2014b ;Yeggoni, et al., 2015a). Thus, a conformational change in protein could be a phenomenon of binding of ligand molecules to the proteins.

3.3. Conclusion

The cytotoxicity of the potent bioactive compounds (APO, ANDR, BAC, 7-HC1, 7-HC 2 and 7-HC 3, COR, EMB, PIP, STL, ROS, MEL and 6-SHG) decreased the cell viability of different cell lines in a dose-dependent manner with an IC_{50} see (Fig 3.1) indicating that these compounds are having potent cytotoxic activity and thus, these compounds can be used as therapeutic agent for hepatic diseases. From the binding analysis, it is clearly evident that all the bioactive compounds had a strong ability to quench the intrinsic fluorescence of HSA through a static quenching procedure. Fluorescence studies indicated that the binding constants of all the bioactive compounds in the range of known FDA approved drugs 10^{3}-10^{6} M^{-1}, which is in the agreement with the binding constants of known drugs. All the compounds binds

with HSA in 1:1 ratio indicating that only one molecule is bound with HSA (Table 3.4). Further, thermodynamic studies revealed that all the HSA-bioactive complexes were spontaneous with negative free energy indicated that HSA-bioactive complexes are stable. Nonetheless, docking studies showed that docking conformer is near and consistent with that of free energy and binding values determined by fluorescence studies. Apparently, the displacement studies revealed that bioactive compounds bind within known binding sites i.e., Sudlow site 1, Sudlow site 2 and subdomain IB. Therefore, the location and the nature of interactions based on the docking studies suggest that the decrease in the emission intensity of HSA is due to the complexation of bioactive compounds in subdomains IIA, IIIA, and IB. In addition, the results obtained from my work have shown that bioactive compounds bind with HSA mainly by hydrophobic interactions and for few compounds with hydrogen bond interactions. These results are in concurrence with the free energy calculations obtained from binding constant which was derived from fluorescence quenching.

Further, I have analyzed the secondary structure of HSA with the increasing concentration of bioactive compounds, from which I deduce that at with an increasing concentrations of bioactive compounds the intensities at 208 and 222 nm decreased along with the decrease in the peaks at a wavelength range of 190-210 nm which are characteristics of α-helix, β-sheets, and random coils respectively. The decrease in the percentages of α-helix, increase in β-sheets and random coils is an indication of the interaction of bioactive compounds which lead to the formation of HSA-bioactive complexes, which is very well supported by the strong affinity of bioactive compounds with HSA as reported in the fluorescence studies. From this, it is inferred that formation of HSA-bioactive compounds led to the partial unfolding of HSA secondary structure, specifically, the loss of helical stability (Table 3.8). This indicates that bioactive compounds are strong enough to bind with HSA which may increase the half-life and efficacy for therapeutic action *in vivo*. This study may give an overview of the expanding field of preclinical and clinical drug applications and developments that use albumin as a protein carrier protein to improve the pharmacokinetic profile of the drug or to target the drug to the pathogenic site addressing diseases with unmet medical needs.

Table. 3.8. Table showing secondary structure of HSA with bioactive complexes

S.No	Drug	α-Helix (%)	β-sheet (%)	Random Coils (%)
1	Artemisinin	58.20 to 54.7	19.2 to 21.1	13.3 to 15.7
2	Ar-tumarone	57.40 to 50.6	19.5 to 22.2	14.1 to 17.20
3	Apocynin	57.3 to 48.5	25.2 to 30.6	17.4 to 20.0
4	Andrographalide	57.5 to 47.2	25.3 to 28.2	17.3 to 20.1
5	Bacosine	57.4 to 44.2	24.2 to 33.2	17.2 to 20.5
6	Corilagin	58 to 52	23 to 25	19 to 22.4
7	Chebulinic acid	57.7 to 51.9	20.1 to 22.6	16.0 to 19.7
8	Chebulagic acid	57.1 to 53.4	19.9 to 21.9	16.8 to 19.10
9	De Andrographalide	57 to 53	25 to 29	18 to 19
10	deForskolin	55.8to52.8	20.9 to 22.1	18.3 to 20.4
11	Embelin	58 to 45.6	23 to 28.4	19 to 26
12	L-dopa	58 to 54	23 to 25	19 to 20
13	Menthol	57.5 to 50.0	25.0 to 29.0	17.5 to 21.0
14	Piperine	58 to 54.0	23.0 to 25.0	19 to 20
15	psoralen	57.9 to 57.4	19.3 to 19.6	13.70 to 14.5
16	Pterostiblene	57.5 to 54.8	20.3 to 21.1	16.60 to 18.8
17	Rosmaric Acid	57.30 to 44.3	24.8 to 33.8	17.9 to 22.2
18	Stigmasterol	57.9 to 55.6	23.3 to 24.70	18.80 to 19.7
19	6-shagoal	57.53 to 49.8	25.01 to30.01	17.46 to 20.0
20	Umb-1	58 to 52.7	20 to 23	22 to 24.3
	Umb-2	58 to 54.7	20 to 21	22 to 24.6
21	7HC-1	58 to 36.5	20 to 32	22 to 31
	7HC-2	58 to 52	20 to 23.6	22 to 24
	7HC-3	58 to 46	20 to 25.6	22 to 28.5

CHAPTER 4

IN SILICO BINDING STUDIES OF BIOACTIVE COMPOUNDS WITH PLASMA PROTEINS

4.1. Binding Studies Using *in silico* Docking

The *in silico* estimation of drug binding to HSA in early drug discovery contributes to the lead optimization process. Local models are useful for the design of new compounds with reduced HSA binding for a particular target receptor, while real-time quantitative structure-activity relationships or global models combining structure and ligand-based approaches serve for compound libraries screening. However, research efforts on other important plasma proteins should be strengthened in the perspective to enable predictions of total plasma protein binding for clinical candidates. Computational molecular docking has been employed to improve the understanding of the interaction of bioactive compounds with HSA. As described in the introduction section, the 3D crystal structure of HSA is a monomer consisting of three homologous domains which assemble to form a heart-shaped molecule. Each of the structurally similar α-helical domains (I–III) has two subdomains (A and B), with six α- helices in subdomain A and four α-helices in subdomain B. The fluorescent tryptophan residue 214 is in subdomain IIA. Several studies have shown that HSA is able to bind many ligands in several binding sites. In the present study, the Autodock v 4.2.3, was chosen to examine the binding site and types of interactions involved in the binding of bioactive compounds with the active site of HSA.

In our study among 30 conformers obtained from docking, only one conformer was taken on the basis of free energy of binding and score ranking (Jones et al.,1997). The minimum binding energy conformer that is very close to the experimentally determined values with the lowest value of inhibition constant was chosen and analyzed for the binding site and type of interactions involved in the HSA-bioactive complexes.

Furthermore, molecular dynamics simulations (MDS) simulations of selected bioactive compounds showed the changes in the root mean square deviation (RMSD) and radius of gyration (Rg) indicating the conformational changes with respective to HSA alone, which are consistent with the circular dichroism spectra. These changes are due to the changes in the interior flexibility of the subdomains IIA, IIIA, and IB domain of HSA which are evident from the root mean square fluctuation (RMSF) studies. Moreover, Rg studies indicated that HSA-bioactive complexes are compact

with respect to HSA crystal structure. With the aid of circular dichroism and MD studies, we conclude that the secondary structural changes are altered upon formation of HSA-bioactive complexes which is not due to the destabilization. We hope that our studies will be pivotal in the pharmacodynamics of bioactive compounds. To understand further, the nature of binding, binding pocket, binding energies etc., of individual bioactive compounds with plasma proteins results were discussed below.

4.1.A. Andrographolide (ANDR)

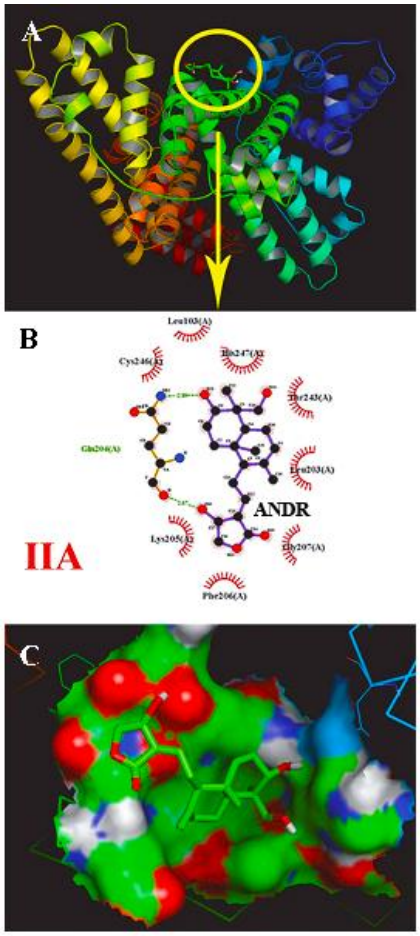

Fig. 4.1. Docking conformation of HSA-ANDR complex obtained from Autodock v 4.2.3 (A) ANDR bound to IIA domain on HSA (Protein represented in ribbon model and ligand represented in stick model). (B) Ligplot of ANDR binding site showing two hydrogen bonds (Gln 204) and hydrophobic interactions of HSA with ANDR. (C) The hydrophobic pocket of IIA domain surrounding the ANDR.

Based on the docking results least binding energy conformed is taken and found that the binding constant to be $1.2\pm0.03\times10^{4}$ M^{-1} and the free energy change to be -5.6±0.031 kcal/mol. Therefore, computationally calculated K and ΔG° values suggest that the binding of ANDR and HSA was similar with fluorescence data. These forces

stabilize the docking conformation and are consistent with the binding mode obtained from the experimental results. It was also observed that ANDR binds at subdomain IIA of HSA in all of these 30 conformers. After analyzing the conformation of the complex it's showed that ANDR binds in the hydrophobic pocket of subdomain IIA and their binding was stabilized by 2 H- bonds formation between ANDR and GLN204 of the HSA with a bond distance of 2.67 and 2.8Å (Fig.4.1 A-C). Further, the vicinity of microenvironment (around 4Å region) *i.e.* the active site of HSA, Cys, Leu, His, Thr, Leu, Gly, Phe, and Lys, *etc.* amino acid residues which are in the proximity of the ligand and conjugated with ANDR. From the binding site analysis, it is clearly evident that ANDR-HSA complex is mainly stabilized by hydrophobic interactions. This supports the quenching of fluorescence which is evident from the location of the ANDR which is in close proximity to the tryptophan residue of HSA (Trp214) suggesting the existence of hydrophobic interaction.

4.1.B. Corilagin (COR)

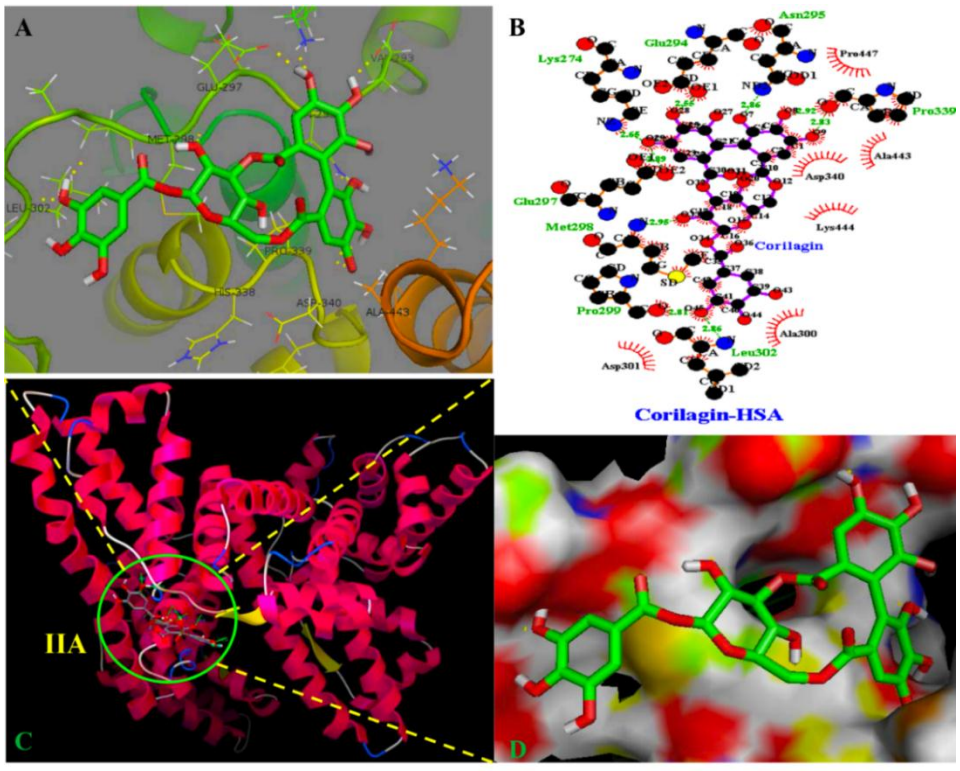

Fig. 4.2. Schematic representation of least binding energy docked conformation obtained from docking simulation (A) Pymol Stereo view of corilagin binding site to HSA IIA domain in which corilagin is rendered as capped sticks and surrounding residues as lines (LYS274, GLU294, ASN295, GLU297, MET298, PRO299, LEU302 and PRO339). (B) A graphical representation of Ligplot data to show the hydrophobic interactions of HSA with corilagin and (C) corilagin bound to IIA domain on HSA (protein and ligand colored blue, red, yellow and green, respectively. (D) The hydrophobic and hydrophilic amino acid residues surrounding the corilagin.

The corilagin complex is stabilized by 8 hydrogen bonds between corilagin to LYS274, GLU294, ASN295, GLU297, MET298, PRO299, LEU302 and PRO339 of the protein with a length of 2.65, 2.56, 2.86, 2.89, 2.98, 2.81, 2.86, and 2.98 Å. The minimum binding energy conformer was observed as -5.71 kcal M^{-1} that is very close to the experimentally determined values (-7.6 kcal M^{-1}) having inhibition constant of 65.16 µM and binding constant was $1.5x10^4$ M^{-1} (Fig.4.2 A). Docking results decipher that corilagin is binding to HSA at subdomain IIA which is Sudlow's site I with most stable docking conformer (Fig 4.2 B and C). It is also observed that corilagin binding site in HSA was fully covered by hydrophobic interactions (Fig.4.2 D). Thus, corilagin is surrounded by hydrophobic and hydrophilic amino acids such as ALA300, GLY328, ASP340, and ALA443. Thus, corilagin binds with HSA mainly by hydrophobic interactions with above-mentioned amino acids involved in the interactions, along with few hydrophilic interactions that are shown in Fig.4.2 C. These results obtained are in accordance with the free energy calculations obtained from binding constant which was derived from fluorescence quenching data.

4.1.C. Embelin (EMB)

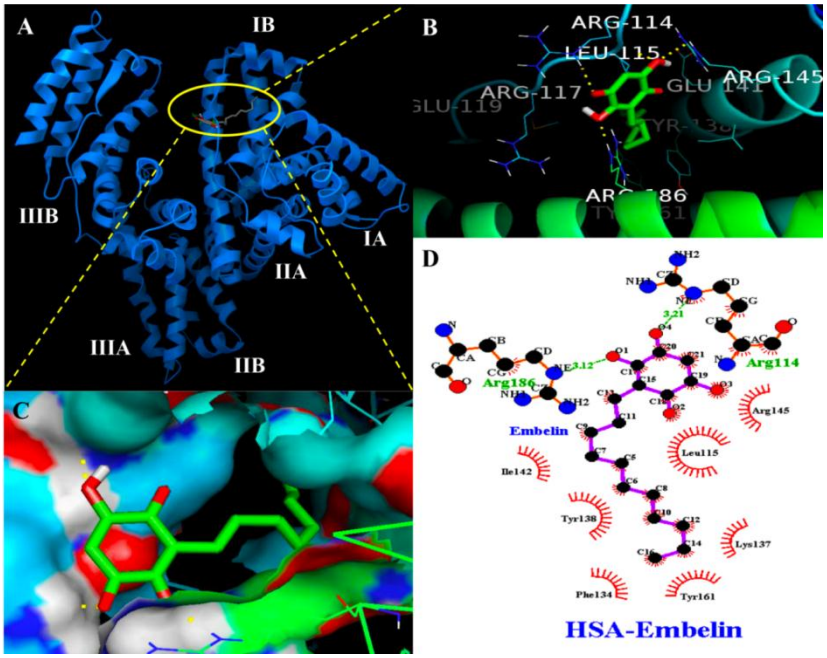

Fig. 4.3. Schematic representation of least binding energy docked conformation obtained from docking simulation (A) EMB bound to IB domain on HSA (protein and ligand colored blue, red, yellow and green, respectively), (B) The hydrophobic and hydrophilic amino acid residues surrounding the probe EMB, (C) A graphical representation of Ligplot data to show the hydrophobic interactions of HSA with EMB and (D) Pymol Stereo view of EMB binding site to HSA IB domain in which EMB is rendered as capped sticks and surrounding residues as lines (LYS137, LEU115, ARG114, ARG186, ARG145, ILE142, TYR138, TRY161 and PHE134).

The lowest binding energy of the conformer (-4.92 kcalM^{-1}) is very close to the experimentally determined values with the lowest value of inhibition constant (246.7 μM) is presented in (Fig. 4.3 A). Of all 30 conformers, the EMB is firmly binding with HSA at subdomain IB which is considered as the third major binding site on HSA. Previous studies revealed that several endogenous compounds and some drugs also bind to subdomain IB (Garg et al., 2013; Zsila et al., 2013). This was also confirmed from molecular displacement results that EMB binds to IB domain (chapter 3). The most stable docking conformer shows that the EMB in the binding site is mostly surrounded by hydrophobic amino acids such as Tyr161, Phe134, Tyr138 and Ile142 than hydrophilic amino acids like Arg114, Arg145, Lys137 and Arg186 (Fig. 4.3 B and C). Thus, it is concluded that the interaction between EMB and HSA is more of hydrophobic in nature. Also, EMB complex is stabilized by a 3-hydrogen bond between EMB to Leu115, Arg114 and Arg186 of the protein with a distance of 3.2 Å, 3.0 Å, and 3.12 Å, respectively. The minimum binding energy conformer was observed as -4.92 kcal M^{-1} that is very close to the experimentally determined values (-5.1 kcal M^{-1}) having inhibition constant of 246.7 μM and binding constant was $4x10^3$ M^{-1}. Our results have shown that EMB binds with HSA mainly by hydrophobic interactions and the above amino acids involved in the interactions are mostly hydrophobic in nature along with few hydrophilic bonds that are shown in Fig. 4.3 D. These results are nearly matching to the free energy calculations obtained from binding constant which was derived from fluorescence quenching.

4.1.D. Piperine (PIP)

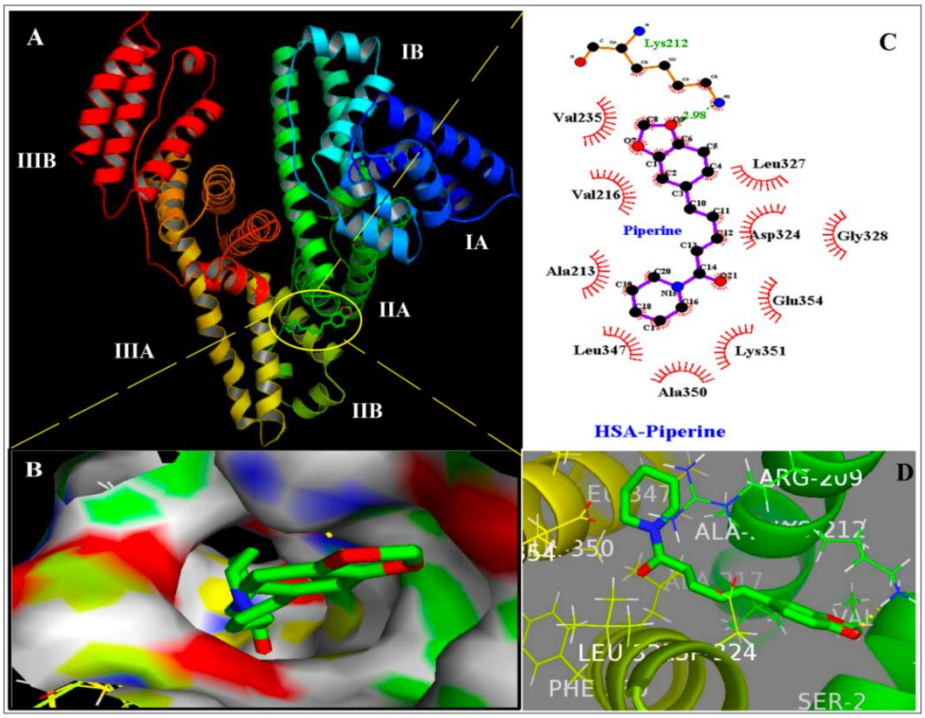

Fig. 4.4. Schematic representation of least binding energy docked conformation obtained from docking simulation (A) Piperine bound to IIA domain on HSA (protein and ligand colored blue, red, yellow and green, respectively), (B) The hydrophobic and hydrophilic amino acid residues surrounding the probe piperine, (C) A graphical representation of Ligplot data to show the hydrophobic interactions of HSA with piperine and (D) Pymol Stereo view of piperine binding site to HSA IIA domain in which piperine is rendered as capped sticks and surrounding residues as lines (LYS351, GLU354, GLY328, ALA350, LEU347, ALA213, VAL216, VAL235, LYS212 and ASP324).

Piperine is an important phytochemical used as spices in our daily food. Further, the piperine complex is stabilized by a hydrogen bond between piperine to LYS212 of the protein with a length of 2.98 Å. The minimum binding energy conformer was observed as - 6.8 Kcal M^{-1} that is very close to the experimentally determined values (-7.8 kcal M^{-1}) having inhibition constant of 3.46 μM and binding constant was $3.3x10^5$ M^{-1} (Fig. 4.4 A). Docking results decipher that piperine is binding to HSA at subdomain IIA which is Sudlow's site I with most stable docking conformer (Fig.4.4 C and D). It is also observed that piperine binding site in HSA was fully covered by hydrophobic interactions (Fig.4.4 D). Thus, piperine occupies mostly surrounded by hydrophobic and hydrophilic amino acids such as LYS351, GLU354, GLY328, ALA350, LEU347, ALA213, VAL216, VAL235, and ASP324. Thus, piperine binds with HSA mainly by hydrophobic interactions with above-mentioned amino acids involved in the interactions, along with few hydrophilic interactions that

are shown in Fig.4.4 C. These results obtained are in accordance with the free energy calculations obtained from binding constant which was derived from fluorescence quenching data.

4.1.E. 7-Hydroxy coumarin derivatives (7HC-1, 7HC-2 and 7HC-3)

The docking results showed that synthesized coumarin derivatives (7HC-1&3) bind within the binding pockets of sub domain IIIA and IIIB (drug site II) and 7HC-2 binds to IIIB domain. The validation of the binding modes as per the amino acid residues, predicted it to be the part of the binding site. There is hydrogen-bonding interactions between the hydroxyl (OH) group of coumarin to HSA.

The present study indicates that these 7HC derivatives binds mainly to the hydrophobic pocket of subdomain IIIA, IIIB and IIIB (Fig.4.5). These compounds are accommodated in the deepest part of the binding cleft largely shielded from a solvent such that the phenyl part is present at the entrance of the pocket and rest of the drug is embedded in the deepest portion of the cleft. The 7HC-1, 7HC-2 and 7HC-3 derivatives complexes are stabilized by the hydrogen bonds with different bond lengths. The 7HC-1 complex is stabilized by a hydrogen bond between the compound and V482 amino acid residue of the protein with length of 2.0 Å, 7HC-2 derivative-HSA complex by a hydrogen bond between the compound and K545 with the bond length of 2.5 Å and 7HC-3 complex by a hydrogen bond with F502 of length 2.2 Å to HSA. These molecules specifically interact with different residues located in the sub domain IIIA, and the complex is stabilized by the hydrogen bonds. The computationally calculated binding energy of lowest energy conformers of 7HC-1, 7HC-2 and 7HC-3 derivatives are -6.15 Kcal/mol, -6.26Kcal/mol and -5.52 Kcal/mol, respectively which are very nearer to the experimentally measured values (chapter 3). Therefore, the molecular docking and free energy calculation results suggested that 7HC derivatives bound to HSA with both hydrophobic and hydrogen bond interactions.

The moiety of 7HC derivatives was located within the hydrophobic binding pocket and several groups of coumarin derivatives (7HC-1, 7HC-2 and 7HC-3) interact with the several residues of sub-domain, IIIA, IIIB, and IIIB. These results were very well supported by molecular displacement analysis by site-specific markers that 7-hydroxycoumarin derivatives are specifically binding to the site II (Fig. 3.19. Almost

all the interactions of 7HC derivatives with HSA was in the vicinity of the active site presented within the 4Å moiety which consists of several residues such as N209, R210, A213, A327, L328, E347, 350, A351, K354, E480, S481, L482, V483 for HSA-7HC-1 complex, as K545, L529, M548, Y401, E400, Q397, F395, L394, K392 and N391for HSA-7HC-2 complex and, Q409, P500, K501, E502, F532, L535, H536, K579, S580 for HSA-7HC-3 complex (Fig.4.5). Therefore, the results of molecular docking indicate that the interaction between 7HC derivatives and HSA are dominated by hydrophobic forces, which is in agreement with the free energy shown by fluorescence data. These coumarin derivatives binding to HSA showed different binding energies and binding sites. This could be because of change in functional groups on each coumarin molecules.

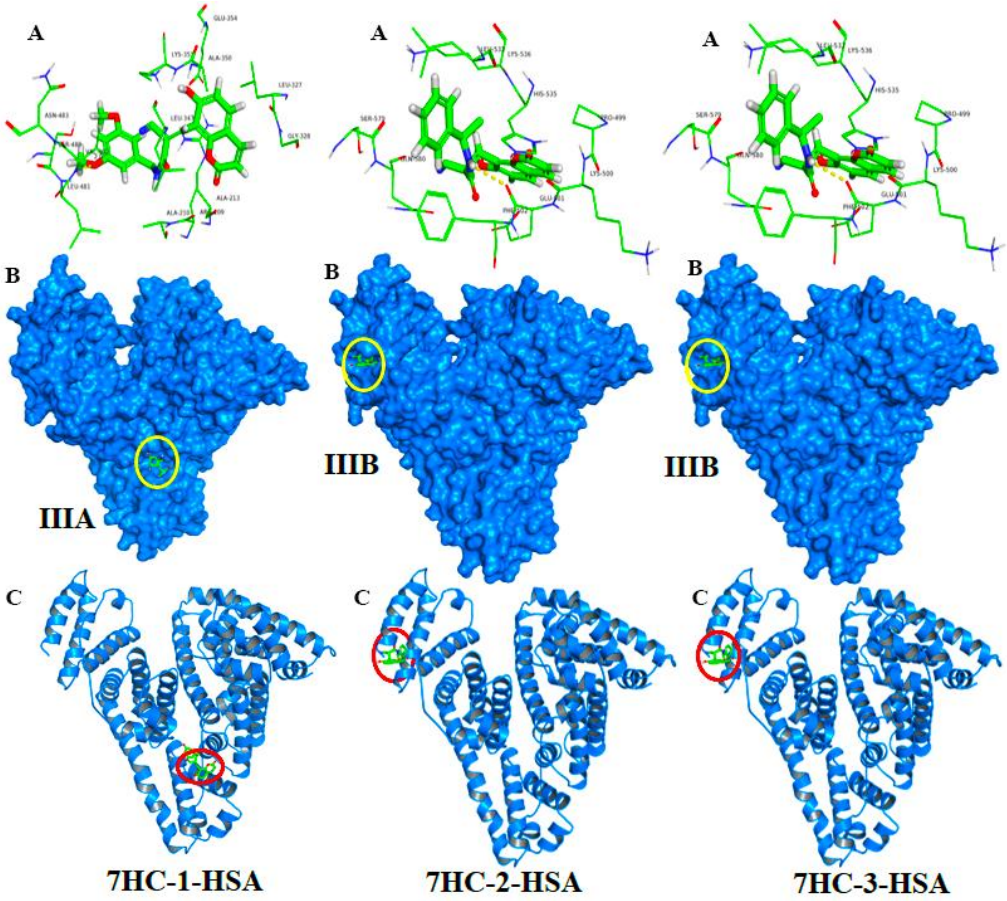

Fig. 4.5. 7HC-1,2 and 3 docked in the binding pocket of HSA using Autodock4.2.3 Different view of HSA and 7HC-1,2 and 3 docked conformation. (A) the docking poses of the HSA-7HC-1,2 and 3 complex depicted in a ball and stick model (blue), and HSA, represented in line model, (B) overview in surface model of 7HC-1, 2 and 3 binding to HSA, cartoon model (C) overview in cartoon model of 7HC-1,2 and 3 binding to HSA. The images are generated using PyMol.

4.1.F. Novel 8-substituted coumarin derivatives

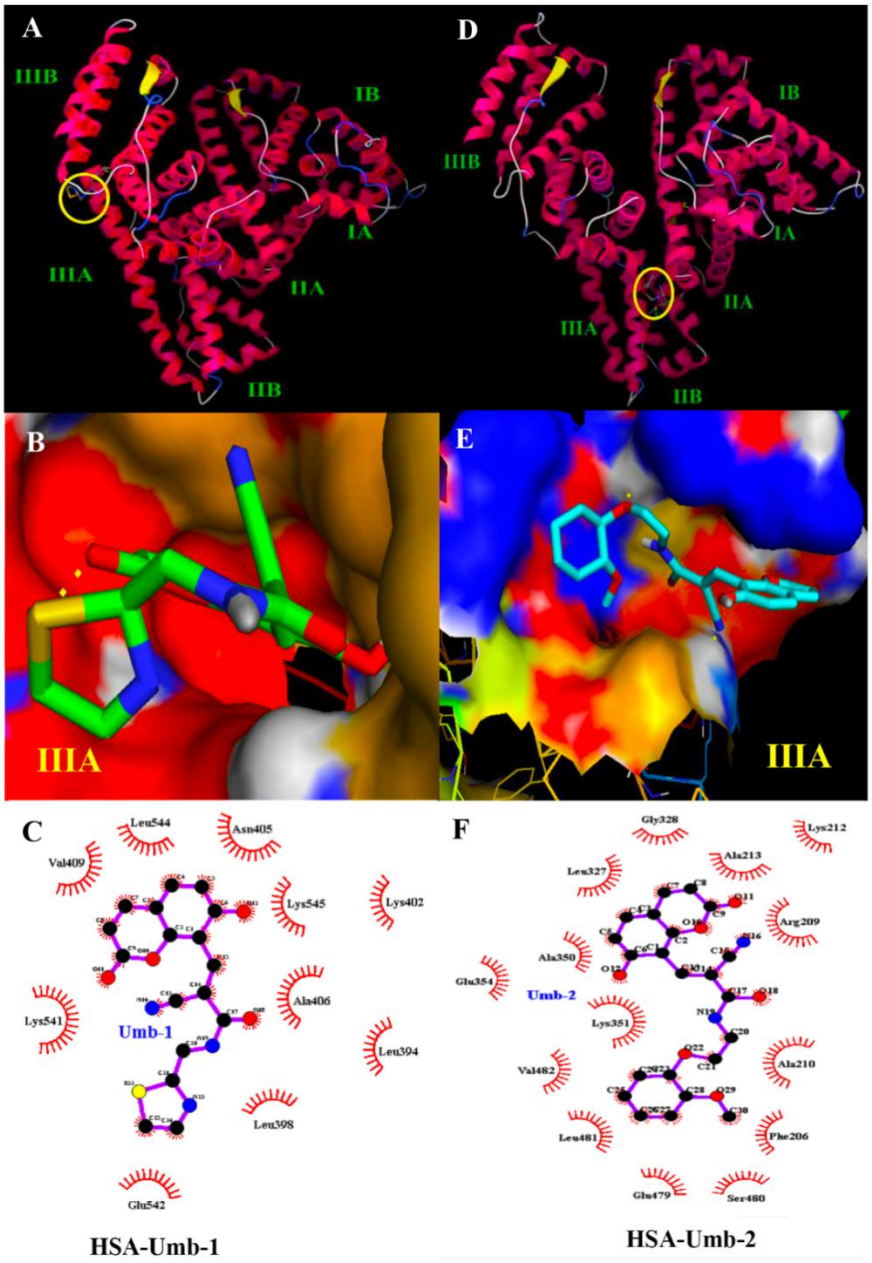

Fig. 4.6. Different views of Umb-1and Umb-2 docked in the binding pocket HSA using Autodock 4.2. (A and D) Overview of cartoon model of Umb-1 and Umb-2 binding to HSA. Pymol is used to generate the images. (B and E) The cavity of hydrophobic and hydrophilic amino acid residues surrounding the probe. (C and F) To the showing, hydrophobic interactions of HSA with Umb-1and Umb-2 Ligplot is used.

The docking results showed the synthesized Umb-1 and Umb-2 derivatives binds within the binding pocket of subdomain IIIA subdomains. The assent of the binding modes as per the amino acid residues, conclude it to be the part of the binding site. Almost all the interactions of Umb-1 and Umb-2 with HSA were in the vicinity of the

active site presented within the 4Å moiety which consists of several residues such as LEU394, LEU398, LYS402, ASN405, ALA406, VAL409, GLU542, LYS545, LEU544, and VAL482, for HSA-Umb-1 complex; as LEU-481,VAL-482,LEU-327,GLY-328,SER-480,GLU-354 and ALA-350 for HSA-Umb-2 complex. It can be seen that the Umb-coumarin derivatives molecule were situated within the hydrophobic cavity of subdomain IIIA (Fig.4.6). Thus, we can conclude that the interaction of Umb-1 and Umb-2 with HSA is mainly hydrophobic, which is in perfect agreement with the thermodynamic results obtained from fluorescence emission. Hydrogen bonding interactions were between the hydroxyl (OH) group of carbon-3 of Umb-1, Umb-2 complexes, and one hydrogen bond is formed between Umb-1 to LYS402 of HSA with a bond length of 2.8 Å, whereas for umb-2 complex one hydrogen bond is formed between GLU354 with a bond length of 2.2 Å respectively (Fig.4.6). The results suggested that the formation of hydrogen bonds stabilize the Umb-1 and Umb-2 -HSA complexes. Similar results were observed for other ligand molecules bound to HSA (Zsila et al., 2003; Schuttelkopf & van Aalten 2004).From docking simulation, the binding constant and free energies of Umb-1 and Umb-2 to HSA were 9.2×10^3 M^{-1} and 1.2×10^5 M^{-1} are -5.4 and -6.9 kcal M^{-1}, respectively. The above results closely harmonized with the experimental data, obtained from fluorescence emission shows the binding constant and free energy values of $K_{umb\text{-}1} = 3.1\pm .01\times10^4$ M^{-1}, $K_{umb\text{-}2} = 7\pm .01\times10^4$ M^{-1}, which corresponds to -6.17 kcal/mol and -6.91 kcal/mol of free energy respectively. Therefore, the results of molecular docking indicate that the interaction between Umb-1/Umb-2 and HSA are dominated by hydrophobic forces, which are in agreement with the fluorescence data.

4.2. Molecular Dynamics Simulations

Moreover, I have done the MD studies for following bioactive compounds (ANDR, COR, EMB, PIP and 7-Hydroxy coumarin derivatives (7HC1, 7HC2, and 7HC3) to authenticate the HSA-bioactive complex conformers from molecular docking results.Furthermore, I analyzed RMSD, RMSF and Rg over the time period of 10000ps which are required parameters for clearly understand the HSA-bioactive compounds interactions at atomic level and provides information on the stability and rigidity of the binding sites on HSA. Which is vital in pharmacodynamics of these selected bioactive compounds.

4.2.A.Andrographolide(ANDR)

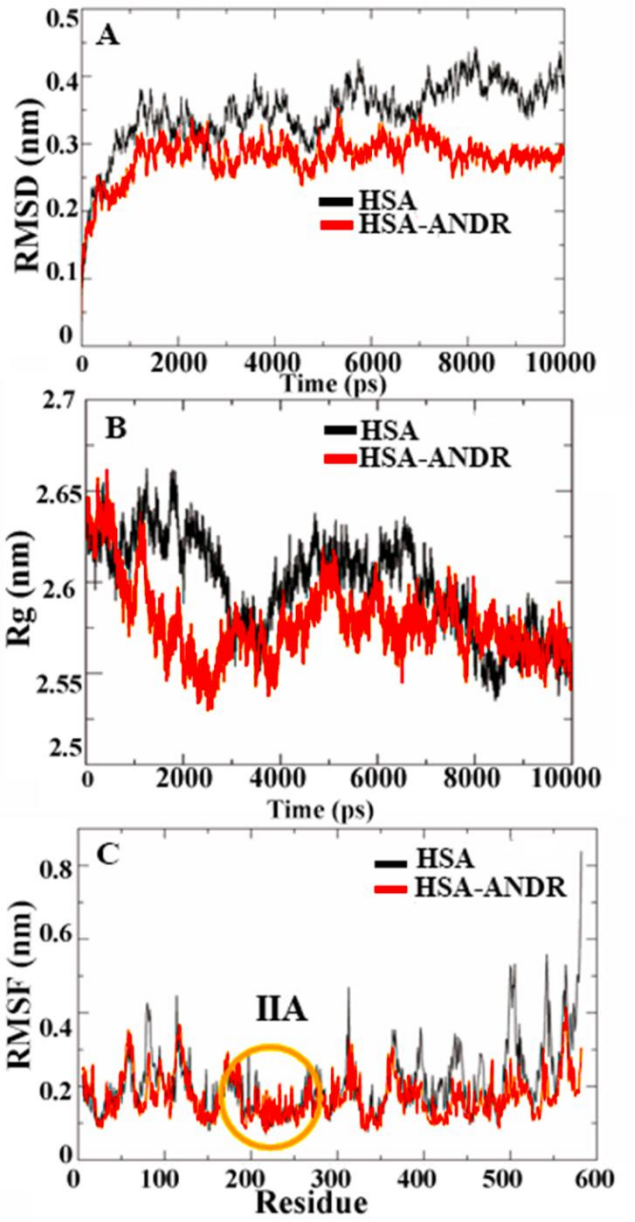

Fig.4.7. Molecular dynamic simulation. (A) Time dependence of Root Mean Square Deviations (RMSD. C_α RMSD values for free HSA (Black) and the HSA- ANDR (Red) complex during a 10 ns MD simulation. (B) Time evolution of the radius of gyration (R_g). The radius of gyration (R_g) values during 10 ns of MD simulation of HSA (Black) and HSA- ANDR (Red) complex. (C) The RMSF values as a function of residue numbers. The RMSF values of free HSA (Black) and HSA-ANDR (Red) complex were plotted against residue numbers.

The rmsd values of atoms in free and ANDR bound HSA were plotted from to 0-10ns as shown in (Fig.4.7) analysis indicates that the rmsd of both systems reaches equilibration and oscillates around in average value after 3ns simulation time. Fig.4.7 A shows the data point of fluctuation was determined as follows: for HSA, 0.40±.035nm; HSA-ANDR, 0.29±0.056nm. attributed rigidity of protein unfolding which is in

agreement with the CD, hence it showed slight changes in the secondary structure. Therefore, the changes are due to partial unfolding but not due to destabilization of HSA. So, we conclude that during MD simulation there is no structural drift from the HSA structure. So, we conclude that during MD simulation there is no significant structural drift from the HSA structure. Recently similar reports were documented from our lab related to protein stability. We also examine the time evolution of the radius of gyration (R_g) in course 10ns of MD simulation of free HSA and HSA-ANDR complex, the result shown in Fig.4.7. The R_g values Fig.4.7B for the complex was stabilized at about 4 ns and achieved equilibrium after 6 ns. Initially, the R_g values of free HSA and the complex with the drug were 2.64nm.

The free HSA and HSA-ANDR were stabilized 2.57±0.02nm and 2.52±0.04nm. As it is expected, by reducing the radius of gyration and increasing the compactness rate in the binding to ANDR and all these findings align with that lupeol and piperine complexes formation with HSA. So based on the RMSD and Rg values obtained from our MD simulation data, it is concluded that HSA exhibits a slight structural change when interacting with ANDR. Thus both experimental and computational results suggest slight conformational changes, probably at the binding region of the protein. Local protein mobility can be determined by RMSF values which were plotted against residue numbers on a 10 ns trajectory. The RMSF plot shows the total amino acid fluctuation that is the total polypeptide chain (Fig.4.7C). The graph strongly indicates that the IIA subdomain for ANDR fluctuated lower than others (IA, IB, IIB, IIIA, and IIIB). This data suggests that the drug molecule (ANDR) binds in the IIA subdomain and forms a rigid structure during MD simulation. The data clearly suggest that the ANDR binds specifically to IIA subdomain, which supports the experimental evidence found from molecular displacement by site-specific markers. The rigidity of the binding sites from RMSF studies indicated that ANDR binds within the subdomain IIA which are in good agreement with the docking studies. These results indicate that ANDR binds specifically to the respective domain, suggesting that binding sites are very specific for ANDR. Thus, during the simulation the HSA-ANDR complex are stable after 4 ns. Nonetheless, the changes in the secondary structure were observed that many be due to partial unfolding of HSA. The unfolding of protein structure may due to orientation changes upon binding of ANDR to HSA.

4.2.B. Corilagin (COR)

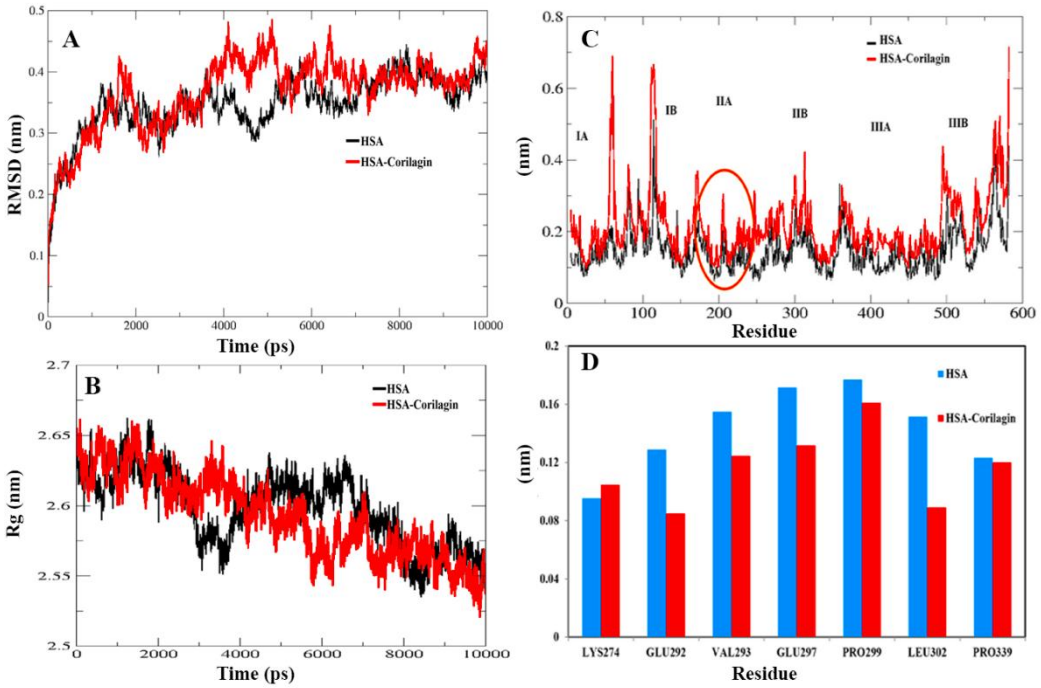

Fig.4.8. (A)The Root mean square deviation (nm) of unligand HSA and ligand HSA (HSA- corilagin). (B) The Time dependence of the radius of gyration (Rg) for the backbone atoms of unligand HSA and ligand HSA (HSA- corilagin). (C)The RMSF values against residue numbers. The RMSF values of unligand HSA and HSA-corilagin complex were plotted against residue numbers (D) The profile of atomic fluctuations.

Atomic fluctuations of free HSA and HSA- corilagin complex to the active site amino acid residues present in the IIB subdomain of HSA which is Site I. Free HSA and HSA–corilagin complex, the RMSD values steadily increase till 1000ps followed by a slow increase up to 4000ps. After this there was no further increment of RMSD values and it reached equilibrium. After reaching the equilibrium the RMSD values of C–Cα–N backbone for both the HSA and HSA–corilagin complex were calculated for the 1-10000ps time scale (Fig.4.8A). For HSA, the data point fluctuations are 0.45±0.053nm whereas for the complex they are 0.40±0.036nm. The decrease in RMSD value of the complex from that of the free HSA indicates that ligand upon binding with protein showed slight structural change, increased rigidity and stability. Thus, the MD simulations studies showed that these complex remain in a stable binding position with slight RMSD fluctuations confirming the integrity of docked conformer which is forecast by AutoDock 4.2.3. Remarkably, our data is in agreement with the earlier reports from our group (Sudhamalla et al., 2010; Malleda et al., 2012; Gokara et al., 2014; Yeggoni et al., 2015a).

The protein reliability is analyzed by plotting R_g values against the function of time. R_g was used to assess the stability of the back bone atoms of HSA and HSA-corilagin complex (Fig.4.8B). The free HSA alone and HSA-corilagin, the R_g value is stabilized at about 2000 ps, which implies that the MD have achieved equilibrium at 4000ps. Firstly, the R_g value of both free HSA and HSA-corilagin complex was 2.64 nm. The free HSA and HSA-corilagin complex was stabilized at 2.57 ± 0.03 nm (Fig.4.8B). The R_g value of HSA, which is shown experimentally by neutron scattering in aqueous solution, was 2.74 ± 0.35 nm which showed that it is synchronizing with the experimental data. The previous studies showed that the R_g of HSA determined experimentally from neutron scattering in aqueous solution 2.74±0.035 nm, which indicates that the simulations performed are identical to the experimental values (Kiselev et al., 2001). Also, the present result is closely related to our previous studies that β-sitosterol, asiatic acid, and piperine stabilizes from 2.59±0.03 nm to 2.40±0.031 nm; 2.42 ± 0.03 nm to 2.45 ± 0.01 nm; 2.64 ± 0.021 nm to 2.57 ± 0.03 nm for free HSA and HSA-with complexes, respectively (Sudhamalla et al., 2010; Gokara et al., 2014; Yeggoni et al., 2015a). So during the simulation the change of Rg value from HSA to HSA–corilagin over simulation time indicates stabilization and slight conformational changes in the secondary structure of HSA when bound to the corilagin. This observation again supports a partial change of CD spectral results as shown and discussed earlier. The local protein mobility which is analyzed by calculating the RMSF value of HSA alone and HSA-corilagin complex. The RMSF were plotted against residue numbers based on the 10000ps trajectory (Fig.4.8C). The profile atomic fluctuations were found to be very similar to those of HSA and HSA-corilagin complex. Here, the results show that except subdomain IIA, rest all domains IA, IB, IIB, and IIIA of HSA are showing high fluctuation which indicates that corilagin is more rigid at the site I, particularly IIA domain (Fig.4.8C). This rigidity was located to individual residues of LYS351, GLU354, ALA213, VAL216, and ASP324 of HSA-corilagin (Fig. 4.2). The specific binding was also confirmed from the site-specific probes showed that corilagin binds to IIA domain (Fig. 3.9). Thus, in the site I, the fluctuations are less when compared with the other drug binding site IB and site II. Thus this study provides an evidence that HSA binding to sites I (IIA subdomain) and interacts specifically with corilagin through conformational adjustments of the protein structure, in aggregation with ligand conformational variation to these sites. Based on

the RMSD, Rg and RMSF values obtained in this work, it can be concluded that the HSA molecule exhibits a slight conformational change when it combines with corilagin which is in agreement with the CD data (Fig. 3.25).

4.2.C. EMB (EMB)

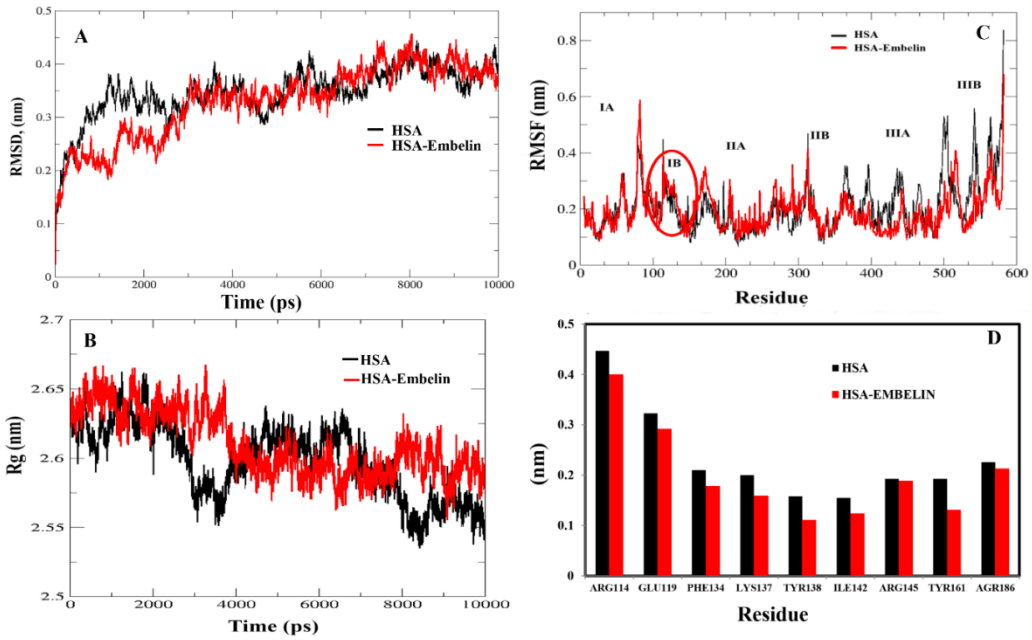

Fig.4.9. (A)The Root mean square deviation of unligand HSA and ligand HSA (HSA- EMB). (B) The Time dependence of the radius of gyration for the backbone atoms of unligand HSA and ligand HSA (HSA- EMB) (C)The RMSF values against residue numbers. The RMSF values of unligand HSA and HSA-EMB complex were plotted against residue numbers (D) The profile of atomic fluctuations. Atomic fluctuations of unliganded HSA and HSA-EMB complex to the active site amino acid residues present in the IB subdomain of HSA which is third major drug binding site.

The results from RMSD values indicate that both systems reached equilibration and oscillate at around a value of 3500ps. RMSD values of atoms in unliganded HSA and HSA-EMB were calculated from the 0-10000ps trajectory, the data points fluctuated by 0.41 ± 0.036 nm for HSA alone and 0.45 ± 0.69 nm for HSA–EMB complexes. Thus, from MD simulations it is ascertained that after 3500ps the EMB interacted complex of HSA is stabilized due to conformational rearrangement (Fig.4.9A). So during the MD simulations, this complex remained in a stable position with low RMSD fluctuations confirming the authenticity of docking results by Auto Dock 4.2.3. The unligand HSA and HSA-EMB, the R_g value is stabilized at about 2000 ps, which suggest that the MD have achieved equilibrium at 4000ps. The R_g value of both free HSA and HSA-EMB complex was 2.64 nm. The free HSA and HSA-EMB complex was stabilized at 2.59 ± 0.03 nm (Fig.4.9B). Further, the experimentally

proved values from neutron scattering in aqueous solution were 2.74±0.035 nm, which illustrate that the simulations performed are identical to the experimental values (Kiselev et al., 2001). The parameter, RMSF is used to investigate the local protein mobility, the values of unliganded HSA and HSA-EMB were plotted against residue numbers on a trajectory of 10000ps, clearly indicates that EMB binding to site IB of HSA, remained rigid when compared to the other subdomains during simulation (Fig.4.9C). The rigidity was located to individual residues of Arg114, Glu119, Phe134, Lys137, Tyr138, Ile142, Arg145, Tyr161 and Arg186 HSA-EMB (Fig.4.9 D). Docking studies proved that EMB binding site is located at IB sub-domain and also the specific binding of EMB to IB subdomain was confirmed from the displacement site-specific probe experiment (chapter 3, Fig. 3.12). Thus, docking and site marker experiments are in good agreement with RMSF of the MD study.

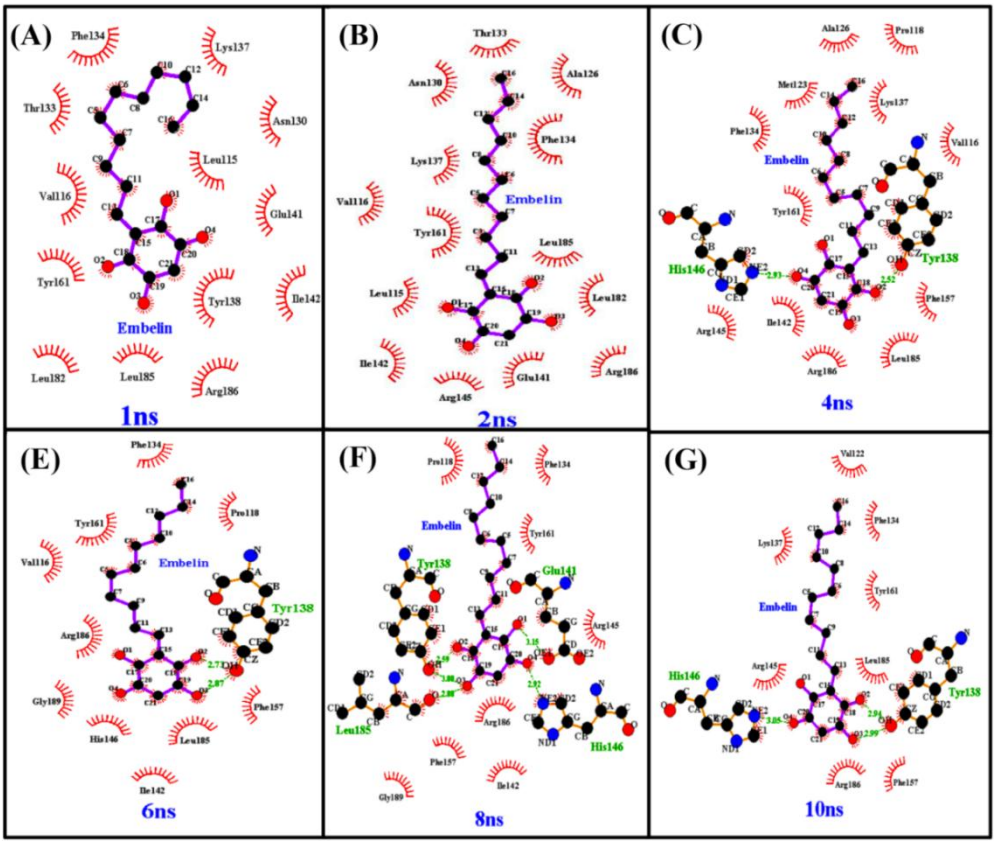

Fig.4.10. A 2D Schematic representation (A-G) of the time-dependent mode of hydrogen bond and hydrophobic interactions of HSA-EMB complex with in subdomain IB at different nanoseconds, using Ligplot.

Results, clearly indicate that during the period of 4ns, the flexibility of the EMB in the binding pocket of subdomain IB of HSA is not much fluctuated which indicates it is more rigid at IB site. Also, the electron micrographs support our data that due to

aggregation of EMB with HSA, a stable complex is formed (Fig. 3.29). Further, slight structural rearrangement of amino residues was seen till 6 ns and then it got stabilized at 10 ns upon binding of EMB with HSA. The structural arrangement and the variation are firmly supported by R_g (Fig.4.10). This study gives that there is a conformational rearrangement of protein structure which implies that EMB binds with subdomain IB of HSA. The results are in very much harmonized with the earlier reports on experimental and simulation of chitosan oligomers and Asiatic acid (Gokara et al., 2014; Gokara et al.,2015). The results available make clear that MD data play a pivotal role in understanding the stability of protein-ligand complex.

4.2.D. Piperine (PIP)

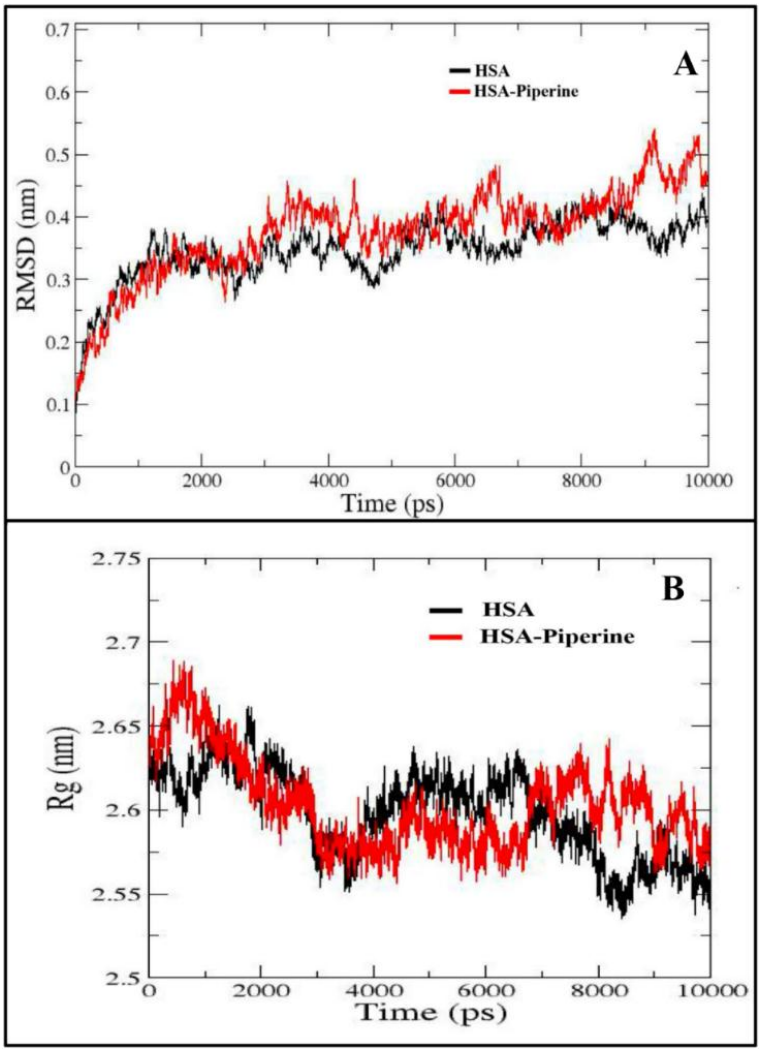

Fig.4.11. (A)The Root mean square deviation (nm) of unligand HSA and ligand HSA (HSA-pipeirne). (B) The Time dependence of the radius of gyration (Rg) for the backbone atoms of unligand HSA and ligand HSA (HSA-piperine).

RMSDs data analysis is used to conform the stability of HSA and HSA-piperine the RMSDs were plotted from 0 to 10000ps (Fig.4.11A). The RMSD values steadily increased from 0 to 1000ps and then it's stabilized at around 3000ps for piperine free HSA and HSA-piperine complex. These results indicate that there was no increment of RMSD and piperine free HSA and HSA-piperine complex reached equilibration and oscillates at around 3000ps. The RMSD values of atoms in unligand HSA and ligand HSA were calculated from a 0 to 10000ps trajectory, where the data points fluctuated by 0.42 ± 0.036 nm for HSA alone and 0.5 ± 0.69 nm for HSA–piperine complexes. During the MD simulations, these complexes remain in a stable binding position with low RMSD fluctuations confirming the credibility of docked conformer which is predicted by Auto Dock 4.2.2. Interestingly, our data is in agreement with the earlier reports from our group (Sudhamalla et al., 2010; Malleda et al., 2012; Gokara et al., 2014; Yeggoni et al., 2014a). R_g data analysis the protein integrity is analyzed by plotting R_g values against the function of time. R_g was used to assess the stability of the back bone atoms of HSA and HSA-piperine complex (Fig.4.11B). The HSA alone and HSA-piperine, the R_g value is stabilized at about 1500 ps, which implies that the MD have achieved equilibrium at 3000ps. Firstly, the R_g value of both free HSA and HSA-piperine complex was 2.64 nm. The unligand HSA and HSA-piperine complex were stabilized at 2.57 ± 0.03 nm (Fig.4.10.i. B). The R_g value of HSA, which is shown experimentally by neutron scattering in aqueous solution, was 2.74 ± 0.35 nm (Kiselev et al., 2001) which showed that it is synchronizing with the experimental data. The previous reports showed that the R_g of HSA determined experimentally from neutron scattering in aqueous solution 2.74±0.035 nm, which indicates that the simulations performed are identical to the experimental values (Kiselev et al., 2001).

Also, the present result is closely matching with our previous reports that β-sitosterol and Asiatic acid stabilizes from 2.59±0.03 nm to 2.40±0.031 nm; 2.42±0.03 nm to 2.45±0.01 nm for free HSA and HSA-with complexes, respectively (Sudhamalla et al., 2010; Gokara et al., 2014). As seen in the Fig.4.11 B, the R_g of piperine-HSA decrease upon binding, this implies a compact structure of HSA. However, the protein microenvironment of HSA is changed upon binding leading to the structural changes of HSA. These results are concomitant with the CD data that upon binding of piperine with HSA, there is a considerable conformational change of secondary structure of protein.

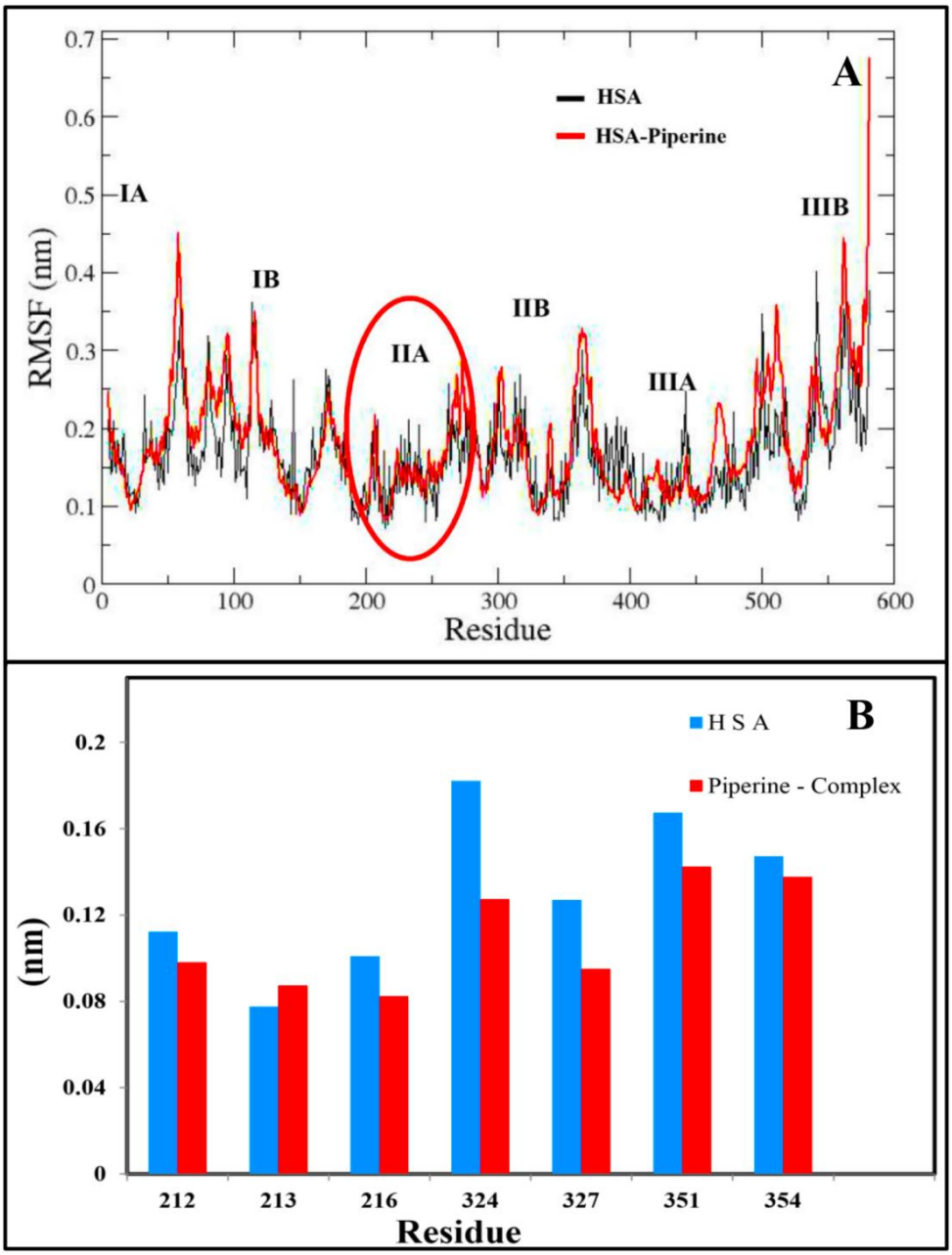

Fig.4.12. (A) The RMSF values against residue numbers**.** The RMSF values of unligand HSA and HSA-piperine complex were plotted against residue numbers (B) The profile of atomic fluctuations. Atomic fluctuations of unliganded HSA and HSA-piperine complex to the active site amino acid residues present in the IIB subdomain of HSA which is Site I.

In MD simulation is an interesting phenomenon that the local protein mobility which is analyzed by calculating the RMSF value of HSA alone and HSA-piperine complex. The RMSF were plotted against residue numbers based on the 10000ps trajectory (Fig.4.12). The profile atomic fluctuations were found to be very similar to those of HSA and HSA-piperine complex. Here, the results show that except

subdomain IIA, rest all domains IA, IB, IIB, and IIIA of HSA are showing high fluctuation which indicates that piperine is more rigid at the site I, particularly IIA. This rigidity was located to individual residues of LYS351, GLU354, ALA213, VAL216, and ASP324 of HSA-piperine (Fig.4.12B). The specific binding was also confirmed from the site-specific markers showed that piperine binds to IIA domain (Fig. 3.15).

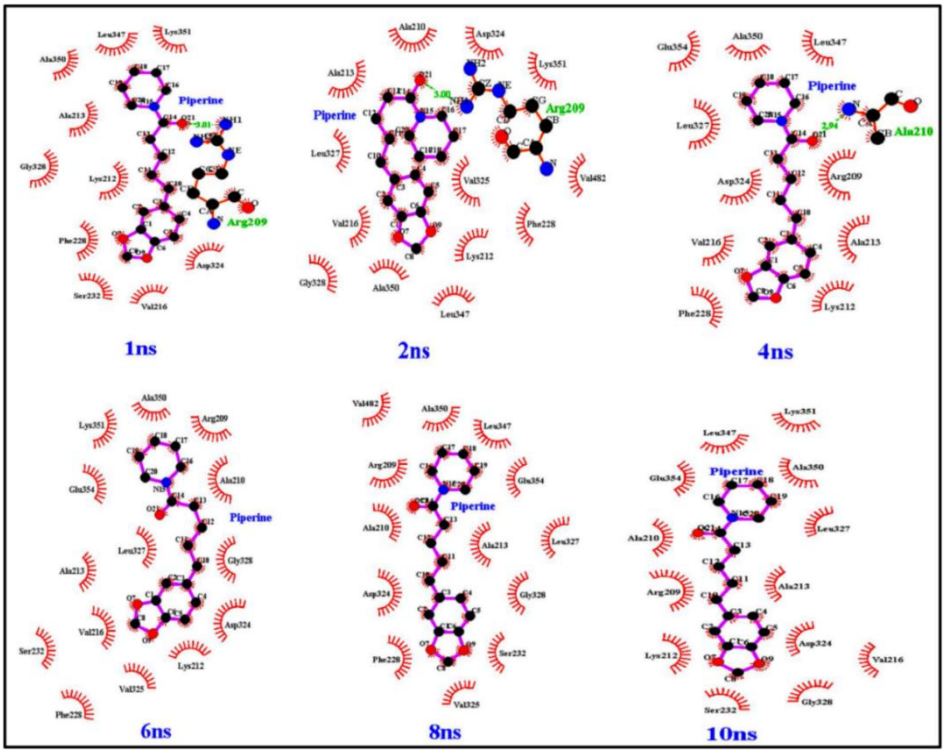

Fig.4.13. Showing hydrophobic interaction with subdomain IIA at different nanoseconds, using Ligplot for HSA-piperine complex.

In order to know the mobility, stability, and flexibility of least energy conformer, we investigated the docked conformer at different intervals of 1–10 ns (Fig.4.13). From these results, it clearly implies that during the period of 4ns, the flexibility of the piperine in the binding pocket of subdomain IIA of HSA is not much fluctuated. Further, slight structural rearrangement of amino residues till 6 ns and then it got stabilized at 10 ns upon binding of piperine with HSA.

The rigidity of binding site is not varied much even in the case of RMSD as whole, indicate that piperine binding is stable enough, which is very well supported by the rigidity of subdomain IIA (Fig.4.12 A and B). Here the structural arrangement and the variation are firmly supported by R_g (Fig.4.13). This study gives that there is a

conformational rearrangement of protein structure which implies the piperine binds with the site I (subdomain IIA) of HSA. The above results are very much supported by our previous experimental and simulation reports on chitosan oligomers and Asiatic acid (Gokara et al., 2014; Gokara et al., 2015).

4.2.E. 7-Hydroxy coumarin derivatives (7HC-1, 7HC-2 and 7HC-3)

In this study, we used molecular dynamics accession to measure the stability of the HSA, and HSA+7HC derivative complex equilibrium. The rigidity, microenvironment of protein and stability of complex in the presence of 7HC derivatives have been discussed from MD simulation based on RMS deviations, rms fluctuations (rmsf's) and the radius of gyration (*R*g) of protein and its complexes results have been analyzed. In addition, the stability of system proved the authenticity of the docking results and other experimental data, where the 7HC derivatives bound to HSA at subdomains IIIA and IIIB were used for MD simulations. The rmsd values of atoms in fat-free HSA and HSA-7HC derivatives complexes were plotted from 0 to 10ns as shown in Fig.4.11. Analysis of the rmsd values indicates that the rmsd of both systems reaches equilibration and oscillates around in average value after 5ns simulation. The rmsd values of atoms in HSA and HSA-7HC derivatives complexes were calculated from a 0-10ns trajectory, where the data points were fluctuated for HSA, 0.73±0.035nm; HSA-7HC1, 1.25 ± 0.056 nm; HSA-7HC2, 0.82 ± 0.32 nm; HSA-7HC3, 0.8 ± 0.39 nm, respectively. It is interesting that our data is almost agreement with our previous report on different 4-methyl umbelliferone coumarin derivatives, where the data points fluctuated for HSA, 0.72 ± 0.036 nm, HSA-CD enamide, 0.85 ± 0.056 nm, HSA-CD enoate, 1.18 ± 0.32 nm, HSA-CDM enamide, 0.82 ± 0.39 nm, respectively (Garg et al., 2013). Similar reports were observed from our group that 0.72±0.036 nm, 0.85±0.023 nm, and 0.81±0.032 nm for free HSA, HSA-β-sitosterol, and HSA-betulinic acid, respectively (Sudhamalla et al., 2010; Malleda et al., 2012), The integrity of the protein is analyzed by plotting the radius of gyration values against time. The radius of gyration describes the overall spread of the molecule and is defined as the root mean square distance of the collection of atoms from their common center of gravity. In the present MD studies, we determined the Rg values of free HSA and HSA-7HC derivatives complexes as shown in Fig.4.14. The *R*g values were stabilized at about 3.5ns in all the three derivatives of 7HC, indicating that the MD simulation

achieved equilibrium after 5ns. Initially, the *R*g values of free HSA, HSA-7HC-1, HSA-7HC-2, and HSA-7HC-3 complexes were 2.7 nm. The free HSA, HSA-7HC-1, HSA-7HC-2 and HSA-7HC-3 complexes were stabilized at 2.52±0.03 and 2.45±0.031, 2.45 ±0.031 nm, respectively (Fig.4.14i). Our previous report on free HSA, HSA-CD enamide, HSA-CD enoate and HSA-CDM enamide complexes were stabilized at 2.39 ± 0.03, 2.54 ± 0.04, 2.45 ± 0.03, and 2.51 ± 0.04 nm, respectively (Garg et al., 2013) which is very close to the present results. This indicates the stabilization of the coumarin-HSA complex is based on the functional groups of the 7HCderivatives.

The previous report showed the *R*g value of HSA by experimentally from neutron scattering in aqueous solution was 2.74±0.035 nm indicated that our MD simulations are identical to the experimental values (Kiselev et al., 2001). Also, the present result is close agreement with our previous report that β-sitosterol and beutilinic acid stabilizes from 2.59±0.03 nm to 2.40±0.031 nm; 2.59±0.03 nm to 2.51±0.01 nm for free HSA and HSA-with complexes, respectively (Sudhamalla et al., 2010; Malleda et al., 2012). These results suggest that the radius of gyration value marginally increased upon binding of 7HC derivatives. The above results emphasize that the 7HC derivatives bind to HSA in MD simulations due to the change in the microenvironment of HSA which leads to the conformational changes of protein. The increase in *R*g values is strongly supported by the experimental CD data that upon binding of 7HC derivatives to HSA, the protein gets partially unfolded (Fig. 4.14). Thus, the MD simulation data clearly showed that HSA-7HC complexes were stabilized due to conformational rearrangements. The similar reports were shown by our group that the conformational changes may occur upon binding of ligands during MD simulation (Sudhamalla et al., 2010; Garg et al., 2013).

The flexibility of local protein was investigated by calculated RMSF values of free HSA and HSA–7HC derivative complexes were plotted on the 10ns trajectory against residue numbers and data shown in our results distinctly indicate that sub-domain IIIA in HSA-7HC-1, subdomains IIIB in HSA-7HC-2 complexes and IIIB in HSA-7HC-3 complex have lower fluctuations as compared to all other domains (IA, IB, IIA, and IIB) which have high fluctuations. Results suggested that the structure of drug binding sites IIIA and IIIB remains rigid during simulation (Fig.4.14). The analysis provides an indication that HSA binding site IIIA interacts clearly with 7HC-1

and IIIB with 7HC-2 and 7HC-3 through remodeling of 7HC derivatives to the specific sites of HSA, which results in structural alteration of the protein. These results suggest that the structure of primary drug binding site I (IIIA) remains rigid during simulation of all the three 7HC derivatives. The binding of 7HC derivatives to HSA mainly affects the loop regions connecting the helices. This study provides evidence that HSA binding site II (IIIA subdomain) interact specifically with 7HC derivatives through conformational adjustments of the protein structure, in conjunction with ligand conformational adaptation to these sites. It clearly indicates that the 7HC derivatives change the microenvironment of HSA leads to the conformational changes in the HSA during MD simulation. This *R*g value is strongly supported by the experimental CD data. Thus, our experimental data (CD) fully supports the MD simulation in which protein conformational changes occur during coumarin derivatives binding to HSA.

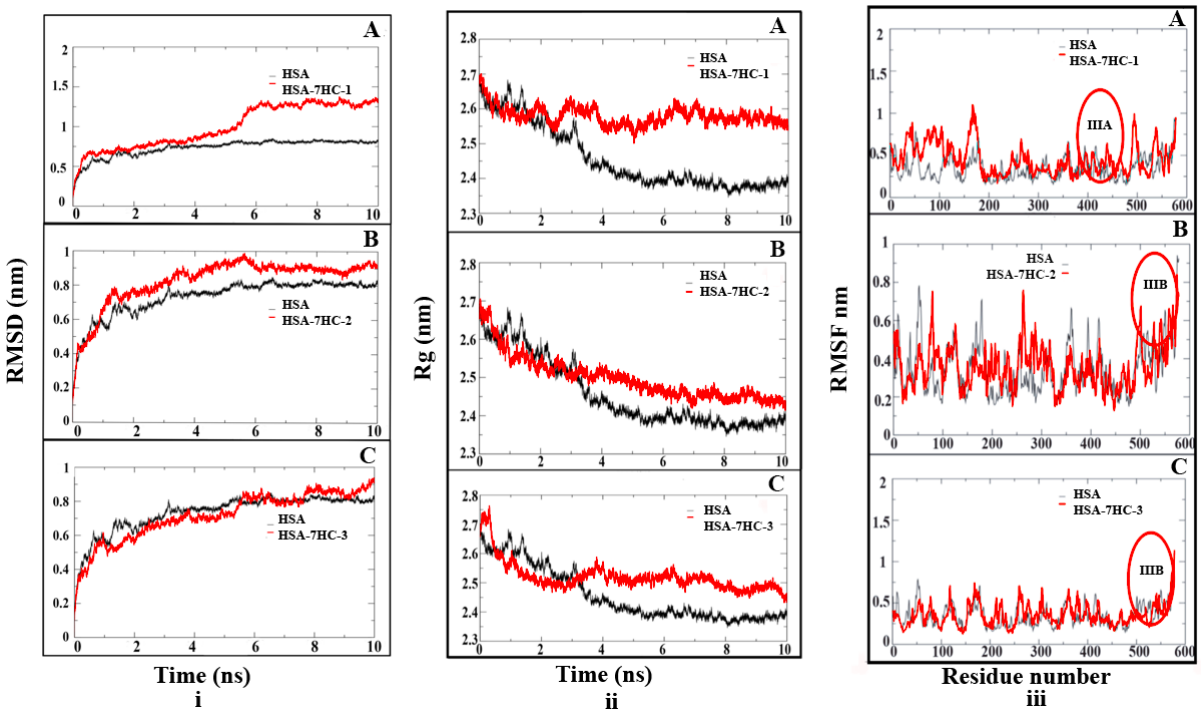

Fig.4.14. (i) The plot of HSA-Coumarin derivatives (7HC-1, 7HC-2 and 7HC-3) RMSD. (A, B and C) C_α rmsd values for free HSA and HSA-7HC-1, 2 and 3 complexes during 10ns MD simulation. **(ii)** (A, B and C) the radius of gyration (*R*g) values during 10ns of MD simulation of HSA and7HC-1,2 and 3 during 10ns of MD simulation. **(iii) (**A, B and C) the RMSF values of free HSA and HSA-7HC-1,2 and 3 complexes were plotted against residue numbers.

4.3. Conclusion

Docking studies showed that docking conformer is close and consistent with the binding constants and free energy values determined by fluorescence studies. Apparently, the docking studies revealed that bioactive compounds bind within known binding sites i.e., Sudlow site 1 and Sudlow site 2 and third major subdomain IB. Therefore, the location and the nature of interactions based on the docking studies suggest that the decrease in the emission intensity of HSA is due to the complexation of bioactive compounds in subdomains IIA, IIIA, and IB (Table 4.1). In addition, the results that I have mentioned shown that bioactive compounds bind with HSA mainly by hydrophobic interactions and for few compounds with hydrogen bond interactions which even few bioactive compounds showed interaction with AGP as well.

These results are in harmonizing with the binding constants and free energy calculations which were derived from fluorescence quenching and SPR. This proves that bioactive compounds are robust enough to bind with HSA which may increase the efficacy of therapeutic action and half-life *in vivo*. Furthermore, MD simulations of selected bioactive compounds showed the changes in the parameters of RMSD and Rg indicating the conformational changes with respective to HSA alone, which are consistent with the circular dichroism spectra. These changes are due to the changes in the interior flexibility of the subdomains IIA, IIIA, and IB domain of HSA which are evident from the RMSF studies. Rg data indicated that HSA-bioactive complexes are stable and compact with respect to HSA crystal structure. With the CD data and MD studies, I analyzed that the changes in the secondary structure are altered upon formation of HSA-bioactive complexes which is not due to the destabilization.

Table. 4.1. *In silico* binding constants, free energy, and binding sites

S.No	Drug	Binding constant (M^{-1})	Free energy (ΔG^0) (Kcal/mol)	Binding site
1	Artemisinin	3.8×10^4	-6.2	IIA
2	Ar-tumarone	1.2×10^4	-5.6	IIIA
3	Apocyanin	3.8×10^3	-4.89	IIA
4	Andrographalide	1.2×10^4	-5.6	IIA
5	Bacosine	2.6×10^4	-6.05	IIA
6	Corilagin	1.5×10^4	-5.7	IIA
7	Chebulinic acid	--------	--------	IIA
8	Chebulagic acid	--------	--------	IIA
9	De Andrographalide	1.3×10^4	-5.6	IIA
10	deForskolin	1.6×10^4	-5.73	IIA
11	Embelin	4.1×10^3	-4.9	IB
12	L-dopa	3.5×10^3	-4.9	IIIA
13	Menthol	2.95×10^4	-4.73	IIA
14	Piperine	3.3×10^5	-6.8	IIA
15	psoralen	2.2×10^4	-5.9	IIIA
16	Pterostiblene	4.0×10^4	-6.2	IB
17	Rosmaric Acid	1.6×10^4	-5.8	IIA
18	Stigmasterol	4.1×10^5	-7.26	IIIA
19	6-shagoal	2.24×10^4	-5.91	IIA
20	Umb-1	9.2×10^3	-5.4	IIIA
	Umb-2	1.2×10^5	-6.9	IIIA
21	7HC-1	3.6×10^4	-6.15	IIIA
	7HC-2	1.2×10^4	-6.2	IIIB
	7HC-3	4.6×10^4	-5.5	IIIB

CHAPTER 5

COMPARATIVE BINDING ANALYSIS OF BIOACTIVE COMPOUNDS WITH HSA AND AGP

5.1. Introduction

Human serum albumin and α-1 acid glycoprotein (AGP) are the most important drug binding proteins in plasma that can have important pharmacokinetic implications. Since plasma concentration of AGP may change under various physiological and pathological conditions (such as during the acute-phase reaction), resulting in alteration of the binding of various drugs and other ligands (Kremer et al., 1988; Fournier et al., 2000). Changes in drug binding and, consequently, alteration in the levels of the unbound (free) drug can have a significant effect on both the pharmacokinetics and pharmacodynamics of drugs. Although the contribution of AGP in the pharmacokinetics of drugs is less when compared with HSA, recently binding studies with AGP is also paid attention (Otagiri et al.,2009). It has been reported that there are few drugs which bind equally to both HSA and AGP, furthermore from the literature, it appeared that there is only one binding site on AGP for acidic drugs (Kalra et al., 2003) excepted for phenobarbital for which two sites have been described (Zsila et al., 2013). In view of the considerable impact of AGP in the binding of drugs, we are interested to know whether the bioactive compounds have any binding with AGP and how it will be comparable with the similar plasma protein like HSA. Here, we examined the binding of selected bioactive compounds (ANDR, COR, EMB, PIP and 7-Hydroxy coumarin derivatives and other bioactive compounds are not binding to AGP) using fluorescence and docking studies.

5.2. Results and Discussion

Fluorescence studies used to characterize the binding constants, free energy and a number of binding sites according to the procedures given in chapter 3. From the fluorescence studies, the mechanism of quenching is found to be a static mechanism which is evident from the bimolecular quenching constants of ANDR, COR and PIP are 5.27×10^{13}, 5.3×10^{13}, 5.5×10^{1} M^{-1} s^{-1} and respectively (See Chapter 3, Table 3.4). It is observed that quenching of emission maximum at 340 nm of AGP was observed with CHN, CHG, COR and PIP (Fig. 5.1, to Fig. 5.6) whereas with 7-Hydroxy coumarin derivatives (7HC-1, 7HC-2 and 7HC-3) and EMB, there is no quenching was observed. Interestingly blue shift and red shifts were observed in the peaks of AGP-ANDR (Fig.3.3.B) and AGP-PIP (Fig.5.4) respectively, whereas with HSA there is no shift in the peaks of these two compounds. This phenomenon might be due to the unfolding of the protein after the binding. The possible explanation for the shift

might be due to the differential exposure of tryptophan residues at various positions in the protein, which may be exposed differentially to the polar environment leading to the shift in the emission maximum at 340 nm, whereas with ANDR, COR and PIP the binding constants are 10 times lesser then HSA. All the compounds (ANDR, COR and PIP) binds with AGP in 1:1 ratio indicating that only one molecule is bound with AGP, similarly with HSA. The negative free energy of all these bioactive compounds is less than the values obtained with HSA (See Table 5.1). There are several studies showed that AGP have moderate to high affinity (10^{3}-10^{6} M^{-1}) with several drugs (Urien et al., 1986; Morin et al., 1997; Israili & Dayton 2001), some drugs showed equal binding with both HSA and AGP (Kumar et al., 1993) and few drugs like acetaminophen, phenobarbital, theophylline, and valproic acid showed negligible binding to AGP (Bailey & Briggs 2004). Not all bioactive compounds binds to AGP and even in my case only specified compounds bound to AGP. The detailed binding analysis has been discussed below.

5.2.A. Binding Analysis of ANDR with AGP using Surface Plasmon Resonance

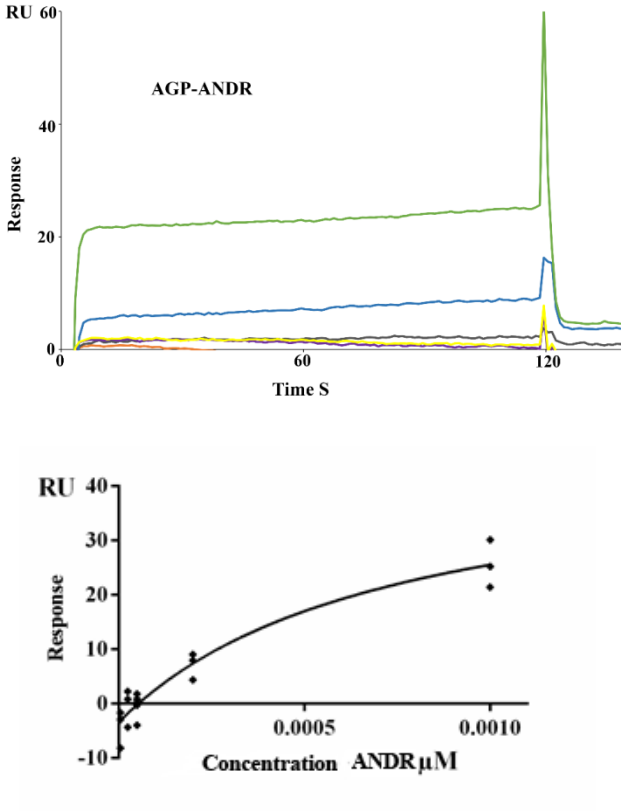

Fig.5.1. Sensorgram of binding of ANDR to AGP immobilized on CM 5 sensor chip (top) and R_{eq} values fitted to the steady state isotherm binding model (bottom) for ANDR binding to the AGP chip surface.

In this study, the interaction between ANDR and HSA and AGP was studied by means of above-mentioned techniques. The results showed that ANDR can be bound to HSA to form a complex. The association constants obtained from the fluorescence and SPR experiments were very close namely, $1.85 \pm 0.02\times10^{4}\ M^{-1}$ (fluorescence) and $3.1 \pm 0.04\times10^{3}\ M^{-1}$ (SPR), respectively.

However, I have even performed SPR by immobilized AGP as well to investigate the interaction of ANDR to AGP under flow conditions. Binding affinity obtained from this fluorescence and SPR spectroscopy were in good agreement with each other with, $1.5 \pm 0.03\times10^{3}\ M^{-1}$ and $1.39 \pm 0.06\times10^{3}\ M^{-1}$, respectively (Fig.3.3.B and Fig.5.1). Steady state analysis (weak and moderate interactions) data initially extracted using Biacore X100 Control Software, version 2.0.1. Hence, the binding constants obtained from the fluorescence and SPR are almost similar.

5.2.B. Binding analysis of Corilagin

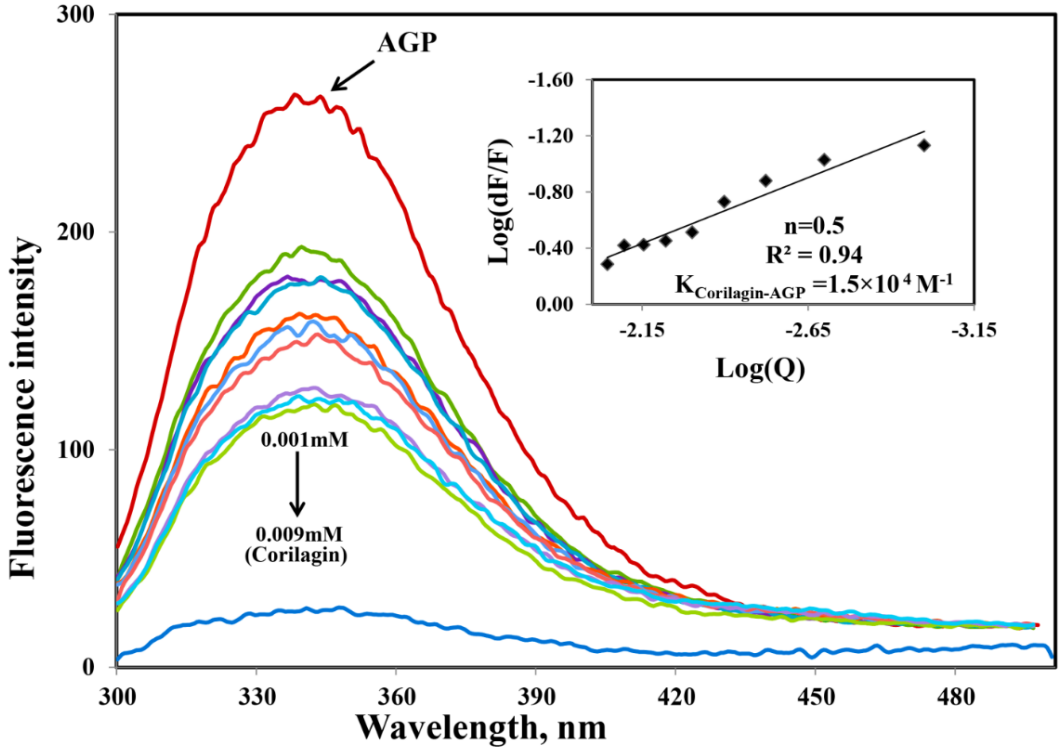

Fig.5.2. Fluorescence emission spectra was measured for AGP along with corilagin in 0.1 M phosphate buffer with pH 7.4, λex = 285 nm, and temperature = 25 °C. Free AGP (0.001 mM) and free AGP with different concentrations of corilagin, 0.001- 0.009 mM. Inset: Plot of log (dF/F) against log [Q]. λex = 285 nm and λem = 340 nm.

Interestingly, the binding of corilagin with AGP was also stronger like HSA ($4.2 \pm .03 \times 10^5$ M^{-1}) and the binding constant was found to be $1.5 \pm .01 \times 10^4$ M^{-1} which is in the range of food and drug administration (FDA) (Fig.5.2). Further, the computational calculated binding constant as 1.0×10^3 M^{-1} obtained as lowest free energy. However, corilagin have good interactions with HSA and AGP, in fact, binding constants with AGP are falling in the range of known FDA approved drugs like furosenamide, imipramine, and benzylpenicillin which are having binding constants 2.6×10^4, 2.5×10^4, and 1.2×10^3 M^{-1} respectively (Varshney et al., 2010). Since these derivatives possess binding constants in the range of 10^3-10^4 suggesting that corilagin binds strongly with HSA and AGP which has importance in the disposition of these molecules. It is known that most of the normal cases HSA acts a carrier for various drug molecules, however, in pathological conditions, the AGP also plays a major role in transporting the drug molecules. Recently, we have also reported that chitosan oligomers were strongly bound to AGP, whereas other molecules like 7-hydroxycoumarin derivatives have shown weak binding to AGP (Yeggoni et al., 2014a; Gokara et al., 2015). Thus, corilagin is a potent phytochemical and can bind to both HSA and AGP which are pharmacologically important proteins. In the case of AGP the free energy calculated from experimental and computational to be -5.6 and -3.83 kcal M^{-1}, respectively. The difference in free energy and binding constants from experimental and computational may be due to differences in arrangement solution and crystal structural. Hence, it is a validation of both the experimental and computationally calculated free energies.

5.2.C. Binding analysis of Chebulinic and Chebulagic acid

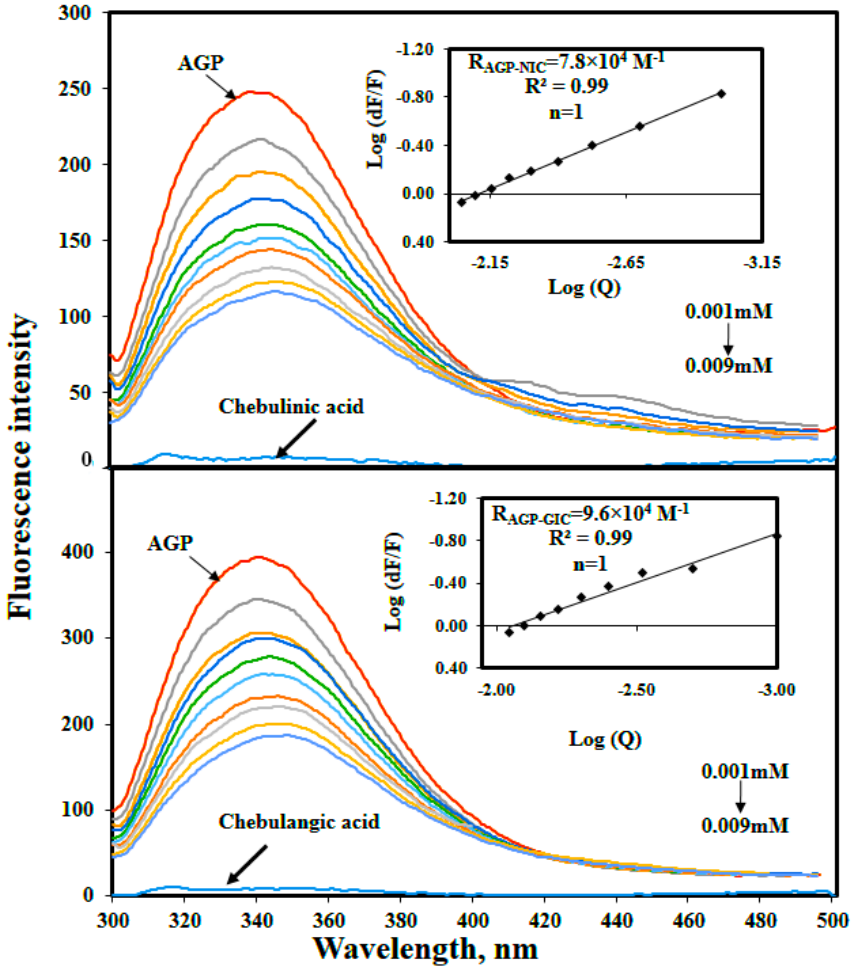

Fig.5.3. Fluorescence emission spectra was measured for AGP along with chebulinic and chebulangic acid in 0.1 M phosphate buffer with pH 7.4, λex = 285 nm, and temperature = 25 °C. Free AGP (0.001 mM) and free AGP with different concentrations of chebulinic and chebulangic acid 0.001, 0.002, 0.003, 0.004, 0.005, 0.006, 0.007, 0.008, and 0.009 mM**.** Inset: Plot of log (dF/F) against log [Q]. λex = 285 nm and λem = 340 nm.

The binding constants of Chebulinic acid and Chebulagic acid with AGP were good and found to be $K_{CHN-AGP}$ = 7.8 ±0.01× 10^4 M^{-1} and $K_{CHG-AGP}$ = 9.6± 0.01 × 10^4 M^{-1}. These results indicate that the binding of CHN and CHG are specific to plasma proteins where binding constants of HSA are $K_{CHN-HSA}$ = 1.2 ±0.01× 10^5 M^{-1} and $K_{CHG-HSA}$ = 3.7± 0.01 × 10^5 M^{-1} (Fig.5.3). Since CHN and CHG are binding to AGP, which is over expressed in pathological conditions and might help in transport of the compounds.

5.2.E. Binding analysis of Piperine

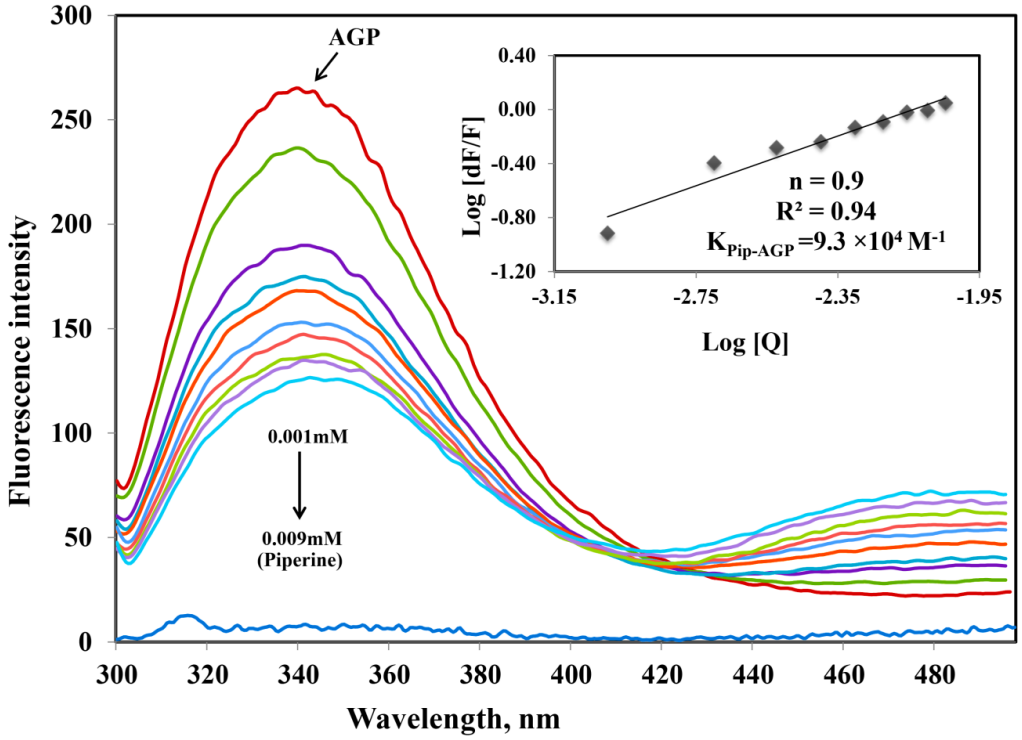

Fig.5.. Fluorescence emission spectra was measured for AGP along with piperine in 0.1 M phosphate buffer with pH 7.4, λex = 285 nm, and temperature = 25 °C. Free AGP (0.001 mM) and free AGP with different concentrations of piperine, 0.001, 0.002, 0.003, 0.004, 0.005, 0.006, 0.007, 0.008, and 0.009 mM. Inset: Plot of log (dF/F) against log [Q]. λex = 285 nm and λem = 340 nm. Inset: Plot of log (dF/F) against log [Q]. λex = 285 nm and λem = 340 nm.

The binding of piperine with AGP was also stronger and the binding constant was found to be 9.3× 10^4 M^{-1} which is in the range of FDA (Fig.5.4) indicating that during acute conditions piperine derived molecules can use a potential drug molecule.

5.2.F. Binding analysis of 7-Hydroxy coumarin derivatives

The binding of 7-hydroxycoumarin derivatives is marginal with AGP in comparison with HSA and their binding constants found to be in the range of K_{7HC1}= 9 ×10^2 M^{-1} ,K_{7HC2} =9×10^2 M^{-1} and K_{7HC3} = 5 ×10^2 M^{-1} which is not in the limitation of drug binding (Fig.5.5). Also, indicates that the binding of coumarin derivatives are specific to serum albumin proteins because all drugs won't bind to AGP and thus, we may not predict the coumarin derivatives binding to AGP because AGP is a positive acute-phase protein.

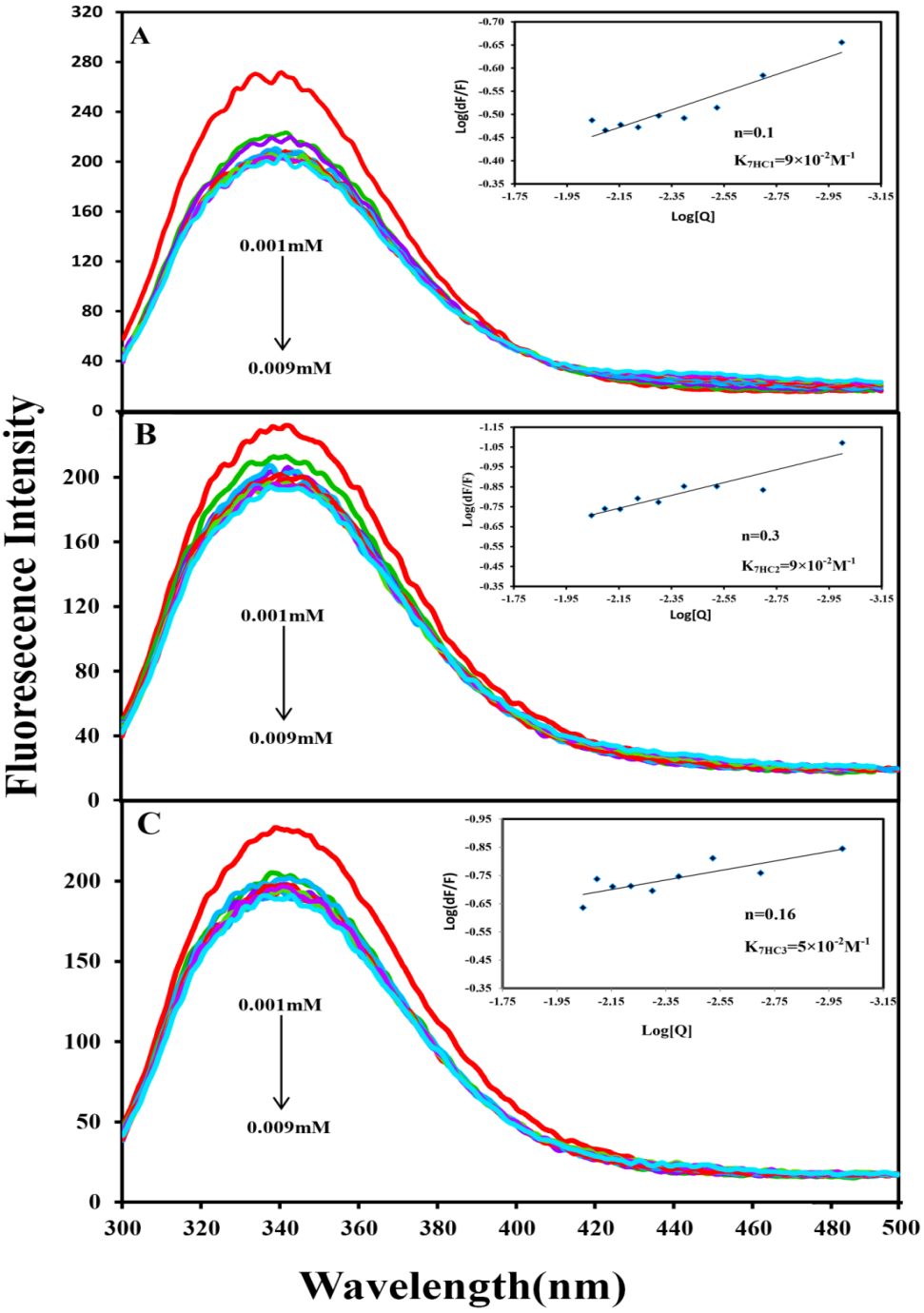

Fig.5.5. Fluorescence emission spectra of AGP-Coumarin derivatives (7HC-1,7HC-2 and 7HC-3) in 0.1M phosphate buffer pH 7.4, λ_{ex} = 285 nm. λ_{em} = 340 nm. Inset: Plot of log (dF/F) against log [Q]. λex = 285 nm and λem = 340 nm.

5.2.G. Binding analysis of novel 8-substituted coumarin derivatives

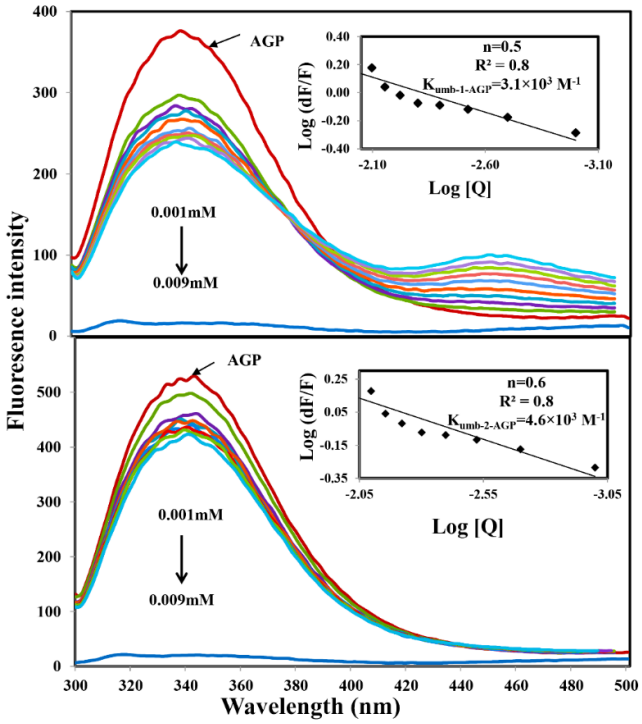

Fig.5.6. Fluorescence emission spectra of AGP-Coumarin derivatives (Umb-1 and Umb-2) in 0.1M phosphate buffer pH 7.4, λ_{ex} = 285 nm. λ_{em} = 340 nm . Inset: Plot of log (dF/F) against log [Q]. λex = 285 nm and λem = 340 nm.

The binding constants of Umb-1 and 2 derivatives with AGP were slightly less when compared with HSA, and their binding constants were found to be $K_{umb\text{-}1\text{-}AGP}$ = 3.1 ±0.01× 10^3 M^{-1} and $K_{umb\text{-}2\text{-}AGP}$ = 4.6± 0.01 × 10^3 M^{-1} (Fig.5.6). We also have calculated the binding constant by using a different computational technique, which shows *K* to be 3.0 × 10^3 and 4.3 × 10^3 M^{-1}, thus these results were in reasonable agreement with the experimental data. These results indicate that the binding of Umb-1 and Umb-2 are specific to serum proteins like HSA and AGP. Since Umb-1 and 2 are binding to AGP, which is overexpressed in pathological conditions, like renal failure, hepatic, pregnant conditions etc. Thus, we could infer that these molecules can be potential therapeutic candidates. However in the case of Umb-1/Umb-2– with AGP, the free energy calculated from experiments and computations were found to be –4.7, -4.9 and -4.74, -4.75 kcal M^{-1}, respectively. Experimentally and computationally calculated values of free energies are in corroboration, therefore we conclude that our results are more authentic. Thus, both proteins HSA and AGP interact with Umb-coumarin derivatives by hydrophobic forces.

It is known that most of the cases HSA are a vehicle to carry the drug molecules, however, in chronic disease conditions, the AGP also play a major role in transporting the drug molecules (Gokara et al., 2010; Gokara et al., 2014; Gokara et al., 2015; Yeggoni et al., 2015 a & b; Yeggoni et al., 2015 a; Yeggoni et al., 2016 a). Acute-phase proteins are proteins whose plasma concentrations increase in response to inflammation like AGP. The abundance of plasma protein levels follows the impact on drug binding extent, cause modifications in the mode of drug action, distribution, disposition, and elimination. Thus, AGP is one of the most important acute phase proteins influences the principal binding proteins for basic drugs.

5.3. Docking studies of the selected bioactive compounds with AGP

5.3.A. Docking analysis of Andrographolide (ANDR)

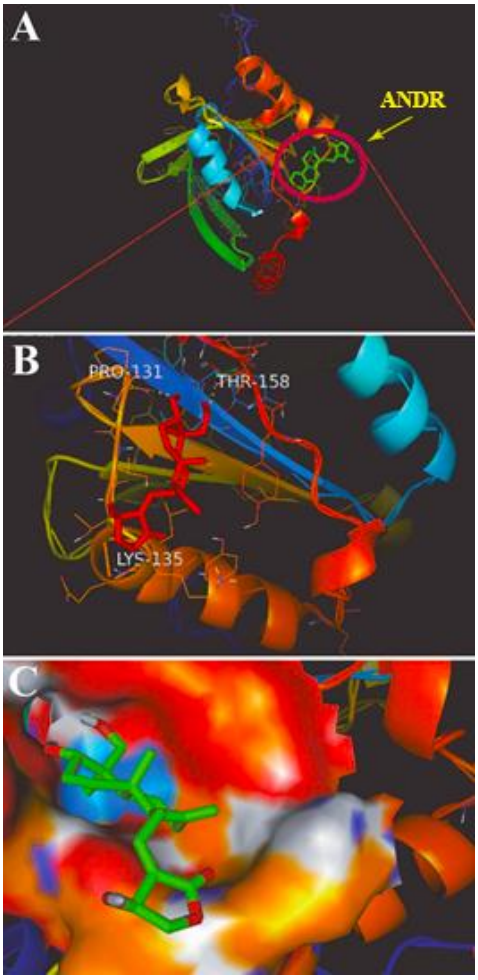

Fig.5.7. Docking conformation of AGP-ANDR complex obtained from Autodock v 4.2. (A) ANDR bound to AGP (Protein represented in ribbon model and ligand represented in stick model). (B) Stereo view of ANDR bound to AGP (prepared by using pymol v 1.5) in surrounding residues is represented as lines (Three hydrogen bonds are Pro 131, Lys 135, Thr 158). (C) The binding pocket surrounding the ANDR.

Whereas, AGP and ANDR interaction was computationally calculated and was found that their interaction was stabilized in ANDR-AGP complex by formation of 3 H-bonds with Pro 131, Lys 135, Thr 158 with a distance of 2.1 Å, 3.2 Å and 3.12 Å, respectively (Fig.5.7.A, B , and C). Further the binding constant (K_{ANDR}) is $7.7\pm0.05\times10^{4}$ M^{-1} and free energy change (ΔG°_{ANDR}) is -6.67±0.21 kcal/mol. These results support the experimental results (K_{ANDR} $=1.5\pm0.03\times10^{3}$ $M^{-1}$and ΔG°_{ANDR} =-4.31±0.031 kcal/mol) found in intrinsic fluorescence of AGP and ANDR interaction. ANDR with HSA is mainly stabilized by hydrophobic interactions along with two hydrogen bonds, whereas with AGP, the main forces involved are three hydrogen bonds. ANDR can show a robust binding to both HSA and AGP. Since AGP is an acute phase protein expressed in pathological conditions hence, binding of ANDR to the AGP warrant in drug binding studies.

5.3.B.Docking analysis of Corilagin

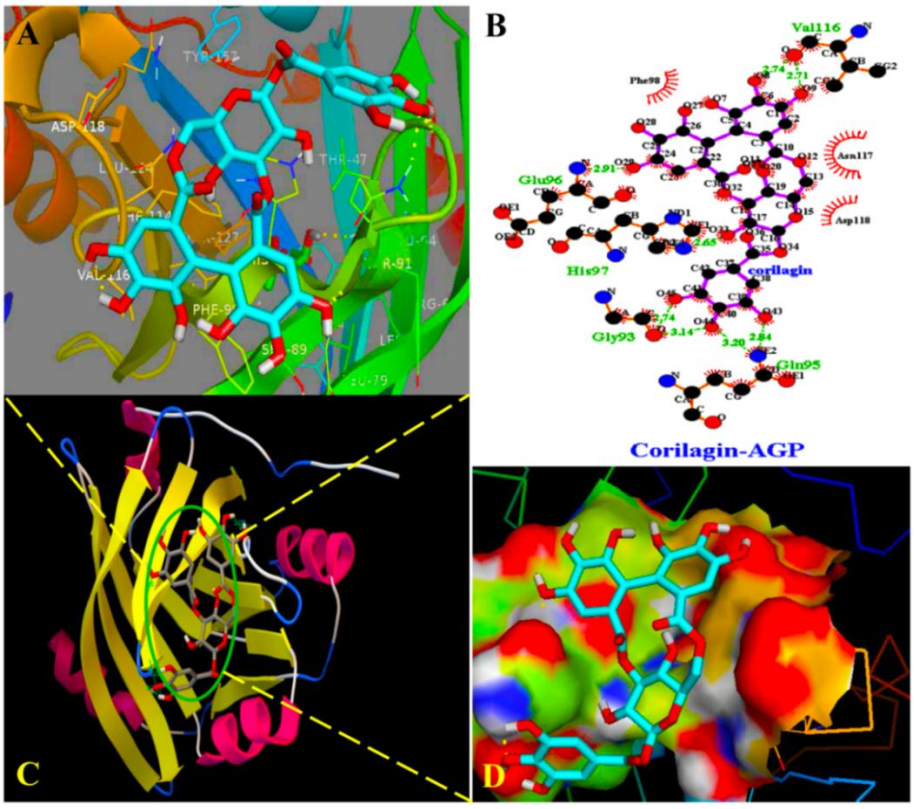

Fig.5.8. Docking conformation of AGP- corilagin complex obtained from Auto dock v 4.2. (A) Pymol Stereo view of corilagin bound to AGP in which corilagin is rendered as capped sticks and surrounding residues as lines (GLY93, GLU96, VAL116, HIS97, and GLN95). (B) Ligplot analysis of AGP with corilagin to show the hydrophobic interactions and The binding pocket showing hydrophobic and hydrophilic amino acid residues surrounding the probe corilagin, (C) corilagin bound to IIA domain on AGP (protein and ligand colored blue, red, yellow and green, respectively. (D) The hydrophobic and hydrophilic amino acid residues surrounding the corilagin.

Interestingly, docking studies revealed that corilagin, interacts with AGP with binding constants of 1.0×10^{3} M^{-1} and free energy was found to be -3.83 kcal M^{-1} which is nearer to the experimental, $1.5\pm .01 \times 10^{4}$ M^{-1}, and -5.6 kcal M^{-1} values (Fig.5.8). The corilagin -AGP complex is stabilized by hydrophobic amino acids and with 8 hydrogen bonds between the compound and GLY93, GLU96, VAL116, HIS97 and GLN95 with a bond length of 2.74, 2.91, 2.71, 2.14, 2.65, 2.84 and 3.20 Å. Over all the interactions of corilagin are varied between HSA and AGP, but the binding constants and free energy of experimental and computational are comparatively less than HSA suggesting that HSA- corilagin complex are more stable than AGP- corilagin complex. The results of docking studies indicate that the interaction between corilagin and HSA, AGP are dominated by hydrogen and hydrophobic interactions, which is in excellent agreement with free energies that are obtained from fluorescence data. However, the pharmacological behavior could change differently in diseased conditions and thus, corilagin binding to plasma protein of AGP would certainly an important process. Particularly, AGP is acute phase protein, hence, there were differential interactions were observed for the corilagin molecule with HSA and AGP.

5.3.C. Docking analysis of Piperine

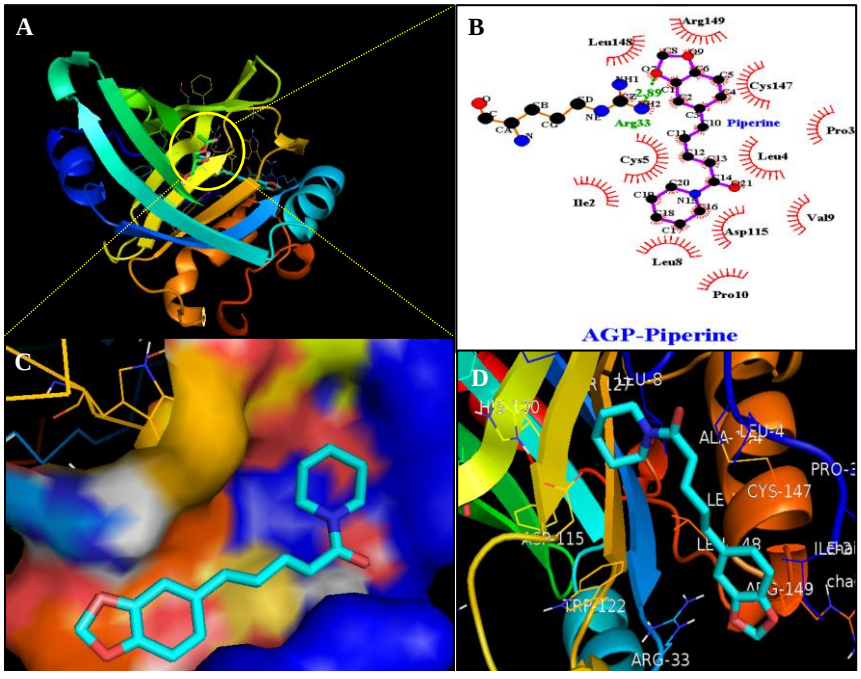

Fig.5.9. Docking conformation of AGP-piperine complex obtained from Auto dock v 4.2. (A) Piperine bound to AGP (Protein represented in ribbon model and ligand represented in stick model) (B) The binding pocket showing hydrophobic and hydrophilic amino acid residues surrounding the probe piperine, (C) Ligplot analysis of AGP with piperine to show the hydrophobic interactions and (D) Pymol Stereo view of piperine bound to AGP in which piperine is rendered as capped sticks and surrounding residues as lines (Lys5, Ile2, Arg149, Lys147, Arg33, Leu8, Pro10, Val9, Leu4 and Asp115).

Docking studies revealed that piperine interacts with AGP with binding constants of 1.2 × 10^4 M^{-1} and free energy was found to be -6.71 kcal M^{-1} which is nearer to the experimental, 9.3× 10^4 M^{-1}, and -6.71 kcal M^{-1} values (Fig.5.9). The Piperine-AGP complex is stabilized by hydrophobic amino acids and with one hydrogen bond between the compound and Arg 33 with a bond length of 2.89 Å. However, piperine-HSA complex is stabilized by hydrophobic interactions along with one hydrogen bond between the piperine and Lys212 with a bond length of 2.98 Å. Overall the interactions of piperine are varied between HSA and AGP, but the binding constants and free energy of experimental and computational are comparatively less than HSA suggesting that HSA-piperine complex is more stable than AGP-piperine complex. However, the pharmacological behavior could change differently in diseased conditions and thus, piperine binding to plasma protein of AGP would certainly an important process. Particularly, AGP is acute phase protein, hence, there were differential interactions were observed for the piperine molecule with HSA and AGP.

5.3.D. Docking analysis of Novel 8-substituted coumarin derivatives

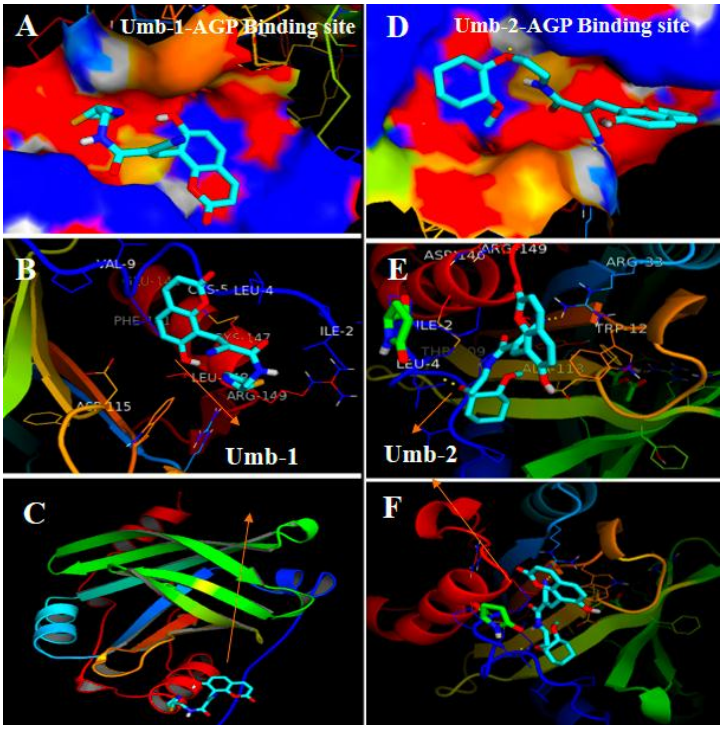

Fig.5.10. Different views of Umb-1 docked in the binding pocket AGP using Autodock 4.2. (A) Showing the hydrophobic cavity region of AGP with Umb-1. Pymol is used to generate the images. (B) The hydrophobic and hydrophilic amino acid residues surrounding the probe. (C) Overview of cartoon model of Umb-1 binding to AGP. (D) Showing the hydrophobic cavity region of AGP with Umb-2. Pymol is used to generate the images. (E) The hydrophobic and hydrophilic amino acid residues surrounding the probe. (F) Overview of cartoon model of Umb-2 binding to AGP.

Interestingly, molecular docking studies revealed that these Umb-1/Umb-2 showed interaction with AGP with binding constants of 3.0×10^3 M^{-1} and 4.3×10^3 M^{-1} and free energies are found to be -4.74 and -4.75 kcal M^{-1} (Fig.5.10). Furthermore, these values seem to be close to the experimental binding constants and free energy values $K_{umb\text{-}1\text{-}AGP} = 3.1 \pm 0.01 \times 10^3$ M^{-1}, $K_{umb\text{-}2\text{-}AGP} = 4.6 \pm 0.01 \times 10^3$ M^{-1} and -4.74, -4.9 kcal M^{-1}, respectively. In this study difference between experimental and computational results may be due to the differential arrangement of crystal and aqueous conditions. The obtained docking results are in good agreement with the above experimental data. Overall when we compare the binding and free energy values of both HSA and AGP, it indicates that Umb-coumarin derivatives- HSA complexes are more stable and has greater stability than AGP

Docking studies revealed that ANDR, COR, PIP, CHG, and CHN interacts with AGP with a binding constant and free energy near to the experimental values which reassure that the interactions of bioactive compounds with AGP which mimic the actual binding *in vitro.* These bioactive compounds interact with AGP by hydrogen bonds (see Table. 5.1 for amino acids, for COR in contrast with HSA, it is stabilized by hydrogen bonds with AGP, whereas with HSA it is stabilized by hydrophobic interactions and for other compounds (ANDR, PIP, UMB-1, and UMB-2) it is observed that these compounds are stabilized by hydrogen bonds with AGP and HSA. Whereas, with HSA the interactions between these compounds are varied and this might be the possible reason for the variation in the binding constants of these compounds with HSA and AGP. ADG with HSA is mainly stabilized by hydrophobic interactions along with two hydrogen bonds, whereas with AGP the main forces involved are three hydrogen bonds. PIP with HSA is stabilized by hydrophobic interactions with only one H-bond, PIP-AGP is stabilized by one H-bonds; HSA-COR is stabilized by eight hydrogen bonds the overall binding constants and free energy of both *in vitro* and *in silico* are comparatively less than the HSA suggesting that HSA-bioactive complexes are stable than AGP-bioactive complexes.

5.4. Conclusion

As observed from the binding studies of selected bioactive compounds with HSA from chapter 3, AGP (acute phase protein) indicated that only ADG, COR, CHN, CHG, PIP, Umb-1 and Umb-2 coumarin derivatives showed binding with AGP. Interestingly, these molecules bind almost equally to the HSA indicating that both proteins are very important in delivering these drug molecules. As AGP concentration increases in many diseases, which, effects the binding of certain drugs and their kinetics. Hence, this study will be helpful and play a pivotal role in pharmacology and clinical medicine as well as methodology. Hence, it is important to study the interaction of bioactive compounds with AGP along with HSA which may have a role in the disposition of drugs in pathological conditions, where HSA concentration is less in hepatic and renal- related diseases. I assume that our results will give a road map to develop inspired drugs to chronic diseases where AGP play a major role in drug transport.

Table 5.1. Comparative chart of binding constants, free energies, number of binding sites (n), type of interactions of selected bioactive compounds with HSA and AGP

S.No	Drug	HSA Binding constant (M^{-1})	HSA Free energy (Kcal/mol)	AGP Binding constant (M^{-1})	AGP Free energy (Kcal/mol)
1	PIP	5.7×10^5	-7.8	9.3×10^4	-6.71
2	7HC-1	4.6×10^4	-6.34	No binding	No binding
	7HC-2	1.3×10^4	-5.58		
	7HC-3	7.9×10^4	-6.65		
3	BAC	2.9×10^4	-6.07	1.8×10^3	-4.4
4	ANDR	1.85×10^4	-5.79	1.5×10^3	-4.31
5	EMB	5.9×10^4	-5.0	No binding	No binding
6	CHC	1.2×10^5	-6.90	7.8×10^4	-6.64
7	CHG	6.8×10^5	-7.57	9.6×10^4	-6.77
8	Umb-1	3.1×10^4	-6.1	3.1×10^3	-4.7
	Umb-2	7.0×10^4	-6.5	4.6×10^3	-4.9

CHAPTER 6

INTERACTION OF BIODEGRADABLE NANOCARRIERS WITH HUMAN SERUM ALBUMIN

6. 1 Introduction

Nanocarriers are materials which are nanoparticulate in size. These are able to encapsulate nano-sized substances to protect and bind, transport and sustain release at the specific site. These nanocarriers (1-100 nm in size) have been made up of a range of polymers and inorganic materials. Nanocarriers can transport a variety of guest materials, such as imaging agent nanoparticles, drugs, enzymes etc. However, most of the research works have been done in this field was focused on the medical application such as diagnostic and drug delivery purposes (Mura et al.,2013; Ang et al., 2014). Soluble macromolecules have an advantage over other biomolecules because of their flexible chains which can accommodate as well as adopt guest molecules. Encapsulation with an appropriate nanocarrier can protect the properties of guest particles against the environment and also from degradation. Hydrophobic drugs can be solubilized and transported in the water and carrier might even be able to transport the drug to the targeted site in the body where it can release and cure by acting on it. Encapsulation, not only protects the drug from the environment but also the system to the drug applied. Further, advantages of macromolecular nanocarriers are their ability to enhance the uptake of drugs or imaging agents by passive and active targeting (Svenson et al., 2012).

For the formation of nanocarriers, there are two main approaches followed such as (1) formation of micelles by self-assembly of block copolymers (amphiphilic) and (2) formation of the multifunctional hydrophobic core molecules surrounded by a functional hydrophilic shell. Dendritic polymers are divided into two major classes one is perfect dendrimers and another is hyperbranched polymers. Dendrimers are perfectly branched architecture with a degree of branching 100% and with a polydispersity index of 1 which indicates that they are monodisperse (Schlüter & Rabe 2000; Newkome et al.,2001). Another so-called hyperbranched are obtained one step reaction of polymerization exhibit similarity as that of perfect dendrimers analogs. Therefore, polymers that are hyperbranched are considered to be a better alternative for perfect dendrimers.

Available hyperbranched polymers are outlined as polyamides, polyamines, polyethers and polyesters (Yan et al.,2011). Nanocarriers are based on the dendritic polymers exhibit an excellent (*in vivo*) stability. However, desirable aspect is to release encapsulated guest for many biological applications.

6.2. Hyperbranched polyglycerols (hPGs)

The hPGs are synthesized by ring-opening multi-branching polymerization of glycidol (Tokar et al., 1994; Sunder et al., 2000) with exclusive properties associated with their nanometer size range. Additionally, hPGs are biocompatible, soluble in water and possessed low viscosity (Kainthan & Brooks 2007; Kainthan et al., 2008). Recently, unimolecular core–shell nanoparticles have attracted interest because of their unique property not fall apart on dilution. Haag's group developed an efficient unimolecular core–shell nanocarrier with a dendritic hydrophobic poly (ethylene) core and a grafted, dendritic, hydrophilic polyglycerol (hPG) shell (Popeney et al., 2012). Furthermore, a new type of unimolecular liposome-like multishell system has developed in the group based on a hydrophilic hPG core, a hydrophobic inner alkyl shell, and a hydrophilic outer mPEG shell. The nanocarriers which are having hPGs (hPG10-A-C18-mPEG350 and hPG10-E-C15-mPEG350) core with the composition of the nanocarriers are same, expect the C18: alkyl chain with 18 Carbon atoms C15: alkyl chain with 15 Carbon atoms (Fig.6.1) is used for my study. (Fleige et al., 2014a; Fleige et al., 2014b).

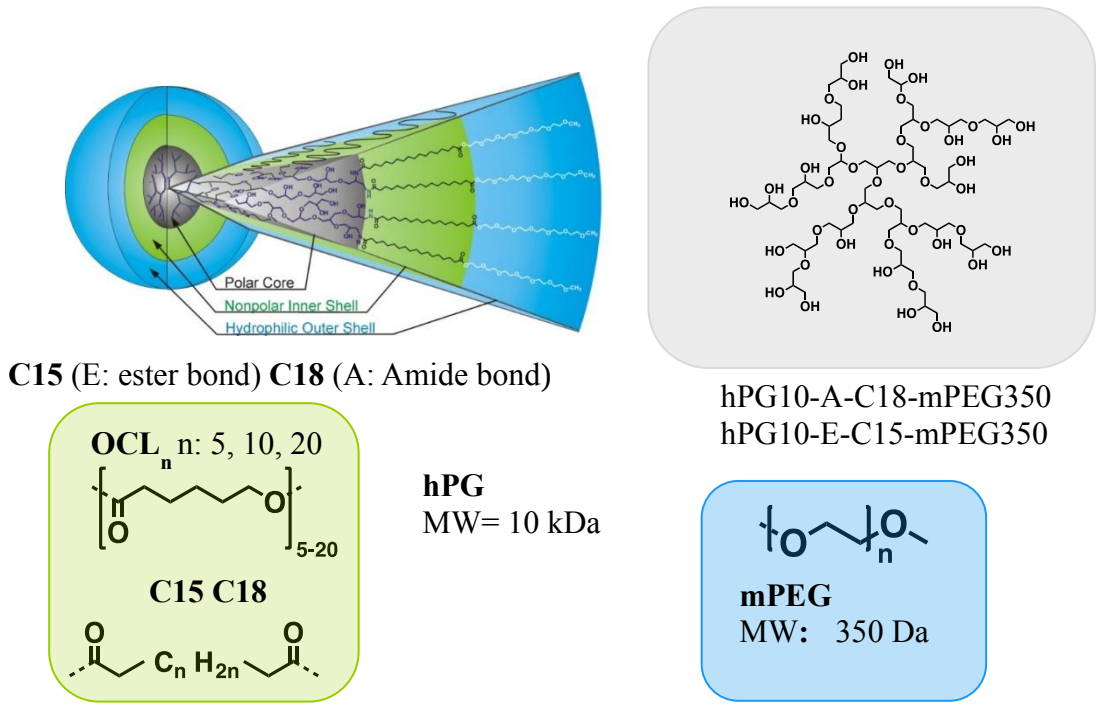

Fig.6.1. Schematic structure of a core–multishell nanoparticle based on a dendritic polyglycerol core (hPG, gray), an inner hydrophobic alkyl shell (green), and an outer hydrophilic shell made of poly(ethylene glycol)methyl ether with an average number averaged molecular weight of 350 g/mol (mPEG350, blue). But differ in the alkyl chain with 15 Carbon and 18 Carbon atoms.

6.3. Hyperbranched polyesters (hPEGs)

The hPEGs nondegradable drug carrier systems may accumulate in different organs, thus causing inflammation and toxic effects. The desirable property of unimolecular micelles for delivery of drugs is biodegradability. Hyperbranched poly esters are one of the biodegradable drug carriers. Additionally, they are nonionic, nonimmunogenic and low in toxicity. The mainstream of reported work focused on solubilizing the drugs with hydrophilic nanocarriers. The water solubility occurred in the branched nanocarrier by covalently attaching biocompatible poly (ethylene glycol) (PEG), which formed the outer shell of the nanocarrier (Kadajji & Betageri 2011). Whereas hyperbranched polyester, hPES32-E-CL8-mPEG2000, CL8: 8 repeating units of caprolactone and mPEG MW 2000 g/mol (Fig.6.2) (Walker et al., 2016).

.

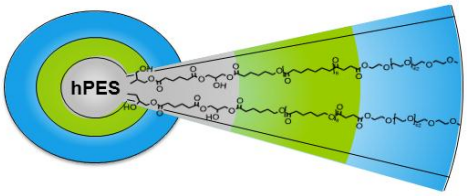

hPES32-E-CL8-mPEG2000

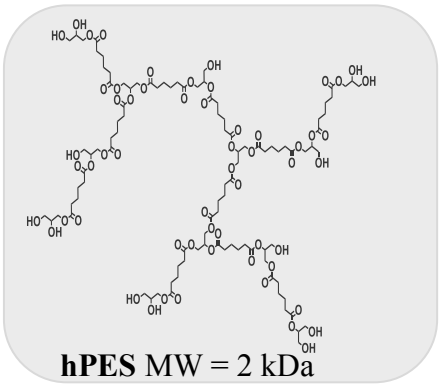

Fig. 6.2. Schematic structure of a core–multishell nanoparticle based on a dendritic polyester core (hPE, gray), an inner hydrophobic alkyl shell (green), and an outer hydrophilic shell made of poly(ethylene glycol)methyl ether with an average number averaged molecular weight of 2000 g/mol (mPEG2000, blue). CL8: 8 repeating units of caprolactone.

HSA acts as a carrier several endogenous and exogenous compounds including fatty acids (Sugio et al., 1999). HSA has long been a major attention of pharmaceutical company due to its ability to bind various ligands and alters their pharmacokinetic properties (Kratochwil et al., 2002). However, the study of nanocarriers is not been adequately studied. Therefore it was of present interest to study the binding of nanocarriers with HSA in aqueous solution in order to evaluate the effect of nanocarrier on HSA secondary structure element, conformation, and stability. In this report, I encapsulated piperine which is a bioactive hydrophobic drug which is highly insoluble

in water with biodegradable CMS nanocarriers.Later carried out the interaction between biodegradable nanocarriers with HSA by the biophysical approach.

Also, I carried out cell viability and *in vitro* cellular uptake of piperine nanoformulation. Nevertheless, I have presented a spectroscopic analysis of the interaction of HSA with nanocarrier at physiological conditions, using protein as a constant concentration and various nanocarrier compositions. Structural information regarding complexation of nanocarrier-HSA is reported here. Further, conventional CMS nanocarrier readily interacts with plasma proteins. The surface properties of nanocarrier remain a major factor that can improve half-life, which is likely to be used for the therapeutic purpose. Therefore, the aim of this study was to examine the interaction of CMS nanocarrier with HSA and as a result, predict the implications of their biological features for *in vivo* application.

6.4. Results and Discussions

6.4.A. Cell viability, cellular uptake, and association of CMS nanocarriers

As per the literature, the nanoparticles of size <200nm can be up taken *via* endo-cytosis through the process of diffusion into cancer cells (Panyam & Labhasetwar 2003; Vasir & Labhasetwar 2007). Therefore, the present study, I have carried out the feasibility of three different CMS nanocarriers for cancer cell uptake, as well as interaction with HSA. CMS nanocarriers have variable particle sizes and morphology (Fig.6.3). hPG10-E-C15-mPEG350, hPG10-A-C18-mPEG350, and hPES32-E-CL8-mPEG2000 nanocarriers have particle sizes of about 18.2±1.3, 25.9±0.6 and 18.7±0.2nm respectively. When nanocarrier incubated with HSA, the morphology of nanocarriers was distinctive in AFM, i.e, HSA corona might have formed or it has shown a behavioral change in their aggregation pattern (Fig.6.4). The change in the morphology of nanocarriers is similar to that caused by the formation of loosely bound proteins on metal or polymer nanoparticle surfaces or soft corona (Monopoli et al., 2011). The observed spot showed a high accumulation in the hPES32-E-CL8-mPEG2000 nanocarrier after HSA incubation is not the nanoparticle aggregation. This might be due to the higher rate of adsorption of HSA and hPES32-E-CL8-mPEG2000 exists through ionic bonding or an inclusion complex. In the case of the hPG10-E-C15-mPEG350, hPG10-A-C18-mPEG350, as HSA is interacting an aligned network was observed in the sample (Fig.6.4, white arrows).

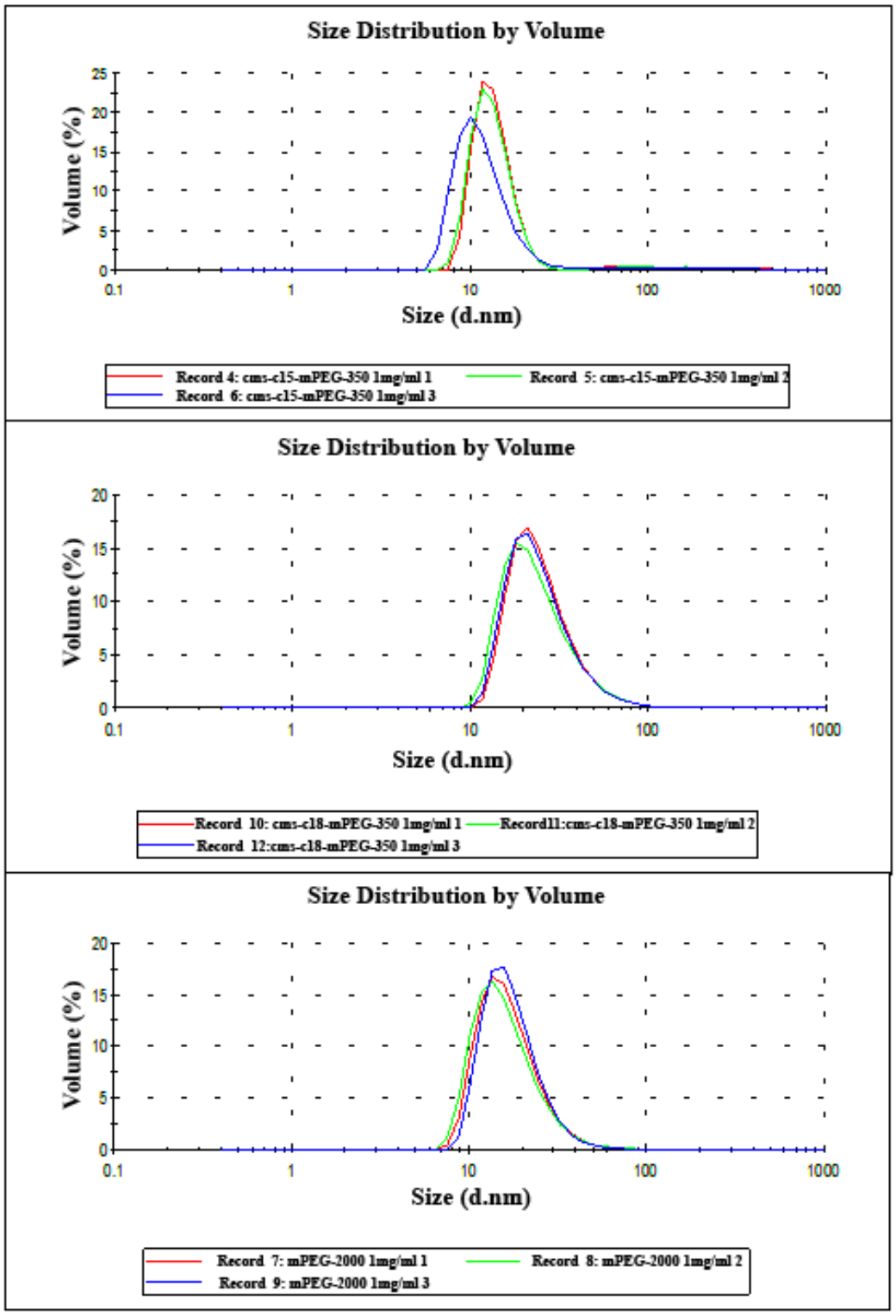

Fig.6.3. Hydrodynamic radii of CMS nanocarriers in PBS, analyzed using DLS.

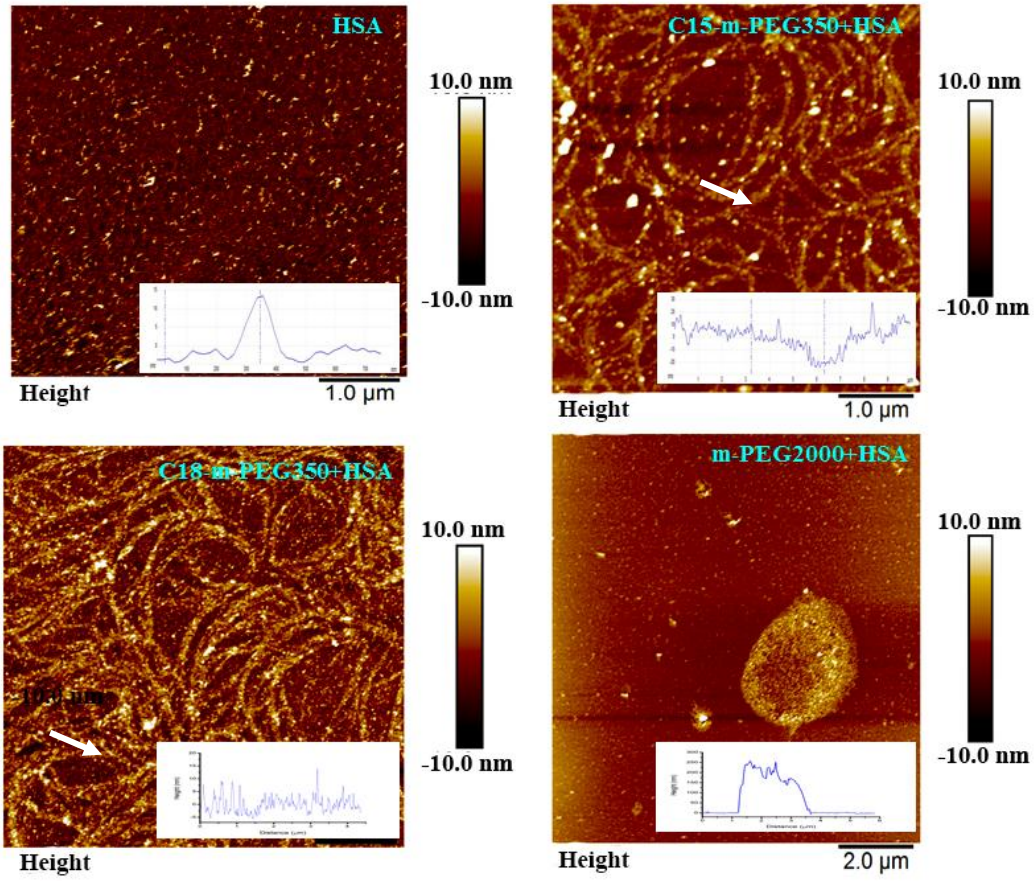

Fig.6.4. Atomic force microscopy images of the CMS nanocarriers (1 mg/mL) before and after incubation with human serum albumin (100 µg). Incubation with human serum albumin was performed for 2 h, after which the CMS nanocarriers were deposited on mica glass slides, and imaged under AFM. White arrows indicate aligned HSA networks.

6.4.B. Stability and release

The stability of pH-CMS nanocarriers loaded with piperine was studied under both i.e, acidic and physiological conditions and loaded piperine pH-CMS-C18-mPEG-350 nanocarriers at pH 5 & pH 7.4 at 37 °C till 48 h. After sample preparation, after 1-48 h, the samples were placed in small SEC columns. Sample at pH 7.4 has shown release about 15 -20% piperine over 48 h (Fig.6.5). Under physiological conditions, the loaded piperine-CMS nanocarriers can consider as relatively stable. The pH-CMS nanocarriers at pH 5 released piperine with time (Fig.6.5). This proves that under slightly acidic conditions piperine-loaded-CMS-C18-mPEG-350 efficiently release piperine. Interestingly, the other bioactive molecules loaded with CMS nanocarriers but encapsulation efficacy is less when compare to piperine which indicates only piperine is a right molecule for this study.

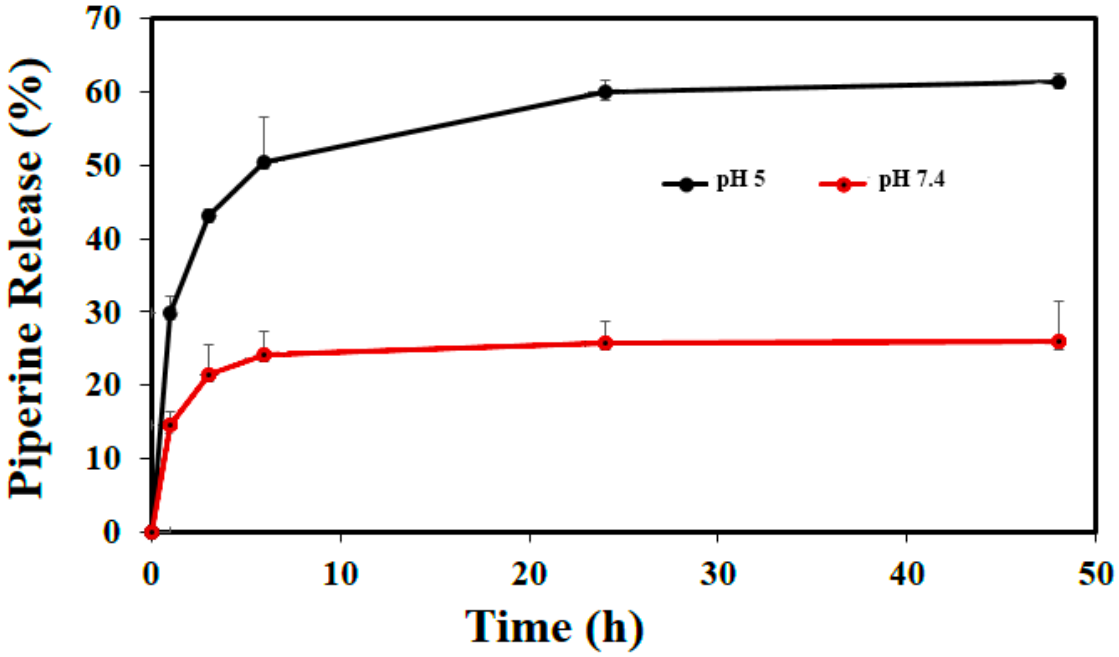

Fig.6.5. The release of piperine loaded CMS-C15-mPEG nanocarrier at a pH 5 and pH 7.4 over 48 h.

6.4.C. *In vitro* studies

The advantage of CMS nanocarriers overstable CMS nanocarriers wherein it lies the possibility to initiate and control the release of piperine. To confirm this advantage *in vitro* real-time cell analysis experiments were performed. The cell viability of unloaded CMS nanocarriers has studied over a period of 48h. Fig.6.6 shows that unloaded CMS nanocarriers are not toxic in nature. Thus at high concentrations (1 mg/mL) nanocarriers showed no toxic effects. Real-time cell analysis of piperine-loaded CMS nanocarriers showed a marginally higher toxicity of CMS nanocarriers compares to unloaded-CMS nanocarriers after 48 h. However, the cleavable systems of nanocarrier showed significantly high toxicity after 48h.

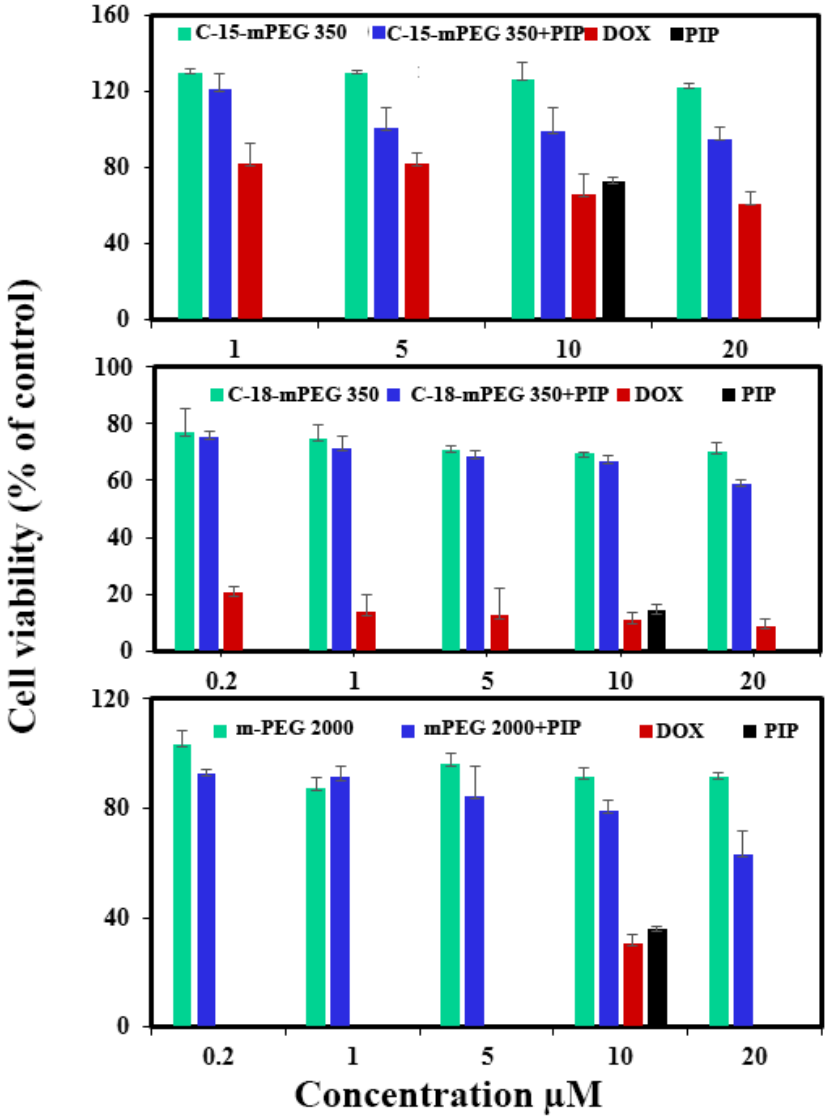

Fig.6.6. Real-time cell analysis of A549 cancer cells that were treated with different concentrations of unloaded and piperine loaded, taken Doxorubicin and piperine alone as control after 48h. Samples were calibrated on the piperine concentrations.

6.4D. Cellular Uptake

I have performed confocal microscopy in order to estimate the cellular uptake of CMS hPG10-A-C18-mPEG350-ICC nanocarrier. As it is seen in the Fig.6.7 the nanocarriers were up taken by A549 cell lines. The ICC fluorescence clearly indicated that there is the localization of the dye in the cytoplasm as well as in nuclei.

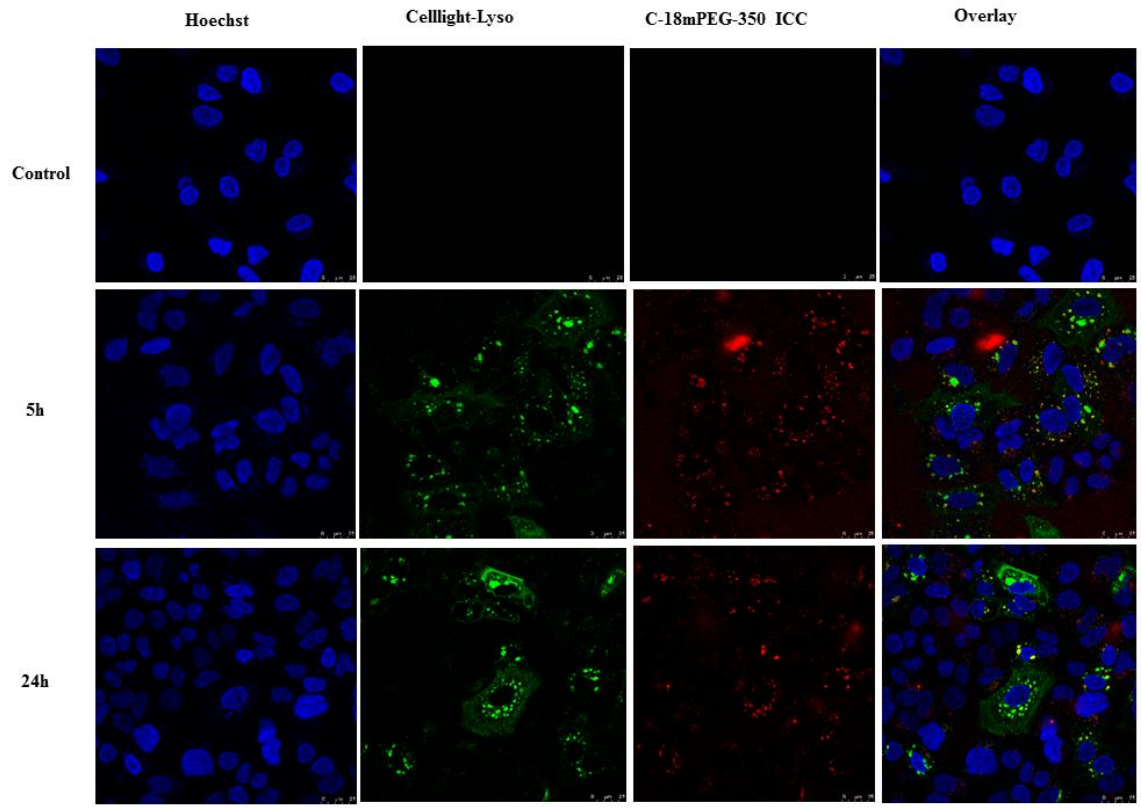

Fig.6.7. Confocal fluorescence microscopy picture of piperine-loaded CMS C-18-mPEG-ICC nanocarrier as well as cell light lyso for comparison, taken up by A549 lung cancer cells after 5 and 24h incubation. The cell nucleus is stained with Hoechst (blue).The CMS C-18-mPEG-ICC is shown in red due to the presence of ICC dye.

6.4.E. Fluorescence Spectra and Stability of CMS nanocarriers-HSA Complexes.

The fluorescence spectroscopy is the best method to calculate the binding constant, free energy of different CMS nanocarriers and also a number of binding sites with HSA. The fluorescence emission of HSA comes from aromatic amino acids of tryptophan, tyrosine, and phenylalanine. The emission spectrum of HSA is mainly from a single tryptophan residue located at the 214 position in subdomain IIA (Il'ichev et al., 2002; Sułkowska et al., 2002). Different concentrations of CMS nanocarriers hPG10-E-C15-mPEG350, hPG10-A-C18-mPEG350 and hPES32-E-CL8-mPEG2000 were used to study the fluorescence emission properties with HSA. Our results have shown that hPG10-E-C15-mPEG350, hPG10-A-C18-mPEG350, and hPES32-E-CL8-mPEG2000 molecules have a very little fluorescence and the addition of increasing concentrations (0.001-0.009 mM) of CMS nanocarriers hPG10-E-C15-mPEG350, hPG10-A-C18-mPEG350 and hPES32-E-CL8-mPEG2000 resulted in a decrease in the maximum emission at 360 nm (Fig.6.8). Hence, the quenching of the fluorescence is concentration

dependent. Decrease in fluorescence intensity may be due to the interaction of excited state of the fluorophore with its surrounding protein molecules (Lakowicz et al., 2009).

An increasing concentration of CMS nanocarriers hPG10-E-C15-mPEG350, hPG10-A-C18-mPEG350 and hPES32-E-CL8-mPEG2000 with HSA, the number of binding ligands were calculated to be 0.89, 0.53 and 0.9 for CMS nanocarriers hPG10-E-C15-mPEG350, hPG10-A-C18-mPEG350 and hPES32-E-CL8-mPEG2000 suggesting that HSA interacts with different CMS nanocarriers hPG10-E-C15-mPEG350, hPG10-A-C18-mPEG350 and hPES32-E-CL8-mPEG2000 in about one-to-one ratio (Fig.6.8). The binding constants of CMS nanocarriers hPG10-E-C15-mPEG350, hPG10-A-C18-mPEG350 and hPES32-E-CL8-mPEG2000 were calculated from the intercept as $1.7 \pm 0.6\times10^{5}$ M^{-1}, $3.0 \pm 0.4\times10^{5} M^{-1,}$ and $1.8 \pm 0.3\times10^{4}$ M^{-1} respectively. Thus, the free energy change calculated upon binding of CMS nanocarriers hPG10-E-C15-mPEG350, hPG10-A-C18-mPEG350 and hPES32-E-CL8-mPEG2000 to HSA were -6.34, -7.14 and -5.8 Kcal M^{-1} respectively at 25 ºC. This indicates that the free energy of HSA- CMS nanocarriers complexes are derived mainly from hydrophobic and possibly hydrogen bond interactions.

To authenticate the presence of static or dynamic quenching in drug-protein complexes have plotted Fo/F against Q and the results are shown in Fig.6.9. (Kq) were calculated to be $5.0 \pm 0.03 \times10^{13}$ M^{-1} s^{-1} for CMS nanocarriers hPG10-E-C15-mPEG350 -HSA and $5.4 \pm 0.02 \times10^{13}$ M^{-1} s^{-1} for, hPG10-A-C18-mPEG350 -HSA and $4.3 \pm 0.05 \times10^{13}$ M^{-1} s^{-1} for hPES32-E-CL8-mPEG2000 -HSA, respectively (Fig.6.9). Since these values obtained were far greater than the maximum collisional quenching constant ($2.0\times10^{10} M^{-1}s^{-1}$) (Agudelo et al., 2012; Zhang et al., 2012), thus the static quenching prevails between CMS nanocarrier-HSA complexes. Further, ITC experiments consist of a number of equal volumes of injections of mPEG-2000 solution from the syringe into HSA solution contained in the sample cell. The results obtained for an exothermic binding process are shown in the upper frame of Fig.6.10, where each peak is the result of the single injection, it can be seen that in the early injections the peaks are of an almost equal size, which indicates that nearly all of the injected ligand is bound by the HSA. The last injections, of very small size, show that saturation is virtually complete by the end of ITC experiment. The figure inset has the best value for stoichiometry n=1, binding constant Ka= $3.03 \pm 4 \times 10^{4}$ M^{-1} , ΔH= -18.5 ± 49.6 and ΔS= 18.8. The

injection point of this curve indicates that the mPEG-2000 binds to HSA in the sample cell with a 1:1 stoichiometry and binding constant obtained from ITC are close the binding constant obtained from fluorescence spectroscopy Ka=1.8 ± 0.3×10^4 M^{-1}. These results are mainly derived from the nanocarrier-induced quenching of intrinsic fluorescence of the HSA. The case of C15-mPEG350 and C18-mPEG350 at higher concentrations they are forming aggregates.

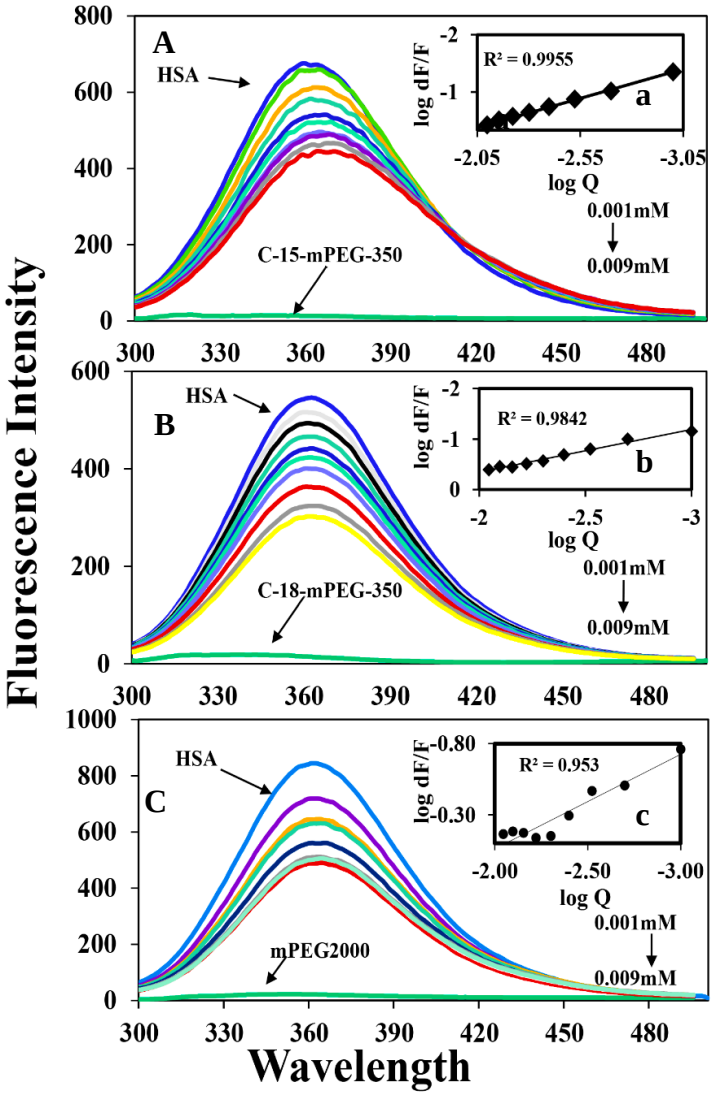

Fig.6.8. Fluorescence emission spectra of CMS nanocarrier-HSA systems in 10 mM PBS buffer pH 7.4 at 25 °C for (A) C-15-mPEG-350-HSA (B) C-18-mPEG-350 HSA and (C) mPEG-2000-HSA: (a) free HSA (0.001mM); CMS nanocarrier ranging from 0.001mM-0.009mM. The plot of log (dF/F) as a function of 1/CMS nanocarriers concentration.Inset: The binding constant K being the ratio of the intercept and the slope for (a) C-15-mPEG-350-HSA (b) C-18-mPEG-350 HSA and (c) mPEG-2000-HSA complexes.

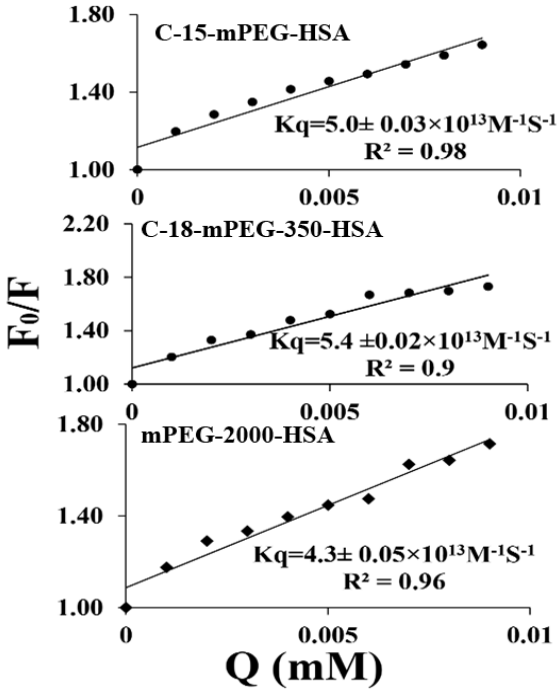

Fig.6.9. Stern volmer plots of fluorescence quenching constants (kq) for CMS nanocarriers-HSA complexes at different concentrations to determine dynamic and static quenching

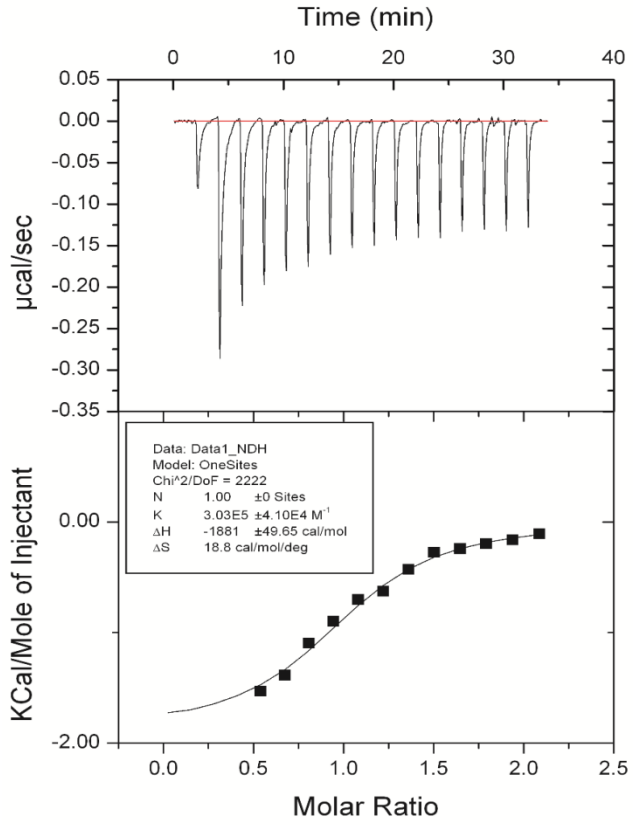

Fig.6.10. Isothermal titration calorimetric (ITC) profile for the titration of HSA in the presence of mPEG-2000 at 293 K. (A) Shows the heat change of dilution as a function of time per injection of the mPEG2000 at 298 K. (B) Shows the heat evolved against the molar ratio of (mPEG2000: HSA) at 293 K (black dots). The solid line is the fitted curve.

6.4.F. CD Spectra and Protein Conformation

CD spectroscopy is one of the best methods to identify the alterations in HSA secondary structure upon additions of different concentrations of hPG10-E-C15-mPEG350, hPG10-A-C18-mPEG350, and hPES32-E-CL8-mPEG2000 nanocarriers in accordance with their sensitivity to the change in the structure of protein. Secondary-structural elements were calculated by using CDNN 2.2 software program. CD spectroscopic results are shown in (Fig 6.11). Secondary structure calculations based on CD data suggest that free HSA has a high α-helix content, 57%, β-sheet 25.9% turn, and random coil 16.6%, which is consistent with the literature report. Upon CMS nanocarriers complexation, a major reduction of α -helix was observed from 57% free HSA to 44.8% in hPG10-E-C15-mPEG350, 43.7%, hPG10-A-C18-mPEG350, and 50.9% hPES32-E-CL8-mPEG2000 (Fig.6.11). The major decrease in α-helix was accompanied by an increase in the β-sheet and random coil structures. The major reduction of the α -helix with an increase in the β-sheet and random is consistent and results that showed a reduction of α -helix and an increase of random coil and turn structure due to a partial protein unfolding. This is very common that protein gets unfold during protein-ligand interactions particularly HSA-ligand complex, where our group have extensively studied (Gokara et al., 2010; Yeggoni et al., 2014 a; Gokara et al., 2015; Yeggoni et al., 2015 a & b; Yeggoni et al., 2016 a &b). These results are in agreement with the AFM pictures that the conformational change attributes to the nanoparticle aggregation and adsorption mechanism.

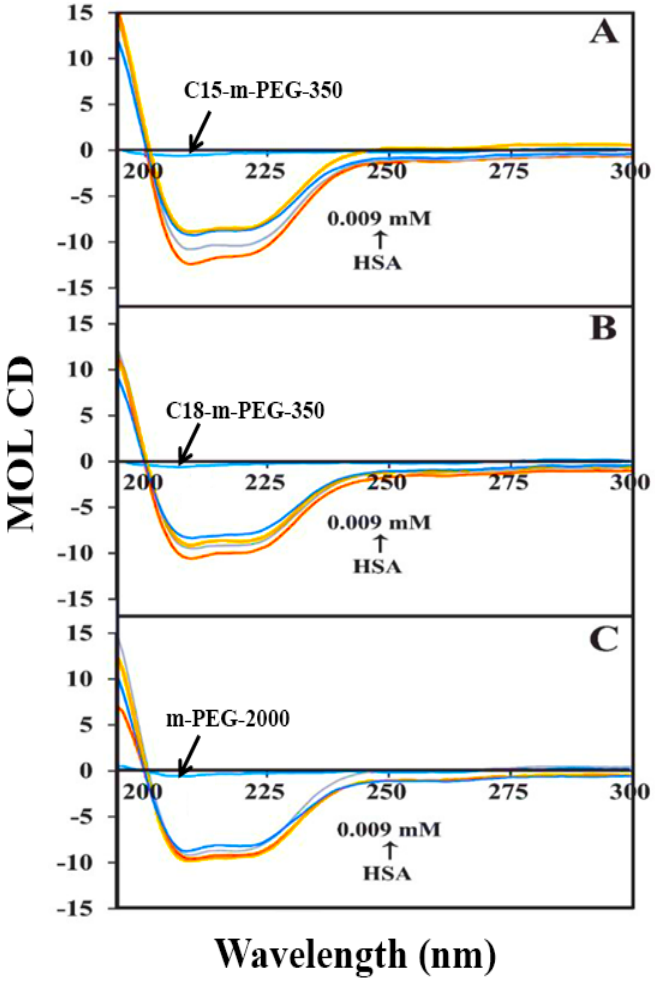

Fig.6.11. Circular dichroism of free HSA and its CMS nanocarriers complexes in aqueous solution with a protein concentration of 0.001mM and CMS nanocarrier concentrations of 0.001, 0.005, and 0.009 mM in PBS buffer, pH 7.4, at 25 °C.

6.5. Conclusion

CMS nanocarriers enabled the versatile nanocarriers to become pH responsive. The ester linkage used was rapidly cleaved at a pH 5. Piperine loaded C15-mPEG350 CMS nanocarrier was stable at pH 7.4 and showed sustained release of the drug. I am able to demonstrate that CMS-C-15-mPEG350 nanocarriers could release piperine more efficiently under the acidic conditions of intracellular compartments and therefore showed higher cell viability in comparison to the stable CMS nanocarrier. Real-time cell analysis C18-mPEG350-ICC were able to demonstrate that nanocarrier could release piperine more efficiently under acidic conditions in intracellular compartments, therefore showed little cell viability due to less encapsulation of piperine in comparison to CMS nanocarrier alone. On the basis of the spectroscopic analysis, CMS nanocarriers bind to HSA with the order of $K_{C18\text{-}350} > K_{C15\text{-}350} > K_{2000}$.

The interaction of CMS nanocarriers leads to a secondary structural change of HSA indicating partial unfolding of protein with an increase in the concentration of CMS nanocarriers. This work clearly demonstrates that CMS nanocarriers interact with HSA. These interactions and secondary structural changes were confirmed using biophysical techniques. High binding of C-15mPEG 350 and C-18 m-PEG350 with HSA which results in the form of aligned networks are observed through AFM images, thus it can be the limiting factor in biological applications. Further extensive research is required for confirming our results.

CHAPTER 7

SUMMARY

Summary

We examined the cytotoxicity of the selected bioactive compounds by MTT assay method for their anti-cancer and anti-inflammatory properties by performing cytotoxic studies on HepG2, MCF-7, HeLa, Raw mouse macrophages and A549 cell lines. Using these cell lines are appropriate *in vitro* model system for studying cancer and inflammatory diseases. The bioactive compounds of Apocynin, Andrographolide, Bacosine, 7-Hydroxy coumarin derivatives, Corilagin, Embelin, Piperine, Stigmasterol, Rosmarinic acid, Menthol, and 6-Shagoal decreased the cell viability of specific cell lines in a dose- dependent manner by significant IC_{50} values (Chapter 3, Fig 3.1). These result clearly indicated the cytotoxic activity of these bioactive compounds, showed a decrease in the viability of particular cell lines. From this study, we concluded that these compounds are having potent cytotoxic activity and thus, these compounds can be used as a therapeutic agent for hepatic diseases.

Consequently, Binding constants and free energy determined by using plasma proteins. All the selected bioactive compounds showed static quenching phenomenon by quenching intrinsic fluorescence of HSA which is apparent from Stern-Volmer plot, where the values are higher than the given collisional quenching constant (Chapter 3, Table. 3.4). Further, binding constants of all the selected bioactive from fluorescence studies are in the range of 10^3-10^6 M^{-1} which are in corroboration with the binding constants of well-known drugs. All the compounds binds with HSA in 1:1 ratio indicating that only one molecule is bound with HSA. The negative free energy of all the selected bioactive compounds indicated that HSA-bioactive complexes are stable with hydrophobic interaction. The conformational changes were obtained from CD spectra of HSA exhibiting two negative bands in the ultraviolet region at 208 and 222 nm. Percentages of α-helix, β-turns and random coils were calculated from the graphs by using CDNN 2.1 software. Change in secondary structure of HSA was observed with an increasing concentration of bioactive compounds. The intensities at 208 and 222 nm decreased in a concentration-dependent manner upon binding of bioactive compounds to HSA. These studies revealed that there is a clear decrease in the α-helical content and an increase in the β-turns and random coils. Specifically, it suggested the loss of helical stability, which may be the result of the formation of a complex between HSA and bioactive compounds. This suggests that the secondary

structure of HSA became partially unfolded due to the HSA-bioactive complex formation. These conformational changes may be due to changes in the interior flexibility of the subdomains IIA, IIIA and IB domain of HSA upon binding of bioactive compounds (Chapter 3). Further, molecular docking studies indicate that all the bioactive compounds under study bind within known binding sites i.e., Sudlow site 1 and Sudlow site 2 and subdomain IB (Chapter 4). The binding constants and free energy of the best docking conformer are close and consistent with the binding constants and free energy values determined by fluorescence studies. Therefore, the location and the nature of interactions based on the docking studies suggest that the decrease in the emission intensity of HSA is due to the complexation of active compounds in subdomains IIA, IIIA, and IB. In addition, our results have shown that bioactive compounds bind/stabilize with HSA mainly by hydrophobic interactions and for few compounds with hydrogen bond were observed. Thus, these interactions (hydrophobic or hydrogen) may be due to the different functional groups attached to the bioactive compounds. These results are in concurrence with the free energy calculations obtained from binding constant which was derived from *in vitro* fluorescence experiments. This indicates that bioactive compounds are good enough to bind with HSA which may increase the efficacy and half-life for therapeutic action (Chapter 3).

Furthermore, the stability of the HSA-bioactive compounds was examined by performing molecular dynamic simulations by using GROMACS 4.5.6. We analyzed the stability of HSA-bioactive complexes by considering the RMSD, Rg, and RMSF with respect to the initial structure of HSA crystal structure. From which we found that RMSD and Rg of HSA- bioactive compounds have fewer fluctuations with respect to the RMSD and Rg of HSA, which are well validated with the CD studies. The rigidity of the binding sites from RMSF studies indicated that bioactive compounds binds within the subdomain IIA, IIIA, and IB which are in good agreement with the docking studies. These results indicate that bioactive compounds bind specifically to the respective domains, suggesting that binding sites are very specific for each bioactive compound. Thus, during the simulation the HSA-bioactive complexes are stable after 4 ns. Nonetheless, the changes in the secondary structure were observed that many be due to partial unfolding of HSA. The unfolding of protein structure may be due to

orientation changes or partial destabilization of the protein upon binding of bioactive compounds to HSA (Chapter 3).

In the 5th chapter, we discussed the comparison of binding studies of selected bioactive compounds with AGP (acute phase protein) and HSA. From which we found that few bioactive compounds (bacosine, andrographolide, piperine, Umb derivatives, corilagin and chebulinic acid and chebulagic acid) showed less binding with AGP than HSA and few compounds (7-Hydroxy coumarin derivatives, embelin, pterostiblene, L-dopa, psoralen, and artemisinin) showed no binding with AGP. Interestingly, some selected bioactive compounds (piperine, bacosine, menthol, andrographolide, corilagin, chebulinic acid and chebulagic acid) showed a strong affinity with AGP like in HSA. Furthermore, from the docking studies found that whatever bioactive compounds bound to AGP were having hydrogen bond interactions and of course, they also stabilized by hydrophobic bonds. Whereas HSA- bioactive complexes are stabilized by both the hydrogen bonds and hydrophobic interactions but it is not particularly having hydrogen bonds like in AGP. From these studies, it is clearly evident that HSA plays a major role in binding of all these bioactive compounds. This explains the versatility of the HSA in carrying and proper disposition of these bioactive compounds.

In the 6th chapter, we carried out the interaction studies of biodegradable CMS nanocarriers with HSA, this versatile nanocarrier to become pH responsive. The ester linkage used was rapidly cleaved at a pH 5. Piperine loaded C15-mPEG350 CMS nanocarrier were stable at pH 7.4 and showed sustained release of the drug. We were able to demonstrate that CMS-C-15-mPEG350 nanocarriers could release piperine more efficiently under the acidic conditions of intracellular compartments and therefore showed higher cell viability in comparison to the stable CMS nanocarrier. Real-time cell analysis C18-mPEG350-ICC were able to demonstrate that nanocarrier could release piperine more efficiently under acidic conditions of intracellular compartments, therefore, showed little cell viability due to less encapsulation of piperine in comparison to CMS nanocarrier alone. On the basis of spectroscopic analysis, CMS nanocarriers bind to HSA with the order of $K_{C18\text{-}350} > K_{C15\text{-}350} > K_{2000}$. The interaction of CMS nanocarriers leads to a secondary structural change of HSA indicating partial unfolding of protein at the increase in the concentration of CMS nanocarriers. This

work clearly demonstrates that CMS nanocarriers interact with HSA. These interactions were confirmed using fluorescence, ITC, and CD techniques, but also change the secondary structure of protein molecules through CD. Stronger binding of C-15mPEG 350 and C-18 m-PEG350 with HSA and from aligned networks through AFM could be a factor excluding the application of this type of nanocarriers in medicine. So obtained results should be taken into the note in the future studies concerning the use of these nanocarriers for medical use.

In summary, the therapeutic significance of this work was evident since HSA serves as a carrier molecule for multiple drugs and the interaction of bioactive compounds with HSA. In addition to HSA binding analysis of bioactive compounds, the AGP is also crucial since AGP is an acute-phase protein. In many diseases like chronic renal failure, hepatic and pregnancy the AGP content increases in blood, which in turn, influences the binding of certain drugs and their pharmacokinetics. In view of the evidence presented, it is imperative to assign a greater role of HSA as a carrier molecule for many bioactive compounds rather than AGP in normal and pathological conditions. It is our hope that the results presented in this thesis may provide new grounds for further investigations of the pharmaceutical potential of these bioactive compounds, and will be useful for monitoring it's biological functions *in vivo.* Based on this study one can think of designing new therapeutic compounds to cure life-threatening diseases.

BIBLIOGRAPHY

A Farco, J. & Grundmann, O. (2013). Menthol-pharmacology of an important naturally medicinal "cool". *Mini Reviews in Medicinal Chemistry 13*: 124-131.

Abraham, S. N., Bishop, B. L., Duncan, M. J., Krishnan, K. R. R., Song, J., Li, G. & Zaas, D. A. (2008). Methods and compositions for treating urinary tract infections using agents that mimic or elevate cyclic amp, Google Patents US20110171195 A11.

Agarwal, R. P., Phillips, M., McPherson, R. A. & Hensley, P. (1986). Serum albumin and the metabolism of disulfiram. *Biochemical Pharmacology 35*: 3341-3347.

Agudelo, D., Bourassa, P., Bruneau, J., Berube, G., Asselin, E. & Tajmir-Riahi, H.-A. (2012). Probing the binding sites of antibiotic drugs doxorubicin and N-(trifluoroacetyl) doxorubicin with human and bovine serum albumins. *PloS One 7*: e43814.

Ahmad, B., Parveen, S. & Khan, R. H. (2006). Effect of albumin conformation on the binding of ciprofloxacin to human serum albumin: a novel approach directly assigning binding site. *Biomacromolecules 7*: 1350-1356.

Amroyan, E., Gabrielian, E., Panossian, A., Wikman, G. & Wagner, H. (1999). Inhibitory effect of andrographolide from Andrographis paniculata on PAF-induced platelet aggregation. *Phytomedicine 6*: 27-31.

Anderson, L. & Anderson, N. G. (1977). High resolution two-dimensional electrophoresis of human plasma proteins. *Proceedings of the National Academy of Sciences 74*: 5421-5425.

Ang, C. Y., Tan, S. Y. & Zhao, Y. (2014). Recent advances in biocompatible nanocarriers for delivery of chemotherapeutic cargoes towards cancer therapy. *Organic and Biomolecular Chemistry 12*: 4776-4806.

Araujo, C. & Leon, L. (2001). Biological activities of Curcuma longa L. *Memorias do Instituto Oswaldo Cruz 96*: 723-728.

Atal, C., Dubey, R. & Singh, J. (1985). Biochemical basis of enhanced drug bioavailability by piperine: evidence that piperine is a potent inhibitor of drug metabolism. *Journal of Pharmacology and Experimental Therapeutics 232*: 258-262.

Atal, C., Zutshi, U. & Rao, P. (1981). Scientific evidence on the role of Ayurvedic herbals on bioavailability of drugs. *Journal of Ethnopharmacology 4*: 229-232.

Athineos, E., Kukral, J. C. & Winzler, R. J. (1964). Biosynthesis of glycoproteins: II. The site of glucosamine incorporation into canine plasma α-1 acid glycoprotein. *Archives of Biochemistry and Biophysics 106*: 338-342.

Azad, M. A., Huang, J. X., Cooper, M. A., Roberts, K. D., Thompson, P. E., Nation, R. L., Li, J. & Velkov, T. (2012). Structure–activity relationships for the binding of polymyxins with human α-1-acid glycoprotein. *Biochemical Pharmacology 84*: 278-291.

Bailey, D. N. & Briggs, J. R. (2004). The binding of selected therapeutic drugs to human serum [alpha]-1 acid glycoprotein and to human serum albumin in vitro. *Therapeutic Drug Monitoring 26*: 40-43.

Bang, J. (2009). H. Oh da, HM Choi, BJ Sur, SJ Lim, JY Kim et al., Anti-inflammatory and antiarthritic effects of piperine in human interleukin 1beta-stimulated fibroblast-like synoviocytes and in rat arthritis models. *Arthritis Research and Therapy 11*: R49.

Baur, J. A. & Sinclair, D. A. (2006). Therapeutic potential of resveratrol: the *in vivo* evidence. *Nature reviews Drug discovery 5*: 493-506.

Beauchemin, R., N'Soukpoe-Kossi, C., Thomas, T., Thomas, T., Carpentier, R. & Tajmir-Riahi, H. (2007). Polyamine analogues bind human serum albumin. *Biomacromolecules 8*: 3177-3183.

Berendsen, H. J., Postma, J. v., van Gunsteren, W. F., DiNola, A. & Haak, J. (1984). Molecular dynamics with coupling to an external bath. *The Journal of Chemical Physics 81*: 3684-3690.

Berendsen, H. J., van der Spoel, D. & van Drunen, R. (1995). GROMACS: A message-passing parallel molecular dynamics implementation. *Computer Physics Communications 91*: 43-56.

Bhattacharya, A. A., Curry, S. & Franks, N. P. (2000). Binding of the general anesthetics propofol and halothane to human serum albumin high resolution crystal structures. *The Journal of Biological Chemistry 275*: 38731-38738.

Bories, P. N., Feger, J., Benbernou, N., Rouzeau, J.-D., Agneray, J. & Durand, G. (1990). Prevalence of tri-and tetraantennary glycans of humanα 1-acid glycoprotein in release of macrophage inhibitor of interleukin-1 activity. *Inflammation 14*: 315-323.

D'Amelio, Sr., CRC Press, Boca Raton. (1999). A Phytocosmetic Desk Reference, Botanicals,

Boussif, O., Lezoualc'h, F., Zanta, M. A., Mergny, M. D., Scherman, D., Demeneix, B. & Behr, J.-P. (1995). A versatile vector for gene and oligonucleotide transfer into cells in culture and in vivo: polyethylenimine. *Proceedings of the National Academy of Sciences 92*: 7297-7301.

Brown, J. R. (1977). *Serum albumin: amino acid sequence*, Pergamon Press, Oxford.

Campos-Toimil, M., Orallo, F., Santana, L. & Uriarte, E. (2002). Synthesis and vasorelaxant activity of new coumarin and furocoumarin derivatives. *Bioorganic & Medicinal Chemistry Letters 12*: 783-786.

Carter, B. A., Taylor, O. A., Prendergast, D. R., Zimmerman, T. L., Von Furstenberg, R., Moore, D. D. & Karpen, S. J. (2007). Stigmasterol, a soy lipid–derived phytosterol, is an antagonist of the bile acid nuclear receptor FXR. *Pediatric research 62*: 301-306.

Carter, D., HE, X.-M., Munson, S. H., Twigg, P. D., Gernert, K. M., Broom, M. B. & Miller, T. Y. (1989). Three-dimensional structure of human serum albumin. *Science 244*: 1195-1198.

Chakravarti, R. & Chakravarti, D. (1951). Andrographolide, the active constituent of Andrographis paniculata Nees; a preliminary communication. *Indian medical gazette 86*: 96-97.

Chen, Y. & Chen, C. (2011). Corilagin prevents tert-butyl hydroperoxide-induced oxidative stress injury in cultured N9 murine microglia cells. *Neurochemistry International 59*: 290-296.

Cheng, X.-X., Lui, Y., Zhou, B., Xiao, X.-H. & Liu, Y. (2009). Probing the binding sites and the effect of berbamine on the structure of bovine serum albumin. *Spectrochimica Acta Part A: Molecular and Biomolecular Spectroscopy 72*: 922-928.

Chiu, K. M., Mortensen, R., Osmand, A. & Gewurz, H. (1977). Interactions of alpha1-acid glycoprotein with the immune system. I. Purification and effects upon lymphocyte responsiveness. *Immunology 32*: 997.

Chuang, V. T. G. & Otagiri, M. (2006). Stereoselective binding of human serum albumin. *Chirality 18*: 159-166.

Correcirc, D. H. & Ramos, C. H. (2009). The use of circular dichroism spectroscopy to study protein folding, form and function. *African Journal of Biochemistry Research 3*: 164-173.

Correa-Basurto, J., Flores-Sandoval, C., Marín-Cruz, J., Rojo-Domínguez, A., Espinoza-Fonseca, L. M. & Trujillo-Ferrara, J. G. (2007). Docking and quantum mechanic studies on cholinesterases

Costello, M., Gewurz, H. & Siegel, J. (1984). Inhibition of neutrophil activation by alpha1-acid glycoprotein. *Clinical and Experimental Immunology 55*: 465.

Curry, S. (2009). Lessons from the crystallographic analysis of small molecule binding to human serum albumin. *Drug metabolism and Pharmacokinetics 24*: 342-357.

Curry, S., Brick, P. & Franks, N. P. (1999). Fatty acid binding to human serum albumin: new insights from crystallographic studies. *Biochimica et Biophysica Acta 1441*: 131-140.

Curry, S., Mandelkow, H., Brick, P. & Franks, N. (1998). Crystal structure of human serum albumin complexed with fatty acid reveals an asymmetric distribution of binding sites. *Nature Structural & Molecular Biology 5*: 827-835.

Darden, T., York, D. & Pedersen, L. (1993). Particle mesh Ewald: An N· log (N) method for Ewald sums in large systems. *The Journal of Chemical Physics 98*: 10089-10092.

Dente, L., Pizza, M., Metspalu, A. & Cortese, R. (1987). Structure and expression of the genes coding for human alpha 1-acid glycoprotein. *The EMBO Journal 6*: 2289–2296.

Dighe, N. S., Pattan, S. R., Dengale, S. S., Musmade, D. S., Shelar, M., Tambe, V. & Hole, M. B. (2010). Synthetic and pharmacological profiles of coumarins: A review. *Archives of Applied Science Research. 2*: 65-71.

Donnelly, A. C., Mays, J. R., Burlison, J. A., Nelson, J. T., Vielhauer, G., Holzbeierlein, J. & Blagg, B. S. (2008). The design, synthesis, and evaluation of coumarin ring derivatives of the novobiocin scaffold that exhibit antiproliferative activity. *The Journal of Organic Chemistry 73*: 8901-8920.

Drmanovic, Z., Voyatzi, S., Kouretas, D., Sahpazidou, D., Papageorgiou, A. & Antonoglou, O. (1998). Albumin possesses intrinsic enolase activity towards dihydrotestosterone which can differentiate benign from malignant breast tumors. *Anticancer research 19*: 4113-4124.

Duan, W., Yu, Y. & Zhang, L. (2005). Antiatherogenic effects of phyllanthus emblica associated with corilagin and its analogue. *Yakugaku zasshi: Journal of the Pharmaceutical Society of Japan 125*: 587-591.

Egan, D., O'kennedy, R., Moran, E., Cox, D., Prosser, E. & Thornes, R. D. (1990). The pharmacology, metabolism, analysis, and applications of coumarin and coumarin-related compounds. *Drug Metabolism Reviews 22*: 503-529.

Emerich, D. F. & Thanos, C. G. (2007). Targeted nanoparticle-based drug delivery and diagnosis. *Journal of Drug Targeting 15*: 163-183.

Epps, D., Raub, T., Caiolfa, V., Chiari, A. & Zamai, M. (1998). Evaluating the binding selectivity of transthyretin amyloid fibril inhibitors in blood plasma. *Journal Pharmacy and Pharmacology 51*: 41-48.

Fasano, M., Curry, S., Terreno, E., Galliano, M., Fanali, G., Narciso, P., Notari, S. & Ascenzi, P. (2005). The extraordinary ligand binding properties of human serum albumin. *International Union of Biochemistry and Molecular Biology 57*: 787-796.

Feroz, S. R., Mohamad, S. B., Bujang, N., Malek, S. N. & Tayyab, S. (2012). Multispectroscopic and molecular modeling approach to investigate the interaction of flavokawain B with human serum albumin. *Journal of Agricultural and Food Chemistry 60*: 5899-5908.

Finn, G. J., Kenealy, E., Creaven, B. S. & Egan, D. A. (2002). In vitro cytotoxic potential and mechanism of action of selected coumarins, using human renal cell lines. *Cancer Letters 183*: 61-68.

Fitzpatrick, F. & Wynalda, M. A. (1983). Albumin-catalyzed metabolism of prostaglandin D2. Identification of products formed in vitro. *Journal of Biological Chemistry 258*: 11713-11718.

Fleige, E., Achazi, K., Schaletzki, K., Triemer, T. & Haag, R. (2014a). pH-responsive dendritic core–multishell nanocarriers. *Journal of Controlled Release 185*: 99-108.

Fleige, E., Tyagi, R. & Haag, R. (2014b). Dendronized core-multishell nanocarriers for solubilization of guest molecules. *Nanocarriers 1:1-9.*

Fleige, E., Ziem, B., Grabolle, M., Haag, R. & Resch-Genger, U. (2012). Aggregation phenomena of host and guest upon the loading of dendritic core-multishell nanoparticles with solvatochromic dyes. *Macromolecules 45*: 9452-9459.

Förster, T. (1996). In O. Sinanoglu. *Modern quantum chemistry vol. 3* p. 93.

Fournier, T., Medjoubi-N, N. & Porquet, D. (2000). Alpha-1-acid glycoprotein. *Biochimica et Biophysica Acta (BBA)-Protein Structure and Molecular Enzymology 1482*: 157-171.

Frostell-Karlsson, Å., Remaeus, A., Roos, H., Andersson, K., Borg, P., Hämäläinen, M. & Karlsson, R. (2000). Biosensor analysis of the interaction between immobilized human serum albumin and drug compounds for prediction of human serum albumin binding levels. *Journal of Medicinal Chemistry 43*: 1986-1992.

Gabay, O., Sanchez, C., Salvat, C., Chevy, F., Breton, M., Nourissat, G., Wolf, C., Jacques, C. & Berenbaum, F. (2010). Stigmasterol: a phytosterol with potential anti-osteoarthritic properties. *Osteoarthritis and Cartilage 18*: 106-116.

Gambacorti-Passerini, C., Zucchetti, M., Russo, D., Frapolli, R., Verga, M., Bungaro, S., Tornaghi, L., Rossi, F., Pioltelli, P. & Pogliani, E. (2003). α1 acid glycoprotein binds to imatinib (STI571) and substantially alters its pharmacokinetics in chronic myeloid leukemia patients. *Clinical Cancer Research 9*: 625-632.

Garg, A., Manidhar, D. M., Gokara, M., Malleda, C., Reddy, C. S. & Subramanyam, R. (2013). Elucidation of the binding mechanism of coumarin derivatives with human serum albumin. *PLOS ONE 8*: e63805.

Gautam, B., Vadivel, V., Stuetz, W. & Biesalski, H. K. (2012). Bioactive compounds extracted from Indian wild legume seeds: antioxidant and type II diabetes-related enzyme inhibition properties. *International Journal of Food Sciences and Nutrition 63*: 242-245.

Ghosh, T., Maity, T. K. & Singh, J. (2011). Antihyperglycemic activity of bacosine, a triterpene from Bacopa monnieri, in alloxan-induced diabetic rats. *Planta Medica 77*: 804-808.

Ghuman, J., Zunszain, P. A., Petitpas, I., Bhattacharya, A. A., Otagiri, M. & Curry, S. (2005). Structural basis of the drug-binding specificity of human serum albumin. *Journal of Molecular Biology 353*: 38-52.

Gokara, M., Kimavath, G. B., Podile, A. R. & Subramanyam, R. (2015). Differential interactions and structural stability of chitosan oligomers with human serum albumin and alpha-1-glycoprotein. *Journal of biomolecular Structure & Dynamics 33*: 196-210.

Gokara, M., Malavath, T., Kalangi, S. K., Reddana, P. & Subramanyam, R. (2014). Unraveling the binding mechanism of asiatic acid with human serum albumin and its biological implications. *Journal of biomolecular Structure & Dynamics 32*: 1290-1302.

Gokara, M., Sudhamalla, B., Amooru, D. G. & Subramanyam, R. (2010). Molecular interaction studies of trimethoxy flavone with human serum albumin. *PLoS One 5*: e8834.

Gonzalez-Burgos, E. & Gomez-Serranillos, M. (2012). Terpene compounds in nature: a review of their potential antioxidant activity. *Current Medicinal Chemistry 19*: 5319-5341.

Gorelik, B. & Goldblum, A. (2008). High quality binding modes in docking ligands to proteins. *Proteins: Structure, Function, and Bioinformatics 71*: 1373-1386.

Gormley, N. A., Orphanides, G., Meyer, A., Cullis, P. M. & Maxwell, A. (1996). The interaction of coumarin antibiotics with fragments of the DNA gyrase B protein. *Biochemistry 35*: 5083-5092.

Hau, D. K.-P., Zhu, G.-Y., Leung, A. K.-M., Wong, R. S.-M., Cheng, G. Y.-M., Lai, P. B.-S., Tong, S.-W., Lau, F.-Y., Chan, K.-W. & Wong, W.-Y. (2010). In vivo anti-tumour activity of corilagin on Hep3B hepatocellular carcinoma. *Phytomedicine 18*: 11-15.

Hauser, R. A. & Zesiewicz, T. A. (1999). Management of early Parkinson's disease. *Medical Clinics of North America 83*: 393-414.

He, X. M. & Carter, D. C. (1992). Atomic structure and chemistry of human serum albumin. *Nature 358*: 209-215.

Heegaard, P. M., Miller, I., Sorensen, N. S., Soerensen, K. E. & Skovgaard, K. (2013). Pig α1-Acid Glycoprotein: Characterization and First Description in Any Species as a Negative Acute Phase Protein. *PloS one 8*: e68110.

Hein, K. L., Kragh-Hansen, U., Morth, J. P., Jeppesen, M. D., Otzen, D., Møller, J. V. & Nissen, P. (2010). Crystallographic analysis reveals a unique lidocaine binding site on human serum albumin. *Journal of Structural Biology 171*: 353-360.

Hess, B., Bekker, H., Berendsen, H. J. & Fraaije, J. G. (1997). LINCS: a linear constraint solver for molecular simulations. *Journal of Computational Chemistry 18*: 1463-1472.

Hochepied T, B. F., Baumann H, Libert C. (2003;). Alpha(1)-acid glycoprotein: an acute phase protein with inflammatory and immunomodulating properties. *Cytokine Growth Factor Rev 14*: 25–34.

Hu, Y.-J., Liu, Y., Wang, J.-B., Xiao, X.-H. & Qu, S.-S. (2004). Study of the interaction between monoammonium glycyrrhizinate and bovine serum albumin. *Journal of Pharmaceutical and Biomedical Analysis 36*: 915-919.

Huang, Z. & Ung, T. (2013). Effect of Alpha-1-Acid Glycoprotein binding on pharmacokinetics and Pharmacodynamics. *Current Drug Metabolism 14*: 226-238.

Ihm, J.-E., Han, K.-O., Han, I.-K., Ahn, K.-D., Han, D.-K. & Cho, C.-S. (2003). High transfection efficiency of poly (4-vinylimidazole) as a new gene carrier. *Bioconjugate Chemistry 14*: 707-708.

Il'ichev, Y. V., Perry, J. L. & Simon, J. D. (2002). Interaction of ochratoxin A with human serum albumin. Preferential binding of the dianion and pH effects. *Journal of Physical Chemistry B 106*: 452-459.

Imamura H, K. T., Ismail A, Suenaga A, Otagiri M. (2002;). Stereoselective protein binding of alprenolol in the renal diseased state. *Chirality 14*: 599–603.

Israili, Z. & Dayton, P. (2001). Human alpha-1-glycoprotein and its interactions with drugs 1 2. *Drug Metabolism Reviews 33*: 161-235.

Jarabak, R. & Westley, J. (1989). The sulfur-cyanolysis sites of serum albumin: Metabolite competition studies. *Journal of Biochemical Toxicology 4*: 255-261.

Jeffrey Fishwicka, W. G. M., Geoffrey Edwardsa, Stephen A Warda (1995). The toxicity of artemisinin and related compounds on neuronal and glial cells in culture. *Chemico-Biological Interactions 96*: 263–271.

Jiang, Y. L. (2008). Design, synthesis and spectroscopic studies of resveratrol aliphatic acid ligands of human serum albumin. *Bioorganic & Medicinal Chemistry 16*: 6406-6414.

Jones, G., Willett, P., Glen, R. C., Leach, A. R. & Taylor, R. (1997). Development and validation of a genetic algorithm for flexible docking. *Journal of Molecular Biology 267*: 727-748.

Jun-Hua, H., Yue-Xin, Y. & Mei-Yuan, F. (2008). Contents of phytosterols in vegetables and fruits commonly consumed in China. *Biomedical and Environmental Sciences 21*: 449-453.

Kabeya, L. M., de Marchi, A. A., Kanashiro, A., Lopes, N. P., da Silva, C. H., Pupo, M. T. & Lucisano-Valim, Y. M. (2007). Inhibition of horseradish peroxidase catalytic activity by new 3-phenylcoumarin derivatives: Synthesis and structure–activity relationships. *Bioorganic & Medicinal Chemistry 15*: 1516-1524.

Kadajji, V. G. & Betageri, G. V. (2011). Water soluble polymers for pharmaceutical applications. *Polymers 3*: 1972-2009.

Kainthan, R. K. & Brooks, D. E. (2007). In vivo biological evaluation of high molecular weight hyperbranched polyglycerols. *Biomaterials 28*: 4779-4787.

Kainthan, R. K., Mugabe, C., Burt, H. M. & Brooks, D. E. (2008). Unimolecular micelles based on hydrophobically derivatized hyperbranched polyglycerols: ligand binding properties. *Biomacromolecules 9*: 886-895.

Kalanur, S. S., Seetharamappa, J. & Kalalbandi, V. K. A. (2010). Characterization of interaction and the effect of carbamazepine on the structure of human serum albumin. *Journal of Pharmaceutical and Biomedical Analysis 53*: 660-666.

Kalra, E. K. (2003). Nutraceutical-definition and introduction. *Aaps Pharmscitech 5*: 27-28.

Kametani, T. & Furuyama, H. (1987). Synthesis of vitamin D3 and related compounds. *Medicinal Research Reviews 7*: 147-171.

Kanakis, C. D., Tarantilis, P. A., Tajmir-Riahi, H. A. & Polissiou, M. G. (2007). Crocetin, dimethylcrocetin, and safranal bind human serum albumin: stability and antioxidative properties. *Journal of Agricultural and Food Chemistry 55*: 970-977.

Katori, N., Sai, K., Saito, Y., Fukushima-Uesaka, H., Kurose, K., Yomota, C., Kawanishi, T., Nishimaki-Mogami, T., Naito, M. & Sawada, J. I. (2011). Genetic variations of orosomucoid genes associated with serum alpha-1-acid glycoprotein level and the pharmacokinetics of paclitaxel in Japanese cancer patients. *Journal of Pharmaceutical Sciences 100*: 4546-4559.

Kinoshita, S., Inoue, Y., Nakama, S., Ichiba, T. & Aniya, Y. (2007). Antioxidant and hepatoprotective actions of medicinal herb, Terminalia catappa L. from Okinawa Island and its tannin corilagin. *Phytomedicine 14*: 755-762.

Kinoshita, S., Inoue, Y., Nakama, S., Ichiba, T. & Aniya, Y. (2007). Antioxidant and hepatoprotective actions of medicinal herb,Terminalia catappa L. from Okinawa Island and its tannin corilagin. *Phytomedicine 14*: 755-762.

Kiselev, M., IuA, G., Dobretsov, G. & Komarova, M. (2001). Size of a human serum albumin molecule in solution. *Biofizika 46*: 423.

Klika, K. D., Saleem, A., Sinkkonen, J., Kähkönen, M., Loponen, J., Tähtinen, P. & Pihlaja, K. (2004). The structural and conformational analyses and antioxidant activities of chebulinic acid and its thrice-hydrolyzed derivative, 2, 4-chebuloyl-β-D-glucopyranoside, isolated from the fruit of Terminalia chebula. *Archive for Organic Chemistry 7*: 83-105.

Kontogiorgis, C. & Hadjipavlou-Litina, D. (2003). Biological evaluation of several coumarin derivatives designed as possible anti-inflammatory/antioxidant agents. *Journal of Enzyme Inhibition and Medicinal Chemistry 18*: 63-69.

Kowalczyk, D., Marsault, J.-P. & Slomkowski, S. (1996). Atomic force microscopy of human serum albumin (HSA) on poly (styrene/acrolein) microspheres. *Colloid and Polymer Science 274*: 513-519.

Kragh-Hansen, U. (1981). Molecular aspects of ligand binding to serum albumin. *Pharmacological Reviews 33*: 17-53.

Kragh-Hansen, U., Chuang, V. T. G. & Otagiri, M. (2002). Practical aspects of the ligand-binding and enzymatic properties of human serum albumin. *Biological and Pharmaceutical Bulletin 25*: 695-704.

Kratochwil, N. A., Huber, W., Müller, F., Kansy, M. & Gerber, P. R. (2002). Predicting plasma protein binding of drugs: a new approach. *Biochemical Pharmacology 64*: 1355-1374.

Kremer, J. M., Wilting, J. & Janssen, L. (1988). Drug binding to human alpha-1-acid glycoprotein in health and disease. *Pharmacological Reviews 40*: 1-47.

Kumar, G., Walle, U., Bhalla, K. & Walle, T. (1993). Binding of taxol to human plasma, albumin and alpha 1-acid glycoprotein. *Research Communications in Chemical Pathology and Pharmacology 80*: 337-344.

Kurniasih, I. N., Keilitz, J. & Haag, R. (2015). Dendritic nanocarriers based on hyperbranched polymers. *Chemical Society Reviews 44*: 4145-4164.

Kurono, Y., Kushida, I., Tanaka, H., and Ikeda, K. (1992). Esterase-like activity of human serum albumin. VIII. Reaction with amino acid p-nitrophenyl esters. *Chemical and Pharmaceutical Bulletin 40*: 2169-2172.

Lacy, A. & O'Kennedy, R. (2004). Studies on coumarins and coumarin-related compounds to determine their therapeutic role in the treatment of cancer. *Current Pharmaceutical Design 10*: 3797-3811.

Laemmli, U. K. (1970). Cleavage of structural proteins during the assembly of the head of bacteriophage T4. *Nature 227*: 680-685.

Lakowicz, J. R. (2009). *Principles of fluorescence spectroscopy*, Springer.

Leckband, D. (2000). Measuring the forces that control protein interactions. *Annual Review of Biophysics and Biomolecular Structure 29*: 1-26.

Lee, E. B., Shin, K. H. & Woo, W. S. (1984). Pharmacological study on piperine. *Archives of Pharmacal Research 7*: 127-132.

Leite, V. C., Santos, R. F., Chen, L. C. & Guillo, L. A. (2004). Psoralen derivatives and longwave ultraviolet irradiation are active in vitro against human melanoma cell line. *Journal of Photochemistry and Photobiology B: Biology 76*: 49-53.

Lichenstein, H. S., Lyons, D. E., Wurfel, M. M., Johnson, D. A., McGinley, M. D., Leidli, J. C., Trollinger, D. B., Mayer, J. P., Wright, S. D. & Zukowski, M. M. (1994). Afamin is a new member of the albumin, alpha-fetoprotein, and vitamin D-binding protein gene family. *Journal of Biological Chemistry 269*: 18149-18154.

Lindahl, E., Hess, B. & Van Der Spoel, D. (2001). GROMACS 3.0: a package for molecular simulation and trajectory analysis. *Molecular Modeling Annual 7*: 306-317.

Litvinenko, V., Popova, T., Simonjan, A., Zoz, I. & Sokolov, V. (1975). Gerbstoffe" und Oxzyzimtsaureabkommlinge in Labiaten. *Planta Medica 27*: 372-380.

Liu, K. C. C., Lin, M.-T., Lee, S.-S., Chiou, J.-F., Ren, S. & Lien, E. J. (1999). Antiviral tannins from two Phyllanthus species. *Planta Medica 65*: 043-046.

Ma, S.-F., Anraku, M., Iwao, Y., Yamasaki, K., Kragh-Hansen, U., Yamaotsu, N., Hirono, S., Ikeda, T. & Otagiri, M. (2005). Hydrolysis of angiotensin II receptor blocker prodrug olmesartan medoxomil by human serum albumin and identification of its catalytic active sites. *DrugMmetabolism and Disposition 33*: 1911-1919.

Madhavan, G. R., Balraju, V., Mallesham, B., Chakrabarti, R. & Lohray, V. B. (2003). Novel coumarin derivatives of heterocyclic compounds as lipid-lowering agents. *Bioorganic & Medicinal Chemistry Letters 13*: 2547-2551.

Maiti, T. K., Ghosh, K. S., Samanta, A. & Dasgupta, S. (2008). The interaction of silibinin with human serum albumin: A spectroscopic investigation. *Journal of Photochemistry and Photobiology A: Chemistry 194*: 297-307.

Malleda, C., Ahalawat, N., Gokara, M. & Subramanyam, R. (2012). Molecular dynamics simulation studies of betulinic acid with human serum albumin. *Journal of Molecular Modeling. 18*: 2589-2597.

Mantena, S. K., Sharma, S. D. & Katiyar, S. K. (2006). Berberine, a natural product, induces G1-phase cell cycle arrest and caspase-3-dependent apoptosis in human prostate carcinoma cells. *Molecular Cancer Therapeutics 5*: 296-308.

Mazzei, M., Nieddu, E., Miele, M., Balbi, A., Ferrone, M., Fermeglia, M., Mazzei, M. T., Pricl, S., La Colla, P. & Marongiu, F. (2008). Activity of Mannich bases of 7-hydroxycoumarin against Flaviviridae. *Bioorganic & Medicinal Chemistry 16*: 2591-2605.

McEwan, D. G. (2007). Cyclic AMP modulation and its effects on chemo-resistant colon cancer cell proliferation and survival, Cancer Research UK.

Means, G. E. & Bender, M. L. (1975). Acetylation of human serum albumin by p-nitrophenyl acetate. *Biochemistry 14*: 4989-4994.

Merdan, T., Kunath, K., Petersen, H., Bakowsky, U., Voigt, K. H., Kopecek, J. & Kissel, T. (2005). PEGylation of poly (ethylene imine) affects stability of complexes with plasmid DNA under in vivo conditions in a dose-dependent manner after intravenous injection into mice. *Bioconjugate Chemistry 16*: 785-792.

Monopoli, M. P., Walczyk, D., Campbell, A., Elia, G., Lynch, I., Baldelli Bombelli, F. & Dawson, K. A. (2011). Physical− chemical aspects of protein corona: relevance to in vitro and in vivo biological impacts of nanoparticles. *Journal of the American Chemical Society 133*: 2525-2534.

Morin, D., Simon, N., Depres-Brummer, P., Levi, F., Tillement, J.-P. & Urien, S. (1997). Melatonin high-affinity binding to alpha-1-acid glycoprotein in human serum. *Pharmacology 54*: 271-275.

Morris, G. M., Goodsell, D. S., Halliday, R. S., Huey, R., Hart, W. E., Belew, R. K. & Olson, A. J. (1998). Automated docking using a Lamarckian genetic algorithm and an empirical binding free energy function. *Journal of Computational Chemistry 19*: 1639-1662.

Morris, G. M., Huey, R., Lindstrom, W., Sanner, M. F., Belew, R. K., Goodsell, D. S. & Olson, A. J. (2009). AutoDock4 and AutoDockTools4: Automated docking with selective receptor flexibility. *Journal of Computational Chemistry 30*: 2785-2791.

Mosmann, T. (1983). Rapid colorimetric assay for cellular growth and survival: application to proliferation and cytotoxicity assays. *Journal of Immunological Methods 65*: 55-63.

Mura, S., Nicolas, J. & Couvreur, P. (2013). Stimuli-responsive nanocarriers for drug delivery. *Nature Materials 12*: 991-1003.

Neelam, S., Gokara, M., Sudhamalla, B., Amooru, D. G. & Subramanyam, R. (2010). Interaction studies of coumaroyltyramine with human serum albumin and its biological importance. *Journal of Physical Chemistry. B 114*: 3005-3012.

Newkome, G., Moorefield, C. & Vögtle, F. (2001). Dendrimers and dendrons. Concepts, syntheses, perspectives. *Wiley-VCH, New York.(b) Tomalia, DA and Dvornic, PR (1994) Nature 372*: 617-618.

Nikolovska-Coleska, Z., Xu, L., Hu, Z., Tomita, Y., Li, P., Roller, P. P., Wang, R., Fang, X., Guo, R. & Zhang, M. (2004). Discovery of embelin as a cell-permeable, small-molecular weight inhibitor of XIAP through structure-based computational screening of a traditional herbal medicine three-dimensional structure database. *Journal of Medicinal Chemistry 47*: 2430-2440.

Nishi, K., Ono, T., Nakamura, T., Fukunaga, N., Izumi, M., Watanabe, H., Suenaga, A., Maruyama, T., Yamagata, Y. & Curry, S. (2011). Structural insights into differences in drug-binding selectivity between two forms of human α1-acid glycoprotein genetic variants, the A and F1* S forms. *Journal of Biological Chemistry 286*: 14427-14434.

Ojala, T. (2001). *Biological screening of plant coumarins*, University of Helsinki.

Ostrov, D. A., Prada, J. A. H., Corsino, P. E., Finton, K. A., Le, N. & Rowe, T. C. (2007). Discovery of novel DNA gyrase inhibitors by high-throughput virtual screening. *Antimicrobial Agents and Chemotherapy 51*: 3688-3698.

Otagiri, M. (2009). Study on binding of drug to serum protein. *Yakugaku zasshi: Journal of the Pharmaceutical Society of Japan 129*: 413.

Pan, M. H., Hsieh, M. C., Kuo, J. M., Lai, C. S., Wu, H., Sang, S. & Ho, C. T. (2008). 6-Shogaol induces apoptosis in human colorectal carcinoma cells via ROS production, caspase activation, and GADD 153 expression. *Molecular Nutrition & Food Research 52*: 527-537.

Panda, S., Jafri, M., Kar, A. & Meheta, B. (2009). Thyroid inhibitory, antiperoxidative and hypoglycemic effects of stigmasterol isolated fromButea monosperma. *Fitoterapia 80*: 123-126.

Panyam, J. & Labhasetwar, V. (2003). Biodegradable nanoparticles for drug and gene delivery to cells and tissue. *Advanced Drug Delivery reviews 55*: 329-347.

Parnham, M. & Kesselring, K. (1985). Rosmarinic acid. *Drugs Future 10*: 756-757.

Pasban Ziyarat, F., Asoodeh, A., Sharif Barfeh, Z., Pirouzi, M. & Chamani, J. (2014). Probing the interaction of lysozyme with ciprofloxacin in the presence of different-sized Ag nano-particles by multi spectroscopic techniques and isothermal titration calorimetry. *Journal of Biomolecular Structure and Dynamics 32*: 613-629.

Pei, Y. Q. (1983). A review of pharmacology and clinical use of piperine and its derivatives. *Epilepsia 24*: 177-182.

Peters, E. A., Hiltermann, J. T. & Stolk, J. (2001). Effect of apocynin on ozone-induced airway hyperresponsiveness to methacholine in asthmatics. *Free Radical Biology and Medicine 31*: 1442-1447.

Peters Jr, T. (1996). *All about albumin: biochemistry, genetics, and medical applications*. San Diego, Academic Press.

Petersen, H., Fechner, P. M., Fischer, D. & Kissel, T. (2002). Synthesis, characterization, and biocompatibility of polyethyleneimine-g raft-poly (ethylene glycol) block copolymers. *Macromolecules 35*: 6867-6874.

Petitpas, I., Grüne, T., Bhattacharya, A. A. & Curry, S. (2001). Crystal structures of human serum albumin complexed with monounsaturated and polyunsaturated fatty acids. *Journal of Molecular Biology 314*: 955-960.

Popeney, C. S., Lukowiak, M. C., Böttcher, C., Schade, B., Welker, P., Mangoldt, D., Gunkel, G., Guan, Z. & Haag, R. (2012). Tandem coordination, ring-opening, hyperbranched polymerization for the synthesis of water-soluble core–shell unimolecular transporters. *ACS Macro Letters 1*: 564-567.

Pos, O., Oostendorp, R. A., Van Der Stelt, M. E., Scheper, R. J. & Van Dijk, W. (1990). Con A-nonreactive human α1-acid glycoprotein (AGP) is more effective in modulation of lymphocyte proliferation than Con A-reactive AGP serum variants. *Inflammation 14*: 133-141.

Poschner, B. C., Reed, J., Langosch, D. & Hofmann, M. W. (2007). An automated application for deconvolution of circular dichroism spectra of small peptides. *Analytical Biochemistry 363*: 306-308.

Privalov, P. L. (1979). Stability of proteins small globular proteins. *Advances in Protein Chemistry 33*: 167-241.

Privalov, P. L. & Gill, S. J. (1988). Stability of protein structure and hydrophobic interaction. *Advances in Protein Chemistry 39*: 191-238.

Radowski, M. R., Shukla, A., von Berlepsch, H., Böttcher, C., Pickaert, G., Rehage, H. & Haag, R. (2007). Supramolecular aggregates of dendritic multishell architectures as universal nanocarriers. *Angewandte Chemie International Edition 46*: 1265-1269.

Reddy, D. B. & Reddanna, P. (2009). Chebulagic acid (CA) attenuates LPS-induced inflammation by suppressing NF-κB and MAPK activation in RAW 264.7 macrophages. *Biochemical and Biophysical Research Communications 381*: 112-117.

Remsberg, C. M., Yáñez, J. A., Ohgami, Y., Vega-Villa, K. R., Rimando, A. M. & Davies, N. M. (2008). Pharmacometrics of pterostilbene: preclinical pharmacokinetics and metabolism, anticancer, antiinflammatory, antioxidant and analgesic activity. *Phytotherapy Research 22*: 169-179.

Ritchie, D. G. & Fuller, G. M. (1983). Hepatocyte-Stimulating Factor: A Monocyte-Derived Acute-Phase Regulatory Protein. *Annals of the New York Academy of Sciences 408*: 490-502.

Riveiro, M., De Kimpe, N., Moglioni, A., Vazquez, R., Monczor, F., Shayo, C. & Davio, C. (2010). Coumarins: old compounds with novel promising therapeutic perspectives. *Current Medicinal Chemistry 17*: 1325-1338.

Roy, D., Dutta, S., Maity, S. S., Ghosh, S., Singha Roy, A., Ghosh, K. S. & Dasgupta, S. (2012). Spectroscopic and docking studies of the binding of two stereoisomeric antioxidant catechins to serum albumins. *Journal of Luminescence 132*: 1364-1375.

Santana, L., Uriarte, E., González-Díaz, H., Zagotto, G., Soto-Otero, R. & Méndez-Álvarez, E. (2006). A QSAR model for in silico screening of MAO-A inhibitors. Prediction, synthesis, and biological assay of novel coumarins. *Journal of Medicinal Chemistry 49*: 1149-1156.

Sarcione, E. J. (1963). Synthesis of α-1-acid glycoprotein by the isolated perfused rat liver. *Archives of Biochemistry and Biophysics 100*: 516-519.

Sashidhara, K. V., Kumar, A., Kumar, M., Sarkar, J. & Sinha, S. (2010). Synthesis and in vitro evaluation of novel coumarin–chalcone hybrids as potential anticancer agents. *Bioorganic & Medicinal Chemistry Letters 20*: 7205-7211.

Sasidharan, I., Sundaresan, A., Nisha, V., Kirishna, M. S., Raghu, K. & Jayamurthy, P. (2012). Inhibitory effect of Terminalia chebula Retz. fruit extracts on digestive enzyme related to diabetes and oxidative stress. *Journal of Enzyme Inhibition and Medicinal Chemistry 27*: 578-586.

Schlüter, A. D. & Rabe, J. P. (2000). Dendronized polymers: synthesis, characterization, assembly at interfaces, and manipulation. *Angewandte Chemie International Edition 39*: 864-883.

Schmid, K., Nimberg, R. B., Kimura, A., Yamaguchi, H. & Binette, J. (1977). The carbohydrate units of human plasma α1-Acid glycoprotein. *Biochimica et Biophysica Acta. 492*: 291-302.

Schmidlin, L., Poutaraud, A., Claudel, P., Mestre, P., Prado, E., Santos-Rosa, M., Wiedemann-Merdinoglu, S., Karst, F., Merdinoglu, D. & Hugueney, P. (2008). A stress-inducible resveratrol O-methyltransferase involved in the biosynthesis of pterostilbene in grapevine. *Plant Physiology 148*: 1630-1639.

Schuttelkopf, A. W. & van Aalten, D. M. (2004). PRODRG: a tool for high-throughput crystallography of protein-ligand complexes. *Crystallographica Section D: Biological Crystallography 60*: 1355-1363.

Shen, Q., Wang, L., Zhou, H., Yu, L.-s. & Zeng, S. (2013). Stereoselective binding of chiral drugs to plasma proteins. *Acta Pharmacologica Sinica 34*: 998-1006.

Shen, Y. C., Chen, C. F. & Chiou, W. F. (2002). Andrographolide prevents oxygen radical production by human neutrophils: possible mechanism (s) involved in its anti-inflammatory effect. *British Journal of Pharmacology 135*: 399-406.

Shuai, X., Merdan, T., Unger, F. & Kissel, T. (2005). Supramolecular gene delivery vectors showing enhanced transgene expression and good biocompatibility. *Bioconjugate Chemistry 16*: 322-329.

Siddiqui, S., Siddiqui, B., Adil, Q. & Begum, S. (1990). Constituents of Mirabilis jalapa. *Fitoterapia 61*.

Singh, N., Kulshrestha, V., Srivastava, R. & Kohli, R. (1973). A comparative evaluation of piperine and nalorphine against morphine-induced respiratory depression and analgesia. *Journal of Indian Medicine* 4:22-26

Spiegel, K. & Magistrato, A. (2006). Modeling anticancer drug–DNA interactions via mixed QM/MM molecular dynamics simulations. *Organic & Biomolecular Chemistry 4*: 2507-2517.

Srinivasan, K. (2007). Black pepper and its pungent principle-piperine: a review of diverse physiological effects. *Critical Reviews in Food Science and Nutrition 47*: 735-748.

Subramanyam, R., Gollapudi, A., Bonigala, P., Chinnaboina, M. & Amooru, D. G. (2009a)

Betulinic acid binding to human serum albumin: A study of protein conformation and binding affinity. *Journal of Photochemistry and Photobiology B: Biology 94*: 8-12.

Subramanyam, R., Goud, M., Sudhamalla, B., Reddeem, E., Gollapudi, A., Nellaepalli, S., Yadavalli, V., Chinnaboina, M. & Amooru, D. G. (2009b). Novel binding studies of human serum albumin with trans-feruloyl maslinic acid. *Journal of Photochemistry and Photobiology B: Biology 95*: 81-88.

Sudhamalla, B., Gokara, M., Ahalawat, N., Amooru, D. G. & Subramanyam, R. (2010). Molecular dynamics simulation and binding studies of β-sitosterol with human serum albumin and its biological relevance. *The Journal of Physical Chemistry B 114*: 9054-9062.

Sudlow, G., Birkett, D. & Wade, D. (1975). The characterization of two specific drug binding sites on human serum albumin. *Molecular Pharmacology 11*: 824-832.

Sudlow, G., Birkett, D. & Wade, D. (1976). Further characterization of specific drug binding sites on human serum albumin. *Molecular Pharmacology 12*: 1052-1061.

Sugio, S., Kashima, A., Mochizuki, S., Noda, M. & Kobayashi, K. (1999). Crystal structure of human serum albumin at 2.5 Å resolution. *Protein Engineering 12*: 439-446.

Sułkowska, A. (2002). Interaction of drugs with bovine and human serum albumin. *Journal of Molecular Structure 614*: 227-232.

Sundararaman, P. & Djerassi, C. (1977). A convenient synthesis of progesterone from stigmasterol. *The Journal of Organic Chemistry 42*: 3633-3634.

Sunder, A., Mülhaupt, R., Haag, R. & Frey, H. (2000). Hyperbranched polyether polyols: a modular approach to complex polymer architectures. *Advanced Materials 12*: 235-239.

Svenson, S. (2012). Clinical translation of nanomedicines. *Current Opinion in Solid State and Materials Science 16*: 287-294.

Tang, D.-Z., Yang, F., Yang, Z., Huang, J., Shi, Q., Chen, D. & Wang, Y.-J. (2011). Psoralen stimulates osteoblast differentiation through activation of BMP signaling. *Biochemical and Biophysical Research Communications 405*: 256-261.

Tang, Y., Chen, R., Huang, Y., Li, G., Huang, Y., Chen, J., Duan, L., Zhu, B.-T., Thrasher, J. B. & Zhang, X. (2014). Natural Compound Alternol Induces Oxidative Stress–Dependent Apoptotic Cell Death Preferentially in Prostate Cancer Cells. *Molecular Cancer Therapeutics 13*: 1526-1536.

Tayeh, N., Rungassamy, T. & Albani, J. R. (2009). Fluorescence spectral resolution of tryptophan residues in bovine and human serum albumins. *Journal of Pharmaceutical and Biomedical Analysis 50*: 107-116.

Tesseromatis, C. & Alevizou, A. (2008). The role of the protein-binding on the mode of drug action as well the interactions with other drugs. *European Journal of Drug Metabolism and Pharmacokinetics 33*: 225-230.

Tokar, R., Kubisa, P., Penczek, S. & Dworak, A. (1994). Cationic polymerization of glycidol: coexistence of the activated monomer and active chain end mechanism. *Macromolecules 27*: 320-322.

Trivedi, N. P., Rawal, U. M. & Patel, B. P. (2007). Hepatoprotective effect of andrographolide against hexachlorocyclohexane-induced oxidative injury. *Integrative Cancer Therapies 6*: 271-280.

Urien, S., Albengres, E., Pinquier, J.-L. & Tillement, J.-P. (1986). Role of alpha-1 acid glycoprotein, albumin, and nonesterified fatty acids in serum binding of apazone and warfarin. *Clinical Pharmacology & Therapeutics 39*: 683-689.

Valeur, B. & Brochon, J.-C. (2012). *New trends in fluorescence spectroscopy: applications to chemical and life sciences*, Springer Science & Business Media.

Van den Worm, E., Beukelman, C. J., Van den Berg, A. J., Kroes, B. H., Labadie, R. P. & Van Dijk, H. (2001). Effects of methoxylation of apocynin and analogs on the inhibition of reactive oxygen species production by stimulated human neutrophils. *European Journal of Pharmacology 433*: 225-230.

Varshney, A., Sen, P., Ahmad, E., Rehan, M., Subbarao, N. & Khan, R. H. (2010). Ligand binding strategies of human serum albumin: how can the cargo be utilized? *Chirality 22*: 77-87.

Vasir, J. K. & Labhasetwar, V. (2007). Biodegradable nanoparticles for cytosolic delivery of therapeutics. *Advanced Drug Delivery Reviews 59*: 718-728.

Walker, J. E. (1976). Lysine residue 199 of human serum albumin is modified by acetylsalicylic acid. *FEBS letters 66*: 173-175.

Walker, K. A., Stumbé, J.-F. & Haag, R. (2016). Polyester-Based, Biodegradable Core-Multishell Nanocarriers for the Transport of Hydrophobic Drugs. *Polymers 8*: 192.

Wang, R., Lai, L. & Wang, S. (2002). Further development and validation of empirical scoring functions for structure-based binding affinity prediction. *Journal of Computer-Aided Molecular Design 16*: 11-26.

Wesche DL, D. M., Tortella FC, Brewer TG (1994). Neurotoxicity of artemisinin analogs in vitro. *Antimicrob Agents Chemother 8*: 1813–1819.

Woody, R. W. & Koslowski, A. (2002). Recent developments in the electronic spectroscopy of amides and α-helical polypeptides. *Biophysical Chemistry 101*: 535-551.

Xia, Y.-F., Ye, B.-Q., Li, Y.-D., Wang, J.-G., He, X.-J., Lin, X., Yao, X., Ma, D., Slungaard, A. & Hebbel, R. P. (2004). Andrographolide attenuates inflammation by inhibition of NF-κB activation through covalent modification of reduced cysteine 62 of p50. *The Journal of Immunology 173*: 4207-4217.

Xu, J., Li, Z., Cao, M., Zhang, H., Sun, J., Zhao, J., Zhou, Q., Wu, Z. & Yang, L. (2012). Synergetic effect of Andrographis paniculata polysaccharide on diabetic nephropathy with andrographolide. *International Journal of Biological Macromolecules 51*: 738-742.

Yamasaki, K., Chuang, V. T. G., Maruyama, T. & Otagiri, M. (2013). Albumin-drug interaction and its clinical implication. *Biochimica et Biophysica Acta (BBA)-General Subjects 1830*: 5435–5443.

Yan, D., Gao, C. & Frey, H. (2011). *Hyperbranched polymers: synthesis, properties, and applications*, John Wiley & Sons.

Yang, J., Petersen, C. E., Ha, C. E. & Bhagavan, N. V. (2002). Structural insights into human serum albumin-mediated prostaglandin catalysis. *Protein Science 11*: 538-545.

Yeggoni, D. P., Gokara, M., Mark Manidhar, D., Rachamallu, A., Nakka, S., Reddy, C. S. & Subramanyam, R. (2014a). Binding and molecular dynamics studies of 7-hydroxycoumarin derivatives with human serum albumin and its pharmacological importance. *Molecular Pharmaceutics 11*: 1117-1131.

Yeggoni,D.P. & Subramanyam, R. (2014b).Binding studies of L-3, 4-dihydroxyphenylalanine with human serum albumin. *Molecular BioSystems 10*: 3101-3110.

Yeggoni, D. P., Rachamallu, A. & Subramanyam, R. (2015a). Cytotoxicity and Comparative Binding Mechanism of Piperine with Human Serum Albumin and α-1-Acid Glycoprotein. *Journal of Biomolecular Structure and Dynamics 33*: 1336-1351.

Yeggoni, D. P. R., Darla, M. M., Reddy, C. S. & Subramanyam, R. (2015b). Investigation of binding mechanism of novel 8-substituted coumarin derivatives with human serum albumin and α-1-glycoprotein. *Journal of Biomolecular Structure and Dynamics* 34:2032-2036.

Yeggoni, D. P., Rachamallu, A. & Subramanyam, R. (2016a). A comparative binding mechanism between human serum albumin and α-1-acid glycoprotein with corilagin: biophysical and computational approach. *RSC Advances 6*: 40225-40237.

Yeggoni, D. P., Rachamallu, A. & Subramanyam, R. (2016b). Protein stability, conformational change and binding mechanism of human serum albumin upon binding of embelin and its role in disease control. *Journal of Photochemistry and Photobiology B: Biology 160*: 248-259.

Yoshima, H., Matsumoto, A., Mizuochi, T., Kawasaki, T. & Kobata, A. (1981). Comparative study of the carbohydrate moieties of rat and human plasma alpha 1-acid glycoproteins. *Journal of Biological Chemistry 256*: 8476-8484.

Zhang, Que, Q., Pan, J. & Guo, J. (2008). Study of the interaction between icariin and human serum albumin by fluorescence spectroscopy. *Journal of Molecular Structure. 881*: 132-138.

Zhang, G., Gurtu, V., Kain, S. R. & Yan, G. (1997). Early detection of apoptosis using a fluorescent conjugate of annexin V. *Biotechniques 23*: 525-531.

Zhang MF, Xu ZQ, Yu-Shu Ge, Jiang FL & Liu, Y. (2012). Binding of fullerol to human serum albumin: spectroscopic and electrochemical approach. *Journal of Photochemistry and Photobiology B: Biology 108*: 34-43.

Zhao, X., Liu, R., Teng, Y. & Liu, X. (2011). The interaction between Ag+ and bovine serum albumin: a spectroscopic investigation. *Science of the Total Environment 409*: 892-897.

Zhao, X., Lu, D., Hao, F. & Liu, R. (2015). Exploring the diameter and surface dependent conformational changes in carbon nanotube-protein corona and the related cytotoxicity. *Journal of Hazardous Materials 292*: 98-107.

Zhou, X., Zhang, G. & Wang, L. (2014). Binding of 8-methoxypsoralen to DNA in vitro: Monitoring by spectroscopic and chemometrics approaches. *Journal of Luminescence 154*: 116-123.

Zsila, F. (2013). Subdomain IB Is the third major drug binding region of human serum albumin: Toward the three-sites model. *Molecular Pharmaceutics 10*: 1668-1682.

Zsila, F., Bikádi, Z. & Simonyi, M. (2003). Probing the binding of the flavonoid, quercetin to human serum albumin by circular dichroism, electronic absorption spectroscopy and molecular modelling methods. *Biochemical Pharmacology 65*: 447-456.

Zunszain, P. A., Ghuman, J., McDonagh, A. F. & Curry, S. (2008). Crystallographic Analysis of Human Serum Albumin Complexed with 4Z, 15E-Bilirubin-IXα. *Journal of MolecularBiology 381*: 394-406.

LIST OF PUBLICATIONS

LIST OF PUBLICATIONS

1. **Yeggoni, D.P**.; Gokara, M.; Mark Manidhar, D.; Rachamallu, A.; Nakka, S.; Reddy, C. S.; Subramanyam, R., Binding and Molecular Dynamics Studies of 7-Hydroxycoumarin Derivatives with Human Serum Albumin and Its Pharmacological Importance. Mol. Pharm. 2014, 11 (4), 1117-1131.

2. **Yeggoni, D.P**.; Rachamallu, A.; Kallubai, M.; Subramanyam, R., Cytotoxicity and Comparative Binding Mechanism of Piperine with Human Serum Albumin and α-1-Acid Glycoprotein. J. Biomol. Struct. Dyn. 2014, 6(33):1336-1351.

3. **Yeggoni, D.P**.; Subramanyam, R., Binding Studies of L-3, 4-Dihydroxy phenylalanine with Human Serum Albumin. Mol. Biosyst. 2014; (10),3101-3110.

4. Kallubai, M.; Rachamallu, **Yeggoni, D. P**.; A.; Subramanyam, R., Comparative Binding Studies of Lupeol Compounds with Plasma Proteins and its Pharmacological Importance. Mol. Biosyst. 2015,(11), 1172-1183 .

5. Surampudi D.; **Yeggoni,D.P**.; Mark Manidhar, D., Design, synthesis and molecular docking of 2-iso propyl amino derivatives of 7-methoxy coumarin as potent acetylcholinesterase inhibitors. Der Pharma Chemica. 2015, 7(7):255-272.

6. **Yeggoni, D.P**.; Mark Manidhar, D.; Reddy, C. S.; Subramanyam, R., Investigation of binding mechanism of novel 8-substituted coumarin derivatives with human serum albumin and α-1-glycoprotein. J. Biomol. Struct. Dyn .2015, 9 (34):1-46.

7. **Yeggoni, D. P**.; Rachamallu, A.; Subramanyam, R., A comparative binding mechanism between human serum albumin and α-1-acid glycoprotein with corilagin: Biophysical and computational approach. RSC. Adv. 2016, 46(6): 40225-40237.

8. **Yeggoni, D.P**.; Rachamallu, A.; Subramanyam, R., Protein Stability, Conformational Change and Binding Mechanism of Human Serum Albumin upon Binding of Embelin and its Role in Disease Control. J. Photochem. Photobiol. . 2016,(160) 248-259 .

9. **Yeggoni, D.P**.; Christian.Kuehne.; Rachamallu, A.; Subramanyam, R., Elucidating the binding interaction of andrographolide to plasma proteins: biophysical and computational approach. RSC.Adv.(Accepted)

10. Sangilimuthu .A.; **Yeggoni, D. P**.; Elsin Raju.D.; Subramanyam, R., Molecular binding mechanism of 5-hydroxyl- 1-methylpiperidin- 2-one with human serum albumin. J. Biomol. Struct. Dyn. (Accepted)

11. **Yeggoni, D.P**.; Rachamallu, A.;Shreya.D.; Argha.M.; Subramanyam, R., Unravelling the Molecular Binding Mechanism of Menthol with Blood Transport Proteins: Biophysical and Computational Approach. J. Biomol. Struct. Dyn. (Accepted)

To be communicated

12. **Yeggoni, D.P**.; Rachamallu, A.; Subramanyam, R., Determination of binding mechanism of Bacosine with serum proteins: A combined biophysical and molecular modeling approach. (to be communicated)

13. **Yeggoni, D.P**.; Rachamallu, A.; Subramanyam, R., Binding mechanism of stigmasterol with Human serum albumin and its biological relevance.(to be communicated)

14. Nakka, S.; **Yeggoni, D.P**.; Rachamallu, A.; Subramanyam, R., Binding mechanism of forskolin with serum proteins.(to be communicated)

15. **Yeggoni, D.P**.; Subramanyam, R., Unravelling the interaction mechanism of chebulinic acid and chebulagic acid with Human serum albumin. (to be communicated)